Modeling Hydrothermal Inputs to Cold-water Streams in Urban Watersheds

A DISSERTATION
SUBMITTED TO THE FACULTY OF THE GRADUATE SCHOOL
OF THE UNIVERSITY OF MINNESOTA
BY

Benjamin David Janke

IN PARTIAL FULFILLMENT OF THE REQUIREMENTS
FOR THE DEGREE OF
Doctor of Philosophy

May, 2011

Acknowledgements

First and foremost, I must thank my advisor Dr. Heinz Stefan, who has been exceedingly helpful and patient over the course of my studies, providing expertise and encouragement when I'd run out of ideas, and never hesitating to make time for me. You have my deepest gratitude.

A special thanks goes to Dr. William Herb, who spent many hours helping me through obstacles in model development and data analysis, and taught me more than a few Excel tricks. I have learned a lot from you, and am very grateful for your patience.

Thanks also to the wonderful people I've met over the years at the St. Anthony Falls Laboratory. It was a great place to call my academic home, and I made a lot of friends during my time there. A special thanks to Chris Ellis, who helped with instrumentation setup and data logger programming for much of the early field work done in this study, and to Eric Novotny and Mike Weiss who helped with this early data collection. Dr. Omid Mohseni provided valuable assistance in various phases of my work and assisted with a major data collection effort.

I would like to thank those whom I've had the privilege of working closely with on various projects, in particular Dr. John Nieber, Kim Chapman of Applied Ecological Services, and Bruce Wilson of the Minnesota Pollution Control Agency (MPCA), who served as project officer for several of the projects.

I acknowledge several individuals and organizations who were involved in data collection and acquisition throughout my studies: the MNROAD Project of the Minnesota Department of Transportation provided temperature data for a number of asphalt and paved surfaces; data for the Plymouth study were collected by James Johnson, formerly of the Three Rivers Park District, and plan drawings of the site were provided by Shahram Missaghi of the City of Plymouth; data for the Vermillion River project

were provided by Applied Ecological Services, Inc., the U.S. Geological Survey, Minnesota Department of Natural Resources, Dakota County Soil and Water Conservation District, Scott County Soil and Water Conservation District, the Metropolitan Council, Emmons and Olivier Resources, Inc., and Barr Engineering Company; support for the Vermillion River study was provided by the MPCA and the Vermillion River Watershed Joint Powers Board. Dr. William Herb developed the MINUHET model, and Jon Beatty and Brant Buchika, formerly of the Minnetonka Audio Software Company, created the user interface for MINUHET.

I must also acknowledge the financial support of the Environmental Protection Agency, which made much of this work possible by providing a three-year fellowship through the Science to Achieve Results (STAR) Graduate Fellowship Program.

Finally, thanks to my parents Bruce and Ellen, my brother Brian, and many friends who have provided love and support in various forms along the way, even if you questioned the sanity of remaining in school as long as I have. Many of you have helped me keep my academics balanced with a variety of right-brain activities; I've enjoyed my time at dinner club, concerts, and happy hours, and with the UMN Concert Band and the pick-up soccer crew.

You all have my most sincere appreciation.

Dedication

To my family, friends, and colleagues who have offered support, critique, and enlightenment at every step of the way. This work is dedicated to you all.

Abstract

This research investigated the impact of urban development on the temperature of cold-water streams, which are crucial to maintaining viable populations of biota (such as trout) that are unable to survive in warmer waters. Since the temperature of these streams is typically maintained by significant amounts of groundwater inflow and riparian shading, the land cover conversion associated with urban development replacement of cropland, natural land, and forests with buildings, roads, lawns, and parking lots has a negative impact, as these land-use changes tend to increase the amount of impervious surface area and reduce the amount of natural shading provided by vegetation. As a result, fluctuations of surface runoff rates and temperatures from rainfall events are amplified, watershed infiltration is reduced, and stream temperature increases.

A primary goal of the project was to produce an assessment tool to be used by city planners and watershed managers to determine the impact of proposed urban development on stream temperatures in a particular watershed. The research procedure focused primarily on understanding and developing models for the hydrologic and heat transfer processes within a watershed, with particular focus on rainfall-runoff processes. Specifically, two process-based models were developed: one for estimation of runoff flow and temperature from urban surfaces, and a second for estimation of groundwater input to a stream from observations of water quality. These models were applied to study sites for validation and sensitivity analyses, and to address questions concerning worst-case scenarios and thermal impacts of various management practices. Fieldwork was performed as necessary to provide data for validation of the models.

The runoff temperature model demonstrated that heat export by rainfall-runoff from a paved surface is determined by antecedent pavement temperature and rainfall intensity/duration, and that longitudinal (stream-wise) gradients in runoff temperature are negligible. The model also contributed to the development of a more comprehensive stormwater modeling tool (MINUHET) by justifying the simpler solution technique used by MINUHETs runoff model. MINUHET was shown to accurately simulate runoff flow rate and temperature at the outlet of a small urban watershed, particularly when

hydrologic data is available for calibration. The roof surface temperature analysis provided evidence that the contribution of rooftops is negligible relative to that of paved surfaces, a common assumption made in runoff temperature modeling. Lastly, the use of temperature as a groundwater tracer was shown to be an effective and inexpensive method for determining groundwater input to a stream, provided that the limitations of the approach are borne in mind when applying the method.

Contents

List of Tables

List of Figures

Thesis Overview

Research Problem

Urban development in the watersheds of cold-water streams can have a detrimental effect on these often-fragile ecosystems. Since the temperature of cold-water streams is typically maintained by significant amounts of groundwater input and riparian shading, the land cover conversion associated with urban development – replacement of cropland, natural land, and forests with buildings, roads, lawns, and parking lots – has a negative impact, because these land-use changes tend to increase the amount of impervious surface area and reduce the amount of natural shading provided by vegetation. As a result, ground surface temperatures increase, surface runoff rates and temperatures from rainfall events are amplified, and infiltration and groundwater recharge from the watershed can be reduced, ultimately leading to an increase in stream temperature (Nelson and Palmer, 2007; Paul and Meyer, 2001; Herb and Stefan, 2008). In previous studies, the increase in impervious surface area associated with urbanization has been correlated with decreased stream flow (Pluhowski, 1970), increased stream temperature (Galli, 1990), and the loss of temperature-sensitive fish species such as trout (Klein, 1979).

In this thesis, the impact of urban areas on stream temperature has been addressed through a detailed investigation and analysis of storm water runoff temperatures, and through the development of a technique for characterizing groundwater inflow to a small stream. There are four chapters:

- Chapter 1: Heat Release from Rooftops During Rainfall,
- Chapter 2: Simulation of Heat Export by Rainfall-Runoff from a Paved Surface,

- Chapter 3: Development and Application of the Minnesota Urban Heat Export Tool (MINUHET), and
- Chapter 4: Estimation of Groundwater Input to a Stream Reach Using a Heat Budget.

Existing stream temperature models are either empirical (e.g. Nelson and Palmer, 2007) and thus are not transferable to other watersheds, or do not explicitly include the effect of surface water runoff (e.g. LeBlanc et al., 1997; Krause et al., 2004). The first two chapters of the thesis are devoted to this issue, specifically investigations and models of runoff from paved surfaces, and heat release from rooftops during rainstorms. In addition to the heat input from surface water runoff, stream temperature models also need to include atmospheric heat exchange and groundwater input, the latter of which can be difficult to quantify. The fourth chapter of the thesis is concerned with this issue. Overall a need exists to better characterize and quantify heat transfer and hydrological processes that control storm water temperatures, and to integrate this knowledge into a process-based tool (model) that can can be used by city planners and watershed managers to assess the impact of proposed urban development on stream temperatures. Such a tool (MINUHET) is described and applied in Chapter 3 of the thesis.

Note that the impact of storm water on stream temperature is not addressed in the thesis, as it has been the subject of field studies mentioned previously (e.g. Pluhowski, 1970; Nelson and Palmer, 2007), as well as in an application of the MINUHET model to a trout stream in Minnesota (Herb and Stefan, 2008). The role of best management practices (BMP's) in the enhancement or mitigation of urban runoff temperature has been addressed in other studies of stormwater ponds (e.g. Van Buren et al., 2000b; Ham et al., 2006; Herb et al., 2009) and rock-filled channels (Roa-Espinosa et al., 2003), and is not included in this work.

Background

The negative impact of urban development on stream temperature is well-documented. In one particular series of studies (Galli, 1990), average stream temperature was found to increase by 0.09 °C for each one percent increase in overall imperviousness in the

watershed. Other studies have shown similar trends (Pluhowski, 1970; Klein, 1979; LeBlanc et al., 1997; Krause et al., 2004). Paved and building surfaces can become hotter than natural surfaces due to low reflectivity and lack of shading by vegetation, and on a short time scale can produce warmer runoff to receiving streams during and after rainfall events. Storm water detention ponds, a common type of storm water management practice, act as heat exchangers by prolonging exposure of surface water to direct solar radiation. Furthermore, since cold-water streams are often fed by groundwater, a loss of infiltration caused by increased imperviousness may reduce the amount of groundwater reaching a stream (Pluhowski, 1970; Klein, 1979; Paul and Meyer, 2001). This can become a significant long-term adverse effect of urbanization on stream temperature.

Temperature is of particular concern due to its great influence on the biological and chemical makeup of a stream. Water temperature can be the determining factor for the type of fish, invertebrates and plants present in a water body, and influences their activity levels, growth rates, and ability to compete (Klein, 1979; Eaton et al., 1995; LeBlanc et al., 1997). Of particular concern is the effect on fish species such as trout; adult brook trout, for example, experience thermal stress when water temperatures exceed 20 °C, and perish when temperatures exceed 24 °C (U.S. Environmental Protection Agency (E.P.A.), 1986). Water temperature also affects geochemical reaction rates and the concentrations of oxygen, nutrients, and pollutants dissolved in the water (LeBlanc et al., 1997; James and Xie, 1999; Paul and Meyer, 2001). Cold-water streams are often dependent on low groundwater temperature to support fisheries and other wildlife that would be unable to survive in warmer waters.

The water and heat budgets of a typical groundwater-gaining stream reach have several components (Figure 1). Major hydrologic components in the water budget are stream flow, stormwater inflow, groundwater inflow, and evaporation. The major heat transfer components are atmospheric heat fluxes (solar radiation, longwave radiation, evaporation, and convection) and the advective heat transfer associated with stream flow, stormwater inflow, and groundwater inflow. Heat exchange by heat conduction between stream-sediment and flowing water can be significant in shallow streams.

In general, heat exchange with the atmosphere is well understood, as the equations relevant to water quality modeling have been developed over decades of research (e.g. Edinger et al., 1968, 1974; Ryan et al., 1974; Theurer et al., 1984; Gulliver and Stefan,

1986). Numerous stream temperature models have been developed and refined. The characterization of advective heat inputs (e.g. from groundwater, tributaries, stormwater or wastewater) usually requires measurements of both flow rate and flow temperature, which often limits modeling accuracy and temporal resolution in watersheds where data are limited or not available. The problem is exacerbated in urbanized watersheds of groundwater-fed streams where external inputs may dominate the stream heat budget.

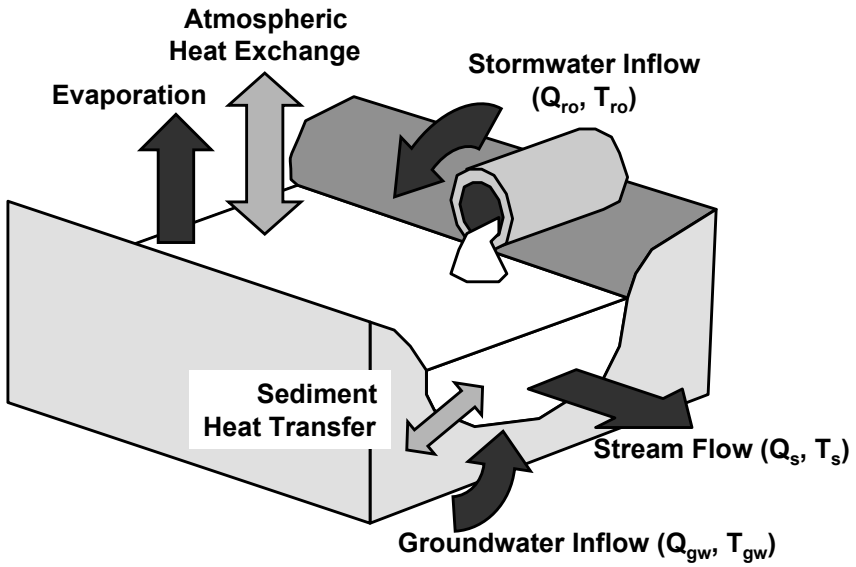

Figure 1: Overview of the heat transfer and hydrologic processes present in a typical groundwater-fed stream located in an urban watershed.

Several models exist for stormwater runoff in urban watersheds (e.g. XPSWMM, HEC-HMS). However, these models were developed for the purpose of storm sewer design and not stormwater temperature simulation. Multi-dimensional groundwater flow and groundwater temperature models (e.g. MODFLOW, VS2D) can be accurate, but tedious to implement and generally require detailed knowledge of sub-surface characteristics (e.g. water table elevation, soil thermal and hydrologic properties). A need exists to develop simple but robust models for characterizing groundwater heat input to a stream.

Research Objectives

The first objective of this thesis research is to develop a better understanding and quantitative process models of:

1. fluxes of heat and water that occur at the earths surface (especially urbanized) during both wet and dry weather,

2. heat and water transfer processes associated with surface runoff from urban surfaces during rainfall events, and

3. heat and hydrologic budgets for a stream, with emphasis on the role of sub-surface water (groundwater) inflow to the stream.

The second objective of the research is to integrate this understanding into process-based numerical simulation models quantifying hydrothermal inputs to a stream: one for predicting flow rate and temperature of surface runoff from a land surface during rainfall events, and another for estimating groundwater inflow to a stream. The models can potentially be used in conjunction with comprehensive watershed runoff models coupled to stream temperature models to assess the impact on stream temperature of future urban development or other land use change in a watershed. The groundwater inflow model can be used independently to identify stream reaches for which groundwater inflow is significant, and to quantify that input. These stream reaches usually maintain the best low-temperature fish habitat in the stream system, and need to receive special attention in the planning of urban development in a watershed.

Basic research, model development, and data analysis will be used to address fundamental questions related to water resources management, specifically the preservation of cold-water streams:

1. Which surfaces (e.g. pavement, rooftops, lawns) exhibit the most heating of runoff?

2. Can the contribution of heat to runoff by certain surfaces, e.g. rooftops and lawns, generally be neglected a common assumption in existing runoff temperature models?

3. What factors (e.g. antecedent conditions, surface properties) have the greatest influence on the heat transfer from a surface to rainfall-runoff?

4. What types of rainfall events (duration, intensity) have the greatest impact on the water temperature rise of runoff?

5. What can be done to improve the accuracy of simulations of flow rate and temperature of rainfall-runoff from an urban watershed?

6. To what degree can groundwater input to a stream be estimated from high-resolution stream and streambed water temperature data?

Methodology

The focus of this research is primarily on the development of deterministic, process-based numerical simulation models. The models are tested against available data, and therefore supplemented by field studies when necessary. Model results are analyzed and compared to observations, and sensitivity analyses are performed.

Model Development

The runoff temperature model for paved (impervious) and pervious surfaces is developed from equations for unsteady heat and mass (water) transfer processes for both wet and dry weather. Runoff is modeled using a numerical solution of the 1-D kinematic wave equation for unsteady flow on a planar surface, producing a solution of runoff depth (and temperature) as a function of time and position along the surface. Interception and infiltration (Green-Ampt) are taken into account for pervious surfaces, although the heat transfer due to infiltrated water is neglected. Modeled atmospheric heat fluxes include solar radiation, long wave radiation, evaporation and convection. Vertical heat conduction below the surface, i.e. within the soil, pavement or roof, is determined from a numerical solution of a 1-D unsteady heat diffusion equation. A formulation is developed for estimating heat flux from the solid surface to the runoff (flowing water). Weather data and physical/thermal properties of the surfaces and sub-surface are needed to operate the model.

The runoff temperature model aided the development of a simulation tool called MINUHET (Herb et al., 2009a), although it was not directly implemented. MINUHET routes stormwater and heat through an urban sub-watershed, producing a time series of flow rates and water temperatures at the outlet (end point) of a sub-watershed for each rainfall event. The tool includes a graphical user interface, and has the capability to model a number of routing elements (storm sewers, pervious and impervious open channels) and a few best management practices (stormwater vaults, rock swales, detention and infiltration ponds).

To model groundwater inflow to a stream reach a detailed, unsteady heat budget that accounts for all major heat transfer processes in the stream reach was used. The groundwater inflow rate (the only major unknown) was extracted from the residual of this heat budget. All other heat flux components were determined from the extensive hydrologic, temperature, and weather data collected on the stream reach. This approach requires accurate modeling of the heat transfer processes, and the availability of accurate model input data: stream flow rate, stream temperature at the upstream and downstream ends of the stream reach, and an estimate of the temperature of the groundwater flowing into the stream, as well as weather data for calculating heat exchange between the water and atmosphere.

Field Data Collection and Analysis

Data were acquired for running the models, for calibrating and/or validating model components, for extracting numerical values of model components (e.g. connected impervious surface area), or for direct analysis, such as in the comparison of wet-weather surface temperatures from a variety of common urban surfaces (Chapter 1). A significant amount of data was acquired from outside sources, but field studies were conducted when necessary to provide a complete data set.

A field study at a small parking lot on Hennepin Island in Minneapolis, MN was used to provide data for validating the runoff temperature model. Runoff flow rate was measured at the outlet of the parking lot using a weir, and runoff temperature was recorded at a number of locations in the lot. Data was collected during the summer months (June to September) of 2007 and 2008. Due to very dry conditions during this period, data for only one suitable event was obtained, which was not enough to provide

a rigorous validation of the runoff model.

A second field study provided surface temperature data for a commercial rooftop. Temperature was measured at 6 locations on the roof of the study site from June through September of 2005. A residential site was monitored over the same time period by another party, providing temperature data for a number of surfaces (e.g. rooftop, driveway, lawn). These temperature data were analyzed during rainfall events to investigate wet-weather roof temperature dynamics, and to assess the heat export potential of different roof types relative to paved surfaces such as driveways.

Runoff flow rate and temperature data were collected in a storm sewer pipe at the outlet of a small (12.5-ac) residential development in Plymouth, MN from August through September of 2005 by the Three Rivers Park District (Hennepin County, MN). The measurements were made as part of an unrelated stormwater management project. The data were analyzed, and also used in a case study of MINUHET (Herb et al., 2009a).

For the groundwater inflow model, relevant data have been collected by a number of state and private entities in the Vermillion River, a trout stream located southeast of Minneapolis, MN. Since 2006, stream temperature, stream flow rate, and groundwater temperature (from shallow wells placed in the stream itself) have been recorded at enough sites to allow for application of the model in several locations and under a variety of weather and stream flow conditions.

Results

The results of this thesis research are presented in four individual chapters: Chapter 1 gives the analysis of the roof temperature data collected at the commercial and residential sites, with emphasis on wet-weather periods; Chapter 2 contains the development and analysis of the runoff temperature model; Chapter 3 presents the application of the MINUHET model to two case studies and an analysis of the data collected; and Chapter 4 includes the development of the groundwater inflow model and its application to the Vermillion River.

The primary outcomes of the rooftop temperature analyses are presented in Chapter 1. Rooftop temperatures were measured over several weeks including multiple rainfall

events. In general, the data analyses show that both residential and commercial rooftops store less heat than a concrete driveway: compared to that concrete driveway, both roof types experienced larger temperature drops prior to the onset of rainfall as storms approached, had lower mean temperatures during rainfall events, and maintained smaller differences with rainfall (dew point) temperature over the duration of rainfall events. The analyses also show that heat release from residential rooftops during rainfall events is negligible, with estimated heat export (per unit surface area) less than 20% of that from a concrete pavement (driveway) for the three rainfall events analyzed. The results for the commercial rooftop were not as conclusive, with heat export ranging from 30% to 90% of that estimated for the concrete driveway. Bearing in mind that the absolute heat export is dependent on the proportions of each surface present in a watershed, the results suggest that the contribution of commercial rooftops to heating of runoff may not be negligible in highly built-up watersheds where these rooftops can make up a large portion of the impervious surface.

The runoff temperature model development and analysis are described in Chapter 2. The model was applied to a small parking lot in Minneapolis, MN for a single, early evening rainfall event in late summer (Aug 11, 2007). While there were not enough rainfall events for a model validation, this case study produced encouraging results with very little calibration (RMSE for flow = 1.14 L/s, RMSE for temperature = 0.61 °C). A sensitivity analysis of the model applied to a hypothetical paved surface revealed that physical properties of the surface (slope, roughness, and length) had little effect on event heat export, which is a measure of the heat contained in the runoff from a surface relative to a reference temperature (in this case 20 °C, a water temperature associated with the onset of thermal stress in some species of trout). Rainfall intensity, rainfall duration, and antecedent pavement temperature were the primary determinants of heat export, with the greatest heat export logically found for long events or those with high rainfall intensity, and particularly for those with high pavement temperatures at the onset of rainfall. Furthermore, simulations showed that gradients of runoff temperature in runoff direction (stream-wise) were relatively insignificant, and thus the detail provided by this model was unnecessary when the primary concern is conditions at the outlet of the modeled surface. This served as motivation for employing a simpler solution technique in the runoff temperature model used by the MINUHET model.

In Chapter 3, the development of the modeling tool MINUHET is summarized, and results of applications of MINUHET to two case studies are analyzed. In the first case study, MINUHET was applied to the same parking lot and rainfall event as the runoff temperature model presented in Chapter 2 for the purpose of comparing the solution techniques employed in the two runoff temperature models. Results showed that the two models differed by 2% or less in terms of total runoff, mean runoff temperature, and event heat export. While the MINUHET model produced slightly higher RMSE values for the observed runoff flow rates and runoff temperatures, the semi-analytic solution technique used in the MINUHET runoff model did not appear to impact the results adversely, and is expected to be suitable for use in future applications of the model.

In the second case study, MINUHET was applied to a 12.5-ac residential development in Plymouth, MN. From observations of runoff volume and rainfall depth, the watershed was found to have an effective impervious area of 19.6%. The use of this calibration parameter, along with calibrated values for the Mannings hydraulic roughness coefficient n and the saturated hydraulic conductivity K of the soil, allowed the simulation of four rainfall events with considerable accuracy in terms of runoff flow rate (RMSE less than 32 L/s), runoff temperature (RMSE less than 1.0 °C), and event heat export (within 10% of the observed value, with exception of one event). A sensitivity analysis showed that the model output was very sensitive to dew point (rainfall) temperature and the thermal properties of the paved surfaces, while thermal properties of the roof and lawn surfaces had no effect on output, and saturated hydraulic conductivity was only important for very large events that produced pervious runoff. It was concluded that MINUHET should be suitable for use in future studies of urban watersheds, and that greater accuracy could be achieved by improving input data quality and by using runoff data for calibration of the model and determination of effective impervious area.

The development and analysis of the model for groundwater input to a stream are presented in Chapter 4. The use of a heat budget approach was found to have a few major advantages: groundwater input representative of a whole stream reach can be obtained rather than a single point value along a reach, and acquisition of the required data and model implementation are straightforward relative to traditional monitoring techniques. However, the approach also has limits in its applicability: it requires periods when a large difference exists in temperature between the stream and

the groundwater, is limited to reaches with very little tributary or stormwater inflows, and works best when groundwater inflow is large relative to the stream flow (i.e. in small streams). The simulation results and a sensitivity analysis showed that the model is able to capture seasonal variability of groundwater inflow rates, but performs poorly in the presence of high stream flows or significant surface inflows. Stream shading, groundwater temperature, and stream temperature were found to greatly impact the results, stressing the importance of high data resolution and quality. Based on these results, criteria were developed for future application of the heat budget technique.

Significance

The negative impact of urban development on the quality of cold-water streams is unmistakable. While temperature is a significant concern, other water quality issues associated with development (e.g. sedimentation, pollution from man-made chemicals, excess nutrients, loss of spawning habitat for fish) are also of importance. The exact cause of warming is not precisely known, and appears to vary from watershed to watershed. Although the loss of groundwater recharge in the watershed and reduced riparian shading can contribute more to the heating of streams than the increased volume and temperature of storm water runoff, this work – which focused primarily on storm water impacts – has refined existing knowledge and quantified relationships that had been assumed but not proven in the management of cold-water stream fisheries.

One contribution of this research has been the development of a robust and accurate process-based surface runoff temperature model. This model was used to substantiate existing assumptions regarding the heat content of urban runoff from rainfall, and also contributed to the development of a more comprehensive stormwater modeling tool (MINUHET) by justifying the simpler solution technique used by MINUHETs runoff temperature model. MINUHET was shown to accurately simulate runoff flow rate and runoff temperature at the outlet of a small urban watershed, particularly when hydrologic data is available for calibration. It is anticipated that this tool can be employed to guide responsible land development as cities continue to expand into the watersheds of cold-water streams.

The analysis of data from a residential and a commercial rooftop clarified a common

assumption made in runoff temperature analysis: the contribution of rooftops is negligible relative to that of paved ground surfaces only for residential roofs; commercial rooftops may produce heating similar to that of a concrete driveway for certain rainfall events.

The use of temperature as a groundwater tracer has been shown to be an effective and inexpensive means for determining groundwater input to a stream, provided that the limitations of the approach are borne in mind when applying the method. The importance of data resolution and data quality when using this method should also be stressed.

Chapter 1

Heat Release From Rooftops During Rainfall

Summary

In the modeling of urban storm water runoff temperatures, the contribution of rooftops to the heating of rainfall runoff is usually neglected or not mentioned in the literature. In this paper we examine the accuracy of this assumption (a) by analyzing temperature data that we recorded on a residential rooftop, a commercial rooftop, and a concrete driveway, and (b) by simulating temperature profiles within rooftops and pavements, and estimating heat transfer amounts from these surfaces to rainfall runoff (heat export). Analysis of both wet- and dry-weather temperature data recorded in the north central USA over periods of several months leads to the conclusion that (a) a concrete driveway has a far greater capacity for heat storage and release than a shingled residential rooftop, and (b) an insulated commercial rooftop is able to store and release more heat than the residential rooftop. Unexpectedly, the rainfall events with the highest dew point (rainfall) and surface temperatures often occurred during late night or early morning hours, and not during daylight hours. The analysis of three rainfall events showed that the heat export from the commercial rooftop (per unit surface area) was roughly three times that of the residential rooftop, but only 30%-90% of the heat export from a concrete driveway. Maximum (potential) heat export was significantly higher for the driveway than for either rooftop. In conclusion, the results of the data analysis

and heat export simulations support the assumption that residential rooftops contribute very little heating to runoff from rainfall. Commercial rooftops may have a thermal impact on rainfall runoff because of their greater thermal storage capacity. Commercial rooftops in addition to asphalt and concrete pavements should be considered when estimating water temperature of rainfall runoff from urbanized areas and the associated impact on the thermal regime of streams and fish habitat.

Originally published as:

> Janke BD, Mohseni O, Herb WR, Stefan HG. 2011. "Heat release by rooftops during rainstorms in the Minneapolis/St. Paul metropolitan area, U.S.A." *Hydrological Processes.* DOI: 10.1002/hyp.7954. (in press).

1.1 Introduction

During the summer months, warm rainfall runoff from impervious urban areas can be a threat to coldwater (trout) streams (James and Xie, 1999; Nelson and Palmer, 2007). Empirical relationships have been developed relating connected impervious surface area to stream temperature (Wang et al., 2003), but no distinction has been made between pavements and roof surfaces. Although rooftops are impervious and cover large portions of urban areas, a common assumption is that they contribute significant water volume but little heat to urban surface runoff from rainfall.

How much water is contributed by rooftops to runoff actually depends on stormwater best management practices (BMPs), which tend to route water from roofs to lawns, rain gardens, infiltration ponds or other places where infiltration into the soil is enhanced. This practice reduces surface runoff. The effect of BMPs on the stormwater volume ultimately contributed by rooftops is not considered in this study.

In the assessment or modeling of urban storm water runoff temperatures, rooftops are ignored, because paved roads and parking lots are expected to have much greater heat storage and release potential than roofs (Herb et al., 2007). No validation of this assumption was found in the literature. The treatment of rooftop runoff is also

not addressed in the literature of some existing runoff temperature models: a model by Van Buren et al. (2000a), developed for urban paved surfaces, does not mention rooftops; the models TURM (Roa-Espinosa et al., 2003; Thompson et al., 2008) and WEP (Jia et al., 2001), which were designed to simulate runoff temperatures and volumes from partially-developed watersheds, either do not treat or do not mention rooftop runoff. MINUHET (Herb et al., 2009a) does consider rooftop runoff. Residential rooftop runoff is taken into account as additional runoff volume, while commercial rooftops can be modeled as separate sub-watersheds, with an assumed mass per unit area that can contribute heat energy to runoff. In this study we will provide information to quantify heat loading from roof runoff.

An experimental (field) and modeling study was conducted to investigate the contribution of rooftops to the heating of rainfall runoff. Rooftop temperatures were recorded and analyzed, and a previously-developed runoff model for pavements was applied to a typical residential (asphalt-shingled) and a commercial (flat tar-and-gravel) roof. Modeling results will be compared in terms of heat export, here defined as the total heat (per unit area) extracted from a rooftop over the course of a rainfall event. The methodology, data and results of the analysis will be presented to support or refute the hypothesis that rooftops contribute little to the heating of rainfall runoff in urban areas.

A vegetated ("green") rooftop was also considered for analysis, but existing documentation suggests that the contribution to runoff heating is minimal. Green rooftops tend to reduce heat flow through the roof (Oberndorfer et al., 2007) and reduce the volume and peak of rainfall runoff relative to conventional rooftops (Liu and Minor, 2005; VanWoert et al., 2005; Carter and Rasmussen, 2006). Heat export from a green roof is therefore expected to be considerably lower than that from any conventional roof, and is not considered in this study.

1.2 Rooftop Structures

Two types of rooftops found in the Upper Midwest of the U.S. were investigated in detail: a residential rooftop and a commercial rooftop in the Minneapolis/St. Paul metropolitan area. Residential rooftops are typically sloping surfaces covered by multiple layers of asphalt shingles, and are found on low-density single-family housing; commercial

rooftops are often flat, tar-and gravel-covered surfaces installed on shopping centers, warehouses, manufacturing and storage facilities, as well as public buildings.

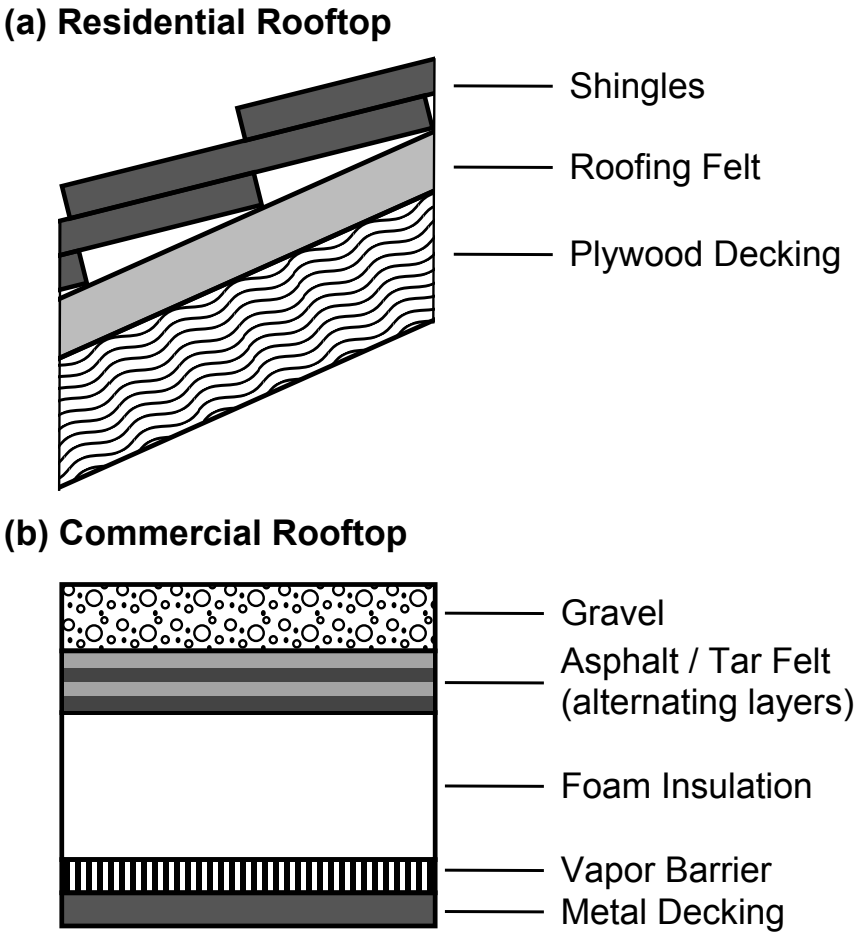

Figure 1.1: Typical structures of (a) a residential rooftop, and (b) a commercial built-up roof (not to scale).

1.2.1 Residential Roof

The residential rooftop is usually constructed with a high slope to facilitate rapid runoff of rainfall from the rooftop to gutters. The roof structure normally consists of a thin (roughly 3/4"), rafter-supported wood decking on which is placed a vapor barrier or roofing felt to prevent moisture transfer (Figure 1.1a). Asphalt shingles are then placed

on top of the felt in overlapping layers to prevent runoff from seeping underneath the shingles and rotting the decking material. The roof is usually constructed over an uninhabited attic space; insulation is placed in the floor of the attic space and the temperature of the space is not controlled as in the rest of the house. The attic space is usually vented through air inlets in the eaves and turbines or air outlets near the top of the attic. The field study was conducted on a roof of this type.

1.2.2 Commercial Roof

The second rooftop structure investigated was a built-up tar-and-gravel rooftop typical of commercial or industrial buildings. The commercial roof is generally flat (on the order of 1% slope). The decking material is usually wood or metal, upon which a layer of foam insulation (2 - 6" thick depending on climate) and a vapor barrier are placed. The roof is then built up by alternating layers of an asphalt-based felt and a liquid hydrocarbon (tar) that fuses with the felt layer. Three to five layers are typical. For the top layer, a coarse gravel or stone is poured into the tar to cap the rooftop and provide resistance to abrasion by wind and rain (Figure 1.1b).

1.3 Data Collection

1.3.1 Field Study Sites

Surface temperature and weather data were collected at two field sites: the roof and driveway of a private residence in Shoreview, Minnesota, and a commercial roof in Minneapolis, roughly 4 miles from the residential site. The latter was the roof of the wind tunnel enclosure at the St. Anthony Falls Laboratory (SAFL) of the University of Minnesota. A weather station at the SAFL site was used to record weather data; precipitation and wind speed were also recorded at the residential site. Data were collected from June through September 2005 at both sites.

At the residential site, temperature was recorded at 1-minute intervals on north-facing and south-facing portions of the roof, on the concrete driveway, and on the lawn (grass) using thermistors (Campbell Scientific model 107). Rooftop thermistors were placed just under the first layer of shingles to prevent direct heating of the probes by

solar radiation, the concrete thermistor was placed in a seam in the driveway and covered with a thin layer of light-colored caulk, and the lawn thermistor was installed such that it was approximately level with the dirt surface and shaded by the grass. Small boxes were placed at the outlet of downspouts from the roof gutters to collect roof runoff. A V-notch weir was constructed at the end of each box and thermistors were placed in the bottom of the boxes. Wind speed (R.M. Young model 03001 anemometer) and precipitation (Texas Electronics model 525 tipping-bucket) were also recorded at the site at 1-minute intervals, and logged along with the temperature data using a Campbell Scientific CR10 data logger.

At the commercial site, thermistors (Campbell Scientific model 107) were placed in the gravel layer of the roof at six locations and roof temperatures were recorded at 1-minute intervals (Campbell Scientific CR10). A well-exposed weather station located at ground level about 200 m from the roof site recorded solar radiation (Li-Cor 200S pyranometer), air temperature and relative humidity (Campbell Scientific CS500 probe), wind speed (R.M. Young model 03001 anemometer), and precipitation (Texas Electronics model 525 tipping-bucket) at 10-minute intervals.

The ages of the various surfaces were similar, and not expected to impact the measurements. Both the driveway and the asphalt-shingled rooftop were roughly 10 years old, and the rooftop at the commercial site was re-surfaced three years prior to the study. While aging could alter surface properties, such as causing an increase in the albedo of asphalt shingles as they lighten with weathering, such changes should have less of an impact on surface temperature during wet-weather than during dry weather, when solar radiation is many times larger.

For surface temperature measurements, it was assumed that the placement on each surface was representative of the whole surface. Surface temperature gradients could exist along the runoff flow path, leading to some error in using a single measurement. However, previous simulations by Janke et al. (2009) showed that the gradients, even on a very long (100 m) paved surface, were almost negligible. On the commercial rooftop, the thermistors were placed at various distances from the roof drain, and the temperature measurements were very consistent (standard deviation of roughly 1.0 °C). For the residential rooftop, the low thermal storage capacity and short residence times likely rendered any stream-wise temperature gradients negligible. The single measurement

locations are therefore expected to represent the temperature of the entire surface.

The installation of the residential rooftop thermistors underneath the top shingle meant that the temperature measurements might not be an exact representation of the shingle surface temperature, although the difference should be small. Heat penetration depth δ in a semi-infinite solid with thermal diffusivity α over a time step Δt is given by $\delta = (4\alpha\Delta t)^{1/2}$ (Eckert and Drake Jr., 1972). Assuming a 1/8-inch thick asphalt shingle with thermal diffusivity of approximately $5\text{x}10^{-8}$ m^2/s (McQuiston et al., 2000), the time required for the bottom of the shingle to reach the temperature of the top is roughly 50 s, which is less than the measurement interval for the study (1 min). Therefore the actual surface temperature should be roughly equal to the measured temperature.

1.3.2 Sample Temperature Records

The general trends of surface temperatures for both dry and wet conditions can be seen in Figure 1.2, which shows temperature measurements at the commercial and residential sites for a 3-day period (June 20 22, 2005); a rainfall event occurred on June 20. High-resolution surface temperature measurements during the June 20 rainfall (Figure 1.3) show the temperature dynamics of the two roof types and the concrete driveway for wet weather. Figure 1.3a shows temperatures measured at the residential site, including the north roof, south roof, east downspout, and driveway. Air temperatures from the SAFL weather station and precipitation from the residential site are also shown. The rainfall was relatively intense: 2.4 cm of rain fell in roughly 40 minutes beginning at 1:45 PM. Hot and sunny conditions were present prior to the onset of the storm.

Figure 1.3b shows surface temperatures at the commercial roof site for the same rainfall event in which 2.6 cm of rain fell at the commercial site. Six individual roof temperature measurements were averaged into one composite roof temperature, as the standard deviation for the entire record was less than 1°C. South roof and driveway temperatures from the residential site are shown for comparison, as well as solar radiation, air temperature, and precipitation as measured by the SAFL weather station. Solar radiation and air temperature were not measured at the residential site; it was assumed that these two parameters are identical in terms of timing and values at the two sites. For wet weather this assumption will sometimes fall short of reality due to the spatial variability of precipitation and air temperature patterns during rainfall events.

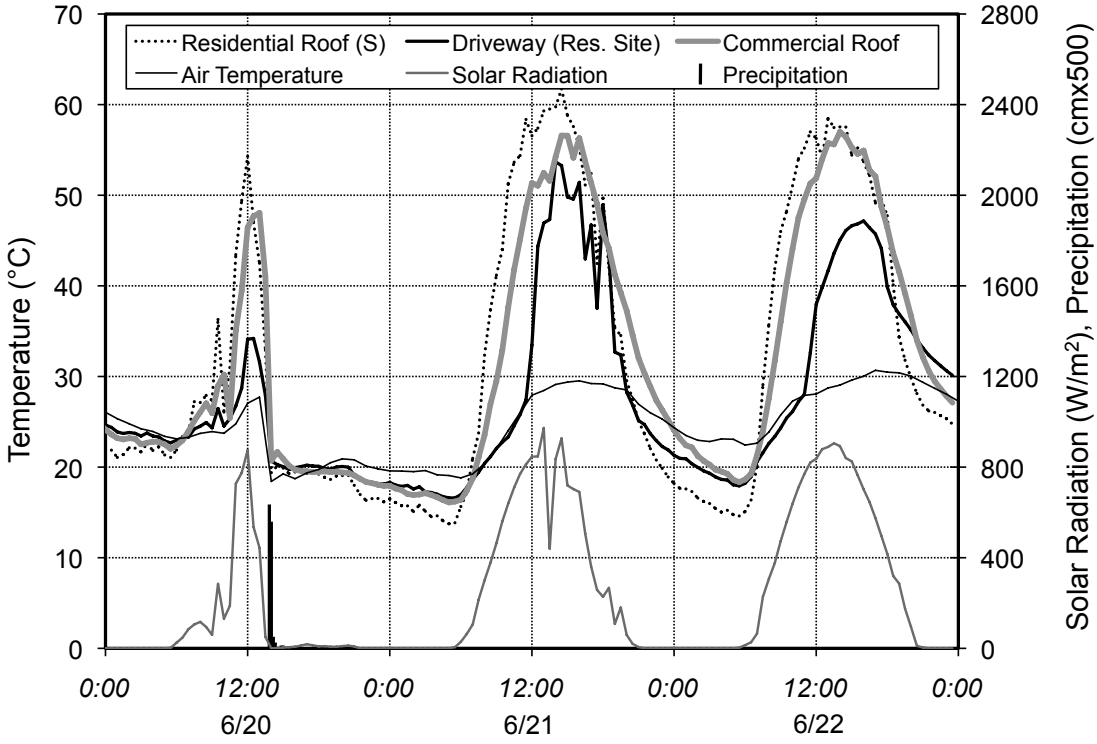

Figure 1.2: Surface temperatures measured at both sites, June 20 - 22, 2005. Air temperature, solar radiation, and precipitation were measured at the commercial site. 2.6 cm of rain fell during the afternoon of June 20. Dry, sunny conditions prevailed on June 21 and 22.

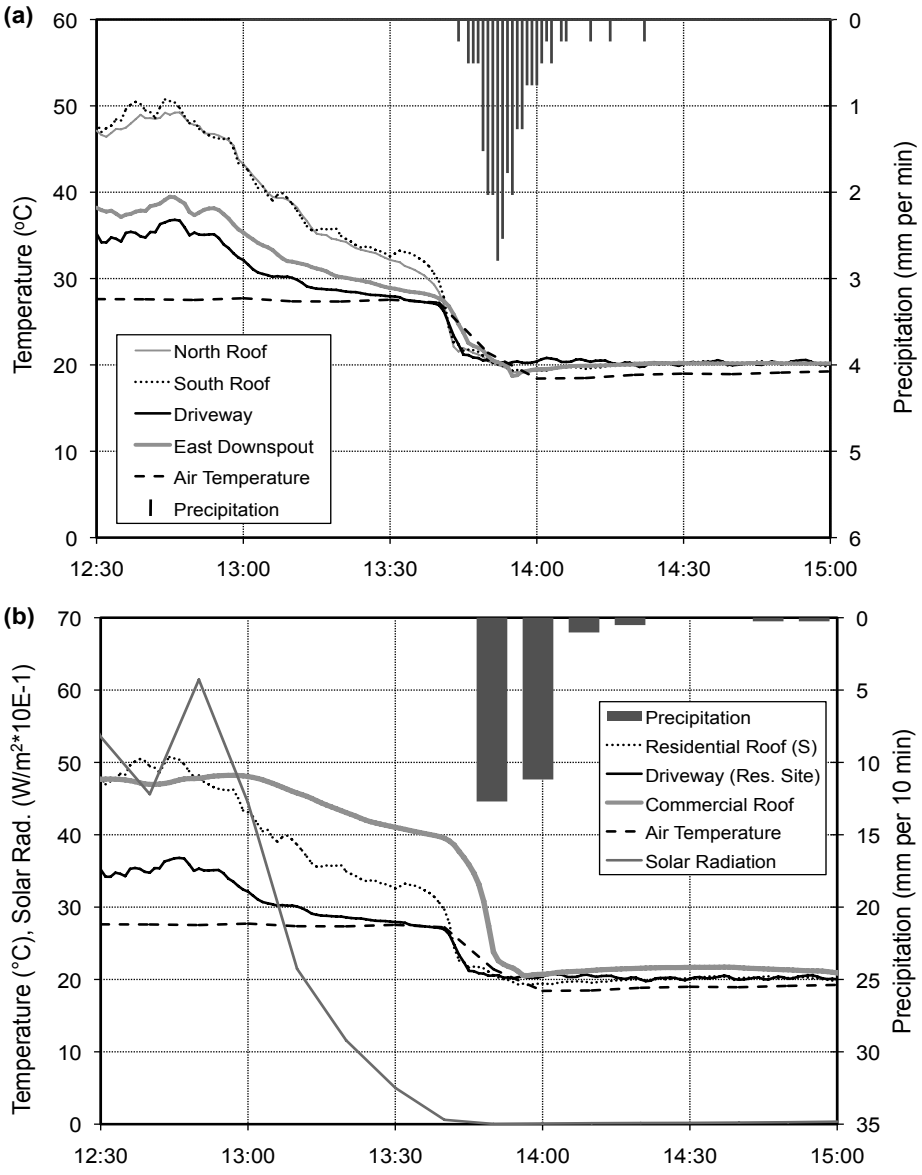

Figure 1.3: Surface temperatures measured at two sites during a rainfall event on June 20, 2005: (a) surface temperatures at the residential site, and (b) surface temperatures at the commercial site, with south roof and driveway temperatures from the residential site given for comparison. Air temperature was measured at the commercial site only. Total rainfall depth was 2.4 cm at the residential site (measured in 1-min intervals) and 2.6 cm at the commercial site (measured in 10-min intervals).

Surface temperature measurements for both sites are shown in Figure 1.4 for a second event that occurred on the morning of Aug 26. This was the largest event in the record, with 4.5 cm of rain measured at both sites over a period of roughly 3 hours beginning at 5:30 am. This event, while occurring at a time when antecedent temperatures should be low, still had a high heat export potential due to the large volume of runoff and relatively high mean dew point temperature (19.4 °C).

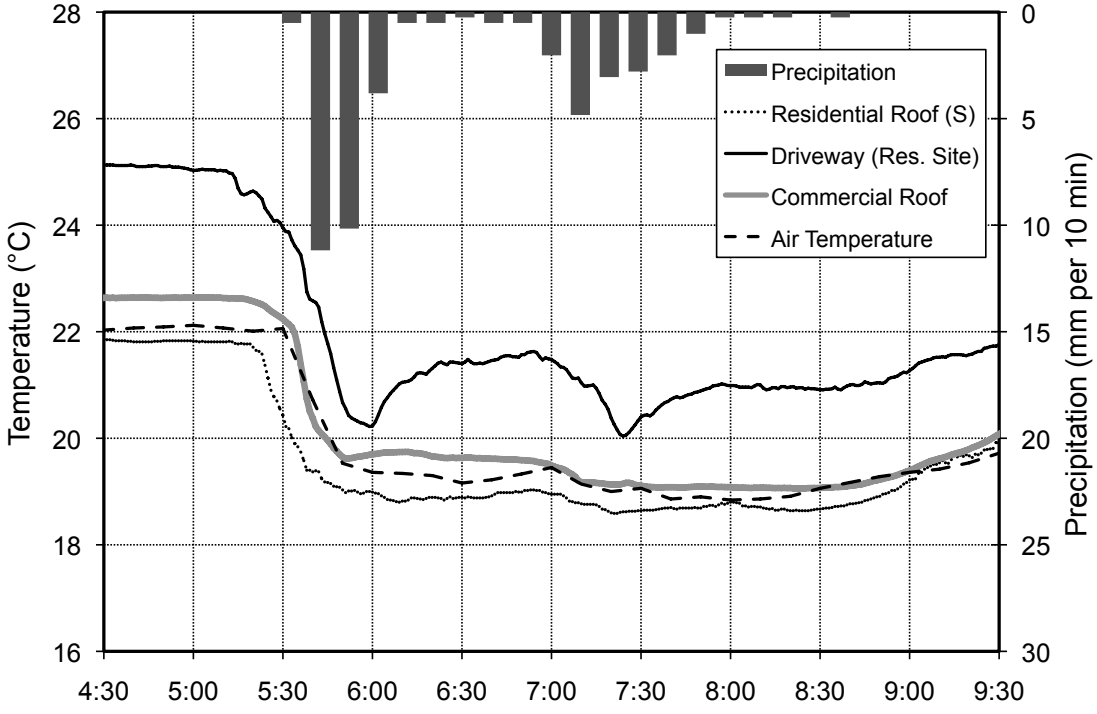

Figure 1.4: Surface temperatures measured at both study sites for a 4.5 cm rainfall event on the morning of Aug 26, 2005. Air temperature and precipitation were measured at the commercial site. Solar radiation is not shown because the rainfall occurred before sunrise.

1.3.3 Interpretation of Sample Records

Under dry-weather and sunny conditions (Figure 1.2), the residential rooftop experiences the highest peak temperatures and the largest diurnal amplitudes: the south

rooftop often exceeds 60 °C in mid-day and drops to below 20 °C at night. The temperature peaks on the residential rooftop are synchronized with the maximum daily solar irradiation, while the peak temperatures of the driveway, the grass, and the commercial rooftop lag behind the peak solar radiation and occur closer to the peaks in air temperature. This behavior is related to the heat storage capacity below each surface; it is smallest for the residential roof and larger for the driveway and commercial roof, which have greater mass. The grass surface experienced the lowest peak temperatures and smallest diurnal amplitudes, and was very similar to air temperature except during the middle of the day when solar radiation was greatest.

At night, when back-radiation from the surface to the atmosphere is the dominant heat flux under dry-weather conditions, the effect of thermal storage is even more pronounced: the residential rooftop rapidly radiates away heat stored during the day and becomes much cooler than air temperature, while the driveway slowly releases stored heat and decreases to a much higher minimum temperature than either the residential or commercial rooftop, at a later point in time, and always in excess of the air temperature. The commercial rooftop reaches minimum temperature slightly later than the residential rooftop and does not become quite as cool, although it drops below air temperature.

Major temperature decreases on all surfaces are observed just prior to the onset of rainfall (Figure 1.3). The drop in temperature begins when clouds move into the area prior to rainfall; this coincides with the recorded decrease in solar radiation roughly one hour prior to the first detected rainfall for the June 20 event. The residential roof, which at 50 °C was the hottest surface prior to rainfall, experienced the greatest cooling, reaching 33 °C just before the onset of rainfall. The commercial rooftop, which was nearly as warm ($\sim$ 48 °C), did not cool off as quickly as the residential rooftop, and the driveway experienced the smallest temperature drop in the hour prior to rainfall, though initially it was not nearly as hot as the other two surfaces. Little difference existed between the north and south roof temperatures at the residential site. A comprehensive analysis of surface temperatures before, during, and after rainfall events is presented in the next section.

The plots in Figures 1.3 and 1.4 show that temperatures generally become very similar for all surfaces after the onset of rainfall, with the exception of the driveway during

the Aug 26 event, which largely maintained its elevated temperature. The temperatures measured on the commercial roof and on the north roof, south roof, driveway, and downspout at the residential site all decrease rapidly in the first 5-10 minutes of both rainfall events. These temperatures eventually level out at around 20 °C in the June 20 event and 19 °C in the Aug 26 event, which in both cases is just slightly higher than the measured air temperature for the event. In this and most rainfall events, relative humidity is near 100%, meaning air temperature is equal to dew point temperature; this is significant because dew point temperature is often used to approximate rainfall temperature. In the context of thermal pollution by surface runoff, it provides evidence that the surface temperatures are near rainfall temperature well before the end of the rainfall event.

The driveway temperature during the Aug 26 event is worth noting, as it illustrates the tremendous capacity for heat storage and release of paved surfaces. Even after the first pulse of rainfall (which involved nearly 3 cm of rain), the surface temperature rebounded almost 2 °C before the second half of the storm, while the other surfaces remained mostly constant. This behavior is especially surprising given the early morning timing of the event, which meant that the heat had been stored in the pavement since the previous day. The temperature increases in all surfaces at the end of the storm is caused by a rapid increase in solar radiation beginning at 8:30 am (not shown).

1.4 Data Analysis: Dynamics of Roof and Pavement Temperatures

1.4.1 Objectives

The first objective of the data analysis was to quantify the temperature dynamics of the two roofs compared to the pavement, and by inference rank the heat release (export) from all three surfaces for multiple rainfall events. A second objective was to relate the roof and pavement temperature records to the weather record, e.g. investigating the difference between dew point (rainfall) temperature and surface temperature for wet weather.

For the data analysis, a rainfall event was defined as all rainfall occurring with a gap

of an hour or less between subsequent measurements of rainfall. It is possible to have multiple events in a single day, or for a single event to begin on one day and end on the next. Some days, particularly in the fall, have sporadic, light rainfall; these rainfalls are included only in the overall analysis. Any other rainfall event is considered "significant." There were 17 "significant" rainfall events in the record from June through September 2005 at the residential site, and 15 at the commercial site. This discrepancy in the number of significant events is due to the 4-mile (6.4 km) distance between the two sites and the often spatially variable nature of rainfall.

Additionally, a separate analysis was conducted for daytime rainfall events, which were defined as all events for which non-zero solar radiation was observed one hour prior to the onset of rainfall. The motivation for analyzing daytime events separately was to investigate presumed worst-case scenarios: rainfall events occurring when rooftop and driveway surfaces have had sufficient time to heat up over the course of the day. Intermittent events are included in overall statistics but not in the "daytime" statistics.

1.4.2 Data Extraction

The first step in the analysis was to assemble specific data. For each of the rainfall events the following was extracted from the weather record: (1) onset, end, and duration of rainfall; (2) solar radiation one hour prior to rainfall and at the onset, the end, and during rainfall (mean); and (3) dew point temperature one hour prior to rainfall and at the onset, the end, and during rainfall (mean). Except for precipitation, which was measured at both sites, weather parameters were taken from data recorded by the weather station at the commercial site.

From the surface temperature records we extracted (1) rooftop and pavement temperature one hour prior to rainfall, (2) rooftop and pavement temperature at the onset, the end and during rainfall (mean), (3) rooftop and pavement temperature change within the hour before rainfall, and (4) rooftop and pavement temperature change during a rainfall event. Water temperature data from the boxes below the downspouts were not included in the analysis because they were inconsistent. Sometimes water was standing in the box from previous rainfall, while at other times the box was dry before the onset of rain (as was likely the case for the June 20 event shown in Figure 1.3a). The north and south residential roof temperatures were averaged into a single characteristic roof

temperature, as they were nearly identical for wet weather.

The changes in rooftop temperatures before and during the rainfall are important characteristics of the event, as is the difference between the rainfall temperature and the roof temperature. These differentials are related to the amount of heat that has been extracted by the rainfall runoff.

Because rainfall temperature is generally not measured at weather stations, we assumed that the rainfall temperature would be equal to the dew point temperature, although that is not always case, e.g. during hailstorms or other events when raindrops do not have the time to fully respond to ambient air conditions while they fall. It is fair to expect that rainfall can be colder than dew point temperature, but rarely warmer. Thompson et al. (2008) found that rainfall temperature was well-approximated by wet-bulb temperature; during rainfall events relative humidity is usually close to 100%, so dew point temperature and wet bulb temperature are roughly equal. Since dew point temperature data was available in this study, it was used in place of wet bulb temperature to approximate rainfall temperature.

1.4.3 Results

The total precipitation measured at SAFL from June 1 to September 30, 2005 was 41.9 cm (16.5 inches). Comparison to long-term averages recorded at the Minneapolis-St. Paul Airport (14.2 inches for 1891 to 2008, and 15.7 inches for 1975 to 2008) indicates that the 2005 data were collected in a slightly wetter than normal year. Events prior to June 18, 2005 were not included in the analysis because thermistors were not installed until this date at the commercial site.

Temperature observations for all surfaces are summarized in Figure 1.5a for daytime rainfall events only, and in Figure 1.5b for all rainfall events. Mean and one standard deviation above and below the mean of wet-weather temperatures are shown for the grass surface, driveway, residential roof, and commercial roof. Dew point is shown as a reference for rainfall temperature.

Roof and Pavement Temperatures Prior to Rainfall

For all rainfall events (Figure 1.5b), the mean temperatures of the driveway and both rooftops are very similar one hour prior to the onset of the rainfall (within 1 °C), while

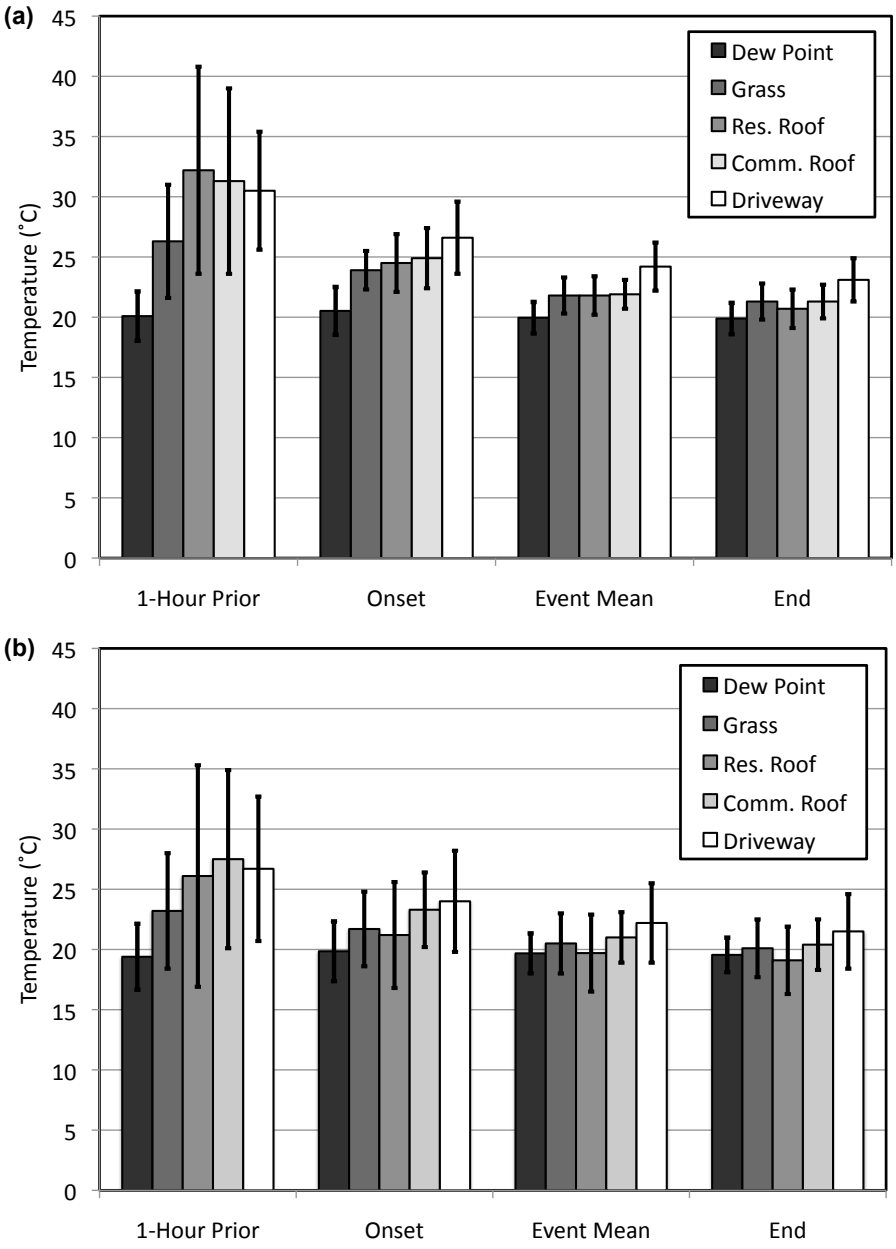

Figure 1.5: Summary of wet-weather surface temperature observations at both the residential and commercial sites during June - Sep 2005 for (a) daytime events only, and for (b) all significant rainfall events. Mean and one standard deviation above and below the mean are shown. Dew point (rainfall) temperature was measured at SAFL.

the lawn surface, as expected, is cooler (by about 4 °C). For daytime rainfall events (Figure 1.5a) the residential roof is slightly warmer than the other impervious surfaces one hour before the rainfall begins: on average 1.7 °C warmer than the driveway and roughly 1°C warmer than the commercial roof. However, this is a far smaller difference in temperature than can be present on a typical sunny mid-summer day. For example, during the dry, sunny period of July 9 - 15, the mean difference between the residential roof and driveway was approximately 8°C during daytime hours (8:00 - 16:00), with instantaneous differences as high as 22 °C.

Changes in surface temperatures both before the rainfall and over the duration of the rainfall are shown in Table 1.1. Roof and driveway temperatures decrease rapidly before many rainfall events due to increased cloud cover that significantly reduces solar radiation. The average drop in residential roof temperature during the hour prior to the onset of daytime rainfall events was 7.7 °C, compared to 6.4 °C for the commercial rooftop and 3.9 °C for the driveway. Temperature changes were slightly less overall when considering all rainfall events in the record. That temperature drops were larger for the rooftop surfaces than for the driveway and lawn is caused by the greater heat storage capacity below the driveway and the lawn; both store more heat and release it more slowly than either of the rooftops.

Roof and Pavement Temperatures During Rainfall Events

For daytime rainfall events only, the mean surface temperatures during the rainfall event are nearly identical for the two rooftops and the grass, while the driveway is roughly 2.3 °C warmer despite being at a lower temperature at the beginning of the rainfall event (Figure 1.5a). When all rainfall events are analyzed together, the mean event temperatures for all surfaces are very similar: the driveway temperature is slightly warmer, and the residential rooftop slightly cooler than the others (Figure 1.5b).

Standard deviations of surface temperatures during rainfall events are similar for the various surfaces and much lower than the standard deviations in the hour prior to rainfall. This is an indication of the considerable variation in antecedent conditions for summer rainfall events, and suggests that surface heat exchange is more dynamic as a storm moves in than during the time when rain is falling.

The change in surface temperature over the course of a rainfall event might be

Period	Parameter	Mean Change	
		All Events	Daytime
During hour before onset	Dew Point (°C)	+0.5	+0.4
	Res. Roof (°C)	-4.9	-7.7
	Comm. Roof (°C)	-4.2	-6.4
	Driveway (°C)	-2.7	-3.9
	Grass (°C)	-1.5	-2.4
Over duration of event	Dew Point (°C)	-0.3	-0.6
	Res. Roof (°C)	-2.1	-3.8
	Comm. Roof (°C)	-2.9	-3.6
	Driveway (°C)	-2.5	-3.5
	Grass (°C)	-1.6	-2.6

Table 1.1: Mean changes in dew point and observed surface temperatures at both roof sites in the hour prior to onset of rainfall and over the duration of rainfall events during June - September, 2005.

expected to provide an illustration of the relative amount of heat storage below the various surfaces. However, the drop in temperature of the impervious surfaces over the duration of daytime rainfall events was essentially the same: 3.8 °C, 3.6 °C, and 3.5 °C for the residential roof, commercial roof, and driveway, respectively (Table 1.1). Given the difference in heat storage capacity below the three surfaces, this implies that a different amount of heat is being extracted from each surface, and that perhaps atmospheric heat transfer or runoff velocity (residence time) is playing a role in the temperature changes experienced by the surfaces.

Difference Between Surface Temperatures and Dew Point (Rainfall) Temperatures During Rainfall Events

The difference between dew point (rainfall) temperature and surface temperature drives the heat flux from storage below the surface into the runoff above the surface; if this number is zero, no heating of the runoff occurs. Similarly, this quantity can be a measure of potential thermal impact if it is calculated with temperatures at the onset of rainfall. The higher the difference between surface temperature and rainfall temperature, the

greater the initial heat extraction rate will be. It is important to bear in mind that the event mean of this parameter will be more useful for estimating total or prolonged heat impact, and that actual heat extraction rates are dependent upon the thermal properties of the surfaces. Differences between surface temperatures and dew point temperatures are summarized in Figure 1.6. Note that all dew point temperatures were measured at SAFL, roughly 4 miles (6.4 km) from the residential site. This distance contributes some uncertainty to the quantities calculated for the surfaces at the residential site (grass, driveway, residential roof).

In general, the results support the expectation that the surface with the least heat storage capacity (residential rooftop) exhibits the smallest temperature difference relative to dew point (rainfall) temperature, while the surface with the greatest heat storage capacity (driveway) maintained a significant temperature difference with dew point temperature. Not surprisingly, the standard deviations of the surface temperature dew point temperature difference were higher in the hour prior to rainfall and at the onset of rainfall than during the event for all surfaces. During rainfall the standard deviation was similar for all surfaces, demonstrating the relative steadiness of heat transfer processes during rainfall when compared to the period leading up to the onset of precipitation.

When daytime rainfall events were analyzed separately (Figure 1.6a), the mean event differences between surface temperature and dew point temperature were similar for the two rooftops and the grass surface (between 1.6 and 2.0 °C), but very different for the driveway (4.0 °C). When all rainfall events were analyzed together (Figure 1.6b) the difference was much higher for the driveway than the other surfaces, with a value of less than 1.0 °C for the residential rooftop. This suggests that the actual heat contribution from rooftops, residential rooftops in particular, may be very small, especially relative to that from concrete driveways.

For potential thermal impact, defined as the difference between surface and dew point temperatures an hour before rainfall, the highest values occur for the two rooftops for daytime events. However, this result is deceiving because by the time the rainfall starts the rooftops have already cooled enough that the driveway surface is once again the warmest surface relative to dew point temperature (6.1 °C versus 4.4 °C and 4.0 °C for the commercial and residential rooftops, respectively). This again illustrates the greater capacity of the driveway for heat storage/release relative to the two rooftops.

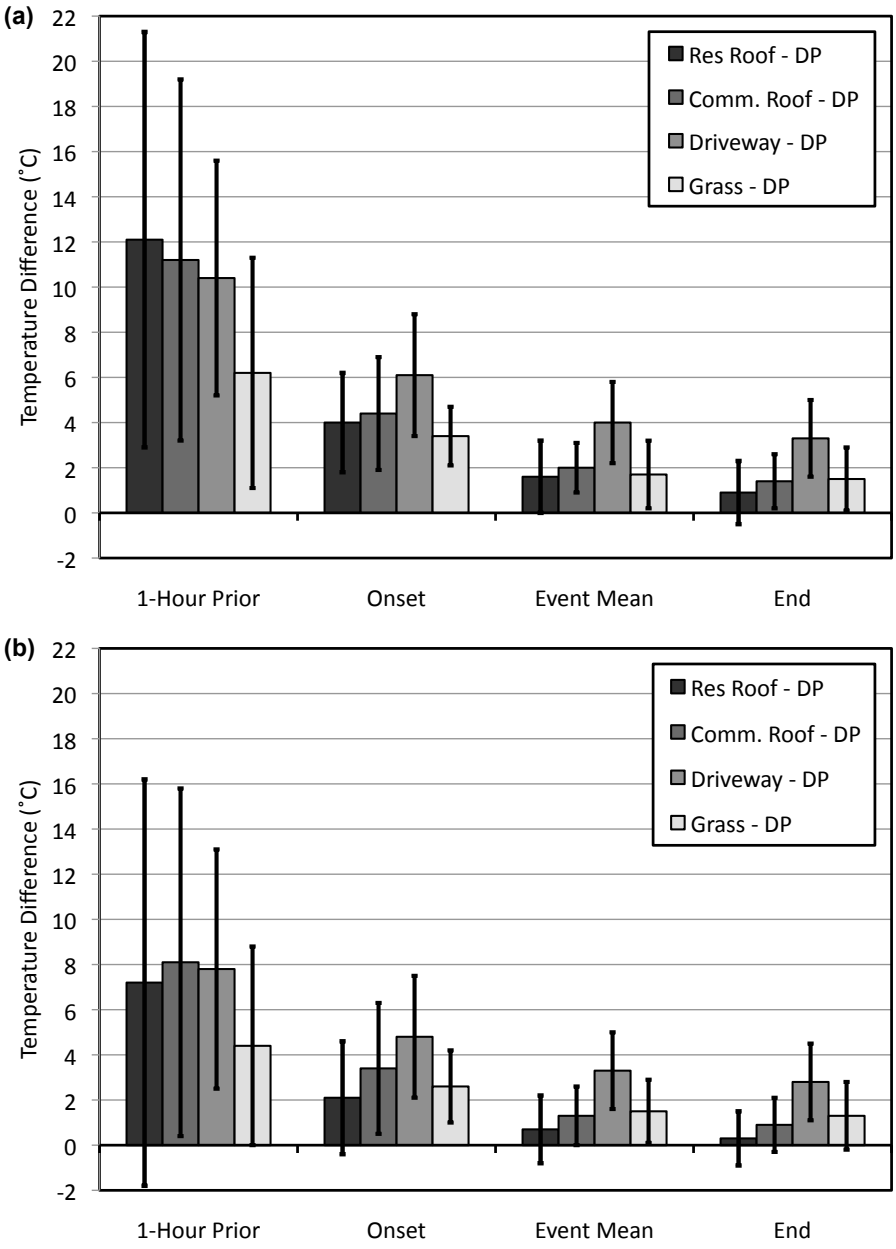

Figure 1.6: Mean difference between surface temperature and dew point (rainfall) temperature for (a) daytime rainfall events only, and for (b) all rainfall events, during the period June - September, 2005. One standard deviation above and below the mean is also shown. Dew point temperature (DP) was measured at SAFL.

Solar Radiation

Solar radiation is a major heat source in determining runoff temperature. Mean observed solar radiation one hour prior to the daytime rainfall events at the commercial site was 157 W/m^2, with a standard deviation of 187 W/m^2 and a maximum value of 615 W/m^2 (not shown). This confirms that antecedent conditions prior to rainfall events are highly variable. However, by the onset of rainfall solar radiation was considerably smaller (mean = 26 W/m^2) and less variable (standard deviation = 39 W/m^2), and over the duration of daytime rainfall events the mean solar radiation remained low at 28 W/m^2. This is a small but potentially significant contribution of heat, and mean event values as high as 107 W/m^2 were observed during daytime rainfall events. By comparison, an event mean solar radiation of 150 W/m^2 was observed by Thompson et al. (2008) for rainfall events in Madison, Wisconsin. Regardless of these differences, it appears that the assumption of zero solar radiation during rainfall events would be erroneous.

Worst-case Scenarios (Extreme Events) for Heating of Runoff by Rooftops

A worst-case scenario of runoff heating by a rooftop would be an event that results in a high temperature of rainfall runoff; this would be expected for events involving high dew point (rainfall) temperature and/or high surface temperature. In our data set, the timing of these worst-case events was, however, contrary to expectations: they did not occur during late afternoon, when antecedent solar radiation and consequently rooftop surface temperatures are at their highest, but often during night and early morning hours.

The four events with the highest mean event temperatures (by surface) are shown in Table 1.2. Overall, more than half of the events occurred during times of the day with presumably low risk for high heat export (i.e. when solar radiation was absent and surface temperatures should have been low): just after midnight on Aug 4, in the early morning hours on June 27, and after sunset on Aug 16 and Sept 12. Only the remainder occurred at the expected time of the day (afternoon) on several dates. However, surface temperatures alone do not control the heat transfer to the runoff, as a relatively high dew point (rainfall) temperature by itself can lead to a high heat content

Parameter	**Temperature (°C)**	**Day**	**Time**
Dew	23.2	Aug 4	0:30
Point	21.6	Sep 12	14:30
Temperature	21.5	June 27	6:40
	21.3	Sep 12	21:20
Residential	24.8	June 27	6:38
Roof	23.1	Aug 4	0:39
Temperature	22.9	Aug 11	12:37
	22.7	July 25	16:44
Commercial	24.7	Aug 4	0:30
Roof	23.8	Sep 12	14:30
Temperature	23.3	June 27	6:40
	22.6	Aug 16	21:50
Driveway	26.7	Aug 4	0:39
Surface	26.7	July 25	16:44
Temperature	26.5	June 27	6:38
	25.3	Aug 11	12:37

Table 1.2: The four highest dew point temperatures and mean event surface temperatures for the residential rooftop, commercial rooftop, and driveway among all rainfall events from June - September, 2005.

of the runoff. Given that solar radiation and other atmospheric heat fluxes are much reduced during rainfall events, dew point temperature and rainfall volume become the primary influences on total event heat export (Janke et al., 2006, 2009). In terms of the event parameters investigated in this study, these late night and early morning storms represent the worst-case scenarios in this particular data set, a result contrary to initial expectations.

These results suggest that because of the lag associated with heat storage and release, the rainfall events with the greatest potential for heat export do not always occur during daylight hours; rainfall events occurring after sunset and during early morning can be worse than mid-afternoon events. This is especially true of surfaces with greater heat storage capacity, such as the driveway and commercial rooftop. The timing of dew point (rainfall) temperature also plays a role in determining the worst-case scenarios.

1.5 Modeling: Roof Temperatures and Heat Storage/Release

1.5.1 Heat Release (Export) From a Rooftop

A comparison of heat export from rooftops and pavements can validate the assumption that rooftops make a negligible contribution of heat to rainfall runoff because of their low thermal storage capability. Heat export is defined here as an amount of heat (Joules) extracted from a rooftop by runoff water from a rainfall event. Since runoff was not measured at the field study sites, heat export could not be calculated from runoff flow rate and runoff temperature data as in previous work (Janke et al., 2009; Herb et al., 2009b). Instead, heat export was estimated by numerical simulation of temperature profiles in the roof materials. The total amount of heat extracted from a roof by a rainfall-runoff event can be estimated by comparing the roof temperature profiles at the beginning and at the end of the rainfall. The amount of heat extracted from the roof (HE) is calculated layer by layer, and the sum is the total heat export ($\mathrm{J/m^2}$):

$$HE = \sum_{i=1}^{n} \rho_i C_{p,i} \Delta z_i \Big(T_{0,i} - T_{f,i} \Big) \tag{1.1}$$

where i is the roof layer number, $\rho C_{p,i}$ is the heat capacity of the layer (J/(m^3 °C)), Δz_i is the thickness of the layer (m), $T_{0,i}$ is the initial temperature of the layer (°C), and $T_{f,i}$ is the final temperature of the layer (°C). Calculation of heat export requires knowledge of the structure of the rooftop, pavement, or asphalt, as well as of the thermal properties of the various layers, which were taken from a number of sources (Chadderton, 1997; McQuiston et al., 2000; Incropera and DeWitt, 2002; ASHRAE, 2005). This particular method of determining heat export was chosen in order to eliminate the need for simulating runoff flow rates and to allow the measured surface temperatures to be incorporated into the calculation. The method is described here in greater detail.

1.5.2 Simulation of Roof Temperature Profiles

Heat transfer within the rooftop is by conduction, and the temperature profile within the rooftop can be found by numerically solving an unsteady 1-D heat diffusion equation.

$$\frac{\partial T}{\partial t} = \frac{\partial}{\partial z}\left(\alpha_p \frac{\partial T}{\partial z}\right) \tag{1.2}$$

where α_p is the thermal diffusivity of the roof material and z is the spatial coordinate perpendicular to the roof surface. The numerical solution of the 1-D equation is identical to the solution for a pavement surface used in Janke et al. (2006). The upper boundary condition for the roof surface was specified by the measured rooftop temperature time series. Equations for atmospheric heat exchange at the roof surface were therefore unnecessary.

The lower boundary condition for the commercial rooftop and the pavement was a specified temperature. Since the underside of a commercial rooftop is typically located in a climate-controlled space, a fixed temperature of 25 °C was used for this roof type. For the concrete pavement, a constant temperature at a depth of 0.6 m was used since at the model time scale (less than one day) the soil temperature at this depth is unchanging. The values used (20.8 °C for June, 27.3 °C for July) were determined from data collected at the Minnesota Department of Transportation's MNRoad pavement research site in Albertville, MN.

Specifying a temperature at the bottom boundary for the residential rooftop is more

difficult, given that the attic space is not climate-controlled. While outdoor air temperature might be a good estimate of attic temperature during cloudy days or in a well-ventilated attic, data collected by the Forest Products Laboratory (Winandy and Beaumont, 1995; Winandy et al., 2000) show that attic temperature can be considerably higher than outdoor air temperature on sunny days, even with moderate solar radiation. The bottom boundary temperature used for the residential rooftop was a temperature 7 °C higher than outdoor air temperature, estimated from these data.

Other options considered for the lower boundary condition were (1) adiabatic and (2) convective heat fluxes. Given the relatively low heat capacity of the residential rooftop, heat exchange with the attic space should be relatively significant over the time-scale of a rainfall event, and thus an adiabatic condition is not accurate. Use of this boundary condition provided the highest estimates of heat export due to the lower final temperatures simulated within the roof materials. The convective heat flux boundary condition investigated used the formulation employed by TenWolde (1997) in a model of roof temperature and moisture. This formulation was based on empirical relationships for an inclined heated plate in a quiescent air volume (i.e. natural convection only).

In general, heat exchange between the attic and rooftop was significant. For a rainfall event on July 25, 2005, the total heat input to the rooftop from the attic was estimated at 64 kJ/m^2 with the convective boundary condition. Using the temperature boundary condition (air temperature plus 7 °C), the heat input to the rooftop was 188 kJ/m^2. This additional heat input causes the final temperatures within the rooftop materials to be higher than when using the other boundary conditions (adiabatic and constant temperature), leading to a lower total heat export for the event. Thus the adiabatic boundary condition provides the highest estimate of heat export, and the temperature boundary condition the smallest. The temperature boundary condition was chosen to avoid over-estimation of the contribution of the roof to heating of runoff (see Section 1.5.6), and also because the choice of boundary condition had less impact on the magnitude of calculated heat export for two other events (June 20 and July 23; not shown).

1.5.3 Maximum Heat Export from Roof

Maximum (or potential) heat export is the maximum amount of heat that can be extracted from a surface by a rainfall-runoff event for given initial conditions. This parameter is useful for investigating the relative potential thermal impact of the various surface types, and for quantifying heat storage.

The method of determining maximum heat export is based on the expectation that the rate of heat extraction is greatest at the beginning of the rainfall and decreases as the difference between rooftop and rainfall temperature decreases, becoming negligible when all available heat has been extracted. Temperature profiles in the roof or pavement at intermediate times during the rainfall event can be used to compute a time series of instantaneous heat export rates by using Eq. 1.1 and dividing by the intermediate time interval. A curve fit to these heat export rates can be used to find additional heat extraction beyond the end of the event to any point in time; integration of the calculated and extrapolated heat fluxes gives the maximum event heat export. To provide a conservative analysis, the heat export over the duration of the rainfall event plus four additional hours was calculated. This is equivalent to assuming that the rainfall event continues for four hours beyond the end of the actual event without any major change in rainfall rate – an unrealistic but not overly-conservative approach.

As an example, consider the commercial rooftop and a rainfall event that occurred on July 23, 2005 from 10:40 to 12:40 (Table 1.3). An indoor air temperature of 25 °C is used as the lower boundary condition, and the upper boundary condition is specified as the time series of observed roof surface temperatures from July 21 – 24. The initial 2 days of temperature observations serve to prime the temperature profile within the rooftop. Applying Eq. 1.1 gives a total heat export of 357 kJ/m^2 for the rainfall event. The maximum heat export rates are calculated from intermediate temperature profiles in the roof and are plotted in Figure 1.7 along with an exponential curve fit ($R^2 = 0.96$). The plot shows, as expected, that considerably more heat is extracted from the rooftop at the beginning than at the end of the event. Extrapolating this curve beyond the end of the rainfall shows that an additional 16 kJ/m^2 (4% of the simulated heat export) would be extracted in the four hours after the rainfall. This results in a maximum heat export of 373 kJ/m^2, and suggests that at least in the case of this particular rooftop and rainfall event, most of the available heat has been extracted by the end of the rainfall.

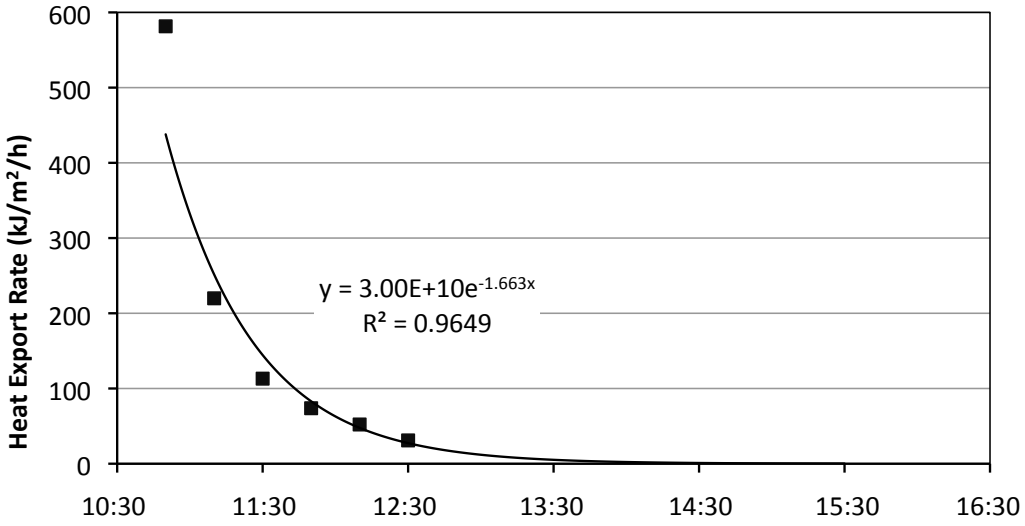

Figure 1.7: Exponential curve fit to a time series of instantaneous heat export rates (kJ/(m^{2}h)) determined from simulated roof temperature profiles and measured rainfall for the commercial rooftop. Rainfall occurred from 10:40 to 12:40 on July 23, 2005.

1.5.4 Selection of Rainfall Events for Analysis

Three rainfall events were selected for the application of the model; they occurred on June 20, July 23, and July 25, 2005. The three events were chosen because of the similarity in timing, depth, and duration between the two sites (Table 1.3), and for their potential for significant thermal impact: all three events were among the largest in the record that occurred during daylight hours with significant solar radiation 1 hour prior to the onset of rainfall. By these criteria, the three events can be considered worst-case scenarios in this data set. It is acknowledged that these might not correspond to the actual worst-case events in the record, as surface temperatures and dew point temperature (a major determinant of heat export) were not considered; thus only one of the events (July 25) appears among the highest-temperature events listed in Table 1.2. However, temperature alone may not be the best indicator of heat export, as the volume of rainfall will also have an impact on actual heat export and tends to depress surface temperatures. This issue was presented in more detail in Section 1.4.3.

	Residential Site			Commercial Site		
Date	**Rainfall Depth** (cm)	**Rainfall Duration** (h)	**Rainfall Start** (h:min)	**Rainfall Depth** (cm)	**Rainfall Duration** (h)	**Rainfall Start** (h:min)
6/20/05	2.4	1.5	13:44	2.6	1.2	13:50
7/23/05	2.2	0.9	10:41	1.9	2.0	10:40
7/25/05	2.9	3.0	16:44	3.5	3.0	16:50

Table 1.3: Depth, duration, and start time of the three rainfall events chosen for analysis of temperature profiles in the residential and commercial roofs.

1.5.5 Results: Heat Export from Residential and Commercial Rooftops and a Concrete Pavement

The above analysis was completed for a residential roof, a commercial roof, and a concrete pavement (driveway) for the three rainfall events in Table 1.3. Results are summarized in Table 1.4. In general, the heat export results support the conclusions of the roof temperature data analysis (Section 1.4). In particular, the residential rooftop contributes little heat to the rainfall runoff; in the case study, the heat export (per unit area) from the residential rooftop was, on average, less than 20% of the simulated heat export (or less than 14% of the maximum heat export) from the concrete driveway. The simulated heat export (per unit area) from the commercial rooftop was on average nearly 3 times that of the residential rooftop, and on average 59% of the simulated heat export (47% of the maximum heat export) from the concrete driveway.

It is important to note that the heat export values are calculated per unit surface area. While the residential and commercial rooftops have considerably lower heat export values than the concrete driveway, the proportion of these three surface types in a particular watershed will ultimately determine their relative influence on heat export from the watershed. However, the results both of this heat export analysis and of the temperature analysis appear to support the assumption that the heat export from the residential rooftops is negligible compared to that from other impervious surfaces for proportions that would be present in a typical residential watershed. The thermal

impact of these rooftops is further diminished by the presence of vegetated surfaces typical of residential areas and practices aimed at disconnecting rooftops from the drainage system. On the other hand, heating of runoff on commercial rooftops appears to be potentially significant, particularly in heavily-urbanized watersheds which contain a large proportion of this roof type relative to other surfaces.

Also noteworthy is that for both rooftops the simulated heat export was only slightly lower than the maximum (potential) heat export. The difference was on average 3% for the residential rooftop, 13% for the commercial roof, and 30% for the driveway. The nearly complete extraction of potential heat from the residential rooftop and the lower extraction rates for the commercial roof and the driveway are clearly related to the heat storage capacity below the surfaces, which is considerably smaller for the rooftops than for the driveway.

Rainfall duration also plays a role in heat export. Roof surfaces reach their maximum heat export, i.e. simulated heat export is approximately equal to maximum heat export, when rainfall events are of long duration, such as the ones that occurred on July 23 and July 25, 2005. The absolute value of maximum heat export for all surfaces is directly proportional to total rainfall depth.

1.5.6 Atmospheric Contribution to Heat Export

Not all heat extracted from the surface (estimated from Eq. 1.1) remains in the runoff water; some of the extracted heat will be quickly lost to the atmosphere, meaning that the actual heat content of the rainfall runoff will be less than that extracted from the roof. This atmospheric heat exchange is generally negative (i.e. has a cooling effect on the runoff water) due to the elevation of the runoff temperature above air temperature in the early stages of rainfall, leading to relatively large outgoing long wave radiative and convective heat fluxes, as well as evaporation at the onset of rainfall. The magnitude of this atmospheric contribution was estimated by separately calculating each atmospheric heat flux component (solar radiation, long wave radiation, sensible, and latent heat flux), and averaging the net heat flux over the duration of the event to find the total heat lost to the atmosphere. Calculations were made using the formulations employed in a previously developed runoff temperature model (Janke et al., 2009, Chapter 2), assuming surface properties of water and using the time-series of observed surface temperatures

Surface	**6/20/05**		**7/23/05**		**7/25/05**		**Average**	
	SimHE	MaxHE	SimHE	MaxHE	SimHE	MaxHE	SimHE	MaxHE
Heat Export in kJ/m^2								
Res. Roof	247	251	115	117	245	257	202	208
Comm. Roof	793	990	357	373	560	610	570	658
Conc. Driveway	876	1288	648	882	1885	2709	1136	1626
As Percent of Heat Export from Concrete Driveway								
Res. Roof	28%	19%	18%	13%	13%	9%	20%	14%
Comm. Roof	91%	77%	55%	42%	30%	23%	58%	47%

Table 1.4: Simulated heat export ("SimHE") and maximum (potential) heat export ("MaxHE") from the residential roof, the commercial roof, and the concrete pavement during three rainfall events (Table 1.3), in kJ per m^2 surface area and as a percentage of the heat export from a concrete pavement.

(in 10-minute averages) and available weather data.

The results of these calculations for the three rainfall events used in the heat export analysis (Table 1.3) were generally inconclusive. The estimated net atmospheric component was from 9% to 88% of the simulated heat export for the surfaces (33% on average for all surfaces combined), with no obvious trends related to surfaces or events. A possible explanation for the high variability in the estimated atmospheric heat flux is that the weather data used in the calculations were collected from the commercial site, causing some uncertainty in the results for the residential rooftop and driveway, which were located roughly 4 miles from the commercial site.

However, these results indicate that the impact of atmospheric heat exchange is significant, and therefore the simulated heat export values can be considered an overestimation of the thermal impact on runoff because not all of the heat extracted from the surfaces is retained by the runoff water. This also serves as a justification for using the less-conservative lower boundary condition (i.e. fixed temperature) for the simulated residential rooftop heat export.

1.6 Summary and Conclusions

In rainfall-runoff temperature modeling, the contribution of rooftops to runoff heating is often neglected or not mentioned in the literature. The assumption can be made that rooftops of all types contribute very little heat to rainfall runoff. We examined the accuracy of this assumption (a) by analyzing temperature data which collected on a residential rooftop, a commercial rooftop, and a concrete driveway, and (b) by simulating temperature profiles and surface heat transfer for these same three urban surfaces. Temperature data were collected at two urban sites in the Upper Midwest (a single family home and a commercial building in Minneapolis, Minnesota) from June through September, 2005.

The surface temperature data were analyzed for all rainfall events in the record. The results (Figure 1.5 and Table 1.1) indicate that the residential and the commercial rooftops store less heat than a concrete driveway. The surfaces cooled significantly in the hour prior to the rainfall events: the surface temperature drop for all surfaces was on average 5.1°C for daytime events (ranging from 2.4 °C for the lawn to 7.7 °C for

the residential roof). Rooftops had slightly higher temperatures (1 – 2 °C on average) than the concrete driveway one hour prior to the onset of rainfall, but had lower mean temperatures during the duration of daytime rainfall events (21.9 °C for the rooftops, versus 24.2 °C for the driveway). This suggests that on sunny days and prior to rainfall, rooftops can reach higher temperatures than paved surfaces, but rooftops do not store much heat and drop rapidly in temperature as cloud cover increases with an approaching storm. Antecedent weather conditions are more important for surfaces with large heat storage capacity (e.g. driveways or lawns) than for those with small storage capacity (e.g. rooftops).

The difference in dew point (rainfall) temperature and surface temperature over the duration of rainfall provides an estimate of how much heat is being extracted by the runoff (Figure 1.6). If this difference is small, little heat is exchanged. The mean roof temperature-dew point temperature difference was 1.8 °C when averaged over all daytime rainfall events, while the mean difference between driveway and dew point temperatures was 4.2 °C. At the end of rainfall events the residential roof had the smallest difference between surface temperature and dew point temperature (0.8 °C for daytime events); it tended towards rainfall temperature faster than the other surfaces. This behavior can be attributed to the low thermal storage capacity of the residential rooftop relative to the other surfaces.

It was expected that daytime rainfall events – in particular those occurring in late afternoon or early evening of hot, sunny days – would have the greatest potential for thermal impact. Instead, it was discovered that the rainfall events with the highest dew point and surface temperatures often occurred late at night or in the early morning (Table 1.2). The highest mean event dew point temperature (23.2 °C), commercial roof temperature (24.7 °C), and driveway temperature (26.7 °C) all occurred for an event beginning at 12:30 AM on Aug 4, 2005. An early morning storm on June 27 also appeared to be a worst-case event based on criteria of highest dew point and surface temperatures. This is contrary to the expectation that worst-case scenarios occur during daylight hours, but is logical, considering that atmospheric heat fluxes, including solar radiation, are significantly reduced during rainfall events, and that heat export by rainfall runoff is often driven primarily by antecedent surface temperatures and rainfall (dew point) temperature.

Simulated and maximum (potential) heat export amounts (J per m^2 surface area) were estimated for three selected daytime rainfall events using a 1-D roof temperature simulation model. The three rainfall events were chosen because they were among the largest daytime storms on the record, and not on the basis of maximum observed surface or dew point temperatures. An unsteady heat diffusion equation was solved using the observed surface temperature time series as an upper boundary condition and a specified temperature as a bottom boundary condition to estimate temperature profiles in the roof material during each rainfall event. Heat export was estimated from the temperature profiles at the beginning and end of the rainfall event (Eq. 1.1). Maximum heat export was estimated by fitting an exponential curve to a time series of calculated heat export rates and extrapolating beyond the end of the event (Figure 1.7).

The results of this heat export analysis for three rainfall events showed that the residential roof contributed, on average, less than 20% of the amount of heat release (per unit surface area) from a driveway surface under the same weather conditions, and that nearly all available heat was being extracted from the roof, i.e. simulated heat export maximum heat export (Table 1.4). Heat extracted from the commercial rooftop was roughly 50% of that from the concrete driveway on a per-unit-area basis. Potential heat export was significantly higher for the driveway than for either rooftop. It is important to note that since heat export is calculated per unit surface area, the actual contribution of heat from each surface will be related to the proportion of each surface type in a particular watershed.

In conclusion, the results of both the temperature data analysis and the heat export simulations support the assumption that heat release from residential rooftops during rainfall is likely negligible, particularly for large and/or long-duration rainfall events. However, the same assumption does not appear completely justified for commercial roofs, which can release a significant amount of heat during rainfall due to their greater thermal storage capacity. How significant this impact might be is not clear, as the estimated heat export for the commercial rooftop was from 30% to 90% of that estimated for a concrete driveway. The contribution could be smaller relative to an asphalt pavement, which may store and release more heat than a concrete driveway. Nevertheless, commercial rooftops should be considered in hydrothermal rainfall-runoff simulation models of urban areas, particularly where they comprise a large percentage

of the total surface area. This statement gains additional weight when considering that the drainage systems of commercial buildings are traditionally connected to storm sewer systems which discharge to streams and rivers. By contrast, residential rooftops and their downspouts often discharge onto lawn areas where infiltration can be significant, although local conditions such as topography, hydraulic conductivity, and antecedent moisture will ultimately determine infiltration rates. Furthermore, previous studies (Herb et al., 2007; Thompson et al., 2008) have determined that runoff from pervious surfaces is generally much cooler than from impervious surfaces, and is therefore less likely to have a thermal impact on receiving waters.

Chapter 2

Simulation of Heat Export by Rainfall-Runoff from a Paved Surface

Summary

The overall goal of our research has been to create a hydro-thermal model to quantify the impact on stream temperature of urban development in watersheds of cold-water streams. In this chapter we describe a significant component of that modeling effort, namely a sub-model for predicting storm water runoff rates and temperatures from paved surfaces during a rainfall event. An unsteady 1-D model has been formulated from basic principles of heat transfer and runoff processes on planar impervious surfaces for both dry- and wet-weather periods. The model predicts runoff flow rates and temperatures as a function of both distance and time on a paved surface, taking into account the magnitude of the radiative, convective, evaporative and conductive heat fluxes at the surface. It also predicts the total heat export for an event, which is defined as the heat contained in the runoff above a reference temperature. A case study is presented in which the model is applied to a parking lot, and simulated runoff flow, temperature, and heat export closely match observations of these quantities for an early-evening rainfall event in August. A sensitivity study was performed to investigate to which extent heat export is affected by antecedent pavement temperature, characteristics of the rainfall event, and

physical parameters of the paved surface. It was found that heat export is more sensitive to rainfall intensity, rainfall duration, and antecedent pavement temperature than the physical properties (slope, roughness, and length) of the paved surface. An increase in rainfall duration increases the total event heat export, especially for high-intensity events. Heat exchange with the atmosphere typically reduces runoff temperature and heat export versus a case in which atmospheric heat fluxes are neglected, with greater effect occurring as rainfall intensity decreases.

Originally published as:

> Janke BD, Herb WR, Mohseni O, Stefan HG. 2009. "Simulation of heat export by rainfall-runoff from a paved surface." *Journal of Hydrology.* 365: 192-212. DOI: 10.1016/j.jhydrol.2008.11.019.

2.1 Introduction

Temperature is a water quality parameter of great influence on the biological and chemical makeup of a stream. Water temperature can be the determining factor for the type of fish, invertebrates, and plants present in a water body, and influences their activity levels, growth rates, and ability to compete (Klein, 1979; Eaton et al., 1995; LeBlanc et al., 1997). Water temperature also affects geochemical reaction rates and the concentrations of oxygen, nutrients, and pollutants dissolved in the water (LeBlanc et al., 1997; James and Xie, 1999; Paul and Meyer, 2001). Cold-water streams are dependent on temperature to support fisheries and other wildlife that would be unable to survive in warmer streams.

Urbanization in the watersheds of cold-water streams threatens to degrade these valuable water resources. Since the temperature of these streams is typically maintained by significant amounts of groundwater recharge and riparian shading, the land cover conversion associated with urban development - replacement of cropland, prairie, and forests with buildings, roads, lawns, and parking lots - has a negative impact, as these land-use changes can dramatically impact heat transfer and hydrology in a watershed.

In general, urban development tends to increase the amount of impervious surface area and reduce the amount of natural shading provided by vegetation; as a result surface runoff rates and temperatures from rainfall events are amplified, watershed infiltration is reduced, and stream temperature increases (Pluhowski, 1970; Paul and Meyer, 2001).

In one particular series of studies (Galli, 1990), average stream temperature was found to increase by 0.09 °C for each one percent increase in overall imperviousness in the watershed. Other studies have shown similar trends (Pluhowski, 1970; Klein, 1979; LeBlanc et al., 1997). Paved and building surfaces can become hotter than natural surfaces due to lack of shading by vegetation, and on a short time scale can produce warmer runoff to receiving streams during and after rainfall events. Storm water detention ponds act as heat exchangers by prolonging exposure of surface water to direct solar radiation, and may have additional adverse effects yet are widely recommended for storm water quality improvement, e.g. sediment and phosphorus removal (Van Buren et al., 2000b; Galli, 1990). Furthermore, since cold-water streams are often fed by groundwater, a reduction of infiltration caused by increased imperviousness in the watershed means that less groundwater will be reaching the stream (Pluhowski, 1970; Klein, 1979; Paul and Meyer, 2001). This can become a significant long-term adverse effect of urbanization on stream temperature.

The overall focus of our research has been to create hydro-thermal modeling tools that can be used to determine if urban development in the watersheds of cold-water streams negatively impacts the fragile nature of these ecosystems. One of these models is the MINnesota Urban Heat Export Tool (MINUHET); while it is still a work in progress, a preliminary version of the model has already been applied to a small residential development with some success (Janke et al., 2007). The motivation for this work is the fact that few tools are currently available to project how stream temperatures are influenced by urban development in the watershed. Available models are either empirical (Nelson and Palmer, 2007) and thus are not transferable to a variety of watersheds, or do not explicitly include the effect of surface water runoff (e.g. LeBlanc et al., 1997; Krause et al., 2004).

One important component of MINUHET was the creation of a sub-model that can predict runoff rates and temperatures from a paved surface during a rainfall event. This paper will describe the development of such a model from basic principles. The model

will be used to address some fundamental questions, such as:

1. Which parameters exhibit the most influence on the heating of runoff?
2. How important are antecedent weather conditions in determining the amount of heat extracted from a paved surface by rainfall runoff?
3. What types of rainfall events have the greatest potential impact on the water temperature of streams that receive the runoff?
4. Are the spatial variations of water depth and temperature important, or can simplified models that average hydro-thermal parameters over a surface area be justified?

The output of this hydro-thermal runoff model, which can be applied to surfaces of different land use, provides the input to models of watershed-scale hydrology and heat transfer (such as MINUHET) and ultimately, of stream temperature. Ease of use is essential if the models are to be used for planning and permit decisions, and it should accept standard weather data as input. However, the model should capture all of the important thermal and hydrological processes at relevant time scales.

A number of models are currently available for the prediction of runoff temperature from paved surfaces, and even from entire urban or partially-developed watersheds. Models developed by Ul Haq and James (2002), Van Buren et al. (2000a), Roa-Espinosa et al. (2003)/Thompson et al. (2008), and Jia et al. (2001) are perhaps the most relevant, but are not the only models available. The models of Ul Haq and James (2002) and Van Buren et al. (2000a) focus on predicting the heating of runoff over impervious surfaces only, while that of Roa-Espinosa et al. (2003) is concerned with runoff temperature from urban watersheds, with the capability to model some best-management practices. The model of Jia et al. (2001) has a much larger scope than the other models, having been developed with the goal of predicting effects of land-use changes on the heat and hydrologic budgets of complex, urban watersheds.

A number of these existing hydro-thermal runoff models have limitations in formulation or applicability. For example, TURM (Roa-Espinosa et al., 2003; Thompson et al., 2008) calculates runoff from both pervious and impervious surfaces by a steady-state analytical solution of the kinematic wave equation, which may not be applicable to real

storm events with irregular rainfall distributions. The Ul Haq and James (2002) model neglects the potentially substantial contribution of both shortwave and long wave radiation to the heat budget of a paved surface during rainfall. While TRMPAVE (Van Buren et al., 2000a) includes a more rigorous surface heat budget, it does not include a runoff model, instead relying on observed or simulated runoff hydrographs for input. This limits its applicability due to the scarcity of this type of data for small watersheds. Conversely, the model of Jia et al. (2001) is very complex and the extensive input data requirements make it difficult to apply the model to a single urban development.

The formulation described herein is the result of an attempt to create a detailed and accurate model from a relatively simple set of inputs. It should be noted that this paper is not concerned with the MINHUET model for runoff flow and temperature prediction in an entire watershed. Rather it is intended to give a detailed multi-dimensional analysis of the unsteady heat transfer processes that contribute to the heating of rainfall runoff from a well-defined land surface, particularly an impervious surface. A model will be developed from basic principles to predict the temperature and flow rate of runoff from such a surface. All heat flux terms will be considered. Water depth, runoff velocity (flow rate) and water temperature will be given as functions of location on the runoff surface, and of time. The model will be applied to a specific study site to assess accuracy, and a sensitivity analysis will be conducted using the model to answer the guiding questions listed previously. The model development and the results of the analysis and the case study are presented in the paper. The results of this study will clarify the hydro-thermal behavior of surface runoff in response to rainfall, and can serve to justify the use of a simpler hydro-thermal runoff model in MINUHET.

2.2 Model Formulation

Figure 2.1 gives a schematic of the water depth distribution for sheet flow on a paved surface in response to a uniform rainfall over some interval of time. The paved surface has a uniform slope S_0 in direction x, a length L in direction x, and a width W perpendicular to x. The model takes into account both the spatial and temporal variation of water depth and water temperature along the length of the paved surface. If a single parcel of water is followed from the end of the paved surface (e.g. parking lot) to the

catch basin, it would be found to increase in depth, velocity and flow rate. It may also increase in temperature as it absorbs heat from the pavement, at least in the initial stages of runoff while the pavement remains warmer than the rainfall.

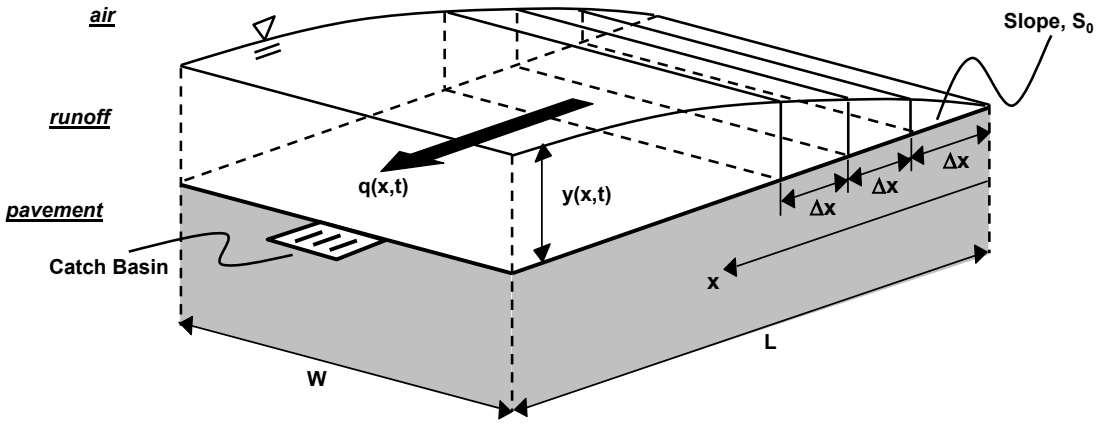

Figure 2.1: Schematic of runoff depth distribution for sheet flow on a paved surface during a rainfall event of uniform intensity.

2.2.1 Water Mass Balance

For unsteady water runoff, the water mass balance at any time t and distance x from the far (upstream) end of the lot is given as

$$\frac{\partial q(x,t)}{\partial x} + \frac{\partial y(x,t)}{\partial t} = i(t) - f(t) - e(t) = z(t) \tag{2.1}$$

where z is the effective rainfall intensity (m/s), q is the runoff flow rate per unit width (m^2/s), y is water depth (m), and $\partial q/\partial x$ represents the change in flow rate along the slope of the parking lot. The $\partial y/\partial t$ term takes into account water storage. Precipitation rate i (m/s) is a known quantity that is a function of time, evaporation rate e (m/s) can be calculated from weather data, and infiltration rate f (m/s) will be negligible for a paved surface. Two unknowns exist in Eq. (2.1): the runoff rate q, and the depth of water y. Each varies with distance x along the paved surface.

The momentum equation is often used to relate flow and depth for sheet flow (Mays, 2001). In its complete form, the equation is complex and difficult to solve. However, if a

kinematic wave approximation is used, i.e. inertial and pressure forces are assumed to be small compared to frictional and gravity forces, and the acceleration and pressure terms are neglected, a relatively simple solution of the runoff problem is obtained: $S_f = S_0$, where S_f is the friction slope, or a measure of the frictional forces. This approximation is justified by the fact that in overland flow the depth of water is small and involves rough surfaces, such that pressure forces will be insignificant, frictional forces will be large, and acceleration negligible. This approach has also been employed in existing runoff models (e.g. Cristina and Sansalone, 2003; Xiong and Melching, 2005). Using Manning's equation and the kinematic wave assumption, the water depth can be eliminated from the water mass balance equation. These assumptions result in a common form of Eq. (2.1), given as

$$\frac{\partial q}{\partial x} + \alpha\beta q^{\beta-1}\frac{\partial q}{\partial t} = z(t) \tag{2.2}$$

where α and β are coefficients determined from Manning's equation: $\alpha = (1/a)^{\beta}$ and $\beta = 1/m$, where $m = 5/3$ for turbulent flow and a is given as follows (Mays, 2001):

$$a = \frac{1.0 * S_0^{1/2}}{n} \tag{2.3}$$

where the coefficient (1.0) in the right-hand side is for SI units; 1.49 would be used for English units. Eq. (2.2) can then be solved by using a variety of numerical schemes to give the per-unit-width flow rate q at any point along the paved surface, for varying intensities of rainfall $z(t)$.

2.2.2 Heat Budget for the Runoff

The heat budget for surface runoff includes the time rate of change of heat storage in the water, which equals the sum of the net horizontal advection by the flow over the pavement, heat inflow from the rainfall h_{rain}, conduction from the heated pavement into the runoff $h_{cond,pv}$, net total (solar and long wave) radiation h_{rad}, evaporation h_{evap}, and convection between the water surface and the atmosphere $h_{conv,atm}$. In equation form, this balance appears as follows:

$$\rho_w C_{p,w} \frac{\partial(y * T_{ro})}{\partial t} = -\rho_w C_{p,w} \frac{\partial(q * T_{ro})}{\partial x} + h_{rain} + h_{cond,pv} + h_{rad} + h_{evap} + h_{conv,atm} \quad (2.4)$$

where T_{ro} is the temperature of the runoff water on the pavement, y is the depth of runoff, and q is the runoff flow rate (per unit width). All three are functions of both time t and distance x along the slope of the paved surface.

Eq. (2.4) is solved numerically using finite-difference techniques to obtain the runoff temperature T_{ro}. The first step in this process is to divide the pavement surface into vertical water-pavement-soil columns of length Δx and width w (Figure 2.1), assuming the heat transfer processes vary in the flow direction x but are laterally uniform. The five heat fluxes designated by the letter h in Eq. (2.4) occur in the vertical direction z in each column, and are assumed to act at the pavement-water interface.

Horizontal heat transfer is through the advection term, i.e. the first term on the right-hand side of Eq. (2.4). The runoff water is assumed to be completely mixed vertically and in quasi-equilibrium with the surface, such that pavement surface temperature is equal to the runoff temperature T_{ro}. The runoff and sub-surface pavement-soil volumes are coupled through the term describing the conduction between the pavement surface and the runoff water, $h_{cond,pv}$.

The volume (depth) of runoff water on the paved surface can be very small. As a result, significant numerical instabilities can develop when atmospheric heat fluxes (i.e. net radiation, atmospheric convection, evaporation) are applied to the runoff volume. To avoid this problem, which arises only for wet weather, the atmospheric heat fluxes are considered to exchange heat with the much larger pavement-soil volume as in the case for dry weather. The resulting surface heat budget for the runoff volume is written as:

$$\rho C_p \frac{\partial(y * T_{ro})}{\partial t} = -\rho C_p \frac{\partial(q * T_{ro})}{\partial x} + h_{rain} + h_{cond,pv} \quad (2.5)$$

where, as before, the $h_{cond,pv}$ term represents the pavement-runoff heat exchange.

2.2.3 Heat Budget for the Pavement/Sub-grade

To quantify the pavement-runoff heat exchange it is necessary to know the pavement/sub-grade temperature profile at all time steps. To keep track of this temperature profile $T_s(z,t)$, an unsteady vertical heat conduction equation is applied to the pavement/sub-grade column:

$$\frac{\partial T_s(z,t)}{\partial t} = \frac{\partial}{\partial z}\left(D_p \frac{\partial T_s(z,t)}{\partial z}\right) \tag{2.6}$$

where D_p is the thermal diffusivity of the pavement/sub-grade column. At the pavement surface a total vertical heat flux h_{total} is applied:

$$h_{total} = h_{rad} - h_{conv,atm} - h_{evap} - h_{cond,pv} \tag{2.7}$$

The first three heat flux terms on the right-hand side of Eq. (2.7) are the heat fluxes that were removed from Eq. (2.4) to give Eq. (2.5). The h_{total} term is the net heat flux at the top of the pavement-soil column, and becomes the upper boundary condition for solving the 1-D heat diffusion equation. The sign convention used assumes that evaporation and atmospheric convection will represent a heat loss from the surface, and the pavement-runoff term $h_{cond,pv}$ will have the opposite sign as in the runoff energy balance (Eq. 2.5).

Eq. (2.6) is discretized using an implicit scheme and the numerical form of this equation is solved via the Tri-diagonal Matrix Algorithm (TDMA). Eq. (2.5) is also solved numerically, with the heat storage and advection terms discretized using an implicit, forward difference scheme known as upwinding (Patankar, 1980).

2.2.4 Atmospheric Heat Fluxes

The atmospheric heat fluxes consist of net solar radiation, net long wave radiation, sensible (convective) heat transfer between the runoff and atmosphere, and latent (evaporative) heat transfer. The formulations used in the model are described briefly here and follow the literature (e.g. Edinger et al., 1968, 1974); for a more detailed discussion see Janke et al. (2006) or Herb et al. (2006).

Net Radiation

The net radiation heat flux consists of two components: the net solar radiation $h_{s,net}$ and the net long wave radiation $h_{lw,net}$. The net solar radiation retained on the surface is $h_{s,net} = h_s(1 - \alpha_s)$, where h_s is the total measured incoming solar radiation at the surface (W/m^2) and α_s is the surface reflectivity (Duffie and Beckman, 1991). Net long wave radiation is a measure of the heat radiated downwards by the atmosphere minus the heat radiated upwards by the ground or water surface. Incoming long wave radiation is modeled as a function of the absolute air temperature T_a (K), vapor pressure of air near the surface e_s (kPa), cloud-cover fraction F_c, and atmospheric emissivity ϵ_a. The Idso (1981) equation is often used to define atmospheric emissivity: $\epsilon_a = 0.7 + (5.95 * 10^{-}5)e_s * exp(1500/T_a)$. We shall use a formulation proposed by Pirazzini et al. (2000) for total incoming long wave radiation, which modifies the Idso (1981) equation. Out-going long wave radiation emitted by the ground or water layer on the ground is determined by the surface temperature T_s (K) and surface emissivity ϵ_s. The formula for net long wave radiation becomes

$$h_{lw,net} = h_{lw,in} - h_{lw,out} = \epsilon_a \sigma T_a^4 \Big(1 + 0.4F_c^2\Big) - \epsilon_s \sigma T_s^4 \tag{2.8}$$

where σ is the Stefan-Boltzmann constant. The sign convention is such that a positive value indicates a net flux into the surface.

Latent (Evaporative) Heat Flux

Latent (evaporative) heat flux h_{evap} is the heat transfer associated with the vaporization of water from the earths surface, and is driven by wind, buoyancy, and atmospheric moisture both at the surface and aloft. The formulation for evaporative heat flux, taken from Stefan et al. (1980) and modified by Herb et al. (2006), accounts for moisture movement via both natural (buoyancy-driven) and forced (wind-driven) convection:

$$h_{evap} = \rho_a L_v \Big(C_{fc} u_2 + C_{nc} \Delta T_v^{1/3}\Big)\Big(q_{sat}(T_s) - q_a\Big) \tag{2.9}$$

In this equation, ρ_a is the density of air (kg_a/m^3), L_v is the latent heat of vaporization of water (J/kg_w), C_{fc} is a forced convection transfer coefficient, C_{nc} is a free

(natural) convection transfer coefficient ($^{\circ}C^{-1/3}*m*s^{-1}$), u_2 is the wind speed measured at a height of roughly 2 m (m/s), ΔT_v is the difference in virtual temperature between the water surface and the air (°C), $q_{sat}(T_s)$ is the saturated specific humidity of the air evaluated at the surface temperature (kg_w/kg_a), and q_a is the specific humidity of the air above the surface. The transfer coefficients and surface temperatures can be modified via the recommendations of Deardorff (1978) to make the formulation applicable to a variety of surfaces, such as different types of canopies, bare soil, open water, or pavement.

Sensible (Convective) Heat Flux

Sensible heat flux $h_{conv,atm}$ is a measure of the heat transferred with the bulk movement of any fluid; in this case the fluid is air in the atmosphere, and it is moved by both mean wind and buoyancy effects. This heat flux is characterized by use of the Bowen ratio (Bowen, 1926; Rasmussen et al., 1995), which relates convective heat flux to evaporative heat flux. Applying the Bowen ratio to the evaporation equation (Eq. 2.9) results in the following formulation:

$$h_{conv,atm} = \rho_a C_{p,a}\Big(C_{fc}u_2 + C_{nc}\Delta T_v^{1/3}\Big)\Big(T_s - T_a\Big) \tag{2.10}$$

where $C_{p,a}$ is the specific heat of air (J/kg*K), u_2 is the wind velocity measured at a height of 2 m (m/s), T_s is the pavement surface temperature (°C), and T_a is air temperature (°C). The other variables, including the transfer coefficients, are the same as in the evaporation equation (Eq. 2.9), and along with the surface temperature can similarly be modified to include the effect of different surface types.

2.2.5 Pavement to Runoff Heat Flux

The pavement-runoff heat flux $h_{cond,pv}$ is a difficult term to describe explicitly. It appears in both the runoff and sub-surface heat budgets (Eqs. 2.5 and 2.7, respectively). It could be estimated using a temperature gradient below the pavement surface, or from empirical flat-plate convection equations. The former would likely suffer from instability and the latter from inaccuracy or a need for calibration. To make the computation robust, we estimate the pavement-runoff heat flux term by the change in heat storage

in the pavement over a time step Δt, essentially computing it as a residual of the heat budget equation. The amount of heat exchanged over a single time step Δt can be defined as:

$$h_{cond,pv} = -\rho_s C_{p,s} \int_t^{t+\Delta t} \frac{\partial T(z,t)}{\partial t} \approx -\rho_s C_{p,s} \frac{\Delta T_s}{\Delta t} \delta_s C_1 \tag{2.11}$$

where ΔT_s represents the change in pavement surface temperature over the time step Δt, δ_s is the depth of penetration of the temperature change, and $\rho_s C_{p,s}$ is the heat capacity of the soil or pavement (J/m^3*K). The shape factor C_1 depends on the temperature profiles at the beginning and the end of a time step; values between 0.25 and 0.5 would be typical. The value of δ_s can be estimated from the thermal diffusivity of the soil or pavement D_p and the length of the time step Δt (Eckert and Drake Jr., 1972):

$$\delta_s = 4(D_p \Delta t)^{1/2} \tag{2.12}$$

2.2.6 Model Input

Operation of the model requires weather data, soil and pavement properties, and selection of several significant parameter and coefficient values.

Required weather data include solar radiation, air temperature, dew point temperature or relative humidity, wind speed, and precipitation. Rainfall temperature can be approximated by the dew-point temperature of air, but that assumption may fall short of reality during extreme events such as hail storms.

Important surface parameter values that must be specified include reflectivity (albedo), emissivity, and wind speed coefficients for convective heat transfer. The surface heat budget also requires thermal properties such as thermal conductivity and specific heat for both the pavement and the subsoil. In this model, properties are assumed to be constant with respect to temperature, moisture content, and soil type. Typical values of thermal properties used are given in Table 2.1. These are similar to published values (Abu-Hamdeh et al., 2000; Incropera and DeWitt, 2002; Luca and Mrawira, 2005).

A description of surface topography is another necessary input to the model, including surface area and average slope for the usually well-delineated paved surface. A

Manning's roughness coefficient n and a surface depression storage value also need to be specified for the paved surface.

Initial conditions are given by the dry weather temperatures of the pavement and sub-surface prior to a rainfall event, which can be simulated continuously with weather data as input. The wet weather equations outlined above are used during rainfall events until runoff disappears; a simplified set of equations are used during dry weather conditions in which the pavement-runoff and evaporation heat fluxes are neglected, and the surface properties of the pavement are used rather than those of water. The governing equations and solution techniques employed in this model are nearly identical to those presented in Herb et al. (2006, 2008), which contain a rigorous validation of the surface temperature model for a variety of surfaces, including asphalt and concrete pavements. Therefore the surface and sub-surface temperatures are assumed to be accurately 'primed' by the use of a continuous simulation with two weeks of dry weather data prior to simulating any single rainfall event.

Property	**Typical Value**	**Units**
Asphalt Pavement		
Albedo	0.12	–
Emissivity	0.94	–
Density	2100 - 2400	kg/m^3
Specific Heat	1120 - 1370	J/kg*K
Thermal Conductivity	1.4 - 1.8	W/m*K
Soil (Medium Texture)		
Density	1300 - 1500	kg/m^3
Specific Heat	900 - 1400	J/kg*K
Thermal Conductivity	0.4 - 1.2	W/m*K

Table 2.1: Typical values of thermal properties of asphalt pavement and soil. Taken from Luca and Mrawira (2005); Abu-Hamdeh et al. (2000).

2.2.7 Solution of Heat Budget Equations

Since $h_{cond,pv}$ cannot be explicitly evaluated until a change in runoff temperature has been estimated, the atmospheric heat fluxes (h_{rad}, $h_{conv,atm}$, and h_{evap}) are evaluated first, giving a value of h_{total} that does not include the $h_{cond,pv}$ term (Eq. 2.7). The 1-D heat diffusion equation (Eq. 2.6) is then solved using h_{total} as the upper boundary condition to get an intermediate surface temperature T'_s. Solution of the runoff heat budget (Eq. 2.5) without the $h_{cond,pv}$ term results in another intermediate runoff temperature T'_{ro}.

Most likely these two intermediate temperatures T'_s and T'_{ro} will not be equal; however, if it is assumed that a quasi-equilibrium must be reached, some heat transfer (in this case, $h_{cond,pv}$) must occur between the pavement and runoff to bring the runoff and surface temperatures into equilibrium. Solution of this simple equilibrium produces a first guess at the actual runoff temperature T_{ro}. The $h_{cond,pv}$ term can then be evaluated explicitly by substituting this new runoff temperature into Eq. (2.11). A second guess at the runoff temperature is provided by re-evaluating the h_{total} term to include the newly-calculated $h_{cond,pv}$ and solving the 1-D heat diffusion equation a second time (again using h_{total} as the upper boundary condition) to get a new surface (runoff) temperature and sub-surface temperature profile. If the two guesses at runoff temperature do not agree, the $h_{cond,pv}$ term can be adjusted and iterations performed until the two guesses converge.

The assumption of quasi-equilibrium between the pavement surface temperature and runoff water temperature is crucial to solution of the heat budget equation. The physical basis for this assumption is that at the molecular scale fluid particles adjacent to the pavement surface are stationary (no-slip condition) and therefore achieve thermal equilibrium with the pavement surface by conduction. This conductive boundary condition at the pavement-runoff interface implies a temperature continuity, except at the moment when the rain first hits the pavement; since the water volume that accumulates in the initial moments of the rainfall event will be very small, the assumption of temperature continuity from time $t = 0$ should not cause significant errors. The remaining issue is then the significance of the temperature gradient in the thin layer of water, as the layer is assumed to be isothermal. The runoff flow on a rough pavement surface is turbulent, and roughness elements will protrude a significant distance into the thin

water layer. Vertical mixing will therefore be strong enough to remove temperature gradients in the water layer, and thus the mean runoff temperature should be close to the pavement surface temperature. Solution of the vertical heat diffusion equation for the water layer (Incropera and Dewitt, 2002) using typical vertical diffusivity values (Fischer et al., 1979; Hondzo, 2002) suggests that even in the case of a 10 °C initial difference in temperature between the pavement and runoff, a 1 cm-thick water layer will be within 10% of the pavement temperature after a single time step (5 sec).

2.2.8 Model Calibration and Validation

The model described herein is developed from basic principles and for an impervious surface of simple geometry. No model calibration should therefore be necessary, except for some material or surface properties, e.g. soil thermal conductivity or Manning's roughness coefficient of a pavement.

An application of the model to a field site will be presented later in this chapter. The RMSE values between simulations and measurements can serve as a measure of the goodness of fit of the model to this particular site. However, this single application is considered to be for illustrative purposes. Applications to additional sites with measurements could be made in the future.

2.3 Model Sensitivity Study

2.3.1 Objectives

Using the model as a tool, a sensitivity study was performed to address the four guiding questions regarding the temperature and rate of runoff from a paved surface (see Introduction). The model output of interest for a single event includes: (1) horizontal distributions of runoff depth and water temperature on the paved surface, and (2) a thermograph, or time-series of water temperature and runoff rate at the outlet of the paved surface. An instantaneous heat export rate from the paved surface can be defined as

$$h_{exp} = \rho_w C_{p,w} \frac{q_{ro}}{L} \Big(T_{ro} - T_{ref} \Big) \tag{2.13}$$

where h_{exp} is in Watts per square meter of surface area. L is the lot length (m), q_{ro} is the per-width flow rate at the outlet (m^2/s), T_{ro} is the outlet runoff temperature (°C), and T_{ref} is some reference temperature (°C). As defined here, h_{exp} is an instantaneous rate of heat export. If h_{exp} is integrated with respect to time over the duration of the entire runoff event, i.e. until runoff ceases, a total heat export H_{exp} can be found:

$$H_{exp} = \int h_{exp} dt = \frac{\rho_w C_{p,w}}{L} \int_0^{t_{ro}} q_{ro} \Big(T_{ro} - T_{ref} \Big) dt \tag{2.14}$$

where t_{ro} is the time between onset of rainfall and cessation of runoff, and H_{exp} will have units of energy per surface area (e.g. J/m^2). The choice of reference temperature will determine the magnitude of the heat export. One option is to use rainfall temperature as the reference temperature, which means that heat export indicates the extent to which the paved surface is heating the rainfall. In this sensitivity study, a temperature near the upper limit of the temperature tolerance range of trout has been selected. In most trout species a water temperature higher than 20 °C induces stress, and can be lethal if exposure occurs for prolonged periods of time (Eaton et al., 1995). A reference temperature of 20 °C was used in this sensitivity study.

It should also be noted that atmospheric heat fluxes are neglected for the purposes of the sensitivity study, both to reduce the number of inputs required for the study and to isolate the effect of a warm pavement on runoff temperature. The only heat sources will be the rainfall and the paved surface.

2.3.2 Model Input for Sensitivity Study

The model input parameters can be grouped into three categories: (1) physical characteristics of the paved surface (lot length, slope, and roughness), (2) rainfall event characteristics (intensity, duration, and temperature of the rainfall), and (3) antecedent conditions (initial paved surface temperature and sub-surface temperature profile). A few simplifications are introduced to keep the number of simulations required for the sensitivity study manageable:

1. Lot slope and roughness are lumped into a single parameter ($S^{1/2}/n$), which appears in Manning's equation and the kinematic wave equation.

2. The rainfall temperature is fixed for the duration of the event at 20 °C.

3. An initial pavement surface temperature of 30 °C is specified, representing conditions prior to a mid-summer afternoon rainfall event.

4. Each rainfall event simulated has a duration of one hour and constant rainfall intensity.

Pavement lot lengths of 25 m and 100 m were selected for the simulations. Lot slopes were in the range from 0.33% to 3.5%, and Manning's n values in the range from 0.022 to 0.088 (0.022 represents a new and smooth surface, and 0.088 is representative of a worn and rough surface). This resulted in a range of $S^{1/2}/n$ values from 0.65 to 8.50, with 0.65 representing a nearly flat, rough surface and 8.50 representing a steep, relatively smooth surface. Rainfall intensities of 0.8 cm/h, 2.5 cm/h, and 7.5 cm/h were chosen. The pavement was assumed to be 10 cm thick, with 50 cm of sub-grade and soil below. A summary of the simulation input parameters for the sensitivity study is given in Table 2.2.

Variables	
Rainfall Intensity (constant over event):	0.8 cm/h, 2.5 cm/h, 7.5 cm/h –
Lot Length:	5 m, 25 m, 100 m
Slope-Roughness, $S^{1/2}/n$:	0.65, 8.50
Constant Parameters	
Event Duration:	1 hour
Rainfall Temperature:	20 °C
Initial Pavement Temperature:	30 °C
Lower-Boundary Temperature:	26.6 °C (at depth of 60 cm)
Reference Temperature:	20 °C
Numerical Model Specifications	
Δt:	5 sec
Runoff Cell Width, Δx:	1.0 m
Number of sub-surface layers:	60
Sub-surface layer thickness, Δz:	1 cm

Table 2.2: Summary of input values and model specifications for sensitivity study.

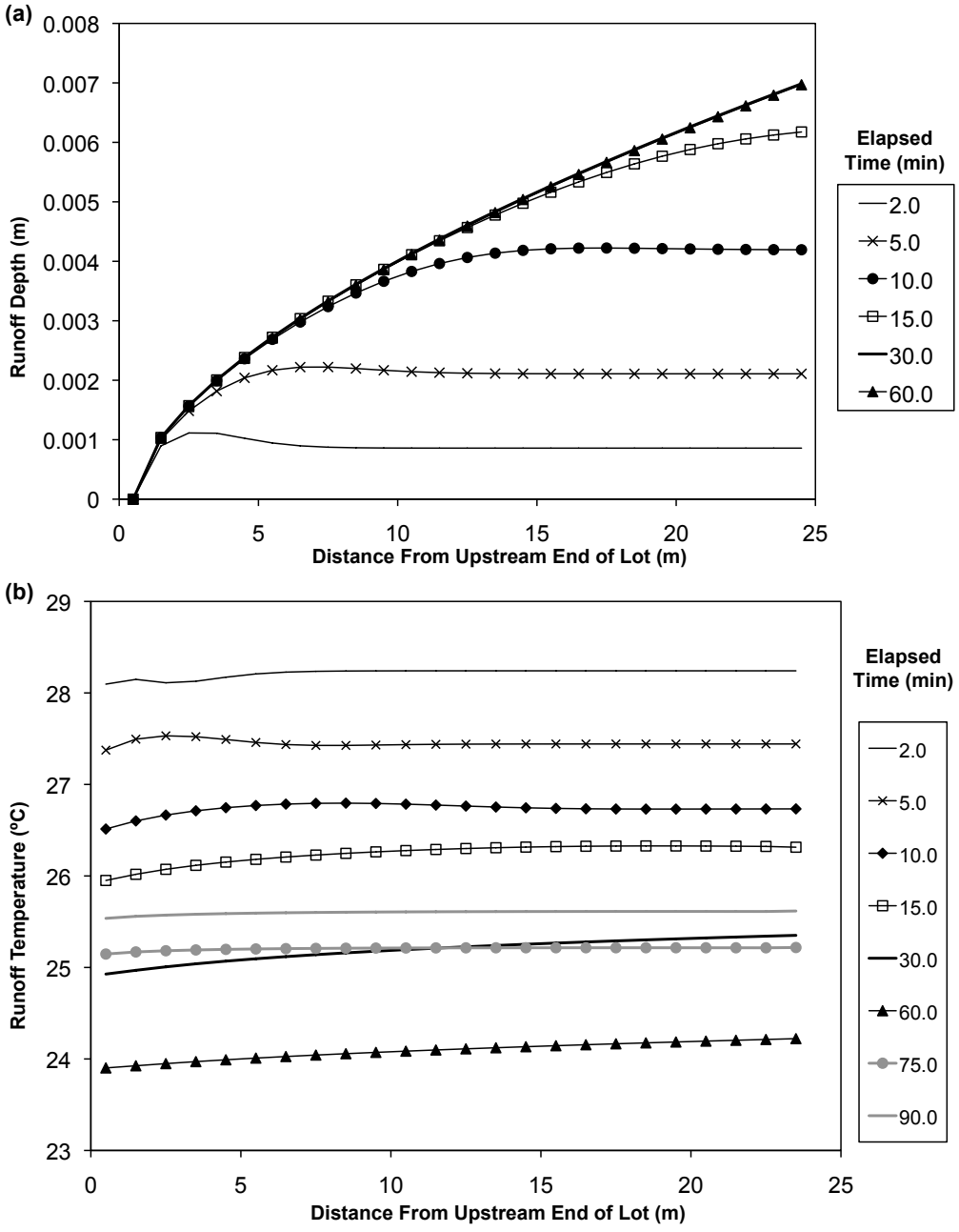

Figure 2.2: Horizontal distributions of (a) runoff depth vs. time, and (b) runoff temperature vs. time, for a one-hour, 2.5 cm/h-intensity rainfall event. Lot length = 25 m, $S^{1/2}/n = 0.65$, rainfall temperature = 20.0 °C, and initial pavement surface temperature = 30.0 °C.

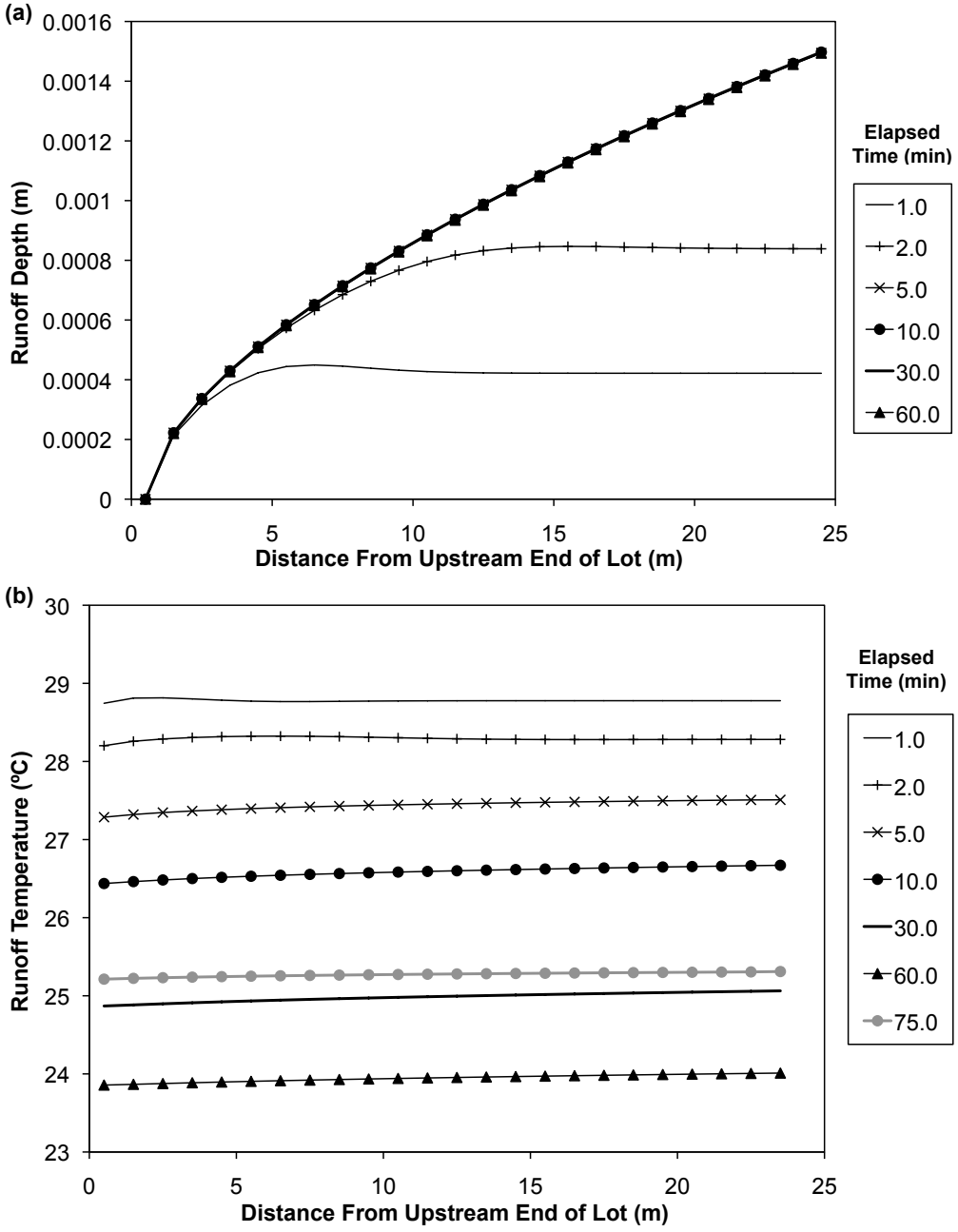

Figure 2.3: Horizontal distributions of (a) runoff depth vs. time, and (b) runoff temperature vs. time, for a one-hour, 2.5 cm/h-intensity rainfall event. Lot length = 25 m, $S^{1/2}/n = 8.5$, rainfall temperature = 20.0 °C, and initial pavement surface temperature = 30.0 °C.

2.3.3 Sensitivity of Runoff Depth and Water Temperature Distributions to Pavement Characteristics

Runoff depth as a function of time and position along the pavement for a rainfall intensity of 2.5 cm/h, lot length of 25 m, and slope-roughness of 0.65 is shown in Figure 2.2a. On this flat, rough surface, a steady state water depth profile is reached after about 30 minutes. Runoff temperature distributions for the event are also shown (Figure 2.2b).

During the rainfall event, the temperature gradient along the slope of the lot is very small; the maximum difference between the upstream and downstream ends of the lot is less than 0.5 C. The water temperature varies more in the first 5 m of the lot than in the lower portion of the lot. This holds true throughout the event. Other features of the plot are (1) the minimum runoff temperature occurs at the very end of the event (60 min), and (2) the runoff temperature increases after the rainfall has ended. This heating of the runoff occurs solely by conduction from the pavement and sub-grade since no atmospheric heat fluxes are calculated in this analysis.

For the steep, smooth surface ($S^{1/2}/n = 8.5$), a steady-state depth profile is reached in less than 5 minutes, i.e. much sooner than in the case of the flat, rough surface (Figure 2.3a). The water depths on the lot of steeper slope were smaller, as to be expected. The temperature gradients along the lot were also smaller in the high slope case (Figure 2.3b), most likely because of smaller water depth and shorter time to equilibrium relative to the low slope case. However, the runoff temperatures on the downstream portions of the paved lots were very similar for $S^{1/2}/n = 8.5$ and $S^{1/2}/n = 0.65$; the difference of the temperature at all points was 0.27 °C on average. Slope and roughness of the lot obviously influence the water depth distributions, but have little effect on the temperature distributions of the runoff.

When the simulations were repeated for a lot length of 100 m with the same slope-roughness values as before (i.e. $S^{1/2}/n = 0.65$ and 8.5), it was found that the temperature and depth distributions for the upstream 25 m of the 100 m lot matched the results of the previous 25 m lot simulation exactly (not shown). This is a logical result, given that there are no 'backwater' effects in the kinematic wave model. To reach a quasi steady-state water depth distribution took longer on the 100 m lot than on the 25 m lot: 60 minutes (i.e. the end of the rainfall event) for the 100 m lot compared to 30 minutes for the 25 m lot under otherwise identical conditions. The temperature

distributions on the 100 m lot had a maximum end-to-end difference of around 0.7 °C. It is therefore concluded that along the length of the lot runoff is close to isothermal, regardless of lot length or slope-roughness.

2.3.4 Sensitivity of Runoff Temperature and Heat Export Rate to Pavement Characteristics

A sample thermograph of the outflow from the lot (at the catch basin in Figure 2.1) is shown in Figure 2.4a, for a one-hour 2.5 cm/h rainfall on a lot of 100 m length with $S^{1/2}/n = 0.65$ (low slope-high roughness). Rainfall temperature is held constant at 20 °C, and there is no atmospheric heat exchange. Initial pavement temperature is 30 °C.

A rapid and large decrease in runoff temperature occurs in the first few minutes of the rainfall event (Figure 2.4a). After the rainfall has ended, the runoff temperature rebounds due to continued heat conduction from the pavement into a water layer of diminishing depth. This trend is similar to observations by Picksley and Deletic (1999) for late afternoon summer storms.

The maximum heat export rate (in W/m^2) from the entire lot occurs near the beginning of the rainfall event, just before the peak runoff rate occurs (Figure 2.4b). The similarity between the runoff hydrograph and the heat export rate time series is logical and suggests a strong influence of water volume on heat export. Heat export is calculated with reference to the rainfall temperature of 20 °C. When integrated over the entire rainfall event, the total heat export in this case is 470 kJ per m^2 of lot area. This is equivalent to the total heat load that would be supplied by the runoff to a receiving water body that has a temperature of 20 °C.

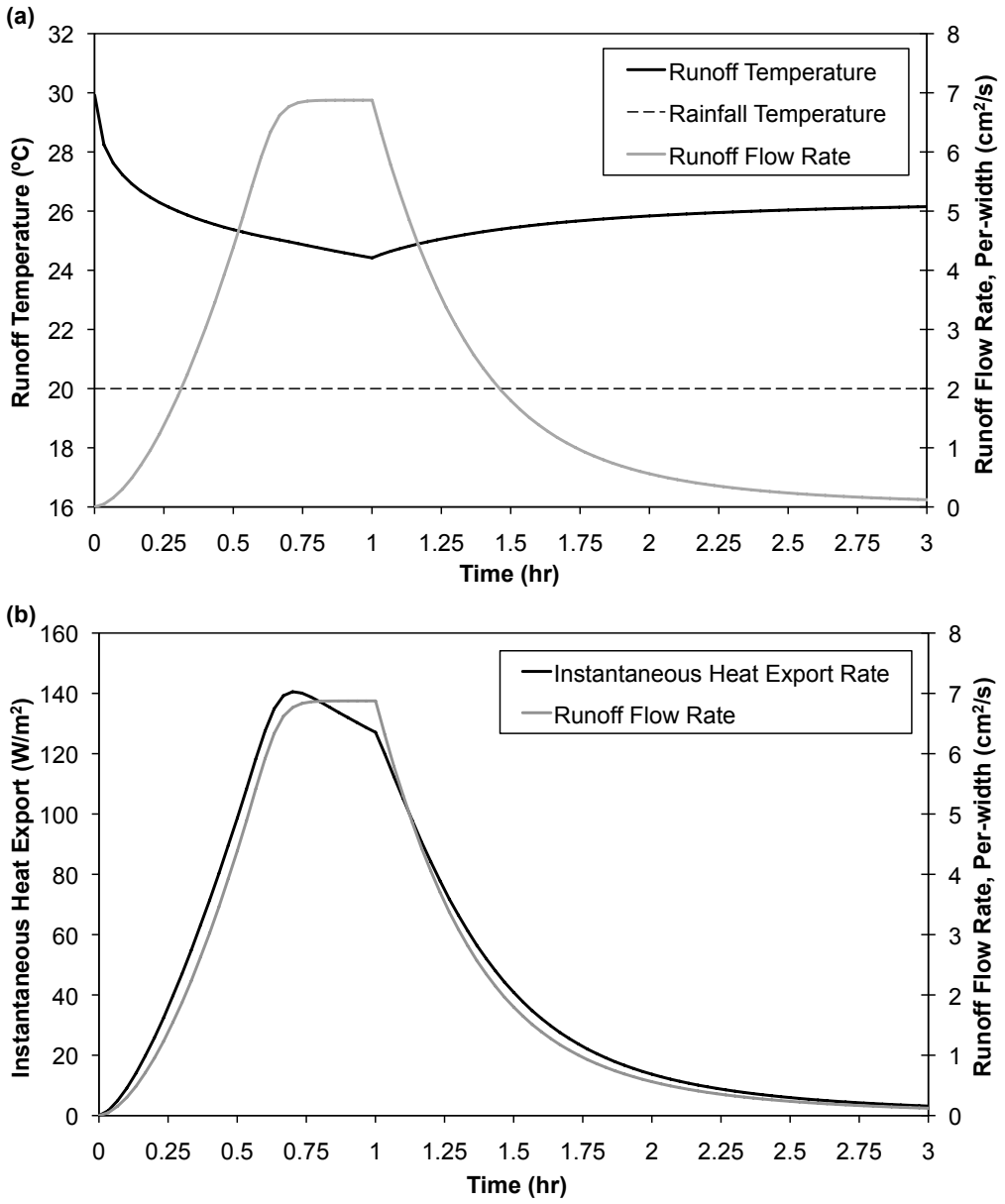

Figure 2.4: (a) Runoff temperature and flow rate, and (b) instantaneous heat export and flow rate, for a one-hour, 2.5 cm/h-intensity rainfall event. Lot length = 100 m, $S^{1/2}/n = 0.65$, rainfall temp = 20.0 °C, initial pavement surface temp = 30.0 °C.

An illustration of the effects of lot length and slope-roughness on runoff temperatures from a paved surface is given in Figure 2.5 for a one-hour rainfall event of 2.5 cm/h intensity. The runoff temperatures are remarkably similar for all cases, and this holds true in general. To explore extreme values we added simulations for a lot length of 5 m to earlier simulations. Extreme runoff temperatures were obtained for the longest lot (100 m) with low slope-roughness (0.65), and the shortest lot (5 m) with high slope-roughness (8.5). The maximum difference in runoff temperatures between these two cases was only 0.46 °C, with a mean difference of 0.25 °C, suggesting that both lot length and slope-roughness do not greatly influence runoff temperature.

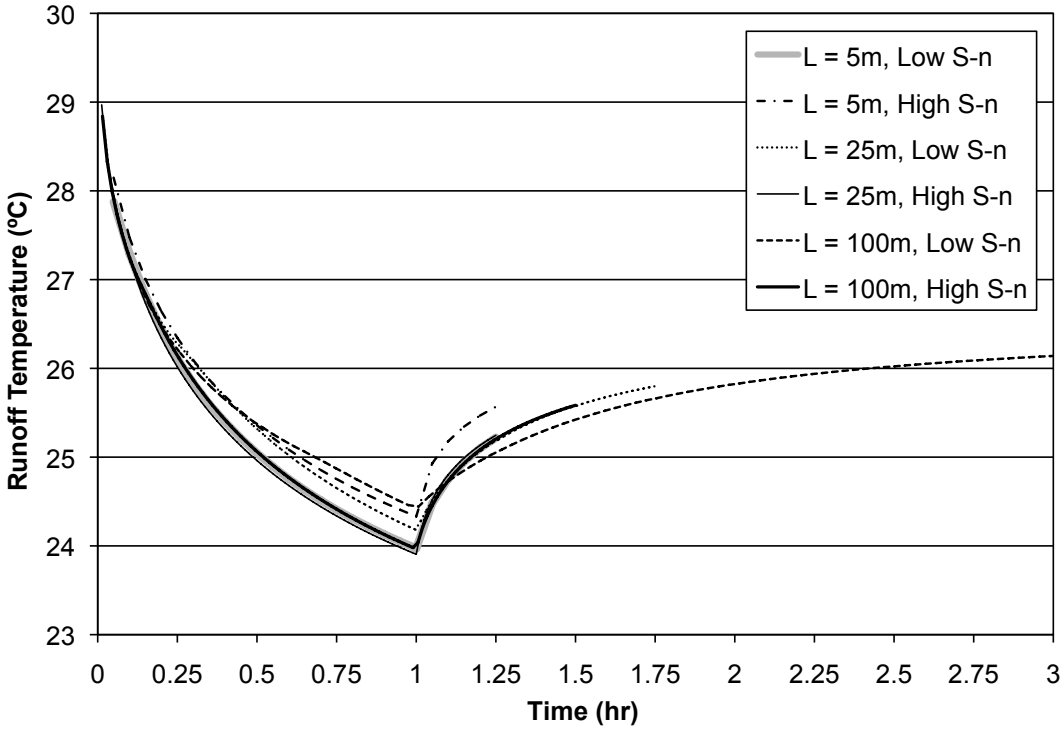

Figure 2.5: Runoff temperature from simulations of six paved surfaces of three lengths (5 m, 25 m and 100 m) and with two different slope-roughness values, for a one-hour, 2.5 cm/h-intensity rainfall. 'Low S-n' corresponds to $S^{1/2}/n$ of 0.65, 'High S-n' corresponds to $S^{1/2}/n$ of 8.50, rainfall temperature = 20.0 °C, and initial pavement surface temperature = 30.0 °C.

While runoff temperature is insensitive to lot parameters, heat export rate (W/m^2) varies greatly with lot length and slope-roughness. Heat export rates from four 25 m-long paved surfaces with different slope-roughness values (0.65, 2.13, 4.55, and 8.5) are illustrated in Figure 2.6. As before, a rainfall of 2.5 cm/h intensity, one-hour duration, and 20 °C temperature was used, and initial pavement surface temperature was 30 °C. As Figure 2.6 indicates, for a higher slope-roughness, peak heat export rate is larger and occurs earlier in the rainfall event. Similar trends were observed when the process was repeated for other lot lengths (not shown).

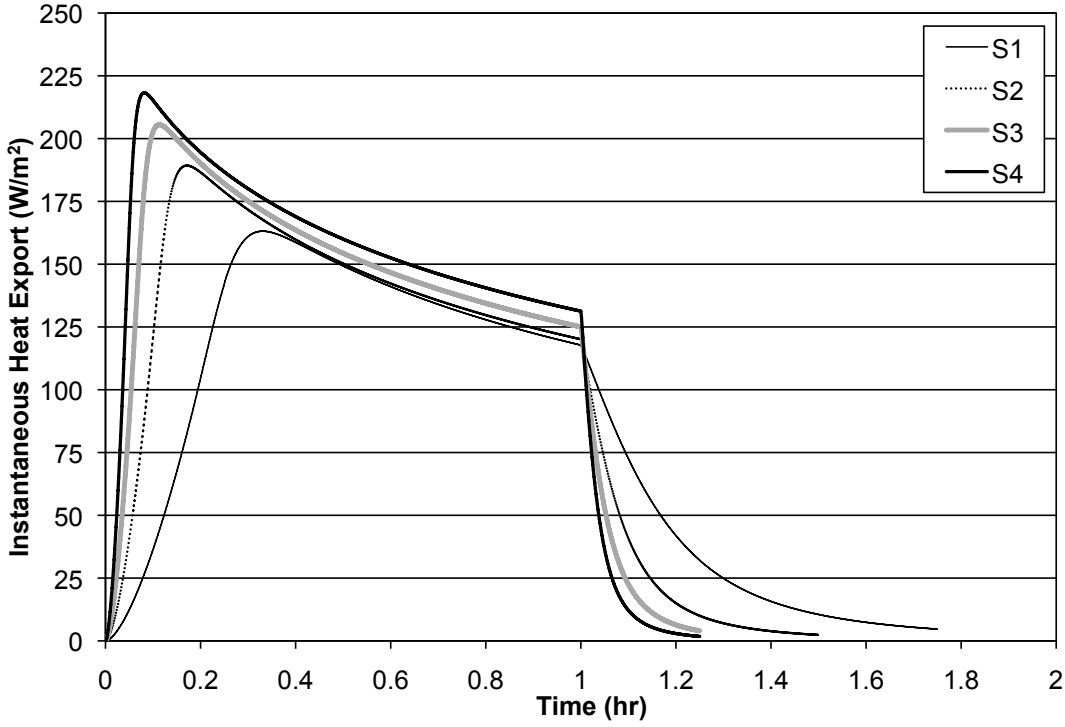

Figure 2.6: Instantaneous heat export rate of runoff from four paved surfaces with different slope-roughness values, for a one-hour, 2.5 cm/h-intensity rainfall event. Lot length = 25 m. S1 = $S^{1/2}/n$ of 0.65, S2 = $S^{1/2}/n$ of 2.13, S3 = $S^{1/2}/n$ of 4.55, S4 = $S^{1/2}/n$ of 8.50, rainfall temperature = 20.0 °C, and initial pavement surface temperature = 30.0 °C.

In Figure 2.7, heat export rate time series are plotted for varying lot length (5 m, 25 m, and 100 m) and a constant slope-roughness of 0.65. Rainfall and antecedent

conditions are the same as in Figure 2.6. The plot in Figure 2.7 indicates that the shorter lot has a peak heat export rate (per unit surface area) that is larger and occurs earlier than on the longer lot for the same rainfall event. For example, with all other parameters held constant for a one-hour, 2.5 cm/h rainfall event, the peak heat export rate for a short (5 m) lot was roughly 180 W/m^2 and occurred $t = 9$ min into the runoff event, while for the long (100 m) lot it was 141 W/m^2 and occurred at $t = 43$ min. However, it should be noted that for a constant lot width, the absolute heat export (in W) would logically be higher for the long lot than the short lot.

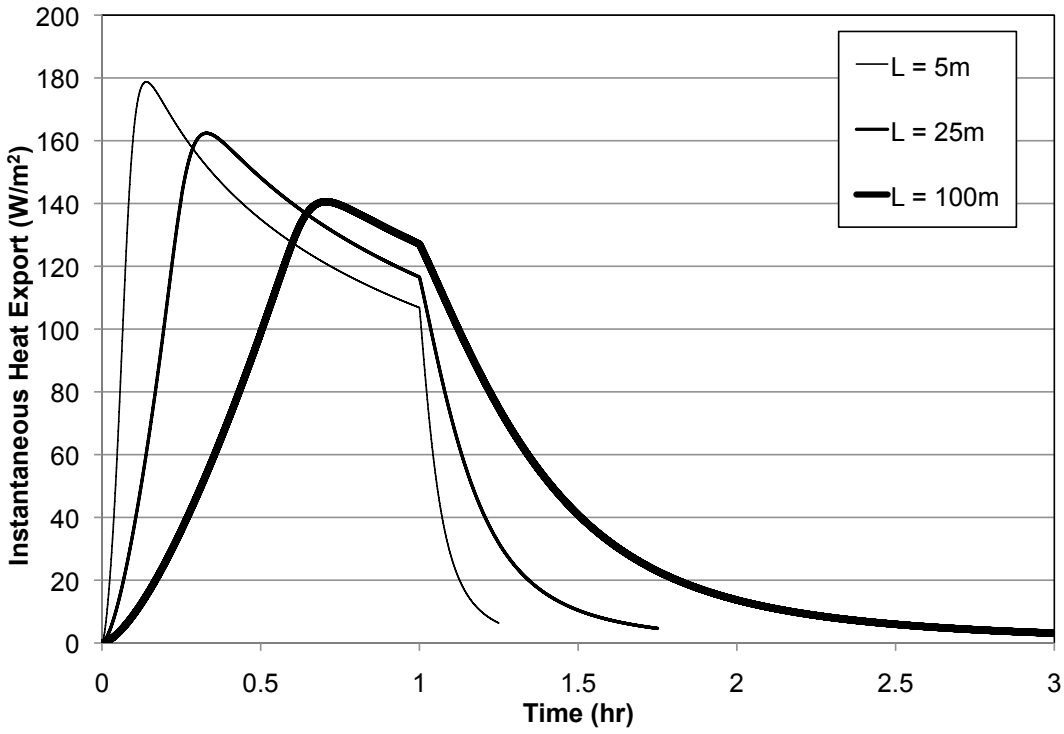

Figure 2.7: Instantaneous heat export rate of runoff from three paved surfaces of lengths $L = 5$ m, 25 m and 100 m for a one-hour, 2.5 cm/h-intensity rainfall event. $S^{1/2}/n = 0.65$, rainfall temperature = 20.0 °C, initial pavement surface temperature = 30.0 °C.

2.3.5 Sensitivity of Rainfall Event Heat Export to Pavement Characteristics

The thermal impact of surface runoff on a receiving water body (such as a stream) depends not only on peak heat export rate, but also on the duration of the heated runoff. A high instantaneous heat export rate does not necessarily imply significant thermal impact on a stream. Total event heat export (J/m^2) is the integral of heat export rate over the duration of a rainfall/runoff event, as defined in Eq. (2.14). It captures the thermal impact potential of a rainfall/runoff event from a surface much better than instantaneous heat export rates.

Simulated heat export values (Table 2.3) suggest that the physical characteristics (length, slope and roughness) of the paved surface do not significantly impact the total event heat export per unit surface area. An increase in slope-roughness leads to slightly higher heat export for medium- and low-intensity rainfall events (a roughly 1% and 5% increase, respectively), with the opposite effect (2% decrease) occurring for the high-intensity events. Short and long lots had virtually the same heat export per unit area (the difference amounted to less than 2% on average). It should be noted that the magnitude of total heat export from a paved surface is, of course, proportional to the surface area of the lot, but the heat export per unit area is only slightly impacted by the lot's physical characteristics. Table 2.3 also gives the time-averaged runoff temperature for each scenario, which shows even less variation with respect to changes in physical lot characteristics than heat export. Interestingly, the highest heat export values, which are associated with the highest rainfall intensity, also correspond to the lowest mean runoff temperatures, suggesting that mean runoff temperature alone is not a good indicator of the potential thermal impact of a rainfall-runoff event.

Rainfall intensity has a much greater impact on heating of runoff, and it is anticipated that pavement surface temperatures due to antecedent weather conditions would have a significant influence, as well. This result seems plausible because the total heat export has to match the amount of heat stored in a pavement before a rainfall event. The speed with which this heat can be extracted depends much more on the rainfall intensity and thermal conductivity of the pavement and sub-grade than on physical characteristics of the lot.

I (cm)	**$S^{1/2}/n$**	**L = 5m**	**L = 25m**	**L = 100m**
0.8	0.65	213 (27.3)	212 (27.3)	216 (27.1)
	8.50	219 (27.2)	228 (27.2)	228 (27.1)
2.5	0.65	499 (25.4)	508 (25.5)	514 (25.7)
	8.50	504 (25.3)	518 (25.2)	515 (25.3)
7.5	0.65	828 (23.1)	846 (23.3)	874 (23.9)
	8.50	826 (23.0)	836 (22.9)	840 (23.3)

Table 2.3: Total event heat export, in kJ/m^2, for three lot lengths L, two slope-roughness parameter values $S^{1/2}/n$, and three total rainfall depths I. Rainfall duration t_d = 1 hr, hence rainfall intensity i (cm/hr) = rainfall amount I (cm). Time-averaged runoff temperature (°C) for each scenario is shown in parentheses.

Thermal conductivity and heat capacity of a pavement show some degree of variability; in a study by Luca and Mrawira (2005), one particular asphalt pavement was shown to vary in thermal conductivity from 1.4 to 1.8 W/m*K, with a range in thermal diffusivity of 4.4 to 6.4 x 10-7 m^2/s. However, when simulations were carried out using this range of diffusivity values for the base scenario (one hour, 2.5 cm/h rainfall event on a 25 m lot with $S^{1/2}/n$ of 0.65 and initial pavement temperature of 30 °C), the calculated total event heat export was found to be within 10% of the original value. Similar results were observed for a lot length of 100 m, and for other rainfall intensities. This behavior suggests that on the time scale of a single rainfall event, pavement thermal properties might not be as critical to computation of runoff temperature as other parameters, and perhaps are more important for determining initial conditions.

Note also that sub-grade (soil) thermal properties show greater variability than pavement thermal properties, due to dependence on parameters such as temperature and composition (i.e. air, mineral, and water content). For medium-textured soils, Ochsner et al. (2001) found thermal conductivity to vary from roughly 0.5 to 1.5 W/m*K, with heat capacity ranging from 1.25 to 2.75 x 10^6 J/m^3*K. However, variation of sub-grade thermal properties within these ranges for the base scenario had an even smaller impact on heat export than was observed for the similar variation in pavement thermal properties, implying that pavement thermal characteristics have a greater impact on runoff temperature (heat export) than soil/sub-grade thermal characteristics.

2.3.6 Sensitivity of Rainfall Event Heat Export and Runoff Temperature to Rainfall Characteristics

It is apparent from the results presented thus far that event heat export is directly proportional to rainfall intensity, i.e. heat export increases with increasing rainfall intensity, regardless of other parameter values. To further assess the effect of rainfall characteristics on heat export, the set of simulations in Table 2.3 was rerun for rainfall duration of 4 hours; the total depth of rainfall I remained constant, thereby reducing the intensity by a factor of 4. The results are presented in Table 2.4. It can be noted that the lowest intensity rainfall event produced no runoff on the low slope-roughness lots, i.e. the depth of water on the surface never exceeded the threshold value required for runoff to occur.

I (cm)	**$S^{1/2}/n$**	**L = 25m**	**L = 100m**
0.8	0.65	n/a	n/a
	8.50	234 (27.3)	234 (27.2)
2.5	0.65	589 (26.1)	591 (26.1)
	8.50	604 (26.1)	606 (26.0)
7.5	0.65	1180 (24.1)	1188 (24.2)
	8.50	1191 (24.0)	1197 (24.0)

Table 2.4: Total event heat export, in kJ/m^2, for two lot lengths L, two slope-roughness parameter values $S^{1/2}/n$, and three total rainfall depths I. Rainfall duration t_d = 4 hr. Rainfall intensity i (cm/hr) = total rainfall depth I (cm) / 4 hr. Time-averaged runoff temperature (°C) for each scenario is shown in parentheses.

The total event heat export for the 4-hour rainfall was larger than for the one-hour rainfall events. The increase was not uniform, however; a mean increase of 3%, 18%, and 43% was observed for the 0.8 cm, 2.5 cm, and 7.5 cm rainfall, respectively. Similar increases were seen for the mean runoff temperature values as well, although the increase was not as large for the high-intensity rainfall. This trend in heat export shows that higher intensity rainfall is able to extract more heat from the pavement if the rainfall event is of longer duration, but that the lower intensity events extract nearly as much heat when the duration is just one hour. The implication is that rainfalls of

longer duration, for a constant rainfall depth, could be a bigger problem for thermal impact (total heat load) than short, intense rainfalls. This behavior also implies that a theoretical maximum total heat extraction exists for a given rainfall intensity, and that a greater duration allows an event to approach this maximum heat extraction. For this particular scenario, if all heat stored in the pavement layer is extracted (i.e. pavement temperature is reduced to the rainfall temperature of 20 °C), the total heat extracted would be 2360 kJ/m^2. This value serves as the upper limit of rainfall event heat export for this particular lot and initial conditions.

As mentioned previously, for a constant length and slope-roughness of the lot, a higher intensity rainfall produces a lower runoff temperature (not shown). For example, in the case of a 25 m-lot with slope-roughness of 0.65, the simulated runoff temperature for the 0.8 cm/h event was as much as 4.5 °C higher than that simulated for the 7.5 cm/h event. This behavior suggests that any heat extracted from the pavement by the runoff is effectively diluted in a large volume of water for higher-intensity events. However, a low runoff temperature does not necessarily correspond to a low total event heat export. Values in Tables 2.3 and 2.4 suggest that the greater the rainfall intensity, the higher the total event heat export, again illustrating the strong tie between hydrology and heat export. This logically implies that the rainfall events with the greatest potential to impact streams will be the larger, rarer events.

2.3.7 Sensitivity of Rainfall Event Heat Export and Runoff Temperature to Antecedent Weather

Both the initial temperature of the paved surface and the rainfall temperature can be expected to be the most crucial determinants of heat export by surface runoff from a paved surface. The difference between the two temperatures determines the potential for heat transfer from the pavement to the runoff; the rate at which the transfer takes place depends on the other parameters.

Simulations to investigate the effect of an increase in the difference between the initial pavement surface and rainfall temperatures were carried out. The temperature difference was doubled to 20 °C by raising the initial pavement surface temperature to 40 °C; rainfall temperature remained at 20 °C. A one-hour rainfall duration was used, and slope-roughness, lot length, and rainfall intensity were varied as before. Heat

input from the atmosphere was again neglected. The simulated total event heat export (kJ/m^2) and mean runoff temperature (°C) results are summarized in Table 2.5.

I (cm)	**$S^{1/2}/n$**	**L = 25m**	**L = 100m**
0.8	0.65	350 (32.1)	342 (31.0)
	8.50	385 (32.1)	381 (31.8)
2.5	0.65	845 (28.9)	831 (28.8)
	8.50	876 (28.8)	871 (28.8)
7.5	0.65	1407 (25.3)	1430 (25.8)
	8.50	1407 (24.9)	1402 (25.1)

Table 2.5: Total event heat export, in kJ/m^2, for two lot lengths L, two slope-roughness parameter values $S^{1/2}/n$, and three total rainfall depths I. Rainfall duration $t_d = 1$ hr, initial pavement temperature = 40 °C, rainfall temperature = 20 °C. Time-averaged runoff temperature (°C) for each scenario is shown in parentheses.

A very significant increase in total event heat export was observed relative to the original case of a 10 °C difference between initial pavement and rainfall temperatures (Table 2.3). The mean increase in total event heat export was 66% and varied little with total rainfall I (65%, 67%, and 66% for I = 0.8 cm, 2.5 cm, and 7.5 cm, respectively). Mean runoff temperature showed a slightly different trend, with a greater increase in runoff temperature being observed for a decrease in rainfall intensity. Slope-roughness and lot length again had very little impact on the change in heat export or mean runoff temperature associated with the increase in initial pavement temperature. Total event heat export values were slightly larger (by a few percent) for lots with higher slope-roughness, with very little effect by changes in lot lengths. These results confirm the expectation that total event heat export by runoff from a paved surface depends much more on initial pavement temperature and rainfall temperature, as well as on rainfall intensity and duration, than on physical lot parameters.

2.3.8 Impact of Atmospheric Heat Exchange on Heat Export

In the foregoing sensitivity analysis, heat flux between the atmosphere and the runoff was neglected in order to illustrate the relative importance of pavement and rainfall parameters. Similarly, the reference temperature and the rainfall temperature were chosen to be equal (20 °C) so that changes in runoff temperature had to be caused solely by heat transfer from the pavement. However, while other models have neglected some components of atmospheric heat exchange (e.g. Ul Haq and James, 2002), our model includes all major components contributing to atmospheric heating or cooling of runoff. In the absence of solar radiation, as is approximately the case for rainfall events, the rate of atmospheric heat exchange is generally proportional to the temperature difference between the surface (runoff) temperature and the dew point temperature (Edinger et al., 1968), suggesting that atmospheric heat exchange is significant when runoff temperatures are appreciably higher or lower than dew point temperature. Such scenarios include those investigated earlier: low-intensity mid-summer rainfall events during daylight hours, when sufficient thermal energy is stored in the pavement to heat runoff to temperatures well above dew point temperature. Conversely, atmospheric contribution is negligible for rainfall events during nighttime or for large rainfall intensities.

Therefore exploratory simulations were made for the same pavement and rainfall conditions used previously (Table 2.2), but including atmospheric heat fluxes. Weather data collected at the Minnesota Department of Transportation's MNROAD research site were used as model input for this portion of the sensitivity study. Solar radiation and wind speed, which were recorded at 15-minute resolution, were averaged during wet weather periods, i.e. when observed precipitation depth was greater than zero. Average solar radiation values were determined from rainfall events that occurred during daylight hours only. Data recorded in July from 1998 to 2001 and from 2003 to 2005 were used. Dew point temperature (used to approximate rainfall temperature) was fixed at 20 °C to match the no-weather simulations completed previously, and air temperature was set at 21 °C. These air and dew point temperature values are only slightly higher than the observed temperatures from the MNROAD data set (19.3 and 18.5 °C, respectively). The chosen weather parameter values are summarized in Table 2.6.

Total event heat export and mean runoff temperature values for the simulations including atmospheric heat fluxes are summarized in Table 2.7. Overall, climate forcing

Parameter	**Value**	**Units**
Solar Radiation	113	W/m^2
Air Temperature	21	°C
Dew Point (Rainfall) Temperature	20	°C
Wind Speed	1.96	m/s
Starting Time	15:00	–

Table 2.6: Weather parameters used in calculating atmospheric heat fluxes. Determined from rainfall events observed during July at MNRoad Project site, 1998-2001 and 2003-2005.

tends to decrease event heat export and mean runoff temperature, but does not have a uniform effect; it is highly dependent on rainfall intensity. Compared to the no weather cases (Table 2.3) the heat export decreased by roughly 34%, 21%, and 6% for the low, medium, and high-intensity rainfall events, respectively, with a similar trend observed in the mean runoff temperature. This behavior suggests that a small amount of runoff is influenced more by atmospheric forcing than a large runoff volume. As was observed before, the pavement lot parameters appeared to have a less significant role.

I (cm)	$\mathbf{S^{1/2}/n}$	**L = 25m**	**L = 100m**
0.8	0.65	145 (25.1)	140 (24.5)
	8.50	164 (25.2)	138 (24.5)
2.5	0.65	402 (24.3)	396 (24.1)
	8.50	420 (24.2)	411 (24.2)
7.5	0.65	787 (23.0)	805 (23.2)
	8.50	795 (22.8)	800 (23.0)

Table 2.7: Total event heat export, in kJ/m^2, for two lot lengths L, two slope-roughness parameter values $S^{1/2}/n$, and three total rainfall depths I, with atmospheric heat flux included. Rainfall duration t_d = 1 hr, initial pavement temperature = 30 °C, rainfall temperature = 20 °C. Time-averaged runoff temperature (°C) for each scenario is shown in parentheses.

Time series plots of runoff temperature simulated both with and without atmospheric heat exchange for identical paved lots are given in Figure 2.8. The rainfall is of

low intensity (i = 0.8 cm/h), the pavement is flat and rough (slope-roughness $S^{1/2}/n$ = 0.65), and the lot length is 25 m. In this case, the atmospheric heat flux is negative, i.e. from the runoff to the atmosphere, and tends to reduce the runoff temperature significantly. This is especially true near the end of the rainfall-runoff event, due to the small amount of water present on the surface.

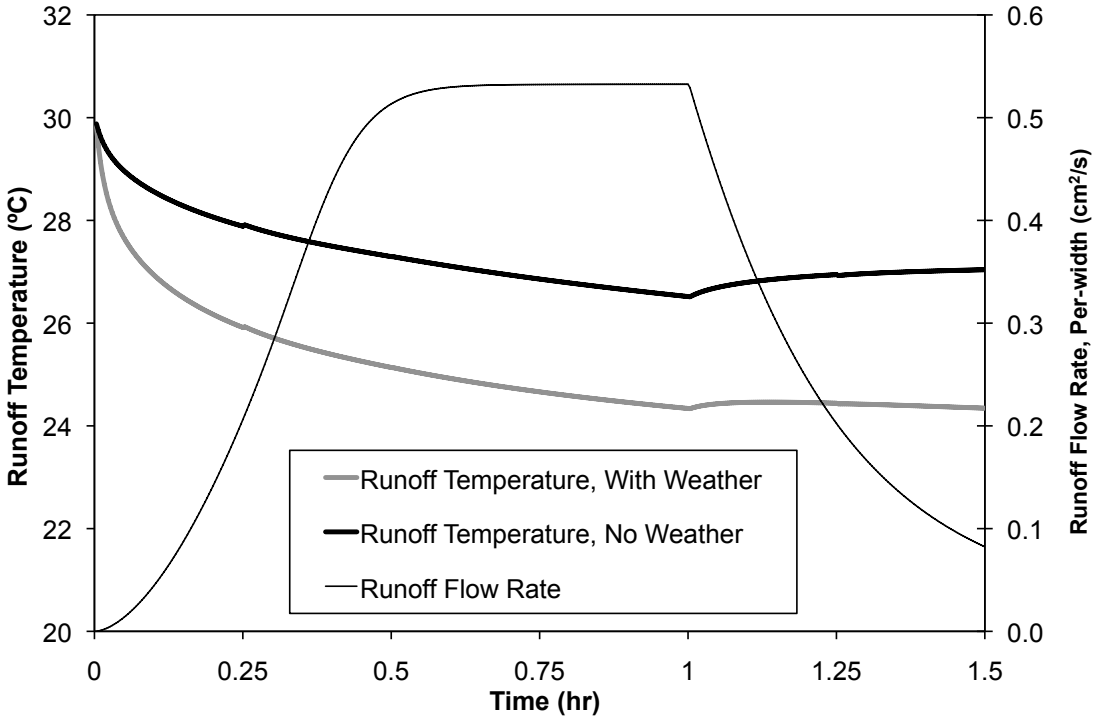

Figure 2.8: Runoff temperature and flow rate for a one-hour, 0.8 cm/h-intensity rainfall event. Lot length = 25 m, $S^{1/2}/n$ = 0.65, rainfall temperature = 20.0 °C, initial pavement surface temperature = 30.0 °C. Runoff temperature is calculated both with and without the effect of atmospheric heat fluxes.

A comparison of runoff temperature time series from the same paved lot was repeated for a high-intensity rainfall event (not shown). In this case, there is very little difference in runoff temperature between the simulations with and without atmospheric heat exchange. The net atmospheric heat flux is again negative, but the cooling effect of the atmosphere is diminished relative to the low-intensity rainfall event because of the greater amount of water on the pavement surface. Again, this effect is most prominent

at the end of the event, when most available heat has already been extracted from the pavement.

Time-averaged values of the atmospheric heat flux components for these two rainfall scenarios illustrate the importance of runoff-dew point temperature difference (Table 2.8). For example, the magnitude of net atmospheric heat flux (-86 W/m^2) for the rainfall event of low intensity was considerably larger than for the high-intensity event (-21 W/m^2), because the runoff-dew point temperature difference is greatest for the low-intensity event. Evaporation, which depends directly on runoff-dew point temperature difference, showed the largest difference between the two rainfall scenarios. These results again suggest that atmospheric heat exchange should not be neglected in a runoff heat budget.

Heat Flux Component (W/m^2)	**i = 0.8 cm/h**	**i = 7.5 cm/h**
Solar Radiation	104	104
Long Wave Radiation	-79	-67
Convection	-21	-11
Evaporation	-90	-49
Net	*-86*	*-21*

Table 2.8: Time-averaged values of atmospheric heat flux components (W/m^2) for two simulations selected from those presented in Table 2.7, which used typical July weather (Table 2.6) to compute heat fluxes. Lot length L = 25 m and slope-roughness $S^{1/2}/n$ = 0.65. Rainfall duration t_d = 1 hr and rainfall intensity i = 0.8 or 7.5 cm/hr.

2.4 Case Study

The model was applied to a field study site in Minneapolis, Minnesota consisting of a small parking lot with a single drainage outlet. The intention was to measure time series of runoff volume and runoff temperature from the lot for a number of rainfall events, and compare these observations with results predicted by the model using weather data collected within 500 m of the site. Unfortunately, the study period (July - October 2007) coincided with near-drought conditions in Minnesota, and yielded few of the late-afternoon thunderstorms that would be expected to produce runoff with significant

thermal impact. Results of the case study are presented as an illustration of model performance, not as a validation exercise.

2.4.1 Study Site and Equipment

The study site was a 0.58-acre, asphalt-paved parking lot on Nicollet Island in Minneapolis, MN. It is a relatively new lot, constructed five years prior to the study. The lot was surveyed and found to be 55 m long and 42 m wide, with a 3.4% slope from the upstream end to the outlet point. The lot is approximately rectangular in shape and its single drainage point is a 1 m-long curb cut, located roughly in the middle of the downstream end. The asphalt is 6 inches thick with a gravel and soil substrate below.

A box containing a composite weir was constructed and fitted into the curb cut to collect runoff water from the lot. A Massa Sonic level gage was mounted to a tripod placed in the box to measure water elevation, which was used to estimate flow rate. Vemco Minilogs (temperature probes with integrated data loggers) were placed at various locations to measure runoff temperature: (1) at the inlet of the box, (2) just upstream of the box, and (3) in the gutter of the curb next to the box. A handheld infrared thermometer was used to take point measurements of temperatures before and during a rainfall event in order to provide initial pavement surface temperatures, and to verify the temperatures measured by the installed Vemco probes. Weather data, including air temperature, dew point temperature, solar radiation, wind speed, and precipitation, were measured at 5-minute intervals at a station at the St. Anthony Falls Laboratory, located roughly 0.5 mi from the study site. Data were collected from July to October, 2007.

2.4.2 Results of the Case Study

To illustrate the performance of the model, observations were required for scenarios in which significant heating of the runoff occurs. This is most likely for rainfalls that occur in the afternoon or evening of hot, dry days. Three such events occurred during the study period, on August 11, September 6, and September 24. Of these events, only the first is useful for application of the model, because the latter two had such high rainfall intensities (greater than 4 in/hr) that runoff poured over the curb of the lot and was

not recorded at the weir.

The August 11 rainfall event was of short duration and moderate intensity, and occurred at approximately 19:00 on a very warm, dry day. Total rainfall depth was only 0.33 cm and fell in a 20-minute period. Initial pavement temperature measured with the infrared thermometer was 39 °C about 10-15 minutes prior to the rainfall, and runoff temperature never fell below 32 °C. This indicates a significant amount of heating by the pavement, as the dew point temperature (our estimate of rainfall temperature) was 24.5 °C. The initial pavement surface temperature simulated by the model from the dry weather data was just over 40 °C, which was deemed a satisfactory match to the observed temperature. Good agreement also existed between runoff temperature as measured by the Vemco Minilogs and as measured with the handheld infrared thermometer, suggesting that measured runoff temperatures are accurate (Figure 2.9). A comparison of simulated and observed runoff flow rate and runoff temperature is shown in Figure 2.9, along with the weather data used as input for the simulation.

Overall, there is fair agreement between the observed and simulated results. The RMSE for flow rate is 1.14 L/s, and the RMSE for runoff temperature is 0.61 °C. The model simulates the general shape of the observed hydrograph, but over-estimates runoff peak flow. A potential source of error in this case stems from the model assuming that sheet flow runs straight off the end of the lot; in reality, the flow collects in a gutter at the downstream end and is routed laterally to the curb cut. While the lot is not extremely wide, this lateral movement of water changes the observed time of concentration and timing of the peak flows. Total volume of runoff was over-predicted by about 14% (4.99 m^3 simulated versus 4.39 m^3 observed), likely the result of a number of factors. First, selection of initial abstraction (assumed equal to surface depression storage) has an impact on predicted total volume of runoff. The surface depression storage used in the model (0.08 cm) is not unreasonable for an asphalt surface (Viessman Jr. et al., 1977; Endreny, 2005), but may be a source of error. However, the over-estimation of observed flow most likely occurred because some portion of the runoff was not measured by the weir box. This could be the case if some flow bypassed the box at the outlet, or if a significant amount of runoff remained in gutters and other large depressions of the lot and failed to be routed to the outlet.

Runoff temperatures are well-matched for most of the event, although the model

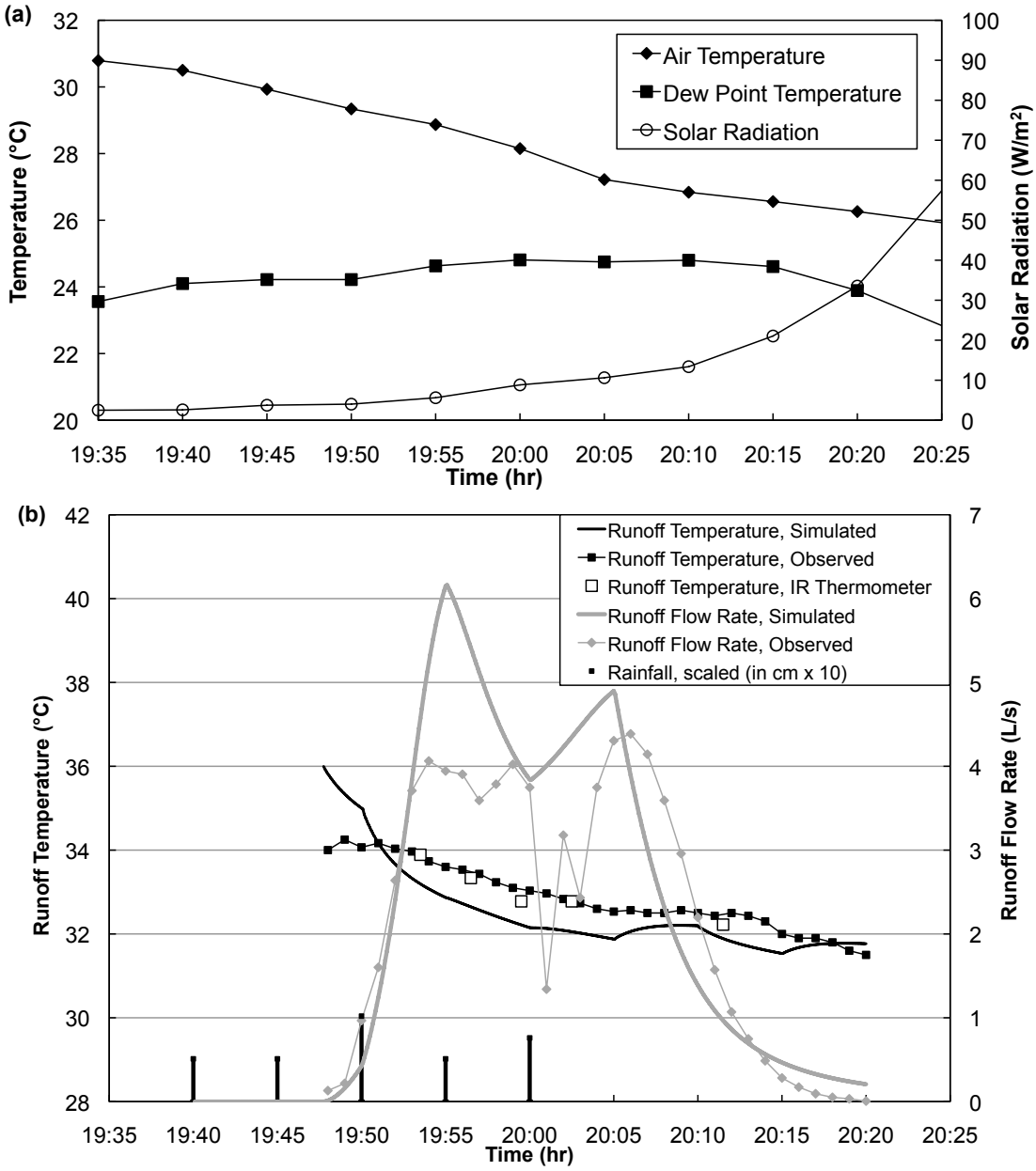

Figure 2.9: Plot showing (a) observed weather data and (b) observed and simulated runoff flow rate and runoff temperature from the Minneapolis, MN study site for a rainfall event occurring on 8/11/2007. Precipitation is shown for reference in (b); it is plotted with reference to the right axis in units of cm*10. Also shown are runoff temperature measurements taken with a handheld infrared thermometer. Weather data was observed at the St. Anthony Falls Laboratory, located 500m from the study site.

predicts a higher initial runoff temperature and a more rapid decline near the beginning of the event than was observed, and generally under-predicts runoff temperature for the remainder of the event. The total heat export values (computed with a reference temperature of 20 °C) matched very well; observed heat export was 278 MJ while the simulated heat export was 260 MJ, a difference of about 6%. The combination of over-predicted runoff volume and under-predicted runoff temperature resulted in an accurate total event heat export value.

Some calibration was needed to achieve these results. Surface depression storage and Manning's n for the asphalt surface were assumed to be small because the lot has a relatively new surface. Both parameters were varied until the shape and duration of the predicted hydrograph closely approximated the observed hydrograph; values used in the simulation were 0.08 cm for depression storage and 0.013 for Manning's n. Thermal properties of the asphalt and sub-grade were not precisely known, and were modified slightly until better agreement was found between the observed and simulated runoff temperature. Values of the calibrated parameters were 1.3 W/m*K, 1750 kg/m^3, and 840 J/kg*K for thermal conductivity, density, and specific heat of the soil, respectively, and 1.2 W/m*K, 2250 kg/m^3, and 925 J/kg*K for thermal conductivity, density, and specific heat of the asphalt pavement, respectively.

2.5 Summary and Conclusions

We have investigated the heat export by rainfall-induced surface runoff from a planar paved surface. A process-based hydro-thermal simulation model of water temperature and flow rate of runoff from the impervious surface was developed. The model uses a water balance equation for the runoff, which is solved via a kinematic wave approximation to provide runoff depth as a function of time and distance along the direction of flow on the paved surface. Heat budget equations for both a runoff control volume and a pavement/sub-grade control volume were formulated. The thin water layer on the pavement was assumed to be well-mixed at all times and provided the time-variable boundary condition for the formulation and solution of a conduction equation for the pavement-soil column. Heat inputs to the runoff control volume were (1) heat fluxes by short and long-wave radiation, evaporation, and convection between the pavement

surface and the atmosphere above, and (2) the conductive heat flux between the runoff on the paved surface and the pavement/sub-grade. To these heat fluxes in the vertical direction a horizontal runoff advection term was added in the runoff heat budget equation. The model requires weather data as well as pavement and sub-grade/soil thermal properties as input.

The hydro-thermal routing model was developed to provide guidance and input at the watershed scale. A case study for a real parking lot was given for illustration and assessment of performance. In the case study, the model was applied to a small parking lot in Minneapolis, Minnesota for a small, early-evening rainfall event occurring on August 11, 2007. Using standard weather data recorded at a nearby station as input, the model was able to predict with a fair amount of accuracy the runoff flow rate and runoff temperature from the parking lot (RMSE for flow = 1.14 L/s; RMSE for temperature = 0.61 °C). Heat export was predicted to within 6% of the observed value. Additional data will be needed to validate the model.

A sensitivity analysis was conducted with the model to answer several basic and conceptual questions (see Introduction). For this sensitivity study the model was applied to very well-defined runoff surfaces (constant slope and surface roughness) with very well-defined initial conditions and rainfall scenarios (constant rainfall temperature and rainfall intensity) that would not be found in natural field settings. Atmospheric heat exchange was initially neglected in order to isolate the effect of a warm pavement on heating of storm water runoff; a set of simulations were repeated with the addition of atmospheric heat fluxes to investigate the potential impact of atmospheric forcing.

Though not exhaustive, the sensitivity analysis assessed the impact of various key parameters on the runoff temperature (°C), maximum heat export rates (W/m^2) and most importantly, total event heat export (J/m^2) from planar paved surfaces. The parameters investigated included lot length L, slope S, and roughness n; rainfall intensity i and rainfall duration t_d; and initial pavement temperature T_{so}. Conclusions of the analysis include:

1. For pavement lengths up to 100 m, simulated water temperatures on the pavement surface did not vary significantly (less than 1°C) in the lengthwise direction in any of the simulated cases.

2. Physical parameters of the paved surface (slope, roughness, and length) have little influence on simulated runoff temperature or total event heat export per unit area (J/m^2).

3. The magnitude of heat export by runoff is strongly linked to rainfall parameters (rainfall intensity, rainfall duration, and rainfall temperature).

4. The lowest runoff temperatures are produced by rainfall events with high rainfall intensities, and the highest runoff temperatures by low rainfall intensities.

5. The highest total event heat export (J/m^2) from a rainfall event is produced by the highest rainfall intensity, even though these events produce the lowest runoff temperatures.

6. The general effect of increasing rainfall duration was to increase the total event heat export, with a greater effect occurring for larger rainfall intensities.

7. An increase in initial pavement temperature logically causes an increase in total event heat export.

8. Atmospheric heat fluxes (i.e. solar radiation, long wave radiation, sensible heat flux, evaporation) likely play a significant role in determining runoff temperature and total event heat export. With the parameters used in this study, the effect of atmospheric forcing was to reduce heat export relative to a no weather case, with a greater reduction occurring for low-intensity rainfall events than for high-intensity rainfall events.

Based on the results of this analysis, the numerous independent variables that influence the heat export from a paved surface during and after a rainfall event can be tentatively ranked in order of relative influence:

- Reference temperature (T_{ref}): this variable directly controls the magnitude of the calculated heat export from a paved surface (linear relationship), and should be related to the temperature of the receiving stream or other surface water body whose ecology is to be protected from excessive water temperatures.

- Rainfall temperature (T_{rain}) and rainfall amount (I): together these parameters determine the total amount of heat received from a rainfall event and exported from a runoff surface (linear relationship). A rainfall that is warm relative to reference temperature can produce an enormous amount of heat export.

- Initial pavement and sub-grade temperatures ($T_s(z)$): this variable, which is determined by weather conditions prior to the onset of rain, controls the amount of heat available in a pavement for release to the surface water runoff. If a pavement is at or below the rainfall temperature it can add no heat to the surface runoff.

- Pavement and sub-grade thermal diffusivity (D_p): this property controls how fast heat is stored in or released from the pavement and sub-grade. Combined with rainfall duration, initial pavement surface temperature, and rainfall temperature it determines the amount of heat released from the pavement to the runoff.

- Physical parameters of a paved lot (slope S, roughness n, and length L): these influence the length of the runoff event and thus the period of heat transfer between pavement and runoff water, but have little effect on total event heat export.

These conclusions are generally consistent with the findings of previous modeling efforts. For example, the model TURM (Roa-Espinosa et al., 2003; Thompson et al., 2008) was also found to be extremely sensitive to the choice of rainfall temperature, with significant sensitivity associated with solar radiation during rainfall events (Arrington, 2003). Higher runoff temperatures were associated with shorter or less-intense rainfall events in TURM simulations, much as in simulations with our model. Picksley and Deletic (1999) found a strong correlation between runoff temperature and both rainfall duration and air temperature for two small watersheds. Given the significant influence of air temperature on pavement temperature, this relationship is similar to our finding that both rainfall duration and pavement temperature are crucial parameters in determining heat export for a rainfall event. Finally, James and Xie (1999) concluded that initial pavement temperature and rainfall rate have a strong influence on runoff temperature, consistent with the results of the sensitivity study presented here.

It can also be concluded that the level of detail provided by the model that was formulated and used in this study would be unnecessary in larger composite watershed

models, given that horizontal gradients of runoff depth and water temperature on uniform paved surfaces up to 100 m length are negligible. This implies that simpler runoff models, such as those employed by MINUHET (Janke et al., 2007; Herb et al., 2009a) or TURM (Roa-Espinosa et al., 2003; Thompson et al., 2008), can likely be utilized without sacrificing too much accuracy. It should also be emphasized that while our model could be used in a standalone fashion, its applicability in such a context is perhaps limited, and is instead intended to provide input to watershed- or development-scale water quality models. Ultimately it is the total runoff volume and the water temperature at the outlet of an impervious parcel that is required by these storm water routing or stream temperature models, and our model is able to provide this information.

The conclusions of the sensitivity analysis and case study have three practical implications regarding thermal enhancement of storm water runoff from impervious surfaces. First, the impact of surface water runoff on a cold-water stream is potentially significant. In our case study, the runoff from a moderately sized parking lot (0.58 ac) for a mid-August rainfall event of only 0.33 cm produced a heat export of more than 250 MJ relative to a temperature of 20 °C the equivalent of a water body at 20°C receiving the runoff completely unmitigated. This example can help explain both the trend of rising observed stream temperatures in watersheds where imperviousness has been increasing (Klein, 1979; Galli, 1990), and the spikes in observed stream temperature associated with small- to moderate-intensity rainfall events in one particular urban development, similar to our case study (Roa-Espinosa et al., 2003). Second, rainfall events with high dew point temperature (i.e. rainfall temperature) and high initial pavement temperature have the greatest potential thermal impact on receiving streams. This scenario can be expected for afternoon or evening rainfall events following days of hot, dry weather in late summer or early autumn, and is consistent with the finding of Roa-Espinosa et al. (2003) that the timing of storm events and antecedent weather determine the thermal impact on receiving streams. This concept of design storms or worst-case scenarios is addressed in more detail in a case study of 280 rainfall events by Herb et al. (2007). Last, runoff temperature alone is not a good indicator of potential thermal impact. In the simulations, the most intense rainfall events, which produced the largest event heat export, also produced the lowest runoff temperatures. This implies that best management practices must be based on heat export, not water temperature.

Chapter 2 Notation and Units

***Parameter*: Description [units]**

a: parameter used in kinematic wave equation

e: evaporation rate [m/s]

e_s: vapor pressure of air near the surface [kPa]

f: infiltration rate [m/s]

$h_{cond,pv}$: heat conduction between pavement and runoff [W/m^2]

$h_{conv,atm}$: convective heat flux [W/m^2]

h_{evap}: evaporative heat flux [W/m^2]

h_{exp}: instantaneous heat export rate [W/m^2]

h_f: heat flux due to infiltrated water [W/m^2]

$h_{lw,in}$: incoming long wave radiation [W/m^2]

$h_{lw,net}$: net (incoming) long wave radiation [W/m^2]

$h_{lw,out}$: outgoing long wave radiation [W/m^2]

h_{rad}: total (solar and long wave) radiative heat flux [W/m^2]

h_{rain}: heat inflow from rainfall [W/m^2]

h_s: total measured incoming solar radiation [W/m^2]

$h_{s,net}$: net solar radiation [W/m^2]

h_{total}: net / total heat flux [W/m^2]

i: rainfall intensity [m/s, cm/h], or spatial index

m: parameter used in kinematic wave equation

n: Manning's roughness coefficient

q, q_{ro}: runoff flow rate per unit width [m^2/s]

q_a: specific humidity of air [kgw/kga]

q_{sat}: saturated specific humidity of air [kgw/kga]

t: time [s]

t_{ro}: duration of rainfall-runoff event [s]

u: wind speed [m/s]

x: coordinate in the direction of overland flow [m]

y: water depth [m]

z: effective rainfall intensity [m/s], or vertical coordinate [m]

C_1: shape factor for sub-surface temperature profiles
C_{fc}: forced convection coefficient
C_{nc}: natural convection coefficient [$^{\circ}C^{-1/3}m/s$]
$C_{p,a}$: specific heat of air [J/kg*K]
$C_{p,s}$: specific heat of soil or pavement [J/kg*K]
$C_{p,w}$: specific heat of water [J/kg*K]
D_p: thermal diffusivity of pavement or sub-soil [m^2/s]
F_c: cloudiness fraction
H_{exp}: total event heat export [J/m^2]
I: total rainfall depth [m, cm]
L: length of modeled surface [m]
L_v: latent heat of vaporization of water [J/kg]
$S^{1/2}/n$: ratio of surface slope (S_0) to Manning's n
$S1$: corresponds to $S^{1/2}/n$ of 0.65
$S2$: corresponds to $S^{1/2}/n$ of 2.13
$S3$: corresponds to $S^{1/2}/n$ of 4.55
$S4$: corresponds to $S^{1/2}/n$ of 8.50
S_f: friction slope [length/length]
S_0: surface slope [length/length]
T_a: air temperature [°C or K]
T_{ref}: reference temperature for heat export calculation [°C]
T_{ro}: runoff temperature [°C]
T_s: surface & sub-surface temperature [°C]
T_v: virtual air temperature [°C]

α: coefficient used in kinematic wave equation
α_p: reflectivity (albedo) of pavement
α_s: reflectivity (albedo) of a generic surface
β: coefficient used in kinematic wave equation
δ_s: heat penetration depth [m]
ϵ_a: atmospheric emissivity

ϵ_s: surface emissivity

ρ_a: density of air [kg/m^3]

ρ_s: density of soil or pavement [kg/m^3]

ρ_w: density of water [kg/m^3]

σ: Stefan-Boltzmann constant [5.67x10^{-8} W m^{-2} K^{-4}]

Δt: time step [s]

Δx: runoff cell width [m]

Δz: thickness of sub-surface layers [m]

ΔT_s: change in surface temperature [°C]

Chapter 3

Development and Application of the Minnesota Urban Heat Export Tool (MINUHET)

Summary

The MINUHET (MINnesota Urban Heat Export Tool) model is a tool used to simulate the flow of heat and storm water through a small urban watershed for a rainfall-runoff event. The tool includes process-based hydrological and thermal models for runoff from developed, undeveloped or vegetated land uses, and for various components of drainage networks, including pervious and impervious open channels, storm sewer systems, detention and infiltration ponds, and some best-management practices such as storm water vaults and rock cribs. The primary output of MINUHET is a time series of runoff flow rate and runoff temperature, which can be used to determine the heat content of the runoff at the outlet of the modeled watershed and aid in the assessment of the thermal impact on receiving waters. MINUHET is designed to simulate the rainfall-runoff from a single rainfall event or a series of events, but can be used in a continuous analysis as well. A graphical user interface and a database of observed and synthetic rainfall events for the state of Minnesota are also included.

This chapter describes the development of the MINUHET model components from

equations describing basic processes of hydrology and heat transfer in an urban watershed, as well as numerical techniques employed in the solution of these equations. Two applications of the model are presented. In the first case study, MINUHET is applied to a small, asphalt parking lot for a late-summer rainfall event. With very little calibration, the model performed well relative to simulations provided by a previously developed runoff temperature model, and to observations of runoff flow and temperature at the study site. In the second case study, MINUHET was applied to a 12-acre residential neighborhood in Plymouth, MN for which runoff flow and temperature data were available for a series of rainfall events. The uncalibrated version of the model did not perform well, with an RMSE for flow and temperature of 148 L/s and 1.57 C, respectively, for one event. Calibration to saturated hydraulic conductivity and thermal diffusivity and heat capacity of asphalt improved simulation results considerably (RMSE of 31.3 L/s and 0.87 C for the same event). Three other events were simulated with similar accuracy using these calibrated parameters. A sensitivity analysis of the model revealed that simulations were very sensitive to dew point (rainfall) temperature and saturated hydraulic conductivity, as well as to thermal properties and thickness of asphalt. These results underscore the importance of data quality and a truthful representation of the modeled watershed in producing accurate simulations with MINUHET.

To be submitted to *Hydrological Processes*, June 2011.

3.1 Introduction

The impact of urban development on the temperature of storm water runoff and the associated impact of heat loading to cold-water streams in urban watersheds has been investigated (e.g. Galli, 1990; James and Xie, 1999; Herb and Stefan, 2008). To address stream temperature response to urban development, process-based models have been developed in recent years to estimate the temperature and flow rate of rainfall runoff from urban surfaces. Examples of such models are TRMPAVE (Van Buren et al., 2000a), a model by Ul-Haq and James (2002), and TURM (Roa-Espinosa et al., 2003; Thompson et al., 2008). Empirical relationships that relate surges in observed stream temperature to land use changes and precipitation have also been developed successfully,

and extended to model the impact of future land use and climate scenarios (Nelson and Palmer, 2007).

The limitations of existing models, described in Chapter 2, were the primary motivation for development of the process-based MINUHET (Minnesota Urban Heat Export Tool) simulation model, with the goal to include a significant array of major heat transfer and hydrologic processes involved in the routing of storm water runoff from a small urban catchment (Herb et al., 2009a). With runoff from paved surfaces expected to have the greatest impact, a model for predicting volume and temperature of runoff from a flat and sloping impervious surface was developed and tested first (Chapter 2; Janke et al., 2009; Herb et al., 2009b). The heat release from rooftops, neglected in existing runoff temperature models, was then investigated (Chapter 1; Janke et al., 2011), with the conclusion that commercial rooftops may contribute significantly to the heating of rainfall runoff, while residential rooftop designs in the Upper Midwest have a negligible impact. Additional components addressed in the analysis of heat export by rainfall runoff from a small urban catchment include: (1) a model for heat transfer associated with runoff from pervious, vegetated surfaces; (2) a model for routing of heat through conveyance systems (e.g. open channels and storm sewers); and (3) models for heat exchange associated with storm water management practices, such as detention ponds, infiltration basins, and rain gardens. Models for these components were developed and incorporated into the comprehensive simulation tool MINUHET. The additional model components will be described only briefly; their development and validation are presented elsewhere. A graphical user interface was also developed for MINUHET to facilitate model setup and application.

The goals of this paper are (1) to give an overview of the processes associated with routing of heat and rainfall runoff through a small urban watershed, (2) describe the models developed to simulate these processes, and (3) to present a case study of the application of the composite model (MINUHET) to a residential development. The individual components of the MINUHET model have been tested with available data, but the composite model has not been assessed against a full urban development. MINUHET will be applied to a residential urban development in Plymouth, Minnesota in which storm water runoff (flow rate and temperature) had been recorded. While the data are limited, the case study will provide evidence that the model can predict runoff

flow rate and temperature from an urban development with reasonable accuracy. The case study will also highlight sources of sensitivity that need to be taken into account in applications of the MINUHET model.

3.2 Hydrologic and Heat Transfer Processes in a Small Urban Watershed: Overview

The hydrologic (water) balance for a rainfall event in an urban watershed primarily requires the partitioning of rainfall (Figure 3.1). Rainfall intercepted by impervious surfaces (e.g. parking lots, roads, rooftops, and driveways) is usually routed to a catch basin or open channel, from where it is conveyed through a storm sewer system to a receiving water body such as a detention pond or infiltration basin. In pervious open channels a portion of this runoff may infiltrate. Storm water BMPs (Best Management Practices) generally require that some runoff from rooftops and driveways in residential areas is routed onto lawns where it pools or infiltrates. These surfaces are known as 'disconnected' impervious (Arrow '1' in Figure 3.1), while impervious surfaces with direct connections to storm water conveyance systems are known as 'connected' impervious (Arrow '2' in Figure 3.1). Precipitation that falls on vegetated surfaces is partitioned into water that is intercepted by the canopy and stored on leaves and stems, and water that falls to the ground surface. Water reaching the ground is further partitioned into water that infiltrates, and water that runs off when the soil becomes saturated because the rainfall rate exceeds the infiltration rate. Water is transferred back to the atmosphere by evaporation and transpiration (for vegetated surfaces) at all points in the routing process, but the magnitude of these fluxes tends to be small during rainfall due to the high water content of the air and the relatively short duration of rainfall.

The surface heat transfer processes during wet weather are summarized in Figure 3.1b. Heat exchange with the atmosphere consists of incoming solar radiation, long wave radiation incoming from the atmosphere and emitted by the wet surface, sensible heat transfer with the atmosphere, and latent heat transfer by evaporation and transpiration. Heat exchange between the runoff and the ground surface can be significant, particularly on paved surfaces (Janke et al., 2009). Heat exchange between the surfaces of storm sewer pipes or open channels and the runoff water also occurs.

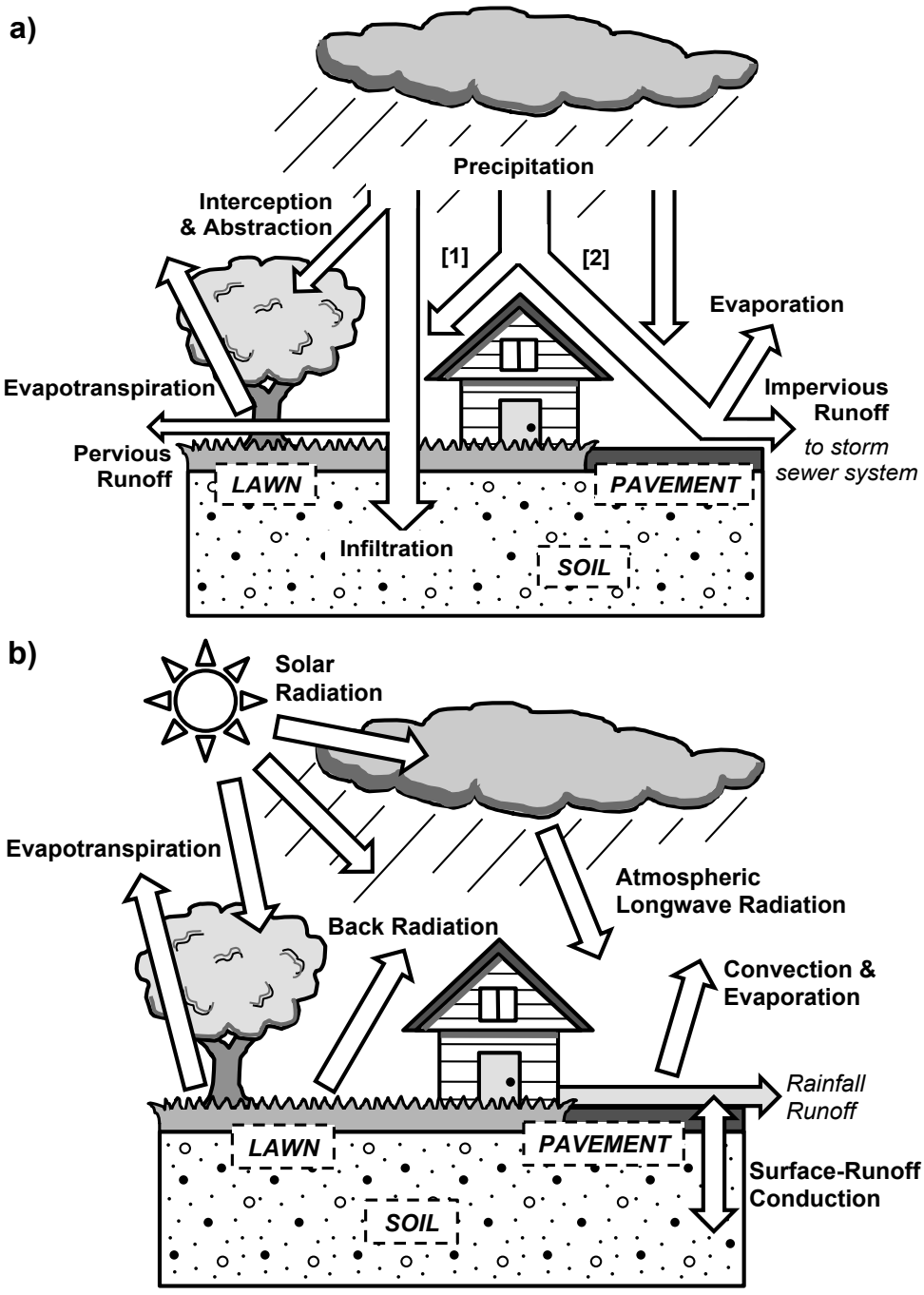

Figure 3.1: Schematic of major (a) hydrologic processes and (b) heat-transfer processes during a rainfall event in a typical urban watershed. In (a), the arrow marked [1] denotes 'disconnected' impervious areas, and arrow [2] denotes 'connected' impervious areas.

The presence of a plant canopy on the ground surface significantly alters the surface heat budget. Heat will be transferred between the canopy and the atmosphere, within the canopy itself, and between the canopy and the ground, primarily by long wave radiation and moisture exchange. In general, a vegetation canopy shades and shelters the land surface, reducing both the solar radiation and the wind speed seen by the surface; this lowers evaporative and sensible heat flux rates. Some precipitation is intercepted by the vegetation, and the loss of water and heat are enhanced by transpiration. Runoff from vegetated surfaces will therefore be cooler and of smaller volume than from paved surfaces (Herb et al., 2007; Thompson et al., 2008). The different approaches to the modeling of heat transfer processes are addressed in the next section.

3.3 Model Development

3.3.1 Background and Model Framework

The MINUHET model is a simulation tool used to route storm water runoff and its heat content through an urban sub-watershed for one or several rainfall events. The tool utilizes unsteady, process-based models for simulating various developed land surfaces, undeveloped or vegetated land uses, pervious and impervious swales or open channels, storm sewer conduits, and ponds. Within each individual model element water and heat are transferred in the vertical dimension only, but between elements water and heat are routed laterally as surface runoff or through pipes or channels. Heat fluxes between the atmosphere and the water on the ground or the ground itself are considered as appropriate, and a vegetation model handles several vegetation types.

MINUHET has four major model components: (1) a sub-watershed model, which can contain a mixture of pervious and impervious land uses that drain to a single point; (2) a routing model for routing of heat and water through the conveyance system (i.e. storm sewer pipes and vegetated or impervious open channels); (3) a pond model for water storage and heat transfer processes in a variety of pond types, including detention ponds, infiltration basins, and dry ponds, with a variety of outlet controls; and (4) a model to simulate the performance of novel BMPs such as underground storm water storage vaults and rock-filled trenches. A schematic of the MINUHET model is shown in Figure 3.2.

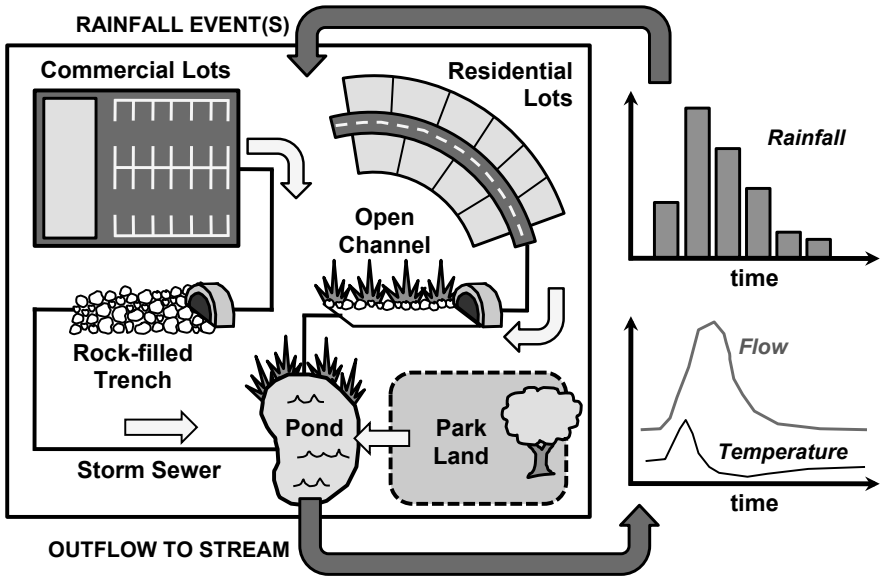

Figure 3.2: Schematic illustrating the typical urban watershed components modeled by MINUHET and their connectivity. For a rainfall event or series of rainfall events, the model simulates time series of runoff flow rate and runoff temperature at the outlet of the modeled watershed.

Model output is in the form of time series of runoff flow rate and runoff temperatures at multiple points and at the outlet of the watershed. The model also uses this information to calculate the heat content of the runoff (relative to a user-specified reference temperature). This heat export time series (J/s) is calculated using Eq. 2.13, and can be integrated over an entire event to give the total heat export (MJ) (Eq. 2.14). Section 2.3.1 contains further details on the determination of heat export and on the selection of a meaningful reference temperature.

A graphical user interface was also developed for the model by the Minnetonka Audio Software Company (Minnetonka, MN) that greatly expedites the model setup, data input, and output visualization processes. The interface provides a schematic representation of the modeled watershed showing connectivity of the various components, and allows editing of the properties for each instance of an element type. A number of rainfall events, both real and synthetic, can be selected for analysis using the interface, though at the moment they are specific to the state of Minnesota. A separate screen shows model output (runoff flow rate, runoff temperature, and heat export rate time

series) in graphical form, which can be exported in a variety of formats to be used in other applications.

3.3.2 Sub-watershed Model

Sub-watershed models are used to describe all land surface areas within the modeled watershed. A single sub-watershed model defines a land area that drains to a single outlet point, and produces a time series of runoff flow rate and runoff temperature at that point. A modeled watershed will likely have multiple sub-watershed models, which are linked by a routing model component.

The sub-watershed model includes of a number of sub-models to describe the transfer of heat and water in the sub-watershed for both wet and dry weather. Sub-models are used to compute land surface and sub-surface temperatures, roof temperatures, runoff flow rates and temperatures, infiltration, and soil moisture. These components are described in detail by Herb et al. (2009a), and summarized here.

Surface Temperature Model

The land surface temperature model uses a heat balance at the ground surface including heat exchange with the atmosphere and/or overlying water, making use of standard weather data and physical properties of the surface and sub-surface (Herb et al., 2006). The heat budget for the land surface appears as follows for a rainfall event:

$$h_{net} = h_{rad} - h_{evap} - h_{conv} - h_{ro} \tag{3.1}$$

where h_{net} is the net heat flux across the ground surface in response to atmospheric heat exchange (net total radiation h_{rad}, evaporation h_{evap}, and convection h_{conv}) and/or to h_{ro}, the conduction between the sub-surface and overlying water layer (Section 3.3.2). The ground serves as either a heat source or sink depending on antecedent conditions and on the thermal storage capacity of the surface, and has a potentially significant interaction with surface runoff during and immediately following rainfall events. For dry weather $h_{ro} = 0$, and for impervious surfaces $h_{evap} = 0$, except when water is pooled on the surface.

Atmospheric heat exchange includes components for net solar radiation (incoming

radiation minus radiation reflected by the surface), incoming long wave radiation from the atmosphere, long wave back radiation from the surface, sensible heat flux, and latent heat flux (evaporation and transpiration). The equations used to describe these components are the same as in the runoff temperature model (Herb et al., 2009b; Janke et al., 2009); the transfer coefficients in the convection and evaporation equations can be modified to represent a variety of surfaces, including pavements, rooftops, and bare soils (Deardorff, 1978).

Vegetation canopies, besides providing shading and sheltering, have the ability to exchange large amounts of heat and moisture with their surroundings through their leaf surfaces, and therefore change land surface and runoff temperatures significantly. In the presence of vegetation, the ground surface heat budget must be modified by more than just altering the values of parameters in the equations for the atmospheric heat transfer components. The general approach to the modeling of vegetation is taken from Deardorff (1978): a heat budget is formulated for the canopy itself, assuming that it has zero heat capacity (i.e. zero mass) and thus does not store heat, acting instead as a heat exchanger between the ground and the atmosphere. Heat fluxes generated or modified by a canopy of vegetation include net long wave radiation between the ground and the canopy, net solar radiation intercepted by the canopy, and both evaporative and convective fluxes from the canopy and the ground surfaces. Estimating these fluxes requires knowledge of the canopy temperature and of the humidity and temperature of the air within the canopy. Parameters to describe canopy structure and phenology (e.g. leaf area index or shading fraction as a function of time) are also necessary.

To simplify the vegetated land cover heat budget, the approach of Best (1998) is employed whereby a dense canopy is assumed, such that evaporative and convective heat exchange between the ground and canopy is negligible. Temperature and humidity of the air in the canopy are thus not needed, simplifying the list of parameters required for heat flux calculations. The resulting canopy heat budget, assuming negligible heat storage by vegetation (i.e. $h_{net,f} = 0$), is given as

$$h_{net,f} = 0 = h_{rad,a} + h_{lw,g} - h_{lw,f} - h_{evap,f} - h_{conv,f} \tag{3.2}$$

where $h_{rad,a}$ is the total radiation (solar and long wave) from the atmosphere absorbed by the canopy, $h_{lw,g}$ is the long wave radiation emitted by the ground and absorbed by the canopy, and $h_{lw,f}$ is long wave radiation emitted by the canopy, $h_{evap,f}$ and $h_{conv,f}$ are the net evaporative and convective heat fluxes from the canopy, respectively. The notation of Deardorff (1978) is adopted here, with the subscripts a, f, and g denoting the atmosphere, foliage (canopy), and ground, respectively.

While the land surface model can theoretically be applied to any land use, it was developed especially for urban land covers, which are highly heterogeneous. Canopy cover is rarely continuous, and even at the scale of a single city block a number of vegetation types or even bare soil can be present. The effect of partial vegetation cover is accounted for in the model by scaling canopy heat flux components with a vegetation density factor v, which ranges from $v = 0$ for a bare soil to $v = 1$ for a dense canopy with a leaf area index (LAI) of roughly 7.0 (Deardorff, 1978). In this way the modeled surface can be partitioned into bare soil and vegetated components (Figure 3.3). The canopy heat budget (Eq. 3.2) remains unchanged by this consideration, while the land surface heat budget, including the runoff heat flux h_{ro}, appears as follows:

$$h_{net,g} = (1 - v)h_{rad,a} + vh_{lw,f} - h_{lw,g} - (1 - C_e v)h_{evap,f} - (1 - C_e v)h_{conv,g} - h_{ro} \quad (3.3)$$

where $h_{net,g}$ is the net heat stored by the ground, and $h_{evap,g}$ and $h_{conv,g}$ are the evaporative and convective heat fluxes, respectively, from the portion of ground not covered by the canopy. The coefficient C_e has been introduced to allow for evaporation and convection to occur for bare soil under a dense canopy; a C_e value of less than 1.0 gives non-zero evaporation for a fully dense canopy with $v = 1$ (Herb et al., 2006, 2008). While soil evaporation and convection were assumed negligible for a completely dense canopy ($v = 1$), allowing some soil evaporation to occur results in greater accuracy of surface temperature simulations for land cover types involving a dense canopy underlain by bare soil, as is commonly the case for agricultural land uses (Herb et al., 2006). The soil convection and evaporation terms are evaluated with equations for a bare soil surface and thus do not use the canopy air temperature or humidity. The loss of accuracy by not using the canopy air parameters is moderated by the small value of the soil evaporative

and convective fluxes for most cover types. That canopy air temperature and humidity do not have to be measured or calculated is attractive.

The complete set of equations used to evaluate all ground and canopy heat flux terms is given by Herb et al. (2006, 2008); an abbreviated description can be found in Appendix A.

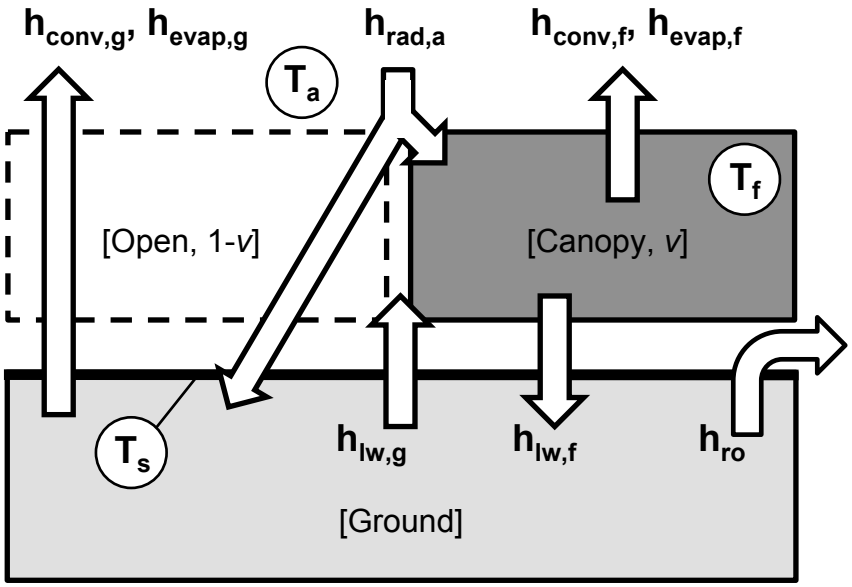

Figure 3.3: Schematic of wet-weather heat fluxes across a ground surface covered by a vegetation canopy (Best, 1998). Heat flux terms are used in Eqs. 3.2 and 3.3. T_a is air temperature, T_f is the foliage (canopy) temperature, T_s is the ground surface temperature, and v is the canopy density factor, which is used to weight heat fluxes across the ground surface.

Sub-surface Temperature Model

Simulating soil temperature as a function of depth below the ground surface is crucial for accurately predicting surface temperatures and for determining heat flux into an overlying water layer (h_{ro}). In the sub-watershed model, heat transfer within the sub-surface is assumed to occur by conduction in the vertical direction only. The vertical soil temperature profile can be determined using an unsteady heat storage-diffusion equation:

$$\frac{\partial T}{\partial t} = \frac{\partial}{\partial z}\left(D_p \frac{\partial T}{\partial z}\right) \tag{3.4}$$

where soil temperature T is a function of depth z and time t, and D_p is the effective thermal diffusivity of the soil or other sub-surface material. The value of thermal diffusivity is modified based on soil water content according to Ochsner et al. (2001).

MINUHETs default values of the thermal properties (heat capacity and thermal diffusivity) of soil, concrete, and asphalt pavements were determined from calibration of the surface and sub-surface temperature models to temperature profile data acquired for these three surface types. The soil temperature data came from a long-term study site at the St. Paul, MN campus of the University of Minnesota, while the pavement data was acquired from a MN DoT pavement research facility (MnRoad) in Albertville, MN. The influence of these thermal properties on simulation results is addressed in Section 3.6.

Roof Temperature Model

Commercial rooftops can make an appreciable contribution of heat to storm water runoff (Chapter 1; Janke et al., 2011). The flat tar-and-gravel rooftops typical of commercial buildings can store enough heat during dry-weather to maintain high temperatures well after the onset of rain. The heat storage capacity of commercial roof can be considerably higher than that of asphalt-shingled (residential) rooftops in the Upper Midwest. Commercial rooftops need to be taken into account in the sub-watershed model.

The MINUHET model simulates rooftops in the same way as land surfaces (Herb et al., 2009a). Atmospheric heat fluxes are calculated for an impervious surface (Eq. 3.3 with $v = 0$), and heat transfer between the rooftop and runoff is determined using the thickness of the rooftop in place of the heat penetration depth δ (Section 3.3.2). The net heat flux serves as the heat input to the rooftop, which is treated as one layer with a single temperature and with a composite mass (per unit area) and heat capacity determined from the properties of the roof materials. Heat transfer at the underside of the rooftop is neglected. The rooftop heat budget is given by

$$\frac{\partial T}{\partial t} = \frac{h_{net,g}}{\rho C_{p,r} m} \tag{3.5}$$

where m is the mass of the roof per unit surface area, heat capacity ($\rho C_{p,r}$) is the composite value determined from the roof structure and materials, and $h_{net,g}$ is the net heat flux from the atmosphere and runoff.

Runoff Model

A model for estimating runoff flow rate and runoff temperature from a variety of surfaces was developed for MINUHET. This model is nearly identical to that described in Janke et al. (2009, see also Chapter 2) for the heat flux calculations, but the two differ slightly in the approach used to determine runoff flow rate: Janke et al. (2009) solves a 1-D kinematic wave model using a numerical approach, while MINUHET solves the kinematic wave equation using a simpler, semi-analytic approach. A comparison of the two models in Section 3.5.1 justifies the use of the simpler runoff formulation of MINUHET.

Runoff Model: Hydrology

Both MINUHET and the model of Janke et al. (2009) make use of the kinematic wave approximation for sheet flow, i.e. that pressure effects on surface runoff are insignificant and that acceleration is negligible due to friction, and thus the momentum balance can be simplified into a balance of the friction and gravity forces ($S_f = S_o$). This assumption also allows Mannings equation to be used with the water depth y as the hydraulic radius R and the surface slope S_o in place of the friction slope S_f:

$$q = \frac{S_0^{1/2} y^{5/3}}{n} \tag{3.6}$$

where n is the Mannings roughness coefficient, and q is the per-width flow rate. Mannings equation provides flow on a per-unit-width basis and therefore requires that the catchment can be defined in terms of a characteristic length and width, i.e. the catchment is roughly rectangular in shape. The catchment should also be small enough, e.g. the size of a parking lot, such that the slope and surface roughness are relatively uniform.

The unsteady runoff mass balance, which neglects lateral inflows, is identical for the two runoff models (Chapter 2; Herb et al., 2009b):

$$\frac{\partial y}{\partial t} + \frac{\partial q}{\partial x} = i \tag{3.7}$$

where y is water depth and q is per-width flow rate, which are both functions of time t and position x along the surface, and i is the excess rainfall intensity (rainfall minus infiltration and evaporation). Substituting Mannings equation (Eq. 3.6) into this equation provides a convenient form of the kinematic wave equation.

The primary difference between the two models lies in the techniques used to solve the governing equations. While Janke et al. (2009) use a numerical solution of the kinematic wave equation for flow rate as a function of time and position along the runoff surface, MINUHET does not solve the kinematic wave equation directly, instead using a semi-analytic approach based on characteristics of kinematic runoff (Herb et al., 2009b). The solution process for both models is compared in more detail in Section 3.4.

Runoff Model: Heat Transfer

The surface heat budget for a wet surface (Eq. 3.3) includes a term h_{ro} for the heat flux by conduction from the ground surface to runoff (water) above it. This term is calculated based on the assumption that during any time step Δt, the runoff temperature T_{ro} will be equal to the surface temperature T_s (Figure 3.4). For this equilibrium to occur, heat addition by the rainfall, which is assumed to fall at dew point temperature, has to be balanced by heat extracted from the sub-surface; the depth δ from the surface over which heat can be extracted is estimated from the thermal diffusivity D of the sub-surface material and the length of the time step Δt (Eq. 2.12; Eckert and Drake Jr., 1972).

It is also assumed that the runoff water layer is well-mixed, i.e. it has a single temperature. With these assumptions the equation for the runoff heat flux can be written as

$$h_{ro} = i\Big(\rho C_p\Big)_w\Big(T_s - T_{dp}\Big) = -\frac{\delta}{2\Delta t}\Big(\rho C_p\Big)_s\Big(T_s - T_{so}\Big) \tag{3.8}$$

where T_s is the runoff temperature (surface temperature) at time $t + \Delta t$, T_{so} is the

initial surface temperature at time $t = t_0$, T_{dp} is the dew point (rainfall) temperature, i is the precipitation intensity, and $(\rho C_p)_w$ and $(\rho C_p)_s$ are the heat capacity for the water layer and sub-surface, respectively.

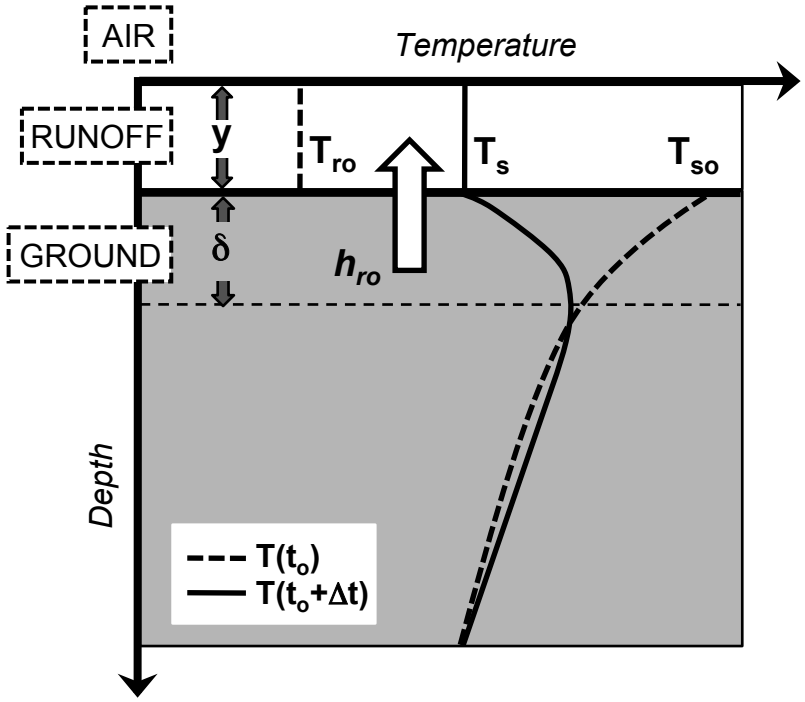

Figure 3.4: Schematic of ground temperature profiles at two consecutive instances of time (t and $t + \Delta t$) used to determine the heat transfer rate h_{ro} between the ground surface and the runoff water layer above it (Herb et al., 2009b).

Infiltration and Soil Moisture Model

Infiltration can appreciably reduce runoff volume from pervious surfaces. Infiltration is included in MINUHET by using the Green-Ampt model, which tracks the downward propagation of a wetting front, defined as the boundary between soil with some pre-rainfall moisture content θ_i and soil that has become saturated as water infiltrates from the top of the soil column (Mays, 2001; Chow et al., 1988). The cumulative infiltrated water depth F is determined from the product of L, the depth of the wetting front, and $\Delta\theta$, the difference in soil moisture between the initial state θ_i and the fully saturated

state θ_s, which is approximately equal to soil porosity η although some air remains trapped even in a saturated soil. Darcys law is used to give an expression for the infiltration rate f:

$$f = \frac{dF}{dt} = K_{hs}\left(\frac{\psi\Delta\theta + F}{F}\right) \tag{3.9}$$

where K_{hs} is saturated hydraulic conductivity and ψ is the soil suction head at the wetting front, which has been determined experimentally by Rawls et al. (1983) for a range of soil textures using the Brooks-Corey equation (Chow et al., 1988). This equation can be integrated to give a non-linear expression for F as a function of time. Given the dependence of the Green-Ampt method on initial soil moisture and saturated hydraulic conductivity (a parameter that can vary over orders of magnitude), MINUHET runoff results from pervious surfaces will be sensitive to the choice of these parameters.

MINUHET also includes a soil moisture model, which is necessary for the accurate prediction of land surface temperatures in a continuous analysis but is less critical when using the model to analyze single rainfall events. In the latter scenario, the specification of initial soil moisture becomes crucial to the calculation of runoff volume due to its impact on infiltration rate.

Details of the soil moisture model are given in Herb et al. (2009a) and Wilson (2005). In general, the transport of moisture in the soil column is governed by an equation that assumes an exponential decay of percolation D_i from a given layer i to the layer below it, similar to the approach used by SWAT (Neitsch et al., 2005):

$$D_i = \Big(\theta_i - \theta_{fc}\Big)\Delta z_i\Big(1 - exp\Big(-\Delta t/\tau\Big)\Big) \tag{3.10}$$

where Δz_i is the thickness of soil layer i, and τ is a time constant representing the residence time of water in the layer, determined from soil moisture content, layer thickness, and the hydraulic conductivity of the layer K_h. This formulation implies that percolation can only occur when moisture content exceeds field capacity.

The hydraulic conductivity can be determined by applying the Brooks-Corey relationship to the definition of relative hydraulic conductivity, and assuming that residual moisture content θ_i is negligible relative to actual moisture content θ and to saturated moisture content θ_s (Wilson, 2005). The resulting equation is:

$$K_h = K_{hs}\left(\frac{\theta}{\theta_s}\right)^{2b+3} \tag{3.11}$$

where b is the Brooks-Corey factor (the inverse of the pore size distribution parameter λ; see Rawls et al., 1989; Wilson, 2005). Soil moisture content is then updated for each layer as the simulation progresses based on the balance of evapotranspiration, infiltration and percolation rates. Water withdrawal from the soil for transpiration by plants is distributed over all layers within the root depth, weighted by the available moisture of the layer, i.e. the moisture in excess of the wilting point.

Mixed Surface Modeling

Urban land use, and ground surfaces of residential areas in particular, can be highly heterogeneous, and modeling each cover type (e.g. rooftop, lawn, driveway) as a separate sub-watershed element would be tedious. MINUHET therefore allows the sub-watershed model to partition the land surface into five categories of cover type: (1) connected pavement, (2) disconnected pavement, (3) rooftop that drains onto connected pavement, (4) rooftop that drains onto pervious area, and (5) pervious land cover (Figure 3.5). This scheme allows a single drainage area of mixed land use, as opposed to a separate sub-watershed for each land classification.

The shape or relative location of the surface types is not included. The connected pavement and pervious land areas are represented only by a characteristic length and total area (Herb et al., 2009a). The length can be varied to modify the time of concentration for a surface, which may be important for areas with non-uniform shapes.

For a selected rainfall event, the MINUHET model determines a time series of runoff flow rates and runoff temperatures for both the connected pavement and the pervious area of each sub-watershed. These two time series, also known as thermo-hydrographs, are then combined at the sub-watershed outlet using a simple mixing scheme as shown in Figure 3.6 (Herb et al., 2009a). This is similar to the approach used in the model TURM (Thompson et al., 2008).

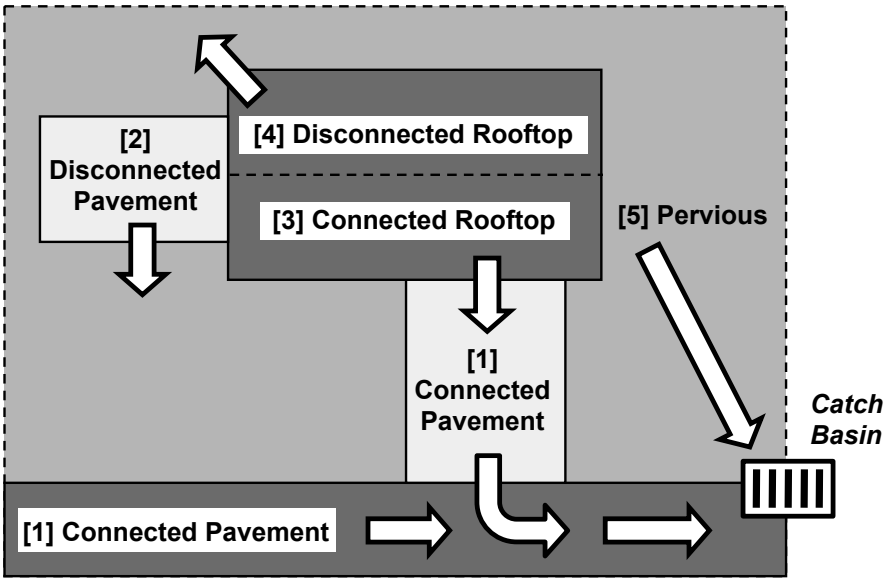

Figure 3.5: Schematic of land-surface showing the partitioning and hydraulic connectivity of a developed residential sub-watershed (Herb et al., 2009a). Five general land-surface types are considered.

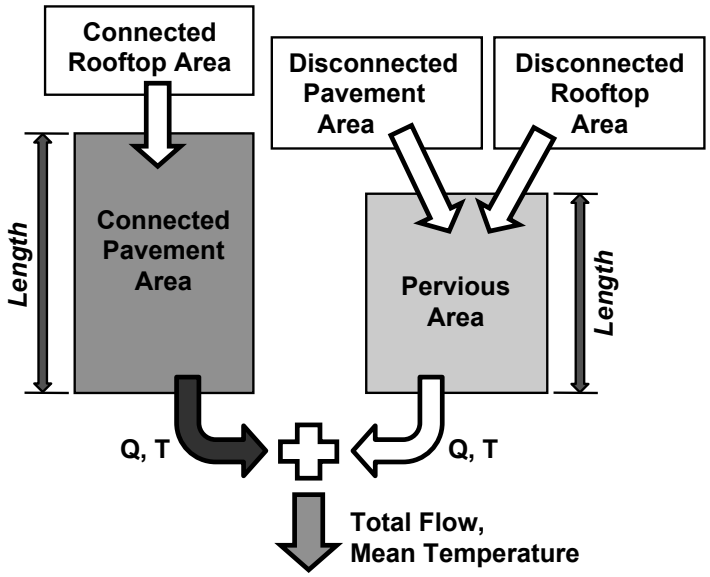

Figure 3.6: Flow chart for modeling of runoff flow rate Q and runoff temperature T at the outlet of a sub-watershed with five surface types (Herb et al., 2009a); see Figure 3.5. Thermo-hydrographs, or time series of Q and T, are produced separately for the paved and pervious portions of the sub-watershed and then mixed at the outlet.

3.3.3 Routing Models

Each sub-watershed model produces a time series of runoff flow rates and runoff temperatures for a rainfall event. The MINUHET model is designed such that a sub-watershed cannot drain to another sub-watershed. Instead, a routing element serves to move water and heat towards the outlet of the modeled catchment. Hydrologic and heat transfer processes must be accurately modeled by the routing components, mostly storm sewers and open channels.

Flow Routing Model

In urban areas, most surface runoff is routed into catch-basins, which drain directly to the underground storm sewer pipe system or to open channels. MINUHET routes water through these components using a kinematic wave model. The governing equation is a combination of an unsteady version of the continuity equation and Mannings equation (Chow et al., 1988; Herb et al., 2009a):

$$\frac{\partial Q}{\partial x} + \alpha\beta Q^{\beta-1}\frac{\partial Q}{\partial t} = q_l \tag{3.12}$$

where Q is the volumetric flow rate, q_l is the lateral inflow rate, x is the stream-wise coordinate. α and β are defined using Mannings equation, and are functions of surface roughness n, slope S_0, and wetted perimeter P of the pipe or channel.

Assumptions made for the routing model should be noted. First, lateral inflows are neglected; in the case of storm sewer pipes this reflects reality since each pipe segment is analyzed separately; in the case of open channels some error may be introduced if the open channel sections are relatively long or happen to receive significant overland runoff. A second limitation is that no backwater effects are modeled, because a kinematic wave model is used. However, a backwater effect can be modeled by placing a pond element upstream of a pipe or channel segment.

Infiltration from pervious open channels is calculated the same as in the sub-watershed model itself (Section 3.3.2). Infiltration is determined for each time step, and subtracted from the flow at the outlet of the channel. Cumulative infiltration depth is calculated separately for each pervious channel element.

Heat Transfer in Pipes and Open Channels

Heat transfer is included in the routing models. For both pipe and open channel routing elements, temperature at the downstream end of the element is calculated - after the flow has been determined - using the following heat balance:

$$\frac{\partial}{\partial t}(V * T) = Q_{in}T_{in} - Q_{out}T + h_a BL + h_{cond} \tag{3.13}$$

where V is water volume in the pipe or channel segment, Q_{in} and Q_{out} are the flows into and out of the segment, respectively, T_{in} is the inflow temperature, h_a is the net atmospheric heat flux across the water surface (for open channels only), B is the water surface width, L is the segment length, T is the volume-weighted water temperature, and h_{cond} is a term to describe the conduction of heat between the stormwater and the pipe wall or open channel.

Heat exchange across the water surface of open channels is calculated as in the sub-watershed runoff model (Section 3.3.2), using the volume-weighted water temperature in the reach as the surface temperature T. Heat conduction h_{cond} between a channel and the surrounding soil is calculated by multiplying the thermal conductivity of the soil k_s by the value of the temperature gradient in the immediate sub-surface over a depth δ, the heat penetration depth for the soil (Eq. 2.12). The sub-surface temperature model for the channel is the same as that used for the sub-watershed model (Section 3.3.2), with the channel water temperature T from the previous time step serving as the upper boundary condition.

For storm sewer pipes, h_{cond} is determined using $h_{cond} = H_w A_w(T_{pw} - T)$, where T_{pw} is the pipe wall temperature, A_w is the wetted area of the pipe or channel, and H_w is a wall heat transfer coefficient. H_w is calculated at each time step using $H_w = 3k/\delta$ (Eckert and Drake Jr., 1972), where k is a composite thermal conductivity of the pipe wall and surrounding soil over the heat penetration depth δ, which is determined using the thermal properties of both the pipe material and soil in Eq. 2.12.

Pipe wall temperature at the onset of rainfall is assumed equal to soil temperature at the depth of the pipe, estimated using a cosine function describing soil temperature as a function of day of the year and of depth below the surface. This function is determined from soil temperature data taken in Saint Paul, MN (Herb et al., 2006).

3.3.4 Detention Pond Model

Detention basins are frequently used in new urban developments as the receiving water body for storm water management. The thermal impact of a detention pond on downstream systems relies on accurate modeling of the heat content and volume of water flowing from a pond. Therefore a detailed pond model has been developed for MINUHET, capable of simulating flow rate and temperature of outflow from a variety of pond or basin types in response to storm water inflows (Herb et al., 2009a, 2009).

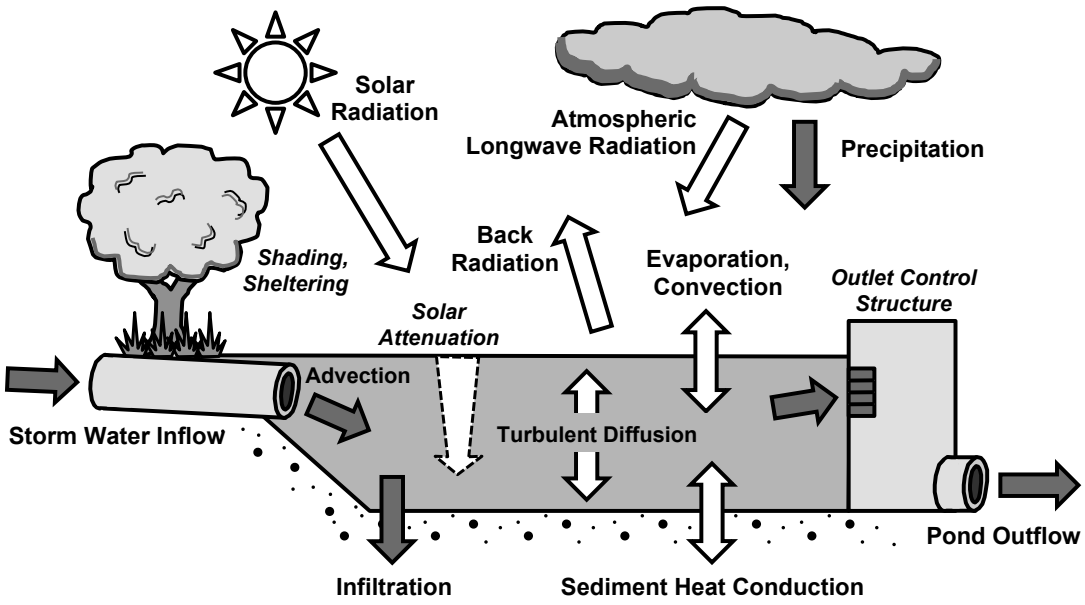

Figure 3.7: Schematic of the heat transfer processes (white arrows) and hydrologic processes (dark arrows) simulated by the MINUHET pond model (from Herb et al., 2009a, 2009).

The one-dimensional, unsteady MINUHET pond model simulates thermal stratification in response to surface heat transfer processes. Modeled heat fluxes include solar radiation, long wave radiation, convection, and evaporation at the water surface; incoming radiation attenuation with depth in the pond; advection of storm water inflows; vertical heat dispersion within the water column by turbulence, Seiche motion and natural convection; conduction to and from the pond sediments; and selective withdrawal from the stratified pond (Figure 3.7). The hydrologic portion of the pond model handles storm water inflows and outflows, infiltration through the bottom of the pond,

precipitation, and evaporation. Mixing by wind is also modeled.

The pond is modeled as a stack of horizontally uniform layers, similar to 1-D lake models (e.g. Ford and Stefan, 1980; Hondzo and Stefan, 1993). Pond bathymetry has to be specified and determines the number of layers, which are allowed to vary in thickness depending on the maximum water depth of the pond. Storm water inflows are modeled as buoyant jets, meaning they can plunge to lower layers of the pond if they have a greater density than the surface water of the pond. Entrainment effects are considered using the models of Fang and Stefan (2000, see also Herb et al., 2009).

A variety of outlet structures can be modeled, including circular ports and pipes at specified outlet elevations, and weirs (V-notch, broad-crested, and sharp-crested). Combinations of outlet types can also be modeled. The equations used to estimate outflow rate and temperature for each outlet type are given by Herb et al. (2009a).

A temperature profile within the pond water and sediment is determined by solving an unsteady, 1-D (vertical) heat transfer equation:

$$\frac{\partial T}{\partial t} = \frac{\partial}{\partial z}\left(D_z \frac{\partial T}{\partial z}\right) + \frac{S}{(\rho C_p)_w} \tag{3.14}$$

where S is an internal heat source term used to describe solar radiation absorbed by the water column as a function of depth, and D_z is the effective vertical dispersion coefficient. The value of D_z in a pond is larger than molecular diffusion, but smaller than in lakes. The heat capacity of each layer ρC_p is weighted by the volume of that layer, as prescribed by the pond bathymetry. Conductive heat transfer in the sediments below the bottom of the pond is also modeled. The lower boundary condition is a constant temperature (mean annual air temperature) at a depth of 10 m below the water-sediment interface (Herb et al., 2009a).

Vertical convective mixing due to density instabilities in the water column is also modeled: a layer mixes with the one below it if it has a greater density, e.g. due to surface cooling, producing a single layer with volume-averaged temperature. A surface mixed layer depth is also calculated based on a balance between kinetic wind energy acting at the pond surface and the potential energy of stable temperature stratification (Ford and Stefan, 1980; Herb et al., 2009). The temperature profile of the pond is calculated in 15-or 60-min time steps.

The MINUHET pond model can be used for either a continuous or event-based analysis. An empirical equation that produces a pond surface and pond bottom temperature as a function of calendar day is used for the pond temperature initialization, and the sediment temperatures are initialized as in the sub-surface model. The pond is simulated using two weeks of antecedent dry-weather data prior to the rainfall event to prime the model for the rainfall event.

The model was developed for a wet detention pond, but can be applied to an infiltration basin or a dry pond by setting the initial water level to zero and treating the pond as a bare soil surface for the antecedent period in order to initialize soil temperature and moisture conditions.

A full description of the equations used in the pond model can be found in Herb et al. (2009a). Herb et al. (2009) present a sensitivity analysis of the model to input parameters, as well as a case study in which the model was applied to a storm water detention pond in Woodbury, MN. The potential mitigating effect of a pond on the temperature and volume of storm water flow from an urban catchment is illustrated.

3.3.5 Other Storm Water BMP Models

MINUHET has the ability to model the mitigation provided by underground storm water storage vaults and rock-filled trenches. Rain gardens can be simulated by use of the infiltration basin model (a special case of the pond model).

Underground Storm Water Storage Vault

Vaults are usually constructed from prefabricated modules, e.g. large sections of corrugated metal pipes. They are buried underground, may be filled with rock, usually have a single inlet, and some inflow and outflow control. A schematic of an underground storm water storage vault is shown in Figure 3.8. The level at which water is withdrawn from the vault is the outlet control; this level is often higher than the bottom elevation to allow some water to remain in the vault, which will cool between events before mixing with warmer runoff from the next event, providing further mitigation. Outflow is calculated using the same approach as for the pond model (Herb et al., 2009). Inflow is restricted either when the vault is filled, or if the inflow rate exceeds some specified

threshold value. In the model, excess flow is routed past the vault inlet, where it is added to the vaults outflow.

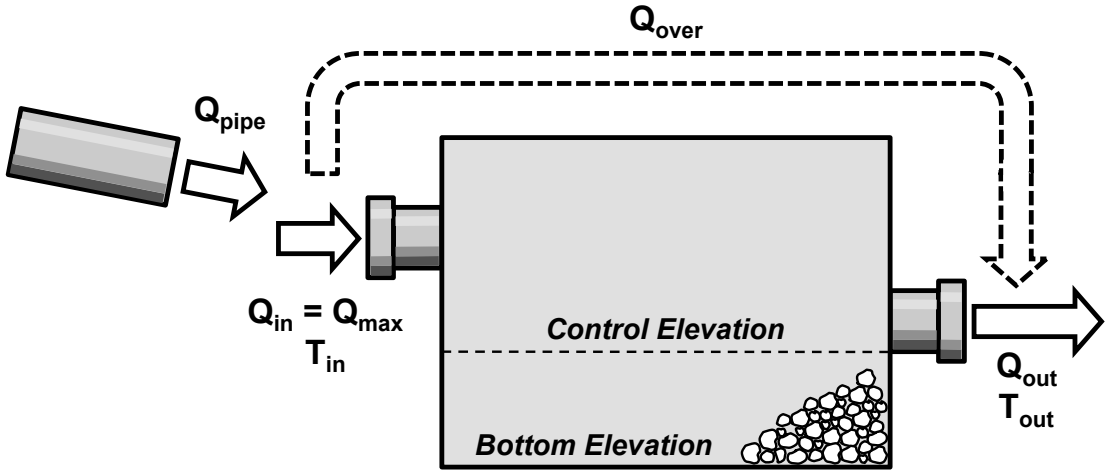

Figure 3.8: Schematic of an underground storm water detention vault. Q_{over} is the excess flow when the flow delivered by the upstream storm sewer (Q_{pipe}) exceeds the inflow capacity of the vault (Q_{max}).

Water in the vault is assumed to be well-mixed, and characterized by a single temperature T_w. The temperatures of the rock fill (T_r) and of the water are tracked in unsteady heat budget equations written for the water volume and for the rock, respectively (Herb et al., 2009):

$$\frac{\partial}{\partial t}(V_w T_w) = Q_{in}T_{in} - Q_{out}T_{out} + \frac{h_r A_{rw}(T_r - T_w)}{(\rho C_p)_w} + \frac{h_s A_{ws}(T_s - T_w)}{(\rho C_p)_w} \tag{3.15}$$

$$V_r \frac{\partial T_r}{\partial t} = \frac{h_r A_{rw}(T_w - T_r)}{(\rho C_p)_r} + \frac{h_s A_{rs}(T_s - T_r)}{(\rho C_p)_r} \tag{3.16}$$

where V_w is the volume of water in the tank, V_r is the volume of rock, Q_{in} is the inflow, Q_{out} is the outflow, T_s is the soil (tank wall) temperature at the tank depth, A_{rw} is the rock surface area in contact with the water, A_{ws} is the surface area of water in contact with the tank wall, A_{rs} is the surface area of rock in contact with the wall, h_r and h_s are heat transfer coefficients for the rock and for the soil, respectively, and

$(\rho C_p)_w$ and $(\rho C_p)_r$ are the heat capacity of the water and rock, respectively. Rock fill is specified by a volume fraction of the vault and an average diameter. Heat exchange between the rock and water in the vault with the soil outside the vault is slow, and needs to be considered only to simulate rock and water temperatures between rainfall events, i.e. for a continuous analysis.

Rock-filled Trenches

Trenches consist of an excavated channel filled with rock, and are used as a storm water BMP in place of an open channel routing element or at the outlet of a catchment. They are similar to storm water vaults, except that they have no outflow control and drain between rainfall events, i.e. they have no standing water.

Heat transfer within the rock-filled trench is modeled using the same equations as for the storm water vault (Eqs. 3.15 and 3.16). The continuity equation for the reach is given by:

$$\frac{\partial A}{\partial t} + \frac{\partial Q}{\partial x} = 0 \tag{3.17}$$

where A is the cross-sectional area of the water, and Q is the volumetric flow. This equation provides a flow solution as a function of time and distance along the trench, which allows calculation of longitudinal water temperature gradients in the trench.

The flow through a trench is modeled using an approach developed by Barr (2001) that allows the flow velocity to be restricted by the presence of rock. A characteristic velocity is calculated as a function of the slope and hydraulic radius of the trench, and of the porosity of the rock fill. Laminar flow is initially assumed, allowing Darcy's equation to be used for computing flow resistance; if turbulent flow is present, a different equation is used. Once the characteristic velocity has been calculated, continuity can be used to determine the flow depth as a function of distance along the trench. Infiltration, computed via the Green-Ampt method, can also be included. See Herb et al. (2009a) for the full set of equations.

3.4 Numerical Model Implementation

The governing equations for the heat and water (mass) balances for the components of the MINUHET model were generally solved using numerical methods. The general approach was to first discretize the balance equations in space and time, and move the solution forward from some initial state by using a time step that varied depending primarily on the presence of surface runoff, the resolution of weather data, and the desired resolution of the results. The details of the solution process and the discretized versions of the balance equations are presented in Herb et al. (2009a); the numerical solution techniques employed by each MINUHET component are described briefly here.

Canopy Heat Budget

The primary unknowns in the set of equations for the canopy surface heat budget (Eq. 3.2) include the canopy temperature (T_f) and the surface temperature (T_s). All other variables are a function of weather parameters or of physical characteristics of the land surface and canopy. The solution process begins with T_f, which is first linearized in the long wave radiation terms, then solved for explicitly using T_f and T_s from the previous time step. Next, the components of the ground heat budget equation (Eq. 3.3) can be evaluated to provide a net ground heat flux ($h_{net,g}$), which is used to update the sub-surface temperatures and the runoff heat flux (h_{ro}). Soil moisture is also updated based on calculations of canopy and soil evaporation, as well as infiltration (if applicable).

Sub-surface Heat Diffusion Equation

The heat diffusion equation (Eq. 3.4) used in the sub-surface temperature model is solved with a finite difference approach that divides the soil column into multiple horizontal layers (Herb et al., 2009a). The boundary condition at the top layer is the net heat flux $h_{net,g}$ from the surface temperature model (Eq. 3.3), and the lower boundary condition is a specified temperature (e.g. mean annual temperature at that depth). The bottom temperature is constant for the analysis of a single rainfall event, but for analyses over longer durations its seasonal variability is accounted for by an empirical equation specific to the land use (Herb et al., 2009a). The total depth of the soil column is also dependent on the time period of analysis. A depth of 1 m is used for analysis

of a single rainfall event since temperature at this depth remains roughly constant over the course of a week, but a deeper soil column is needed for a continuous simulation or an analysis of a series of events. Herb et al. (2006) used a depth of 10 m for seasonal simulations of surface temperatures.

Roof Heat Budget Equation

The heat budget equation for the rooftop (Eq. 3.5) is discretized using the temperature derivative of atmospheric heat exchange ($\partial h_{net,g}/\partial t$), which is calculated from values of temperature and climate variables in the previous time step. The use of the derivative makes the solution more robust, since the relatively small mass of the rooftop (particularly for the residential rooftop) can cause instabilities in the solution.

Runoff Models

The hydrologic balance equations for the runoff model are presented in Section 3.3.2 for both MINUHET and the model of Janke et al. (2009; Chapter 2). The approach of Janke et al. (2009) is to solve the kinematic equation numerically, producing a runoff solution as a function of time and position along the runoff surface; this approach divides the surface into a series of in-line cells of unit width and length Δx, with the final cell producing the outflow for the surface. For further details, see Section 2.2.1.

By contrast, MINUHET does not solve the kinematic wave equation directly, and instead uses an analytical approach that assumes the water depth profile on a surface of length L can be divided into two portions: one from the upstream end ($x = 0$) to some point $x = L_e$ along which equilibrium flow exists and runoff depth varies with distance x, and a second portion (from $x = L_e$ to the outlet at $x = L$) over which flow depth y is constant (Figure 3.9). The equilibrium length L_e can be described as a function of rainfall intensity i and of the time to equilibrium t_c by using Manning's equation and assuming a steady-state mass balance (Mays, 2001; Herb et al., 2009b):

$$L_e = \frac{S_0^{1/2} i^{2/3} t_e^{5/3}}{n} \tag{3.18}$$

L_e generally increases as a rainfall event progresses, and can span the entire length of the runoff surface for long events.

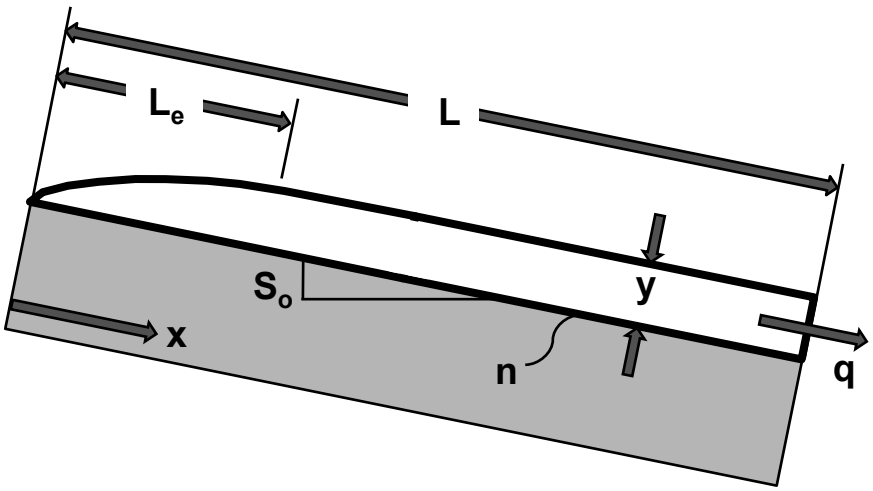

Figure 3.9: Schematic of the semi-analytic approach to modeling runoff depth on a planar surface (from Herb et al., 2009b). Runoff varies from a depth of 0 to a depth of y at the equilibrium distance $x = L_e$. Along the remaining length of the surface, runoff has a constant depth y.

The runoff mass balance (Eq. 3.7) can be simplified when considering the entire length of the surface. The time rate of change in water storage v on the pavement is equal to the balance of rainfall input $i * L$ and the outflow rate q_L:

$$\frac{dv}{dt} = iL - q_L \tag{3.19}$$

A forward-difference discretization of the mass balance provides an estimate of the runoff volume at some incremental time $t + \Delta t$:

$$v(t + \Delta t) = v(t) + iL\Delta t - \frac{\Delta t}{2}\Big(q_L(t) + q_L(t + \Delta t)\Big) \tag{3.20}$$

Using Manning's equation and the steady-state flow rate q (given by $i * L$), the volume of water on the pavement v can also be found as a function of the equilibrium length L_e and water depth y over the constant-depth portion of the lot:

$$v(t) = y(t)\left(L - \frac{3}{8}L_e(t)\right) \tag{3.21}$$

Manning's equation can be used to eliminate y from Eq. 3.21, yielding a form of

$v(t + \Delta t)$ in terms of $q_L(t + \Delta t)$ and L_e that is substituted into Eq. 3.20. A Taylor series expansion is then used to linearize Eq. 3.20 to allow it to be solved explicitly for q_L at time $t + \Delta t$. The effect of time-variable rainfall intensity is incorporated by using a running average of rainfall intensity and allowing it to vary between solution steps. The full set of runoff equations and a description of the solution process are given by Herb et al. (2009b).

Calculation of the surface-runoff heat flux h_{ro} (Eq. 3.8) does not require a special solution technique, but its value is dependent on the choice of time step Δt since it is based on an equilibrium between the precipitation added and the heat extracted from the ground over the time period during Δt. The net heat flux across the ground surface $h_{net,g}$ (Eq. 3.3) is calculated in each time step, and a new sub-surface temperature profile is determined after each time step.

Infiltration and Percolation Equations

In the soil moisture model, the soil column is modeled as a series of uniform, horizontal layers, each with a thickness (Δz) of 0.5 m, which is a coarser resolution than used in the sub-surface temperature model. No special techniques are required for solving the percolation equation (Eq. 3.10); however, infiltration depth F is determined from a linearized version of the Green-Ampt infiltration equation (Eq. 3.9), as given by Li et al. (1976, see also Wilson, 2005; Herb et al., 2009a).

Flow Routing Model

The kinematic wave equation (Eq. 3.12) used for routing flow through sewer pipes and open channels is discretized using an implicit, forward-difference scheme, as given by Chow (1964). The reach is treated as a series of inline cells, with infiltration, evaporation, and lateral inflows accounted for in each cell. Newton's method is used to solve the wave equation, with the solution progressing from the upstream to the downstream end of the pipe or reach for each time step. An initial guess at the flow into the next downstream cell is provided by a linearized version of the flow equation (Chow, 1964).

The heat budget for the reach (Eq. 3.13), which is written for the entire reach rather than for each cell, is solved using an explicit forward-difference approach and a

reach-averaged water temperature. The full set of discretized equations for the routing model is described in Herb et al. (2009a).

Pond Heat Budget Equation

In the pond model, the heat conduction equation (Eq. 3.14) is solved using an implicit, central-difference scheme to calculate a temperature profile in the water column. The upper boundary condition for the pond is the net atmospheric heat transfer, calculated using the same equations as for the runoff model. The lower boundary condition is a constant temperature (mean annual air temperature) at a depth of 10 m below the water-sediment interface. Additional details of the solution process can be found in Herb et al. (2009a).

Storm Water Vault and Rock Crib Models

The coupled equations (Eqs. 3.15 and 3.16) used to model heat routing through the storm water vault are discretized using a forward-difference method and the previous value of the rock temperature T_r. Once the new water temperature T_w is acquired, the rock temperature is updated for the time step.

The rock-filled trench is modeled by dividing its length into a series of cells, and within each cell the heat budget employed in the vault model is used to determine rock and water temperatures. The flow equation (Eq. 3.17) is solved using an implicit forward-difference method to find the volume of water in each cell, which is used in the heat budget equations.

3.5 Model Application

Two applications of the MINUHET model are presented here: an asphalt-paved parking lot in Minneapolis, MN, and a residential development in Plymouth, MN. In the first application, simulations by MINUHET and by the runoff model of Janke et al. (2009, Chapter 2) are compared to measurements of runoff flow rate and temperature for a rainfall event. This case study is intended to illustrate that the simpler solution technique employed by MINUHET in the runoff model is sufficient to predict runoff flow

rate and temperature. The second case study is an application of MINUHET to a mixed-land surface watershed for which both runoff flow rate and runoff temperature data are available. Neither application is intended to provide a validation of the model, because both data sets are too small to serve this purpose. However, more rigorous validations and analyses of the various model components have been presented in previous work, including the surface/sub-surface temperature model for a variety of land cover types (Herb et al., 2006, 2008), the runoff model (Herb et al., 2009a,b), and the pond model (Herb et al., 2009). The composite model has been used in a stormwater analysis for both residential and commercial sites (Herb, 2008), in a stormwater thermal impact study for a trout stream in southeastern Minnesota (Herb and Stefan, 2008), and in the development of a temperature TMDL for a trout stream in northeastern Minnesota (Herb et al., 2009).

In both case studies, model results will be compared with observations of runoff volume and flow rate, runoff temperature, and total heat export (Eq. 3.1). Total heat export will be calculated from the time series of runoff flow rates and runoff temperatures representing the heat content of the runoff above a reference temperature (in this case 20 °C) for an entire rainfall event.

3.5.1 Case study 1: Asphalt-paved parking lot

A field study was conducted on an asphalt-paved parking lot on Nicollet Island in Minneapolis, MN, not far from the St. Anthony Falls Laboratory. Data were collected during one summer period (2007), and compared to simulation results by the MINUHET model and an earlier model (Janke et al., 2009, Chapter 2). This study was a test of the runoff component of the models for an impervious surface.

Field Study Description

The study site was a rectangular, 0.58-acre (55 m long x 42 m wide) asphalt-paved parking lot located on Nicollet Island in Minneapolis, MN. The lot has a roughly 3.4% slope from the upstream end to the outlet point, which is a 1 m-long curb cut located roughly in the middle of the downstream end. The asphalt is 6 inches thick with a gravel and soil substrate. Runoff from the parking lot discharges into the Mississippi

River, and its thermal impact is negligible. However, similar parking lots are located near trout streams in Minnesota.

A box containing a composite weir was constructed and fitted into the curb cut. A level gage (Massa Sonic) was mounted to a tripod placed in the box to measure water elevation, which was used to estimate flow rate. Water temperature recorders (Vemco Minilogs) were placed at various locations to measure runoff temperature: (1) at the inlet of the box, (2) just upstream of the box, and (3) in the gutter of the curb next to the box. These measurements were verified by temperature readings taken throughout the rainfall event with a handheld infrared thermometer, which also provided the initial pavement surface temperatures used to ensure that the simulation was properly primed. Climate data, including air temperature, dew point temperature, solar radiation, wind speed, and precipitation, were measured at 5-minute intervals at a weather station at the St. Anthony Falls Laboratory, located roughly 500 m from the study site.

The field study was conducted from July to October, 2007, which unfortunately coincided with a period of dry weather, and yielded only a few late-afternoon thunderstorms. Rainfall events in the afternoon or evening of hot, dry days are expected to result in the greatest heating of runoff by a paved surface; three such events occurred during the field study. Of these, only the August 11 event was likely to produce good results, as the other two involved such high rainfall intensities that a significant amount of runoff poured over the curb and was not measured by the weir. Additional information on the field study can be found in Chapter 2.4.

Results: Comparison of the Runoff Models

The runoff temperature model of Janke et al. (2009, Chapter 2) was previously applied to the data from the asphalt parking lot in Minneapolis on which runoff flow rate and runoff temperature had been measured. In general, the model performed well; a 0.33-cm rainfall event on August 11, 2007 was simulated with a 7% over-prediction in runoff volume and less than 1% error in volume-averaged runoff temperature, resulting in a heat export that was within 6% of the observed value for the storm.

Here MINUHET is applied to the same field study site for the August 11 rainfall event. This will serve two purposes: (1) to compare the MINUHET runoff temperature model to that of Janke et al. (2009, Chapter 2) in order to justify the use of a simpler

solution technique for the runoff calculation, and (2) to compare MINUHETs simulation output to observations of runoff flow rate and temperature for a simple watershed.

The selected rainfall event, which occurred on the evening of August 11, 2007, was ideal for application of the models due to the short duration and high temperatures involved: 0.33 cm of rain fell in roughly 20 minutes and initial pavement temperatures were high (around 40 °C), with an event mean dew point temperature of 24.5 °C, indicating that this was an event with potentially significant thermal impact.

The output of the two runoff models are compared with observations of runoff flow rate and runoff temperature for the rainfall event in Figure 3.10, with summary statistics in Table 3.1. The simulated output is after calibration, both models using the same parameter values. The calibrated values of Mannings $n = 0.013$ and surface depression storage of 0.8 mm were obtained by modifying default values until the shape of the simulated hydrographs and the total runoff volumes matched the observations as well as possible. Both values are reasonable for a paved surface (Viessman Jr. et al., 1977; Mays, 2001; Endreny, 2005). Thermal conductivity k_a and specific heat $C_{p,a}$ of the asphalt were modified in small increments until the runoff temperatures nearly matched the observations. Calibrated values ($k_a = 1.7$ W/m*K and $C_{p,a} = 1300$ J/kg*K) are within the range of published values (Incropera and DeWitt, 2002; Luca and Mrawira, 2005).

	Observed	**Model 1**	**MINUHET**
T_{ro} **Mean (°C)**	32.9	32.8	32.1
V_{ro} **Total (m^3)**	4.39	4.71	4.66
Heat Export (MJ)	278	252	254
RMSE, Q (L/s)	–	0.75	0.93
RMSE, T_{ro} **(°C)**	–	0.39	0.55

Table 3.1: Summary statistics for the Aug 11, 2007 rainfall-runoff event, as determined from observations, MINUHET (Herb et al., 2009a), and the runoff temperature model ('Model 1') of Janke et al. (2009, Chapter 2). Quantities include flow-averaged runoff temperature, total runoff volume, total heat export from the rainfall event, and RMSE between observed and modeled values of runoff flow rate and runoff temperature.

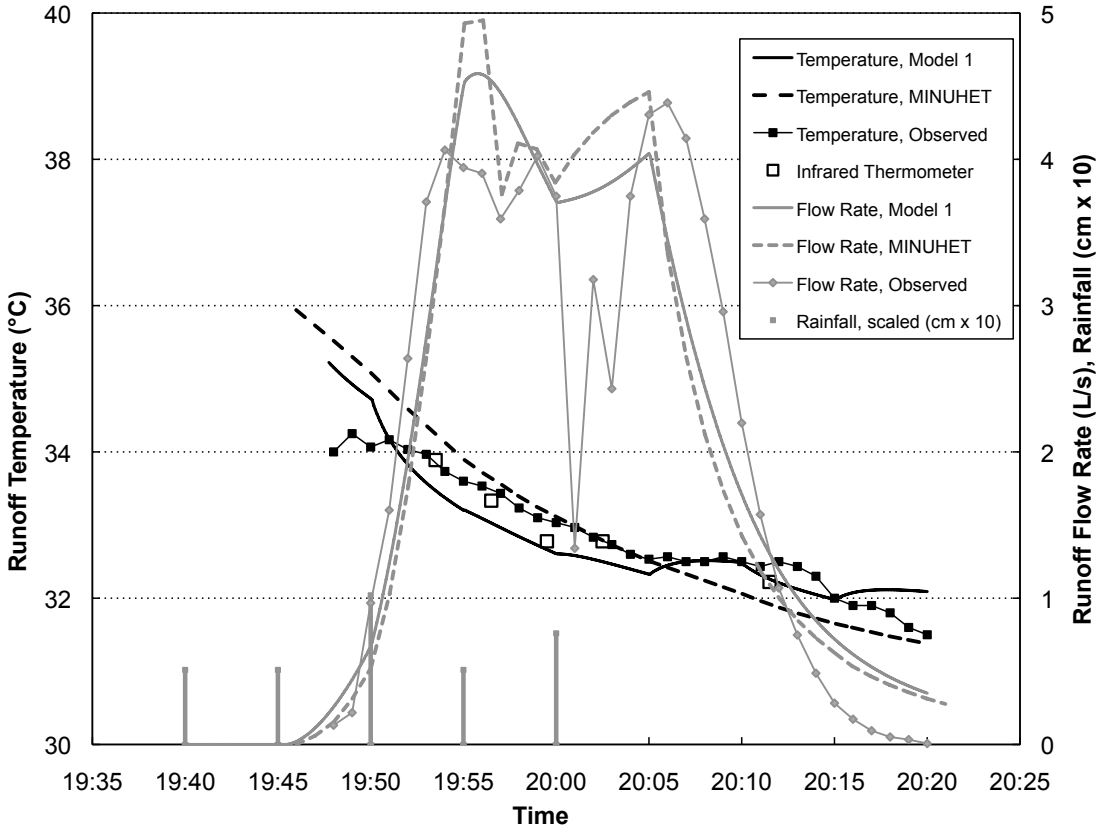

Figure 3.10: Runoff flow rate and runoff temperature from a small parking lot in Minneapolis, MN for a 0.33-cm rainfall event on Aug 11, 2007. Observations are compared with the simulations of two models: MINUHET (Herb et al., 2009a) and the runoff temperature model of Janke et al. (2009, Chapter 2), labeled 'Model 1'. Rainfall should be referenced to the right axis, and has units of cm x10.

Overall, the two models give very similar results for this particular site and event. The simulated peak flow rates are slightly higher from the MINUHET model than the other runoff model, but the rising and falling limbs of the hydrograph are nearly identical for the two models. Both models slightly over-predicted the total runoff volume, likely the result of a much more gradual recession simulated at the end of the event than was observed. RMSE values for flow rate were less than 1.0 L/s for both models.

Both models performed very well for the prediction of runoff temperature and heat export. Simulated flow-averaged runoff temperatures were within 1.0 °C of the observed value, and the RMSE values for water temperature were around 0.5 °C for both models. The models slightly under-predicted total event heat export as a consequence of under-predicting runoff temperature, but the error was less than 10%.

These results are encouraging even though they reflect the use of calibration. Unfortunately, the data set produced no other rainfall events with which to test the models and calibrated input parameters. While the runoff temperature model of (Janke et al., 2009, Chapter 2) produced slightly lower RMSE values for flow and runoff temperature than MINUHET, the differences in the solution techniques of the two models does not appear to significantly impact the results.

3.5.2 Case Study 2: Residential Site

MINUHET has also been applied to a watershed in a residential development in which runoff temperature and flow data were collected in a field study. Given the various land surfaces present in this watershed (lawns, rooftops, driveways, and roads), this case study represents an assessment of the composite MINUHET model rather than of a single component as in the first case study.

Field Study Description

The study site is located in a residential development of Plymouth, MN, a city in the Minneapolis/St. Paul metropolitan area. The sub-watershed tested has 39 houses on roughly 12.5 acres of land, of which 38% is impervious area (24% connected impervious). Construction of the development began more than 20 years ago; the area has more mature trees and vegetation than would be typically found in a new development. A schematic of the study site is shown in Figure 3.11.

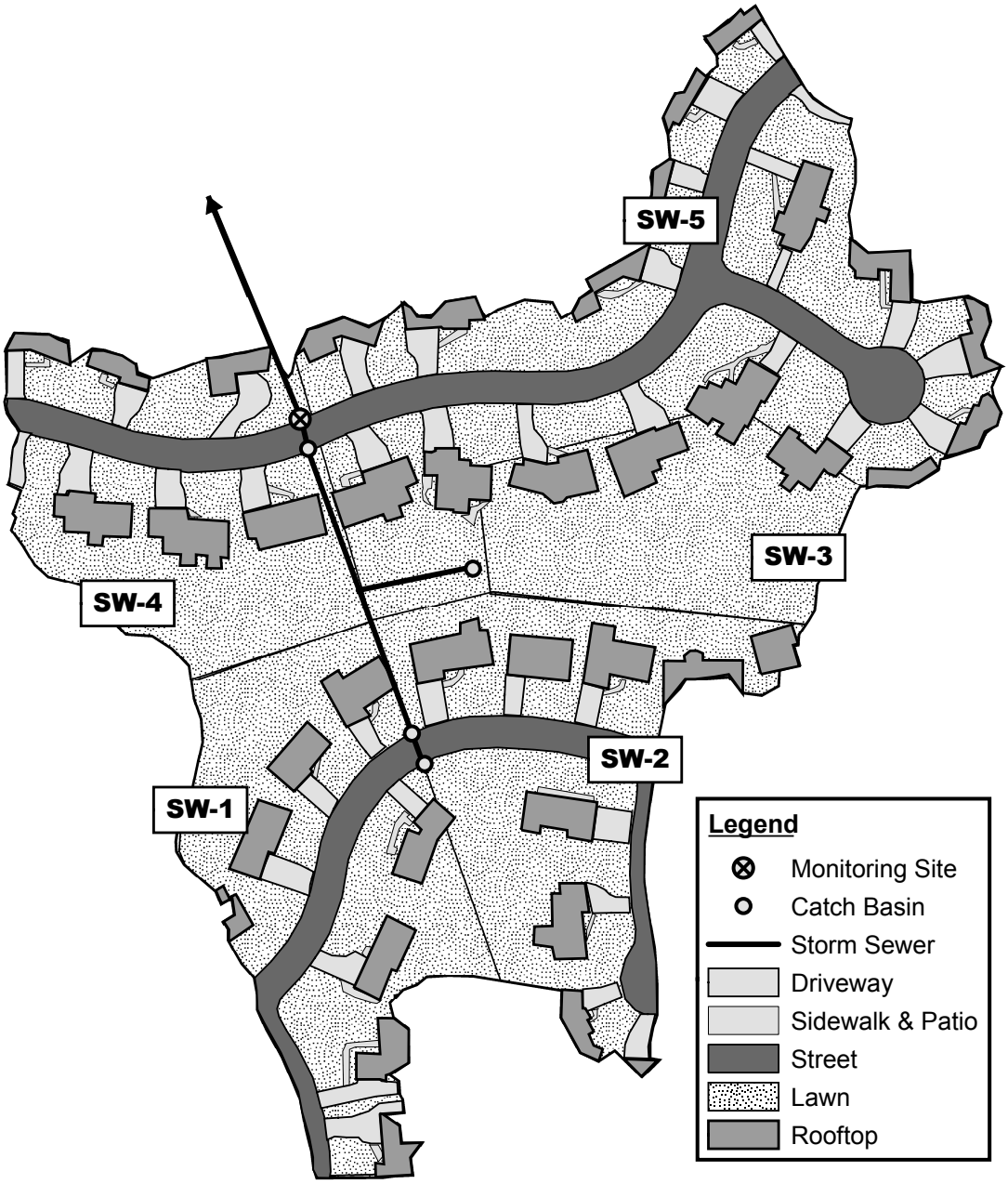

Figure 3.11: Study site, a 12.5-acre watershed located in a residential development in Plymouth, MN. A catch basin at the outlet of the development (near the top of the map) was instrumented for monitoring runoff flow rate and runoff temperature. Also shown are land cover types and sub-catchment divisions, which are used for application of MINUHET to the development.

The relatively simple configuration of the storm sewer system and the small catchment area made the site attractive for application of the model. Field surveys were conducted during rainfall and snowmelt events to delineate the watershed drainage area and partition rooftops into portions draining to lawns ('disconnected' rooftops) and portions draining to driveways and streets ('connected' rooftops). The area occupied by each surface type (e.g. lawn, street, driveway, and sidewalk) was estimated from these surveys and from aerial photography. This information was used to construct GIS data layers, which cannot yet be imported directly into MINUHET but expedite the data input process. Storm sewer plans as well as elevation contour maps for both pre-development and post-development conditions for the drainage area were provided by the city of Plymouth.

A storm sewer pipe at the outlet of the watershed was instrumented with an Isco automatic water sampler by the Three Rivers Park District from July – Oct, 2005 as part of storm water quality monitoring project. Depth of water was recorded in the sewer pipe at 1-minute intervals, and an Isco area-velocity flow module was used to develop a rating curve for flow rate in the pipe. A water temperature logger (HOBO Water Temp Pro) was used to measure storm water temperature at 1-minute intervals in the same location; it was installed in mid-July and removed on Sep 21.

Solar radiation and precipitation depth were recorded at 2-minute intervals beginning on Aug 24 at the Three Rivers Park Districts office less than 1 km from the study site. Air temperature, relative humidity, and wind speed were available at one-hour intervals from the airport in Crystal, MN, located roughly 8 km (five miles) northeast of the study site.

Unfortunately, the delayed installation of the rain gauge and pyranometer, and the removal of the temperature logger in late September made for a short (Aug 24 – Sep 20) data set available for analysis. However, several rainfall events occurred in that short interval and produced a sufficiently large data set for application of MINUHET to the catchment.

'Effective' Impervious Area Analysis

In our analysis, each rainfall depth (event) was defined as the sum of sequential precipitation that occurred with less than a one-hour gap between measured rainfall; by

this definition multiple rainfall events can occur on the same day, e.g. on Sep 12 three distinct rainfall events occurred. A total of 14 rainfall events occurred on 8 different days from Aug 24 to Sep 30, 2005, with a cumulative depth of 17.7 cm. Rainfall depths ranged from 0.48 to 5.0 cm, and rainfall intensities from 0.14 to 2.07 cm/h.

The pervious portion of the study watershed is made up entirely of lawns, most of which contain a number of mature trees. With an abstraction capacity of 0.5 to 1.5 cm for this surface type (Endreny, 2005), very little runoff would be expected to occur from the surfaces for the majority of rainfall events in the record because they were small or of light intensity. The one exception is a very large (5.0 cm) rainfall on the morning of Aug 26; 2.8 cm of rain fell in the first hour. The observed runoff volume for this event (616 m^3) exceeded the runoff volume estimated by multiplying the rainfall depth by the connected impervious area (579 m^3, assuming a 0.1 cm impervious abstraction depth), suggesting that some runoff occurred from the pervious surfaces. For this reason the event was removed from the initial analysis.

The recorded precipitation depth data and the runoff volume data were first used to determine the 'effective' connected impervious surface area in the watershed, which can be compared to that determined from GIS data. While directly connected impervious area can be defined as the sum of all sidewalk, driveway, rooftop, and street surface areas in the catchment, some of these areas (especially sidewalks and driveways) may in fact drain to a pervious area, where runoff will infiltrate or evaporate and never reach the storm sewer system. Thus the effective connected impervious area will be less than the total impervious area connected to the storm sewer system.

In several other studies, effective impervious area has been estimated by methods ranging from detailed analyses of small developments similar to the Plymouth study site (Lee and Heaney, 2003; Roy and Shuster, 2009) to an analysis of hundreds of rainfall events from dozens of catchments (Boyd et al., 1993). For the available runoff volume and precipitation data from the Plymouth, MN site we employed the approach of Boyd et al. (1993). The watershed-averaged runoff depth was plotted against the observed precipitation depth for all recorded events and a straight line was fitted to the data. The slope of this line gives an estimate of the fraction of total watershed area occupied by the effective impervious area, and the x-intercept is the initial abstraction depth of this impervious fraction.

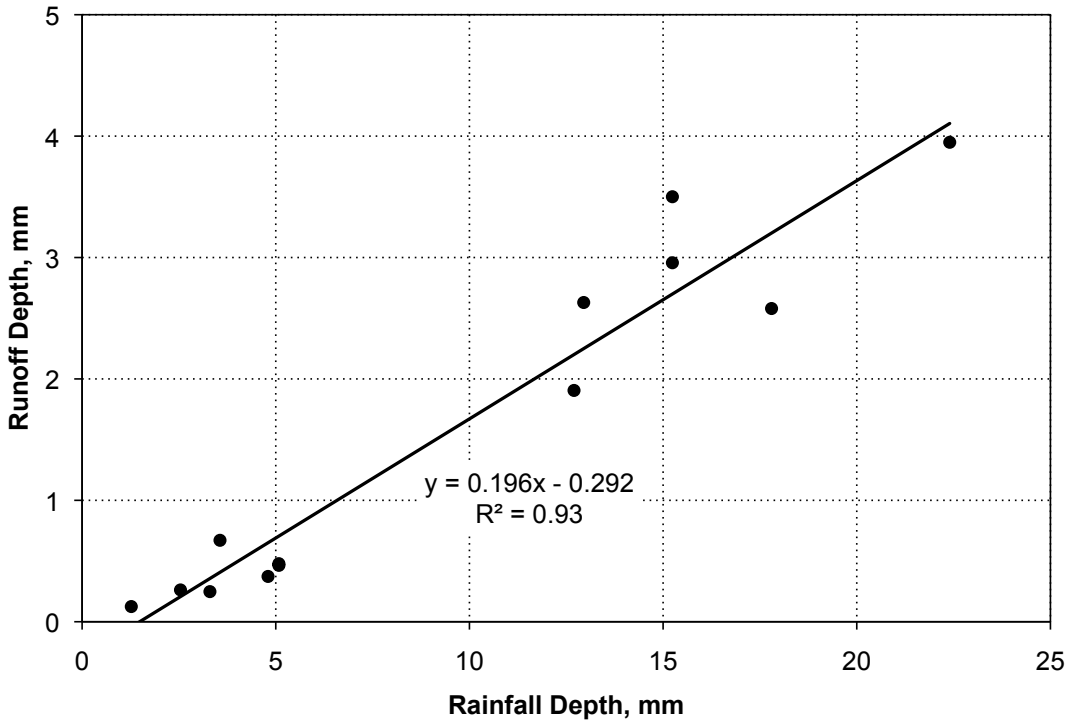

Figure 3.12: Observed runoff depths vs. observed rainfall depths in a residential development in Plymouth, MN for 14 rainfall events that occurred from Aug 26 to Sep 30, 2005. The slope of the linear least-squares fit line (0.196) is the fraction of the total watershed area occupied by the 'effective impervious area. Note that 4 events are clustered around the point for $\sim$ 5 mm rainfall and $\sim$ 0.5 mm runoff depth.

A plot of runoff depth (observed runoff volume divided by total watershed area) versus rainfall depth is shown in Figure 3.12. The linear least-squares fit has an R^2 = 0.93, a slope of 0.196 and an x-intercept (initial abstraction depth) of 1.48 mm. Thus the effective impervious area constitutes 19.6% of the total watershed area, less than the 24% of the total area that was determined from maps to be connected impervious area. The ratio of effective impervious area to connected impervious area (C_a) is 0.83, which is similar to the average value of 0.87 determined by Boyd et al. (1993) from an analysis of 38 catchments (R^2 = 0.76).

Points below the line indicate a smaller contributing area than predicted by the fitted line, while points above the line indicate that (1) the intensity or depth of the rainfall is such that more of the connected impervious area is contributing to runoff, or (2) some surface runoff has occurred from pervious surfaces. The mean intensity for events plotting above the line is 8.2 mm/h, while that for events plotting below the line is 4.7 mm/h, supporting the idea that rainfall intensity affects the size of the effective impervious area (Boyd et al., 1993) and the abstraction capacity of the surfaces (Chow, 1964).

MINUHET Model Setup

A total of three drainage points were identified in the Plymouth catchment: two were sets of street catch basins, and the third was a single drain at a low point in a park area behind the houses in the development. A single sub-watershed was used to characterize the park, and two sub-watersheds were identified to drain to each set of catch basins (one from the east and one from the west), for a total of five sub-watersheds (Figure 3.11). The sub-watersheds were delineated on contour maps of the development. The characteristic lengths of the impervious and pervious surface areas in each sub-watershed were estimated from the longest flow-paths of surface water on each surface type; average slopes along these paths were also determined from the contour maps.

GIS data provided a total connected impervious area of roughly 12,000 m^2 (24% of the total watershed area of 50,400 m^2) while the previous data analysis of the rainfall and runoff data suggested an effective impervious area of 9900 m^2 (19.6% of the total watershed area of 50,400 m^2). The connected impervious area was scaled down to the effective area by using the C_a factor determined from the data analysis (0.83). The

remaining 17% impervious area was re-classified as disconnected, and added to the initial estimate of disconnected impervious areas that initially included only rooftops draining to lawns. The additional disconnected areas are probably sidewalks and portions of driveways.

Impervious surfaces can be partitioned into 'connected' and 'disconnected' areas based on considerations of individual sub-watersheds, e.g. presence of curb and gutter. However, four of the five modeled sub-watersheds in Plymouth were similar enough to justify constant partitioning using $C_a = 0.83$, rather than considering rooftop, driveway, and street areas in each sub-watershed individually. The obvious exception was a green-space sub-watershed (SW-3), which was 100% pervious.

MINUHET Model Results

Simulations were run for the four largest rainfall events in the record (Table 3.2); they occurred on Aug 26, Sep 3, Sep 12, and Sep 19, 2005. The largest events were chosen to reduce the effects of uncertainty in initial abstractions and surface thermal properties on the simulation results. Sensitivity of model output will be analyzed in the next section.

Simulated and observed runoff flow rate and runoff temperature time series at the outlet of the catchment for the Aug 26 event are shown in Figure 3.13a. 5.0 cm of rain fell in 3.5 hours beginning around 5:00 am, with roughly half falling in the first hour. The high rainfall intensity produced runoff from the pervious portions of the watershed (roughly 20% of the total runoff volume). This was the only event in the record with a significant runoff contribution from pervious areas.

Date	**Onset**	**Duration**	**Intensity**	**Depth**
	time	*hr:min*	*cm/h*	*cm*
8/26/05	5:00	3:22	1.49	5.00
9/3/05	15:44	3:50	0.58	2.24
9/12/05	22:32	1:10	1.09	1.27
9/19/05	4:16	2:08	0.83	1.78

Table 3.2: Characteristics of the rainfall events at the Plymouth, MN study site simulated by the MINUHET model. They are the four largest events in the data record.

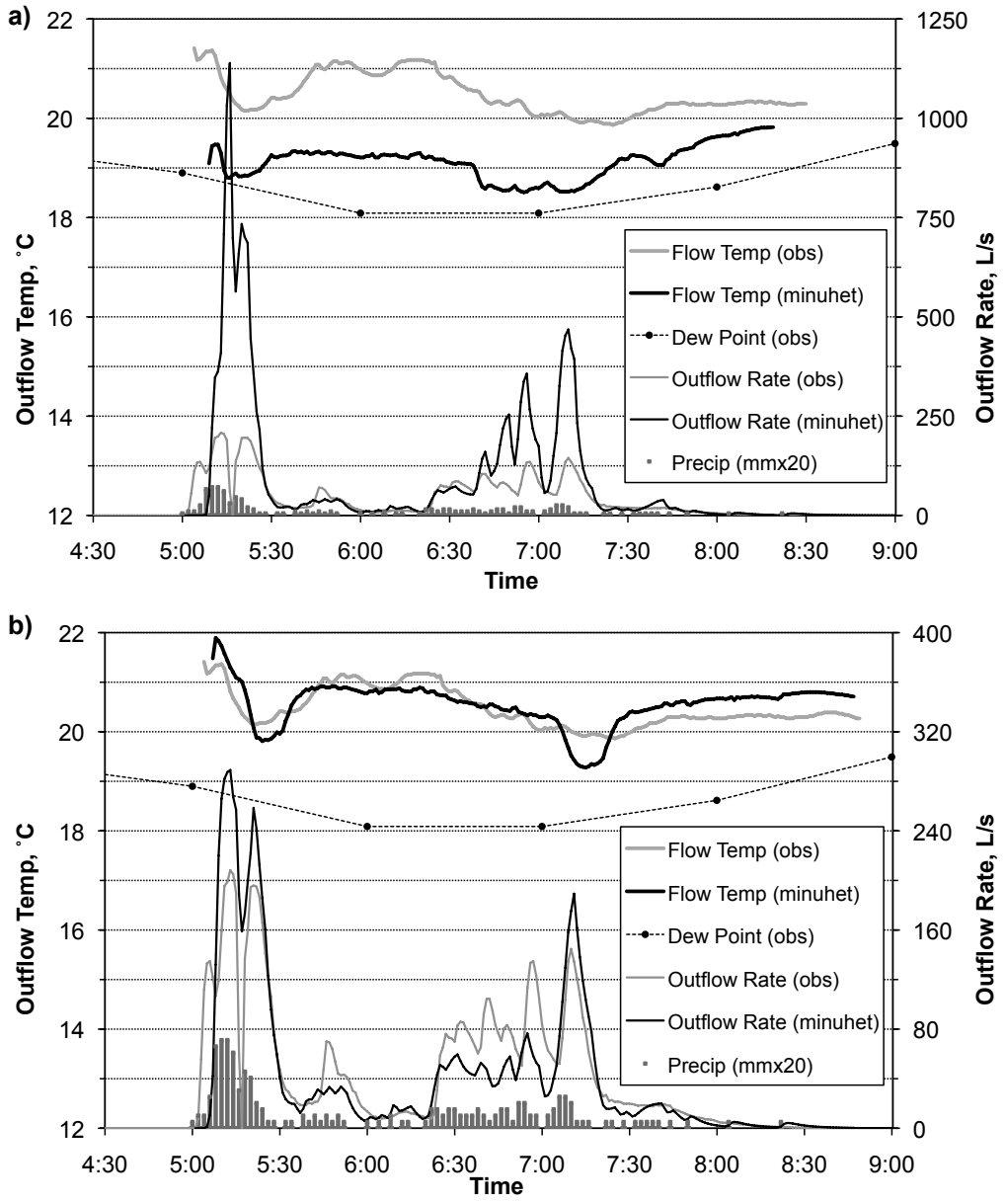

Figure 3.13: Observed and simulated outflow rate and outflow temperature for a 50-mm rainfall event on Aug 26, 2005 at the Plymouth, MN study site. Simulations produced by MINUHET using the default values of input parameters (top), and calibrated values of sat. hyd. cond. of the soil, and thermal diff. and heat cap. of the asphalt and gravel sub-grade (bottom). Note the difference in scale on the right axis of the two graphs.

Using MINUHET's default values (Table 3.3) for hydrologic and thermal properties, i.e. saturated hydraulic conductivity, Manning's roughness n, and thermal diffusivity of the asphalt pavement, the model did not perform well: runoff volume was over-predicted by roughly 100%, and RMSE for flow and temperature were 148 L/s and 1.57 °C, respectively.

The MINUHET model was then calibrated. Saturated hydraulic conductivity (K_{hs}) was increased until the simulated and observed runoff volumes nearly matched; this required a doubling of the initial K_{hs} value – a very reasonable adjustment, given that values of K_{hs} can span three orders of magnitude. Thermal diffusivity and heat capacity of the asphalt surface had to be increased significantly so that heat was more readily transferred from the paved surface to the runoff, but values were within ranges specified in the literature (e.g. Incropera and DeWitt, 2002; Luca and Mrawira, 2005). The values of the calibrated parameters used in the simulations and literature values are shown in Table 3.3. It should also be noted that if the actual thickness of the asphalt pavement in the study watershed was less than the value specified in the simulations (6 in.), an increase in thermal conductivity would have been necessary to compensate for this extra mass of asphalt.

Parameter	**Units**	**Default Value**	**Calibrated Value**	**Literature Value**
Saturated Hydraulic Conductivity, Soil	m/s	$1.7\text{x}10^{-6}$	$3.5\text{x}10^{-6}$	$1.67\text{x}10^{-7}$ (clay)[a] $5.8\text{x}10^{-5}$ (sand)[a]
Thermal Diffusivity, Asphalt	m^2/s	$4.0\text{x}10^{-7}$	$7.0\text{x}10^{-7}$	$4.42 - 6.39\text{x}10^{-7}$ [b]
Heat Capacity, Asphalt	J/m^3K	$2.0\text{x}10^{6}$	$3.5\text{x}10^{6}$	$2.7 - 3.7\text{x}10^{6}$ [b]
Thermal Diffusivity, Sub-grade	m^2/s	$1.0\text{x}10^{-6}$	$5.0\text{x}10^{-7}$	$1.2 - 3.5\text{x}10^{-7}$ (dry)[c] $3.2 - 12.6\text{x}10^{-7}$ (wet)[c]

Table 3.3: Default and modified values of key input parameters used in the calibration of the MINUHET model for the Aug 26 rainfall event at the Plymouth, MN study site. *Sources:* [a] *Rawls* et al. *(1989, from Wilson, 2005),* [b] *Luca and Mrawira (2005),* [c] *Baver* et al. *(1972), for sand, loam, and clay.*

Simulation results for the August 26, 2005 rainfall event improved considerably with calibration. Comparison of the time series is given in Figure 3.13b and statistics are given in Table 3.4. The RMSE in flow and temperature improved to 31.1 L/s and 0.87 °C, respectively. Total volume was slightly under-predicted (580 m^3 simulated versus 616 m^3 observed), and heat export was slightly over-predicted (1342 MJ simulated versus 1254 MJ observed).

Date	**Total Runoff Volume**		**Mean Runoff Temperature**		**Total Event Heat Export**		**RMSE, Runoff Rate**	**RMSE, Runoff Temp.**
	Obs	Sim	Obs	Sim	Obs	Sim		
	m^3	m^3	$°C$	$°C$	MJ	MJ	L/s	$°C$
8/26/05*	616	1247	20.5	18.8	1254	-6105	148	1.57
8/26/05	616	580	20.5	20.6	1254	1342	31.3	0.87
9/3/05	199	214	18.1	18.4	-1561	-1421	9.4	0.58
9/12/05	96	105	20.9	20.9	365	395	11.6	0.50
9/19/05	130	170	19.2	19.1	-435	-626	14.5	0.31

Table 3.4: Summary of observed and simulated event parameters for four rainfall events at the Plymouth, MN study site. Runoff temperature is a flow-weighted average, and total event heat export is defined using a 20 °C reference temperature (see Eq. 3.1). All simulations used calibrated input parameters except for the first storm, as noted. *The top line, denoted by *, shows the MINUHET model output when default (un-calibrated) values of the input parameters given in Table 3.3 were used.*

Overall, the MINUHET model output captured the general dynamics of both the observed outflow and the observed temperature of the August 26 rainfall event quite well. The following minor deviations and potential remedies can be noted:

- MINUHET missed the initial pulse of outflow while over-predicting the second pulse. This effect could perhaps be captured by using smaller sub-watersheds, because the first pulse is likely coming from impervious areas in the immediate vicinity of the catch basin set closest to the outlet. The large times of concentration associated with the relatively large sub-watersheds means that these small-scale effects might be missed.

- The local peaks at roughly 5:20 and 7:10 (Figure 3.13b) are associated with runoff from the pervious areas. The model seems to be over-predicting their runoff contribution, which would also explain the under-predicted runoff temperatures associated with those peaks. Increasing the abstraction depth for the pervious surfaces to reflect the presence of mature trees could improve the simulation results.

- Runoff from impervious surfaces is under-predicted later in the event, e.g. at 5:45 and beginning again at 6:20, which combined with the under-predicted total runoff volume suggests that for a high-intensity event such as this one, the effective impervious area is larger than that obtained from the data analysis in Section 3.5.2.

- The over-prediction of runoff temperature at the end of the rainfall event is likely the product of an increase in dew point temperature, which is set equal to rainfall temperature. There is some uncertainty associated with the dew point temperature, which was measured 8 km (5 miles) from the study site. Because little runoff is occurring at this point in the rainfall event, estimation of total heat export for the event is not much affected by the error.

Simulations were extended next to the three smaller rainfall events in September listed in Table 3.2. The time series plots for comparison of simulation results with observations are shown in Figure 3.14. Statistics of the goodness of fit are given in Table 3.4. Simulation results for all four rainfall events are compared with measurements of total runoff volume (m^3), flow-averaged runoff temperature (°C), total event heat export (MJ), and RMSEs of flow rate (L/s) and flow temperature (°C) time series in Table 3.4. The values of the calibration parameters were kept unchanged from the Aug 26 event simulation for the simulation of the three other rainfall events, with a single modification for the Sep 3 event in which the asphalt thermal conductivity was decreased by 10 - 20% to get a better match with runoff temperature. No other changes were made to the calibration parameters for the other events.

With the exception of the Aug 26 event, MINUHET over-predicted runoff volume. This is an expected result given that the three September events plotted below the regression line in Figure 3.12, suggesting that the 'effective' impervious area for these events was less than that determined by the data. The deviations in total volume were less than 10%, except for the Sep 19 event in which the error was around 30%.

The reason for this large over-prediction of runoff volume is not readily apparent, but could be related to the longer antecedent dry period compared to the other three rainfall events. Dry weather is likely to increase surface storage in the watershed, and to decrease effective impervious area. RMSE values for flow rates were relatively consistent between the four events, ranging from 9.38 L/s to 31.3 L/s for rainfall events. This level of error is acceptable given the large magnitude of runoff flows for the storms.

Flow-averaged runoff temperatures were simulated remarkably well by the MINUHET model for all events, with differences of 0.3 °C or less to observations. RMSE values ranged from 0.31 to 0.87 °C. As a result, total event heat export was accurately predicted by MINUHET for three of the four events, with errors around 9% for those events. The error for the Sep 19 event was 44%, which resulted from the 30% over-prediction in runoff volume.

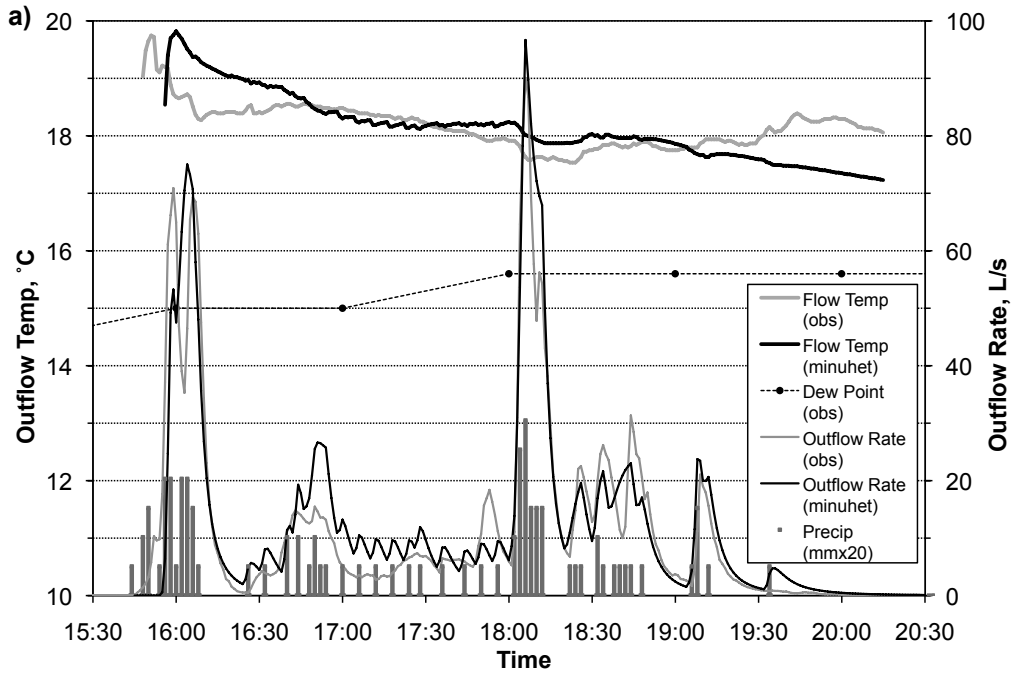

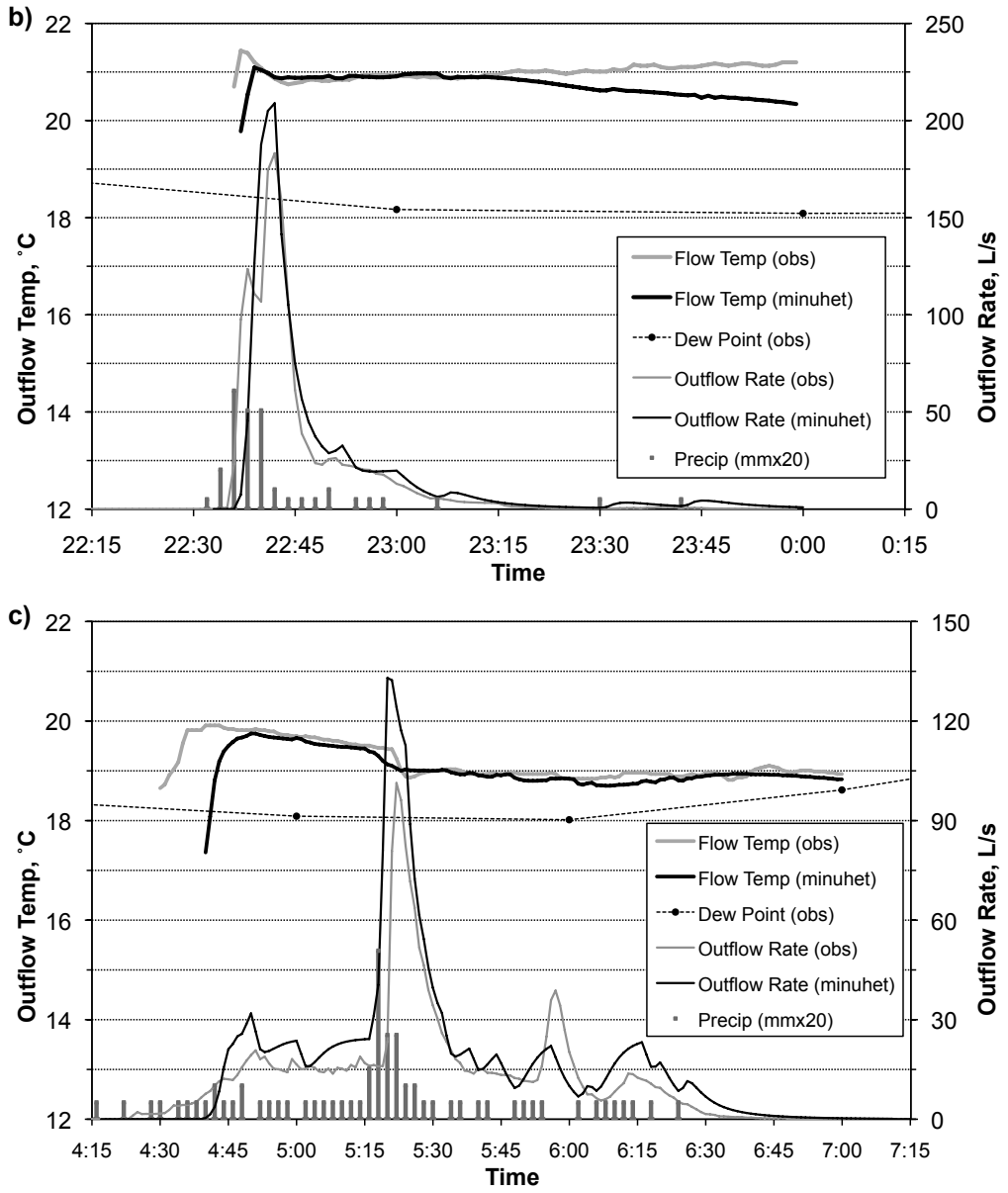

Figure 3.14: Observed and simulated outflow rate and outflow temperature for three rainfall events at the Plymouth, MN study site in Sep, 2005: (a) 2.24-cm event on Sep 3, (b) 1.27-cm event on Sep 12, and (c) 1.78-cm event on Sep 19. Simulations produced by MINUHET using calibrated inputs from the Aug 25 event (see Figure 3.13).

3.6 Model Sensitivity to Input Parameters

Sensitivity analyses for some of the MINUHET model components have been performed previously, including the surface temperature sub-model (Herb et al., 2006, 2008), the runoff temperature sub-model (Herb et al., 2009b), and the pond model (Herb et al., 2009). A sensitivity analysis for the composite (MINUHET) model has not been given, but is necessary to identify those input parameters which will strongly affect the model results and have to be specified or explored with care when the MINUHET model is applied to a developed watershed. A sensitivity analysis can also identify which processes dominate heat export by rainfall-runoff events in a watershed.

A sensitivity analysis of MINUHET applied to the Plymouth study site was conducted. The Aug 26 rainfall event is used for the analysis since it was the only event that produced significant runoff from the pervious portions of the watershed (approximately 20% of the total runoff volume). The sensitivity of the following MINUHET model output quantities was assessed: total runoff volume, flow-averaged runoff temperature, and total event heat export. The investigated input parameters fall into two categories: (1) climate parameters, including dew point temperature and rainfall intensity, and (2) properties of the surface and sub-surface, including heat capacity (J/m^3*K) and thermal diffusivity (m^2/s) of the asphalt, rooftop, and lawn surfaces; asphalt layer thickness (m); and saturated hydraulic conductivity (m/s) of the soil.

The sensitivity analysis was carried out by increasing a given input parameters value by 20% while leaving all other input parameters unchanged. A simulation was run for the Aug 26 rainfall event using the modified parameter values, and the output was then compared to the base case with nominal values of the input parameters. The sensitivity of the model to dew point temperature was assessed by increasing both dew point and air temperatures by 1 °C over the entire duration of the event. Results are shown in Table 3.5.

The model shows considerable sensitivity to climate parameters. A 1°C increase in air and dew point temperature results in a 1.0 °C increase in runoff temperature and a 157% increase in heat export. This result seems reasonable given that dew point temperature, which is used as an approximation of rainfall temperature, has a direct influence on the runoff temperature. Rainfall intensity and total rainfall depth logically

influence runoff volume and heat export: a 20% increase in rainfall intensity resulted in a 43% increase in runoff volume, but produced a smaller heat export than the base case due to lower runoff temperature.

The sensitivity analysis also indicated that properties of the surface materials have a significant influence on the heat export from a rainfall event, with the strongest response obtained for changes of the asphalt surface. A 20% increase in asphalt heat capacity increased heat export by 61%, and a 20% increase in thermal conductivity of asphalt pavement increased heat export by 14%. Given this degree of influence, an accurate estimate of the asphalt layer thickness is also important; a 20% change in this parameter increased the heat export by almost 30%. By contrast, modifications of the thermal properties of the roof and soil surfaces had a negligible effect on runoff temperature and heat export, illustrating that paved surfaces control runoff temperature and heat export from rainfall events.

Parameter	**Model Input Change**	**Model Output Change vs Base Case**		
		Runoff Volume m^3 (%)	Mean Runoff Temp. $^\circ C$ (%)	Total Event Heat Exp. MJ (%)
Dew Point Temp	+ 1 °C	-44 (-8%)	1 (5%)	2179 (157%)
Rainfall Intensity	+ 20%	250 (43%)	-0.2 (-1%)	-51 (-4%)
Heat Capacity, Asphalt	+ 20%	0 (0%)	0.3 (2%)	841 (61%)
Heat Capacity, Roof	+ 20%	0 (0%)	0 (0%)	0 (0%)
Heat Capacity, Soil	+ 20%	2 (0%)	0 (0%)	6 (0%)
Conductivity, Asphalt	+ 20%	0 (0%)	0.1 (1%)	199 (14%)
Conductivity, Roof	+ 20%	0 (0%)	0 (0%)	0 (0%)
Conductivity, Soil	+ 20%	0 (0%)	0 (0%)	2 (0%)
Asphalt Thickness	+ 20%	0 (0%)	0.1 (1%)	407 (29%)
Sat. Hydraulic Conductivity	+ 20%	-77 (-13%)	0.2 (1%)	212 (15%)

Table 3.5: Sensitivity of MINUHET output to climate variables, and to physical properties of asphalt pavement, roof, and soil surfaces at the Plymouth, MN, study site. A 5.0-cm rainfall event on Aug 25, 2005 was used for the analysis.

Simulation results also appear to be very sensitive to saturated hydraulic conductivity of the pervious land surfaces for rainfall events that are large enough to produce significant runoff from these surfaces. Runoff from pervious surfaces tends to be considerably cooler than that from impervious surfaces and decreases mean runoff temperature and total event heat export. However, for lighter rainfall events that do not produce runoff from pervious surfaces, or for highly-developed watersheds which have little or no pervious surface areas, estimation of saturated hydraulic conductivity is less crucial.

3.7 Summary

The MINnesota Urban Heat Export Tool (MINUHET) is a modeling tool for routing of storm water and its heat content through small mixed-land use watersheds. The model output is a high-resolution time series of runoff flow rates and runoff temperatures at various points within and at the outlet of the modeled catchment. MINUHET can model pervious and impervious land surfaces, with a particular emphasis on those found in urban or developing watersheds: lawns, rooftops, driveways, sidewalks, and roads, with routing elements for pervious or impervious open channels, storm sewer systems, and detention ponds (wet ponds, dry ponds, and infiltration basins). Some storm water BMPs can also be modeled, including rock cribs and underground storm water vaults.

MINUHET has not been evaluated as a composite model for a developed watershed, except for a commercial building site and a shopping center near a trout stream in Duluth, MN. MINUHET model components have been applied and validated, including the surface temperature model (Herb et al., 2006, 2008), the runoff temperature model (Herb et al., 2009b), and the pond model (Herb et al., 2009).

Two applications of MINUHET were presented in this chapter. In the first case study, MINUHET was applied to a small, asphalt-paved parking lot for which climate data were available, and runoff flow rate and runoff temperature had been measured for several late-summer rainfall events. MINUHET model output was compared to both observations and simulation results produced by a second runoff temperature model (Chapter 2; Janke et al., 2009) that solves the surface runoff equations in MINUHET by a more rigorous method. In the second case study, MINUHET was applied to a small (12.5 ac) watershed in a suburban residential development that had been instrumented

for the recording of runoff flow rates and runoff temperatures; this was the first application of the composite MINUHET model (as opposed to single component models) to a watershed with mixed surface types (lawns, roads, driveways, roofs, etc). MINUHET was applied to four rainfall events.

The results of the first case study were encouraging. Very little calibration was needed to match simulation results to within 10% of the observed runoff volume and observed heat export for the rainfall event. Mean runoff temperatures matched within 1°C. The MINUHET model and the second runoff temperature simulation model gave very similar output for the case study, with a difference of 2% or less for total runoff and heat export, and less than 0.5 °C for mean runoff temperature. While the model of Janke et al. (2009, Chapter 2) produced slightly smaller RMSE values for runoff rate and runoff temperature than MINUHET, the differences in the solution techniques of the two models does not appear to significantly impact the results. The MINUHET runoff and temperature model is therefore sufficient for application to a composite surface area, and a more complex runoff model appears to be unnecessary.

The Plymouth study site did not test the open channel or detention pond model components because there were none in the watershed. It did have a variety of urban land covers and demonstrated the ability of MINUHET to accurately route heat and water through a small watershed with a simple storm sewer system. The second case study produced reasonably accurate simulation results, and provided information on the hydrology of the watershed. From the rainfall and runoff volume data for 14 events, the study watershed was determined to contain roughly 20% effective impervious area – less than the 24% connected impervious area estimated from surface area maps derived from site surveys. The analysis also provided an estimate of 0.15 cm for the impervious surface abstraction depth. These two pieces of information contributed to a greater accuracy of the simulations.

Of the four rainfall events simulated by MINUHET for the second case study, two reproduced field measurements with considerable accuracy when calibrated input parameters from the first event (Aug 26) were used. The error in the model output for heat export from the fourth rainfall event (Sep 19) can be attributed to over-prediction of total runoff volume, likely the result of increased surface storage in the watershed due to relatively dry antecedent conditions. While the runoff temperature was well-simulated

for this event, the over-estimation of runoff volume led to an inflated value of event heat export.

In a sensitivity analysis of the MINUHET model output for the Aug 26 rainfall event, the only event with significant runoff from pervious surfaces in the second case study, MINUHET was found to be incredibly sensitive to dew point (rainfall) temperature. This is a logical result given that runoff temperature is directly linked to rainfall temperature. Rainfall intensity appeared to have a considerably smaller effect; a 20% increase in rainfall intensity resulted in a small decrease in heat export. Data quality, particularly for dew point temperature, is therefore of great importance.

Properties of the land surface also had a significant impact on simulation results. The thermal properties (heat capacity and conductivity) and thickness of asphalt pavements had the greatest effect on runoff temperature and heat export, while thermal properties of rooftops and lawn surfaces had almost no effect. Simulation results for the Aug 26 event were also sensitive to changes in saturated hydraulic conductivity, a property that is essential to modeling of infiltration and runoff from pervious surfaces. However, it is likely that in the urbanized watersheds that MINUHET is designed to model, runoff from pervious surfaces will not be a significant concern since it typically makes such a small contribution to the overall runoff volume. A similar conclusion was reached in the development and application of other storm water models, e.g. TURM (Thompson et al., 2008).

Taken together, the results of the sensitivity analysis suggest that a truthful representation of the impervious portion of the urban watershed is crucial for producing accurate simulations. Parameters associated with the pervious areas of the watershed, such as surface abstraction, interception, and saturated hydraulic conductivity, are important only for less densely populated areas or more intense rainfall events.

In both case studies calibration was used to improve the simulations, since the default values rarely provided a good match to the observations. This was especially true for the hydrologic parameters (saturated hydraulic conductivity, Mannings n, and surface depression storage); once hydrologic accuracy was attained the simulations generally improved significantly and little adjustment of surface thermal properties was needed. It is therefore our recommendation that some calibration be performed in future applications of MINUHET, especially for the hydrologic portion of the model. While hydrologic data

is not always available or feasible to collect, it must be emphasized that runoff volume or flow rate information can dramatically improve the accuracy of the simulations.

While neither case study included a large enough data set to provide a rigorous validation of MINUHET, the results are encouraging, and suggest that MINUHET should be applicable to a variety of watersheds. The model has already been used in a storm water heat export analysis for a trout stream in southeast Minnesota (Herb and Stefan, 2008) and has contributed to the development of a temperature TMDL for a trout stream in northeastern Minnesota (Herb et al., 2009). It is expected that the MINUHET tool will prove useful in similar studies in the future.

Chapter 3 Notation and Units

***Parameter*: Description [units]**

b: Brooks-Corey factor

f: infiltration rate [m/s]

h_a: net atmospheric heat flux across a water surface [W/m^2]

h_{cond}: conductive heat flux between storm water and pipe wall / channel bottom [W/m^2]

h_{conv}: convective heat flux [W/m^2]

$h_{conv,f}$: convective heat flux from a canopy [W/m^2]

$h_{conv,g}$: convective heat flux from the ground [W/m^2]

h_{evap}: evaporative heat flux [W/m^2]

$h_{evap,f}$: evaporative heat flux from a canopy [W/m^2]

$h_{lw,f}$: long wave radiation emitted by a canopy [W/m^2]

$h_{lw,g}$: long wave radiation emitted by the ground [W/m^2]

h_{net}: net / total heat flux [W/m^2]

$h_{net,f}$: net heat flux to a canopy [W/m^2]

$h_{net,g}$: net heat flux at the ground surface [W/m^2]

h_r: heat transfer coefficient for rock fill in a vault or channel [J/m^3 K]

h_{rad}: total (solar and long wave) radiative heat flux [W/m^2]

$h_{rad,a}$: total radiative heat flux from the atmosphere to the canopy or ground [W/m^2]

h_{ro}: heat flux between pavement and runoff [W/m^2]

h_s: heat transfer coefficient for soil adjacent to vault or crib [J/m^3 K]

i: rainfall intensity [m/s, cm/h], or spatial index

k_a: thermal conductivity of asphalt [W/m*K]

k_s: thermal conductivity of soil [W/m*K]

m: mass of roof per unit surface area [kg/m^2]

n: Manning's roughness coefficient

q: runoff flow rate per unit width [m^2/s]

q_a: specific humidity of air [kgw/kga]

q_l: lateral inflow rate [m^2/s]

q_L: outflow rate for a planar surface of length L [m^2/s]

q_{sat}: saturated specific humidity of air [kgw/kga]

t: time [s]

t_0: arbitrary initial time [s]

t_e: time to equilibrium flow [s]

v: vegetation density factor, from 0 (bare) to 1.0 (full canopy); also runoff volume per unit width [m^2]

x: coordinate in the direction of overland flow [m]

y: water depth [m]

z: vertical coordinate [m]

A: cross-sectional area of water flowing through a rock-filled channel [m^2]

A_{rs}: surface area of rock in contact with tank wall (vault) [m^2]

A_{rw}: surface area of rock in contact with water (vault / rock crib) [m^2]

A_w: wetted area of pipe or channel [m^2]

A_{ws}: surface area of water in contact with tank wall (vault) [m^2]

B: water surface width [m]

C_a: ratio of effective impervious area to connected impervious area

C_e: bare soil evaporation scaling coefficient [0 - 1.0]

C_{fc}: forced convection coefficient

C_{nc}: natural convection coefficient [$°C^{-1/3}m/s$]

$C_{p,a}$: specific heat of air, or of asphalt [J/kg*K]

$C_{p,r}$: composite specific heat of roof materials, or rock (vault/rock crib model) [J/kg*K]

$C_{p,s}$: specific heat of soil or pavement [J/kg*K]

$C_{p,w}$: specific heat of water [J/kg*K]

D_i: percolation rate from soil layer i [cm/h, m/s]

D_p: thermal diffusivity of pavement, soil, or other sub-surface material [m^2/s]

D_z: vertical dispersion coefficient (pond model) [m^2/s]

F: cumulative infiltration depth [m]

F_c: cloudiness fraction

H_w: heat transfer coefficient for pipe wall - storm water [$J\ m^{-2}\ s^{-1}\ K^{-1}$]

K_h: un-saturated hydraulic conductivity [cm/h, m/s]

K_{hs}: saturated hydraulic conductivity [cm/h, m/s]

L: length of modeled surface or segment [m]

L_e: equilibrium flow length for surface runoff [m]

P: wetted perimeter [m]

Q: volumetric flow rate [m^3/s]

Q_{in}: volumetric flow rate into a pipe or channel segment, vault or rock crib [m^3/s]

Q_{out}: volumetric flow rate out of a pipe or channel segment, vault or rock crib [m^3/s]

Q_{over}: flow rate of water in excess of the capacity of a vault [m^3/s]

R: hydraulic radius [m]

S: internal heat source (pond model) [W/m^3]

S_f: friction slope [length/length]

S_0: surface slope [length/length]

T: temperature; volume-weighted water temperature in pipe/channel model [°C or K]

T_a: air temperature [°C or K]

T_{dp}: dew point (rainfall) temperature [°C or K]

T_f: foliage (canopy) temperature [°C or K]

T_{in}: temperature of flow into a pipe or channel segment [°C or K]

T_{out}: outflow temperature (vault or rock crib) [°C or K]

T_{pw}: pipe wall temperature [°C or K]

T_r: rock fill temperature [°C or K]

T_{ref}: reference temperature for heat export calculation [°C]

T_{ro}: runoff temperature [°C or K]

T_s: surface & sub-surface temperature [°C or K]

T_{so}: initial surface & sub-surface temperature [°C or K]

T_v: virtual air temperature [°C]

T_w: water temperature (vault or rock crib) [°C or K]

V: total volume of water in a pipe or channel segment [m^3]

V_r: total volume of rock fill in a stormwater vault or rock crib [m^3]

V_{ro}: total runoff volume [m^3]

V_w: total volume of water in a vault or rock crib [m^3]

α: coefficient used in kinematic wave equation

β: coefficient used in kinematic wave equation

δ: heat penetration depth [m]

η: soil porosity

θ: soil moisture content

θ_i: initial soil moisture content

θ_{fc}: soil moisture content corresponding to field capacity

θ_s: soil moisture content at saturation

λ: pore size distribution parameter

ρ_a: density of air [kg/m^3]

ρ_r: composite density of roof materials, or of rock (vault / rock crib model) [kg/m^3]

ρ_s: density of soil or pavement [kg/m^3]

ρ_w: density of water [kg/m^3]

τ: time constant for percolation model [hr, s]

ψ: soil suction head (at the wetting front, in Green-Ampt equation) [m]

Δt: time step [s]

Δz_i: thickness of sub-surface layer i [m]

$\Delta\theta$: difference in soil moisture content at wetting front ($\theta_s - \theta_i$)

Chapter 4

Estimation of Groundwater Input to a Stream Reach Using a Heat Budget

Summary

Information on groundwater inflow is needed for the management of fisheries in coldwater streams, particularly in watersheds where stream temperature is becoming a concern due to expanding urbanization. This paper presents a model that has been developed for estimation of the groundwater inflow rate to a stream reach from an unsteady heat budget of the stream that takes into account heat exchange with the atmosphere, between the sediment and stream, and due to groundwater inflow. The model has the advantage of using integral heat fluxes for a stream reach rather than point measurements, and both acquisition of the required data and model implementation are relatively straightforward. However, the heat budget approach limits application of the model to groundwater-gaining reaches during periods when a significant temperature difference exists between the stream and groundwater, and to reaches or periods when little tributary or storm water inflow is present due to the model lumping these surface inflows into the calculated groundwater inflow. The model is applied over two summer periods to five stream reaches in the Vermillion River, a trout stream located in southeastern Minnesota, USA. The simulation results and a sensitivity analysis reveal that the model

is able to capture seasonal variability of groundwater inflow rates, but performs poorly in the presence of high stream flows or significant surface inflows. Model results are also highly dependent on stream shading, groundwater temperature and stream temperature, stressing the importance of data resolution and quality. Criteria for guidance of future model application are also developed from the analysis.

Submitted to *River Research and Applications*, June 2010.

4.1 Introduction

Thermal pollution of coldwater streams resulting from urban growth is a concern for fisheries in the U.S. Urban development increases surface water runoff temperature and volume, reduces natural groundwater recharge, and heats shallow aquifers below paved surfaces (Klein, 1979; Galli, 1990; Paul and Meyer, 2001; Taylor and Stefan, 2009). Rising stream temperatures are of concern because they impose a stress on temperature-sensitive biota, especially coldwater fish such as trout and juvenile salmon.

The thermal impact of a proposed urban development in the watershed of a coldwater stream can be projected by simulation models of storm water runoff and stream temperature (Nelson and Palmer, 2007; Thompson et al., 2008; Herb et al., 2009a). One crucial component of coldwater streams is the groundwater input (flow rate and temperature), and the other is shading. While riparian shading can be responsible for the low temperatures present in a trout stream, many are maintained by inflow of cold water, which commonly comes from shallow aquifers (with high hydraulic conductivity) and from springs of deep aquifers, but also from shaded wetlands or snowmelt in the mountains. Groundwater inflow in particular is not only an important input to coldwater stream temperature models, but also identifies the location of gaining stream reaches which are usually particularly cold, and need to receive special attention when urban developments in a watershed are planned.

Estimating groundwater flow rate into a stream can be complicated. Existing estimation methods rely on direct measurement with seepage meters, measurement of water levels in piezometers located within and adjacent to the stream, or measurements of streamflow rates at consecutive stream gaging stations. However, the distance

between stream gaging stations is often so large (e.g. many kilometers) that the resolution in stream flow data is insufficient to determine groundwater input, which can be concentrated in stream reaches as short as 10 to 100 meters. The spatial variability of groundwater input can be difficult to quantify with seepage meters, which can be challenging to install in moving water, or with piezometric head data, which requires knowledge of the hydraulic conductivity of the streambed, a parameter that can vary by orders of magnitude.

In light of these difficulties, the use of temperature as a tracer for groundwater movement has become common in recent decades (Anderson, 2005; Constantz, 2008; Thompson et al., 2008). Water temperature has been employed to identify stream reaches as gaining or losing based on comparisons of streambed temperature and stream water temperature (e.g. Silliman and Booth, 1993; Dumouchelle, 2001). Temperature differentials have also been used in conjunction with head data to estimate hydraulic conductivity and direction of movement of groundwater (e.g. Conant, 2004; Su et al., 2004), and streambed temperature profiles have been used to determine flow rates from 1-D or 2-D solutions of the heat transport equation (e.g. Bartolino and Niswonger, 1999; Essaid et al., 2008; Duque et al., 2010). The use of temperature data is attractive because commercially available temperature loggers are robust, accurate, and of relatively low cost, which makes it possible to monitor temperature fields at fine spatial and temporal resolutions.

In this chapter we demonstrate how measured stream temperatures and streambed temperatures can be used to estimate groundwater inputs to small, groundwater-fed stream reaches. Measured vertical temperature profiles in streambeds have previously been used to calculate groundwater inflow rates to coldwater streams by solving the vertical heat transport equation in the stream sediments (e.g. Stonestrom and Constantz, 2003; Constantz et al., 2008). In our study we use a temperature measurement at a single depth in the streambed and the surface water temperatures at the beginning and the end of a stream reach to estimate the groundwater inflow rate from a heat budget equation. This methodology will be described and applied to the Vermillion River in Minnesota, USA. The advantages and limitations of this approach will be addressed.

4.2 Model Development

4.2.1 Basic Equations

Water temperature in a stream reach responds to heat fluxes across the water surface (solar radiation, long wave radiation, evaporation, and heat convection between the atmosphere and the water), across the streambed (heat conduction into and out of the sediment), advection of groundwater inflow, and net heat advected by the flow in the stream. Heat stored in a stream reach changes in response to these heat fluxes. A heat balance for a stream reach can be written in 1-D form as:

$$\frac{\partial}{\partial t}(AT_s) + \frac{\partial}{\partial x}(QT_s) = S \tag{4.1}$$

where A is the cross-sectional area of the stream [m^2], T_s is stream temperature [°C], Q is the stream flow rate [m^3/s], S is the net heat source term [°C*m^2/s] which is the sum of all heat fluxes into and out of the stream reach; t is time and x is distance along the stream. The term S incorporates the contributions of atmospheric heat exchange, sediment heat transfer, and groundwater inflow, and is given as:

$$S = B\left(\frac{h_{atm} + h_{sed}}{\rho_w C_{p,w}}\right) + q_g T_g \tag{4.2}$$

where B is the mean or characteristic stream width [m], h_{atm} is the total (net) atmospheric heat exchange rate [W/m^2], hsed is the conductive/convective heat transfer to or from the stream sediments, q_g is the groundwater inflow rate (per length of stream reach) [m^2/s], and T_g is the groundwater temperature [°C]. In Eq. 4.2 it is assumed that both the groundwater inflow rate and groundwater temperature are constant (average values) along the stream reach. Although only one characteristic stream width B is shown in Eq. 4.2, it should be noted that B is different for the atmospheric and sediment heat transfer terms; for atmospheric heat transfer B is the stream width at the water surface, and for sediment heat flux B is the wetted perimeter. In shallow and wide streams, the two B values are almost the same.

The mass (water) balance for a stream reach is relatively simple. The main water fluxes are stream flow Q and groundwater inflow q_g, which are related by the mass balance (continuity equation) for the stream reach:

$$Q_{ups} + q_g L = Q_{ds} \tag{4.3}$$

where Q_{ups} is the upstream (inlet) flow rate [m^3/s], L is the total length of the stream reach [m], and Q_{ds} is the observed downstream (outlet) flow rate [m^3/s]. While groundwater inflow can actually be variable along a stream reach, in the model it is assumed to be constant along the reach. The assumption that there are no significant tributaries in the reach to contribute flow to the mass budget is also made. Water losses by evapotranspiration (uptake of water by plant roots) are assumed negligible.

The net heat exchange with the atmosphere h_{atm} [W/m^2] and the heat exchange with the stream bed sediments h_{sed} need to be determined by separate relationships.

4.2.2 Heat Exchange at the Water Surface

The net heat flux through the water surface (h_{atm}) is characterized by equations that quantify solar radiation, long wave radiation, evaporation (latent heat flux), and convection (sensible heat flux) as the principal heat flux components. The equations used to characterize these fluxes are identical to those employed in the runoff temperature model presented in Chapter 2 (see also Janke et al., 2009), as well as in that of Herb et al. (2009b). The flux equations are based primarily on those developed by Edinger et al. (1968, 1974) for heat exchange at the surface of cooling ponds, with net long wave radiation calculated using the formulation of Idso (1981) as modified by Pirazzini et al. (2000). Computing each heat flux component separately provides greater accuracy when the necessary weather data are available, which includes solar radiation, air temperature, relative humidity, and wind speed; water surface parameters such as emissivity and reflectivity also have to be specified.

4.2.3 Heat Exchange with the Streambed

The heat flux across the sediment surface at the bottom of a stream can be estimated by relationships ranging from simple bulk-transfer equations to models that utilize temperature gradients in the streambed. Given that heat transfer into and out of the streambed is not usually a large component of the heat budget of a stream reach, a heat conduction equation similar to that employed in the SNTEMP stream temperature model is

used (Theurer et al., 1984). Heat exchange between the sediment and stream water is assumed to be linearly proportional to the difference between stream temperature T_s and the source temperature T_{ref} representative of the streambed temperature:

$$h_{sed} = \frac{K_{sed}}{\Delta z}\Big(T_{ref} - T_s\Big) \tag{4.4}$$

where K_{sed} is the sediment-water heat exchange coefficient [W/m/K] and Δz is the distance between the stream-sediment interface and the location of the source temperature. K_{sed} has a value of about 1.65 W/m/K (Theurer et al., 1984). In our study the source temperature is a streambed temperature when possible, measured at a depth (Δz) of roughly 0.5 m. Otherwise the mean stream temperature for the period of interest is used, lagged by 36 hours (the approximate time required for a temperature pulse to conduct 0.5 m into the streambed).

4.2.4 Model Formulation

The approach used in modeling groundwater input in the stream reach was to visualize the stream reach as a series of n adjacent cells of length Δx with a constant groundwater inflow q_g along the reach (Figure 4.1). Within each cell i, geometry is assumed constant. Each cell is assumed to be well-mixed, such that stream temperature is constant within the cell; temperature varies from cell-to-cell, i.e. stepwise with distance x along the stream. The heat and mass balances for a single cell are shown in Figure 4.1.

The unsteady heat budget equation (Eq. 4.1) is discretized using a Crank-Nicholson scheme for the time derivative (storage term) and a forward-difference approximation for the spatial derivative (advection term). Application of these schemes results in the following form of the governing equation for some cell i within the stream reach at some time level k:

$$\left(\frac{(Q_i^k T_{s,i}^k - Q_{i-l}^k T_{s,i-1}^k) + (Q_i^{k+1} T_{s,i}^{k+1} - Q_{i-l}^{k+1} T_{s,i-1}^{k+1})}{2\Delta x}\right) + S = A\left(\frac{T_{s,i}^{k+1} - T_{s,i}^k}{\Delta t}\right) \tag{4.5}$$

where S is the heat source term, defined by Eq. 4.2 and evaluated using a cell temperature ($T_{s,i}^k$).

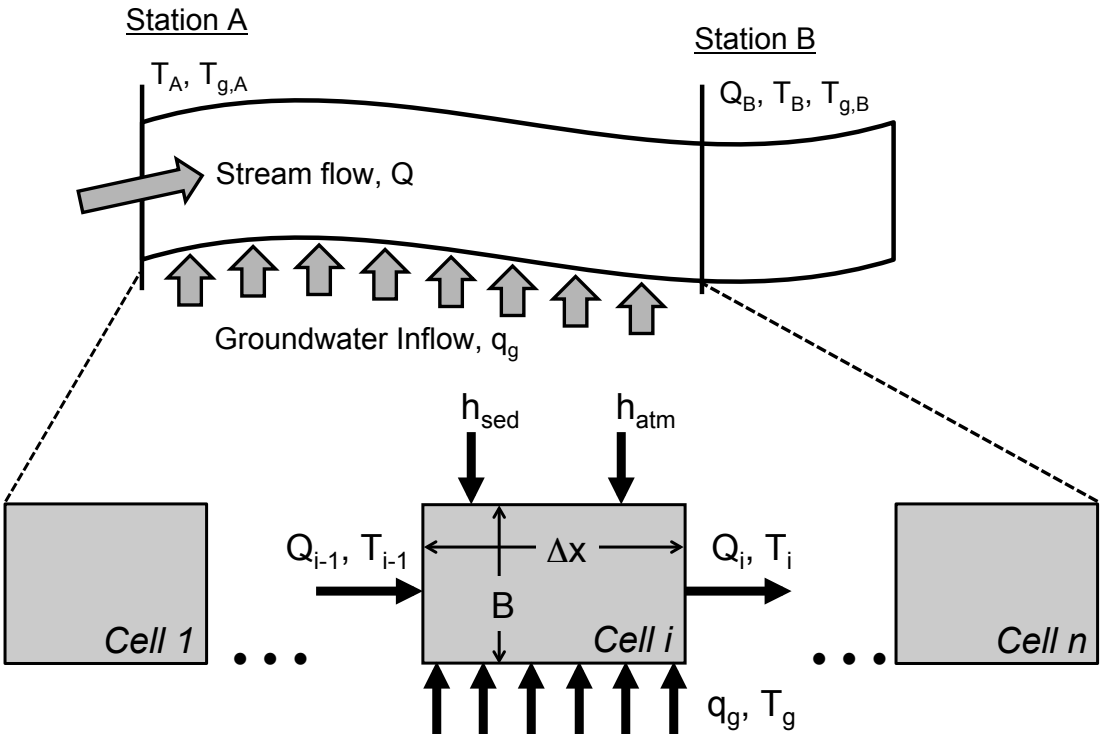

Figure 4.1: Schematic of the cells-in-series model as applied to a stream reach. The stream reach is divided into n cells of length Δx and width B. Stream temperature T, streambed temperature T_g, and stream flow Q data are collected at selected stations. H_{atm} = net heat flux across the water surface, H_{sed} = diffusive heat flux across the sediment surface, and q_g = groundwater inflow rate per unit length.

With a guessed value for the groundwater inflow rate q_g, Eq. 4.5 can be written for each of n cells and solved explicitly for the stream temperature T_s in each cell i, ultimately producing a temperature at the outlet of the reach. This predicted outlet temperature is then compared to the observed temperature at the outlet; if the temperature difference is within a specified tolerance the model proceeds to the next time step, otherwise a new guess is made at the groundwater flow rate and the calculation sequence is repeated to produce a new outlet temperature. This process is repeated until acceptable agreement exists between the simulated and observed temperatures at the end of the stream reach. After the first few time steps this iteration procedure does not have to be repeated often. By this iteration method groundwater inflow can be determined as a function of time.

The model formulation allows for spatial (stream-wise) variation of atmospheric heat fluxes as well as stream geometry, which is common. The model can handle unsteady flow and weather conditions, capturing temporally variable heat inputs to a stream reach. The thermal properties of the streambed do not have to be specified in this model, and a single streambed temperature measurement (or an average of multiple measurements within the stream reach) will suffice as model input.

4.2.5 Model Input

The following data input is required to run the model:

1. stream temperature at the upstream and downstream ends of the stream reach;
2. groundwater temperature or stream bed temperature at one or more locations within the stream reach;
3. stream flow at either end of the stream reach;
4. weather data (solar radiation, air temperature, dew point temperature, and wind speed), preferably measured in the immediate vicinity of the stream reach;
5. stream geometry, including stream reach length and wetted width, which can be either an average value for the reach or allowed to vary along the length if multiple cross-sections are available;

6. stream shading/sheltering, averaged for the stream reach and estimated e.g. from aerial photography.

The model can be applied to estimate groundwater inflow rate to a stream reach on a continuous basis for the period during which the data were collected.

4.2.6 Model Constraints

The groundwater inflow rate is calculated from the residual of the heat budget of a stream reach. The residual is completely attributed to the groundwater inflow, and not to errors in the data or to the presence of surface inflows, which could be, but currently are not included in the model formulation. To separate the residual into components for groundwater and surface water (small tributary) inflows, flow and water temperature measurements in the surface inflows would be required. Without this information, the model will give groundwater inflows only if the following criteria are met: (1) the reach must be a "gaining" reach, i.e. it has significant groundwater inflow relative to any surface inflows; (2) the reach cannot have any large, persistent tributaries or other surface inflows; and (3) the model should be applied during relatively dry weather conditions, when surface inflows (e.g. from storm water outlets, drainage ditches, or overland runoff) are minimal.

The groundwater inflow should also be large relative to the stream flow, i.e. contributing greater than roughly 10% of the observed flow in the reach. This is necessary to be certain that groundwater has a measurable impact on stream temperature and is not simply being calculated from errors in the input data. This implies that the model is likely to perform poorly for reaches or periods with large stream flows. Similarly, the model should be applied during time periods when a significant difference exists between stream temperature and groundwater temperature, such as during late summer. If stream temperature and groundwater temperature are nearly identical, even a large groundwater inflow will not appreciably change stream temperature and will thus not be detectable from the heat budget analysis.

4.3 Case Study

4.3.1 Stream System

The Vermillion River (Figure 4.2), a tributary of the Mississippi River located at the southern fringe of the Twin Cities metropolitan area in Minnesota, was used for a case study. The Vermillion River stream system has a number of designated trout stream reaches that are threatened by urban development in the watershed. Roughly 80% of the flow in the upper Vermillion River is base flow from groundwater sources (Erickson and Stefan, 2008a). The low stream temperatures required to maintain a viable brown trout population are generally provided by localized groundwater inputs; riparian shading is lacking in many reaches of the Vermillion River and its major tributaries.

The principal groundwater source in the Vermillion River basin is a surficial aquifer of high hydraulic conductivity. Its thickness varies generally from 7 to 30 m, with a maximum depth of 61 m. Some bedrock outcroppings are also present (Erickson and Stefan, 2008b). Transmissivity is highest near the stream, where the surface aquifer consists primarily of coarse glacial outwash; areas of finer-textured glacial till further from the river lead to lower transmissivity values with distance from the stream (Palen, 1990a,b; Emmons and Olivier Resources, Inc. (EOR)., 2007). The water table is just a few feet below the ground surface and the surface aquifer responds quickly to rainfall and groundwater recharge.

Below the surficial aquifer are several bedrock aquifers that can potentially leak water to the stream, including the St. Peter and Prairie du Chien aquifers. The St. Peter formation is present in the northwest part of the watershed, and consists primarily of coarse sandstone. The Prairie du Chien group consists mostly of dolomite, and underlies the rest of the watershed (Dakota County, 2006). This aquifer is largely confined except where cut by buried valleys, the deepest of which is located in the far eastern part of the watershed.

Due to the large variations in hydrogeology in the watershed, groundwater inflows to the Vermillion River are expected to be spatially variable. In addition, climatological differences between years, and errors or inconsistencies in the input data will cause temporal variability in groundwater inflows. This situation will potentially complicate the interpretation of the results.

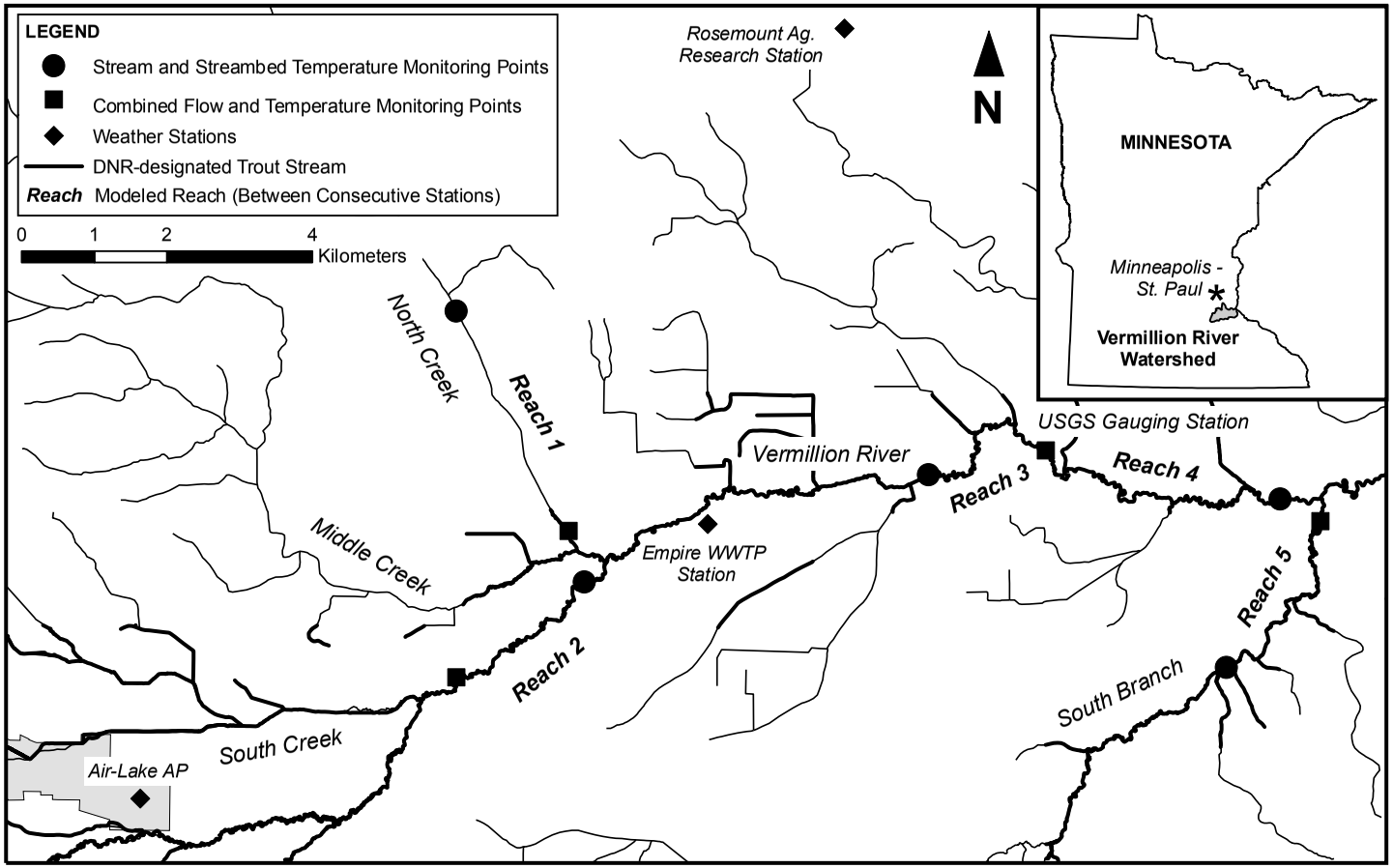

Figure 4.2: Map of the upper Vermillion River showing designated trout stream reaches and modeled stream reaches. The model was applied to Reaches 1 to 5. Data collection points including weather stations, stream gauging stations, stream temperature and streambed temperature monitoring points are identified; only sites contributing data to this study are shown.

4.3.2 Hydrologic Data Acquisition

Data Collection

Hydrologic data collection in the Vermillion River basin has historically been irregular, but has intensified since 2000 because of urban development in the watershed. Numerous individuals, government entities, and consultants to agencies have contributed to the database, and are acknowledged at the end of the paper. A map of the watershed showing the locations of weather stations, stream gauging stations, and stream and streambed (groundwater) temperature monitoring points is shown in Figure 4.2. Only the stations used in this study are shown; data was collected at dozens of other locations in the watershed.

Mean daily stream flow has been recorded for nearly 30 years by the USGS at gaging station No. 05345000 near Empire, MN, and by state agencies since 2000 at 7 other sites on the main stem and three major tributaries (South Branch, North Creek, and Middle Creek) of the Vermillion River. Stream width, cross-sectional area (or mean depth), and stream slope were measured at the gaging sites or obtained from contour maps. Shading and sheltering coefficients were estimated from aerial photography.

Temperatures in the flowing stream and in the streambed have been measured at up to 30 sites since fall 2006. Measurement sites were gaging stations and additional locations on the main stem and in lesser tributaries. At each site, a 1.5 in (3.81 cm) diameter tube was driven up to two feet into the streambed. This tube was sealed at the bottom, and perforations in the lower end allowed groundwater to flow into the tube. An integrated temperature probe and logger (Onset Hobo Water Temp Pro) was placed in the bottom of the tube to record water temperature in the streambed; another integrated probe and logger was placed a few inches above the streambed in the same location to record stream water temperature. A one-week sample record from a 2-mile reach in the upper main stem of the Vermillion River ('Reach 2') is shown in Figure 4.3. The smaller diurnal amplitude and slight lag of the downstream water temperature relative to the upstream water temperature record indicates the presence of groundwater inflow and shading in this reach. After a small rainfall event on 8/3, the downstream temperature is elevated because of storm water inflows near this point. Streambed temperature remains unaffected by the rainfall event, indicating that this is

a groundwater gaining reach.

Groundwater temperature can be measured in the streambed of a "gaining" reach or in wells near a stream reach. The measurements are point measurements and the temporal record gives a range of groundwater temperatures for a stream reach. In the model, one reference groundwater temperature was specified for simulation periods of two weeks. Although temperature measurements in a few shallow wells near the Vermillion River were available, the streambed temperatures recorded in the modeled stream reaches were used because all these reaches were gaining reaches and the spatial variability of hydrogeology in the watershed prohibits using the temperature record from a single site for the entire watershed.

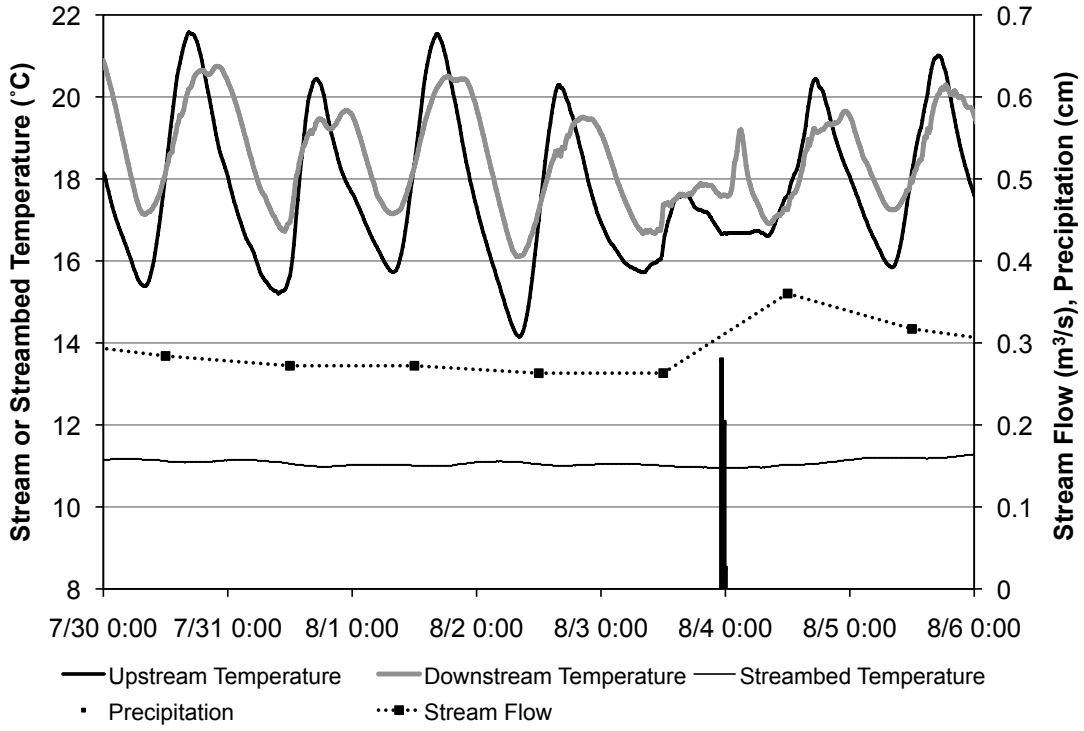

Figure 4.3: Sample of weekly data record for modeled Reach 2 in the upper Vermillion River, July 30 - August 6, 2008. 0.64 cm of precipitation fell just before midnight of August 4.

Limitations of Stream Temperature and Groundwater Temperature Measurements

Only a portion of the watershed could be modeled with the available data. Placement of additional stream temperature gauges along the main stem of the Vermillion River, primarily above major confluences, would have been desirable. Probes had to be removed for the winter and reinstalled in spring. Inconsistent installation of temperature probes and loggers after the ice-cover period lowered the data quality.

Additionally, a single temperature probe in a groundwater fed stream may not measure the mean or characteristic temperature of the stream at that location. If placed too near the stream surface, the sensor will be heated by short-wave solar irradiance and therefore read artificially high temperatures, especially on sunny days. If placed too near the streambed or shore it might be measuring an artificially low temperature closer to that of groundwater. Some probes exhibited signs of being placed too near the surface or the streambed.

A best guess and a likely range of groundwater temperatures were estimated as a function of time for a few modeled reaches having periods of poor-quality or missing data, with temperatures measured in 3.0 m (10 ft) groundwater wells located near the Vermillion River used to provide a lower bound on the estimate of groundwater temperature. This approach was generally limited to periods in August - September, 2007 in Reaches 3, 4, and 5. Additional details regarding selection of groundwater temperatures are given in Janke et al. (2008).

4.4 Weather Data Acquisition

Weather data have been collected at three sites in the Vermillion River watershed: (1) the Rosemount Agricultural Research Station (2007), (2) the Air-Lake Airport in Lakeville (2007-2008), and (3) the Empire wastewater treatment plant (2008; see Figure 4.2). The air temperature, dew point, wind speed, solar radiation, and precipitation data from these stations are assumed to be representative for any stream reach within 20 km. Gaps in the data had to be filled by data collected at the St. Anthony Falls Laboratory in Minneapolis, located roughly 40 km from the watershed.

For the model application weather data with one-hour resolution were used. Stream

temperatures were recorded at 15-minute intervals and averaged over 1-hour periods to match the timescale of the weather data. Recorded mean daily stream flows were converted by interpolation to hourly flow rates as model input, so that instabilities in the simulation resulting from step-flow changes at midnight could be avoided.

The seasonal precipitation totals in the two years simulated (2007 and 2008) were significantly different. The summer of 2007 was wet, with 36.5 cm of rainfall between June and September; large storms occurred at the end of August. By contrast, 2008 was a dry year, with only 23.1 cm of rainfall between June and September, nearly one-third of which fell in the first two weeks of June. This will be important to remember as the model results are reviewed and interpreted.

Shading of stream surfaces by the canopies of trees, bushes and other tall plants on the stream bank, as well as by emergent vegetation in the stream itself, reduces solar radiation input to a stream, which is by far the most significant heat source. Wind sheltering by vegetation canopies or stream banks reduces wind access to the water surface of a stream and thereby influences sensible and latent heat transfer. The wind sheltering coefficient was set equal to the shading coefficient.

4.5 Model Application

4.5.1 Stream Reach Selection

Stream reaches were selected based on location of monitoring stations, availability of data and the constraints for model application listed previously. Five modeled stream reaches with a total length of 21.1 km (13.1 miles) are shown in Figure 4.2; a summary of geometry and flow parameters for each reach is shown in Table 4.1.

4.5.2 Time-scales of Model Application

Model input was varied in hourly time steps, and groundwater inflows were computed for every hour in a simulation period. Groundwater inflow rate was averaged in the model over each day, but allowed to vary from day to day. This was considered sufficient to represent the rapid response of the shallow aquifer. The daily values of groundwater

Reach	**Type**	**Length** *km*	**Shading**	**Mean Width** *m*	**Mean Flow[a]** m^3	**Travel Time** *hr*
1	Tributary	3.5	30%	3.2	0.20	3.0
2	Main Stem	3.2	70%	4.8	0.44	2.0
3	Main Stem	3.7	20%	12.7	1.20	3.0
4	Main Stem	5.9	30%	12.9	1.20	4.2
5	Tributary	4.8	70%	4.7	0.30	4.1

Table 4.1: Summary of stream geometry and flow parameters for modeled reaches. Shading/sheltering, stream width, and flow rate are mean values over the entire length of the reach. [a] *Mean observed flow for all summer periods (June - Sep) of 2007 and 2008 at the gauging station in the modeled reach*

inflow rate were then averaged over each period of analysis, which was roughly two weeks (half-month). Over this period, groundwater temperature is fairly constant, based on observations, and small variations in estimated daily groundwater inflow rate that result from changes in input data can be smoothened out.

4.5.3 Extraneous factors

At least three extraneous events may have affected the groundwater inflow estimation:

1. Dewatering flows from construction sites near the Reach 1 in North Creek likely led to an over-prediction of groundwater inflow rates in 2008.

2. The treated effluent from the Empire wastewater treatment plant that had been discharged to the Vermillion River several miles upstream of Reach 3, the main stem reach upstream of the USGS gauging station, was permanently diverted in a pipeline to the Mississippi River in March 2008. This effluent had contributed a relatively steady 0.28 - 0.42 m^3/s (10 - 15 cfs) to the Vermillion River main stem at an unknown temperature, and the disappearance of this flow in 2008 might explain some of the differences between the 2007 and 2008 groundwater inflow results for Reach 3.

3. A change in the datum for the stream gauging station in the South Branch tributary between the 2007 and 2008 modeling periods led to a new flow rating curve for 2008, and the resulting discrepancy in flows likely had an effect on the estimated groundwater inflow rates for Reach 5.

4.6 Results: Estimates of Groundwater Inflows

Two sets of results will be presented: (1) the seasonal (June - September) averages of predicted groundwater inflows by stream reach and by year, and (2) the predicted groundwater inflow rates to the stream reaches as a function of time over the simulation periods (June - September 2007 and 2008, with additional periods in 2006), along with relevant precipitation and stream flow observations. Gaps in the simulation results are generally due to a lack or poor quality of water temperature data. Estimated groundwater inflow rates are presented as inflow per unit stream length (L/s/km), or as volumetric inflow rate (m^3/s) relative to the observed stream flow (m^3/s) at the end of the investigated stream reach. Both approaches can identify significant groundwater-gaining stream reaches.

4.6.1 Seasonal Averages of Estimated Groundwater Inflow

The estimated mean seasonal (June - September) groundwater inflow rates to each stream reach in 2007 and 2008 are shown in Figure 4.4. Results are presented both in cfs/mile and as the percentage of observed stream flow contributed by groundwater inflow in the modeled stream reach. All five stream reaches investigated are gaining reaches with significant groundwater contributions (22% to 40% of streamflow in 2007 and 11 to 67% in 2008). The map in Figure 4.4 shows considerable spatial variation of groundwater inflows, which is related to both the hydrogeology of the watershed and to modeling errors at high stream flow.

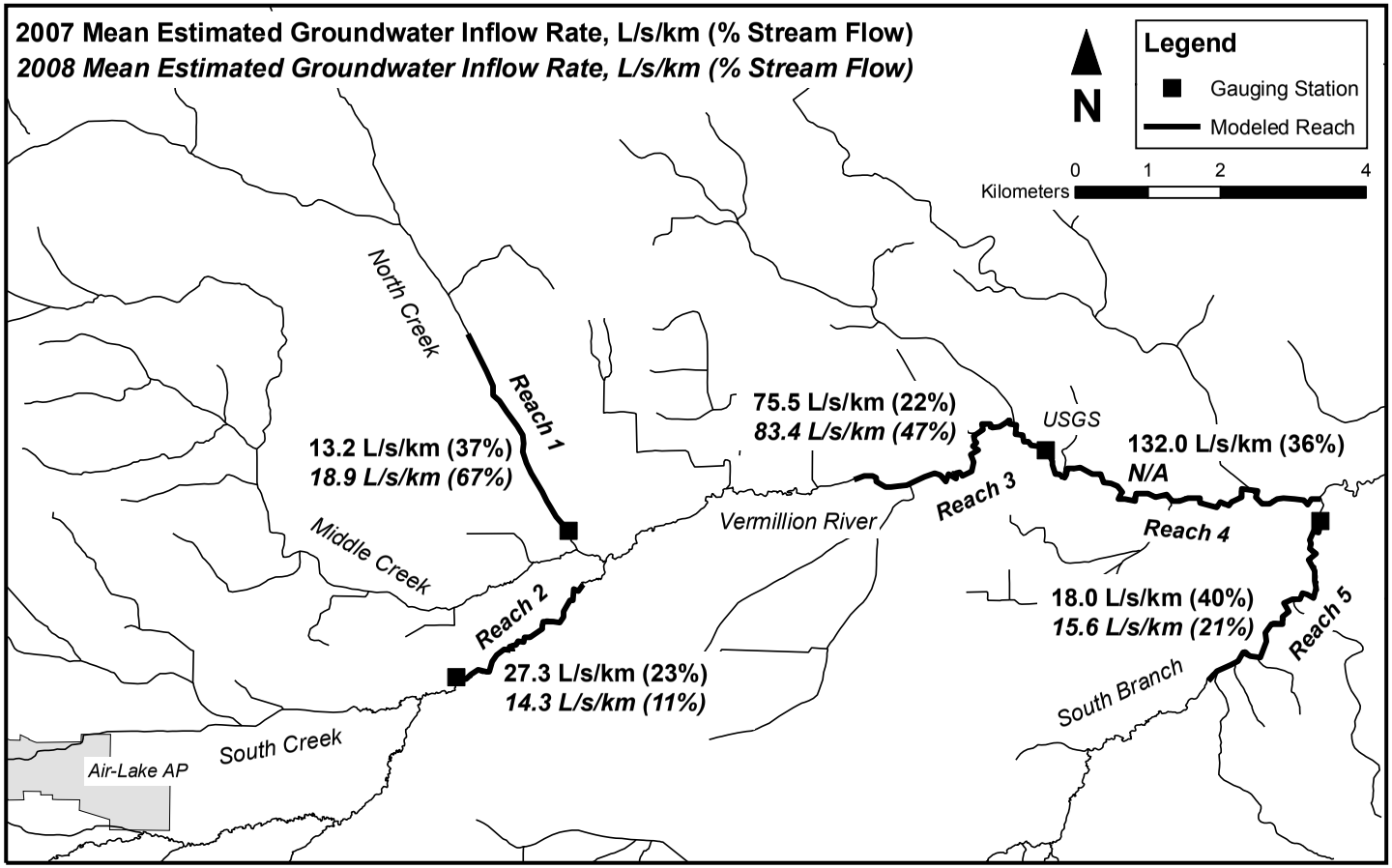

Figure 4.4: Estimated mean seasonal groundwater inflow rates (L/s/km) into the five modeled stream reaches for June - Sep, 2007 (solid text), a relatively wet summer, and for June - Sep, 2008 (italics), a very dry summer. In parentheses is the percentage of observed stream flow at the downstream end of each reach that is contributed by the modeled groundwater input in that reach. 1.0 L/s/km = 0.057 cfs/mile.

The mean groundwater inflow rates are of similar magnitude in 2007 and 2008, despite different seasonal precipitation totals (36.5 cm in 2007 vs. 23.1 cm in 2008). In two of the stream reaches (North Creek and the main stem upstream of the USGS gaging station), the estimated groundwater inflow rates were higher in the drier year; in two other stream reaches (South Branch and upper main stem reach) they were lower for the drier year. Possible explanations for the higher inflow in the drier year are: (1) the middle main stem reach appears to receive some groundwater from a deeper aquifer, as indicated by streambed temperatures that are consistently low throughout the year; (2) North Creek received a construction site de-watering discharge in 2008; and (3) lower stream stages create a larger head gradient between the water table and the stream, which may enhance groundwater inflow.

4.6.2 Seasonal Distribution of Groundwater Inflow

Reach 1: North Creek

Estimated groundwater inflow, measured average stream flow, and observed precipitation are shown for North Creek in Figure 4.5. Simulations were run for the summer period (June - September) of 2007 and 2008, and results were averaged into half-month intervals. This 3.5-km reach is not well-shaded, with a shading/sheltering coefficient of roughly 30%.

The simulation results suggest that North Creek receives significant groundwater inflow (16.9 L/s/km on average, or 52% of observed stream flow) in Reach 1, and that this inflow is highly variable with time, ranging from 7.9 L/s/km to 25.5 L/s/km (10% to 97% of stream flow) with a standard deviation of 5.6 L/s/km (32%).

In general, groundwater inflow makes up a greater percentage of stream flow during low-flow periods, such as in much of 2008 (a drought year). During high-flow periods, such as August 2007, the absolute groundwater inflow rate increases slightly but makes up a smaller portion of the stream flow, which is dominated by storm water runoff. Surface water inputs over the length of the stream reach are not accounted for in the model, and will cause errors in groundwater inflow estimates during wet periods. The large estimated groundwater inflow in early September 2007 following the heavy rains in August may be an example, but it can also be caused by a fast coupling between

infiltrated rainfall, the shallow groundwater system, and the stream in the North Creek watershed.

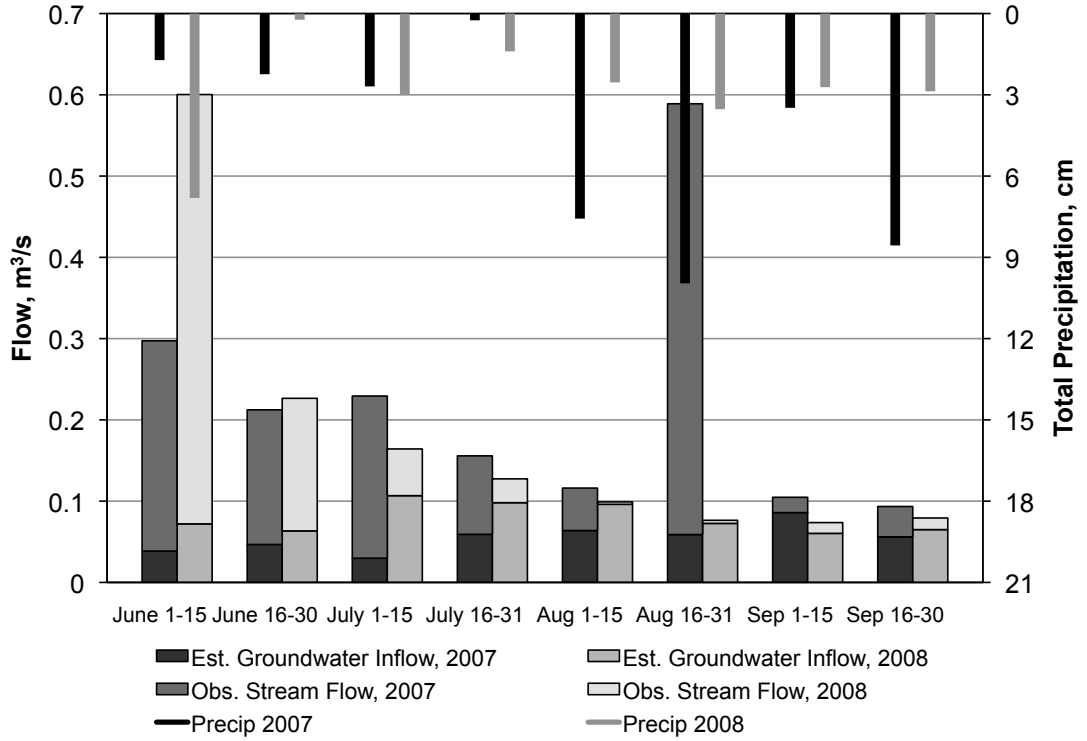

Figure 4.5: Mean observed stream flow (m^3/s) and estimated groundwater inflow in Reach 1 (North Creek) in 2007 and 2008, and total precipitation (cm) by half-month periods. The groundwater inflow in the reach (m^3/s), estimated by the model, is shown as the darker-shaded section at the bottom of each column. Reach length is 3.5 km. 1.0 $m^3/s = 35.3$ cfs.

Reach 2: Upper Main Stem of the Vermillion River

Simulations were run for a 3.2-km section of the upper Vermillion River main stem, just upstream of the confluence with North Creek, for 2006 to 2008. This is the only reach for which data existed for the summer months (June - August) for three years. Shading/sheltering was estimated to be 70% for this reach, which is covered heavily by tree canopies. Results are shown in Figure 4.6.

The results indicate a variable groundwater inflow to the upper main stem; estimated groundwater input ranged from 2% to 49% of observed stream flow (2.5 to 68.1 L/s/km) for the three-year record, with a standard deviation (13%, or 17.2 L/s/km) that was nearly as large as the mean value (14%, or 18.5 L/s/km). Mean seasonal groundwater input was 4%, 23%, and 11% of observed stream flow for 2006, 2007, and 2008, respectively.

Of note are consistently lower groundwater inputs in 2006 and 2008, both of which were relatively dry summers, suggesting that the groundwater entering the system is from shallow sources. This is opposite to the results for North Creek in which the highest groundwater inflow rates were predicted for the dry, low-flow summer of 2008. The consistently low percentage of stream flow contributed by groundwater suggests that Reach 2 is not a strong groundwater-gaining reach.

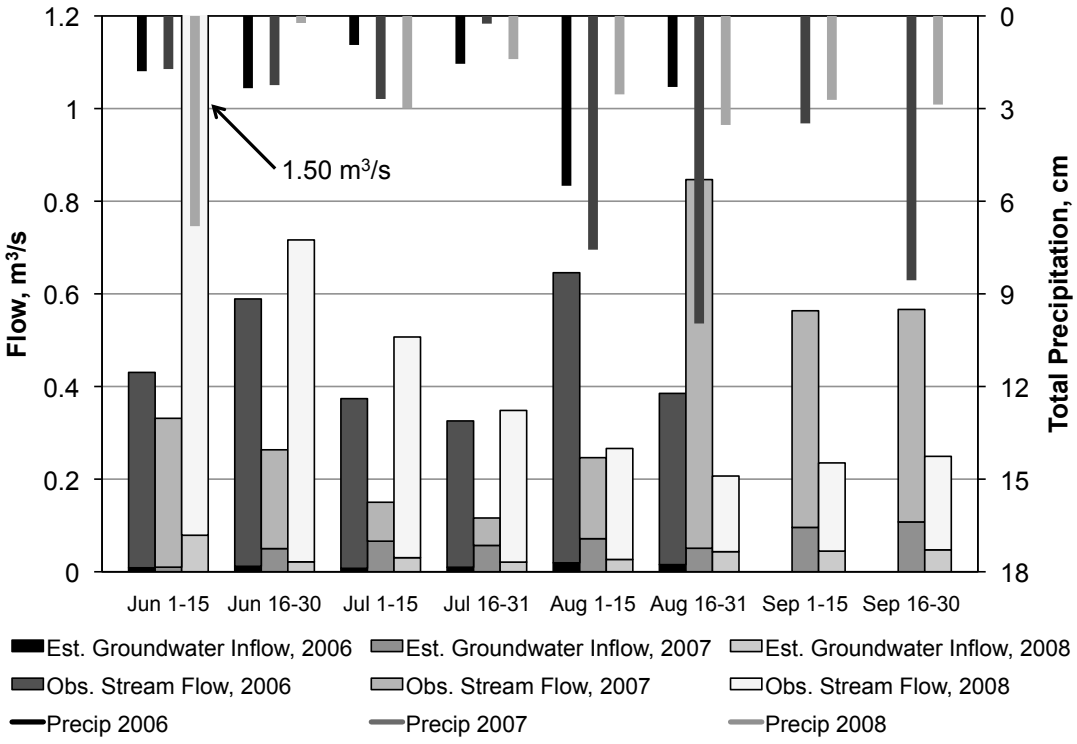

Figure 4.6: Mean observed stream flow (m^3/s) and groundwater inflow in Reach 2 (upper main stem of the Vermillion River) in 2006 - 2008, and total precipitation (cm) by half-month periods. The groundwater inflow in the reach (m^3/s), estimated by the model, is shown as the darker-shaded section at the bottom of each column. Reach length is 3.2 km. 1.0 m^3/s = 35.3 cfs.

Reaches 3 and 4: Middle Main Stem of the Vermillion River

The model was also applied to two consecutive reaches of the middle Vermillion River: a 3.7-km stretch upstream of the USGS gaging station near Empire (Reach 3), and a 5.9-km reach downstream of the gaging station (Reach 4). Reach 4 could only be analyzed for summer and fall of 2007 due to the loss of a temperature logger in 2008. Neither reach is particularly well-shaded; shading/sheltering was estimated to be 20% for the first reach and 30% for the second reach. Results are shown in Figures 4.7 and 4.8.

For Reach 3, mean groundwater contribution is 26% of observed stream flow for 2007 versus 47% for 2008, whereas the mean absolute groundwater inflow rates, while unnaturally large, are very similar in the two years (75.7 L/s/km in 2007 and 82.7 L/s/km in 2008), suggesting the presence of consistent, deep groundwater inflow in the reach. In 2007, results show a highly variable groundwater inflow to the Reach 3, with a range of 5.8 to 140.8 L/s/km (6% to 44% of stream flow); in 2008, the range is 40.5 to 109.1 L/s/km (12% to 83%). The higher percentages in 2008 are thought to be the result of lower stream flows, caused by the lack of precipitation and the diversion of wastewater treatment plant effluent upstream of this reach in March of 2008.

The simultaneous occurrence of large rainfalls and large stream flows, particularly in 2007, most likely indicates that significant tributary and surface inflows were present. These conditions are expected to result in over-predicted groundwater inflow rates and are the likely cause of the many unrealistically high inflow values simulated for this reach.

Even higher groundwater inflow rates were calculated for Reach 4 (the downstream reach) than for Reach 3 (the upstream reach) for 2007. Values ranged from 89.7 to 195.3 L/s/km (20% to 42% of stream flow), with a higher estimated mean inflow rate (126.7 L/s/km) than in the upstream reach (75.7 L/s/km). Again, the absolute values of groundwater inflow are unreasonably high. While the reach downstream of Empire is likely a groundwater-gaining reach, the presence of high stream flows and significant tributaries in the reach as well as the availability of only one year of data allow for only qualitative conclusions.

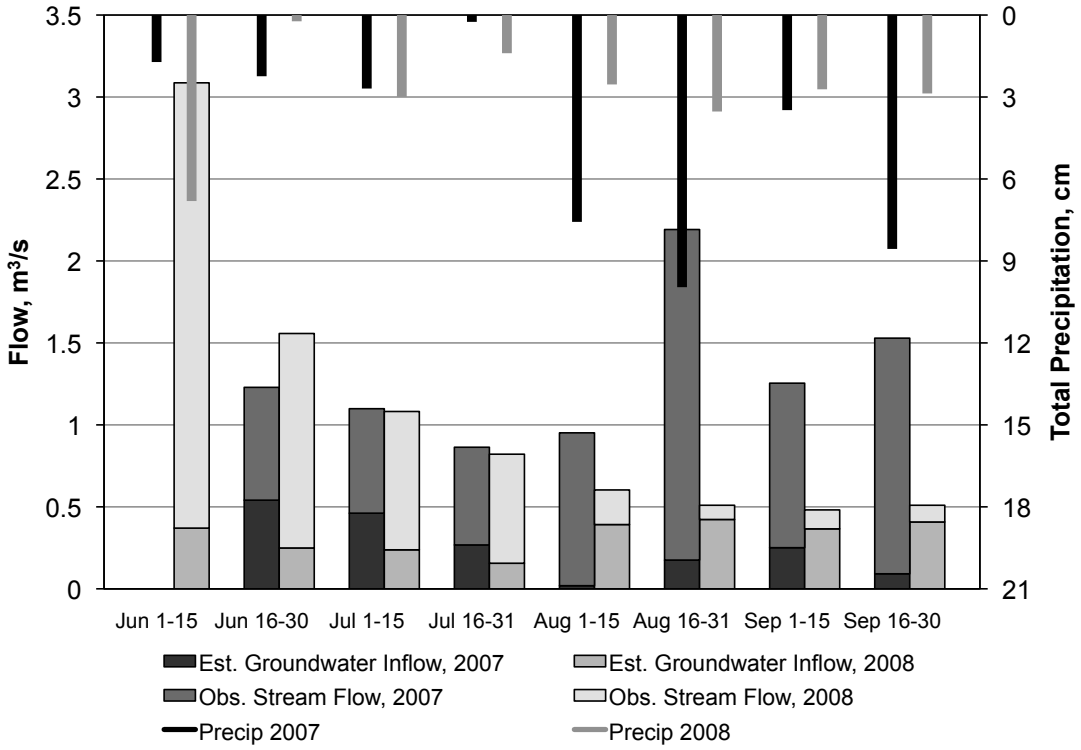

Figure 4.7: Mean observed stream flow (m^3/s) and groundwater inflow in Reach 3 (middle main stem of the Vermillion River upstream of Empire) in 2007 - 2008, and total precipitation (cm) by half-month periods. The groundwater inflow (m^3/s) in the reach, estimated by the model, is shown as the darker-shaded section at the bottom of each column. Reach length is 3.7 km. 1.0 m^3/s = 35.3 cfs.

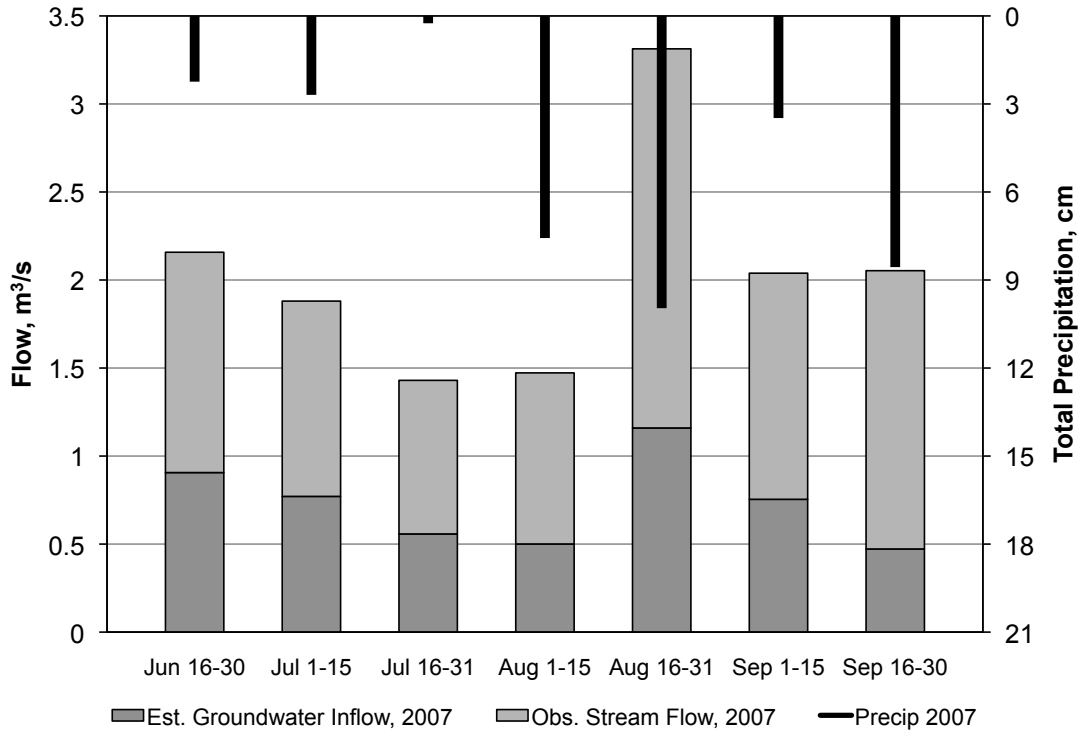

Figure 4.8: Mean observed stream flow (m^3/s) and groundwater inflow in Reach 4 (middle main stem of the Vermillion River downstream of Empire) in 2007 - 2008, and total precipitation (cm) by half-month periods. The groundwater inflow in the reach (m^3/s), estimated by the model, is shown as the darker-shaded section at the bottom of each column. Reach length is 5.9 km. 1.0 m^3/s = 35.3 cfs.

Reach 5: Lower South Branch

The model was last applied to Reach 5 in South Branch, a major tributary, just upstream of its confluence with the Vermillion River a few miles downstream of Reach 4. The 4.8 km-long reach has more shading than most of the other reaches, estimated at 70%. Results are shown in Figure 4.9.

Estimated mean groundwater inflow rates were similar in 2007 and 2008 (17.9 L/s/km on average in 2007, and 15.7 L/s/km in 2008), although mean contribution of groundwater to stream flow was much higher in 2007 (40%) than in 2008 (21%). During periods of heavy rainfall (e.g. August 2007), stream flow increases by nearly an order of magnitude but groundwater inflow increases by only a factor of 2 or 3. These results suggest that the groundwater input to South Branch is significant and perhaps a combination of both shallow and deep groundwater.

The 2008 results had more variability, with a range of 3.5 to 28.9 L/s/km (15% to 34% of measured stream flow), than the 2007 results, with a range of 10.6 to 26.4 L/s/km (25% to 63%). While the 2008 results may be more accurate due to the presence of base flow conditions, they should be considered with caution because the discharge in the stream reach was determined from a different rating curve in 2008 than in previous years, resulting in higher stream flows for the drier year (2008) than for the wetter year (2007) – the only reach in the system for which this was the case. This discrepancy might explain the high variability and generally lower groundwater inflow rates in 2008. The presence of irrigation and significant drain tile systems in the South Branch watershed also introduces some uncertainty to the results.

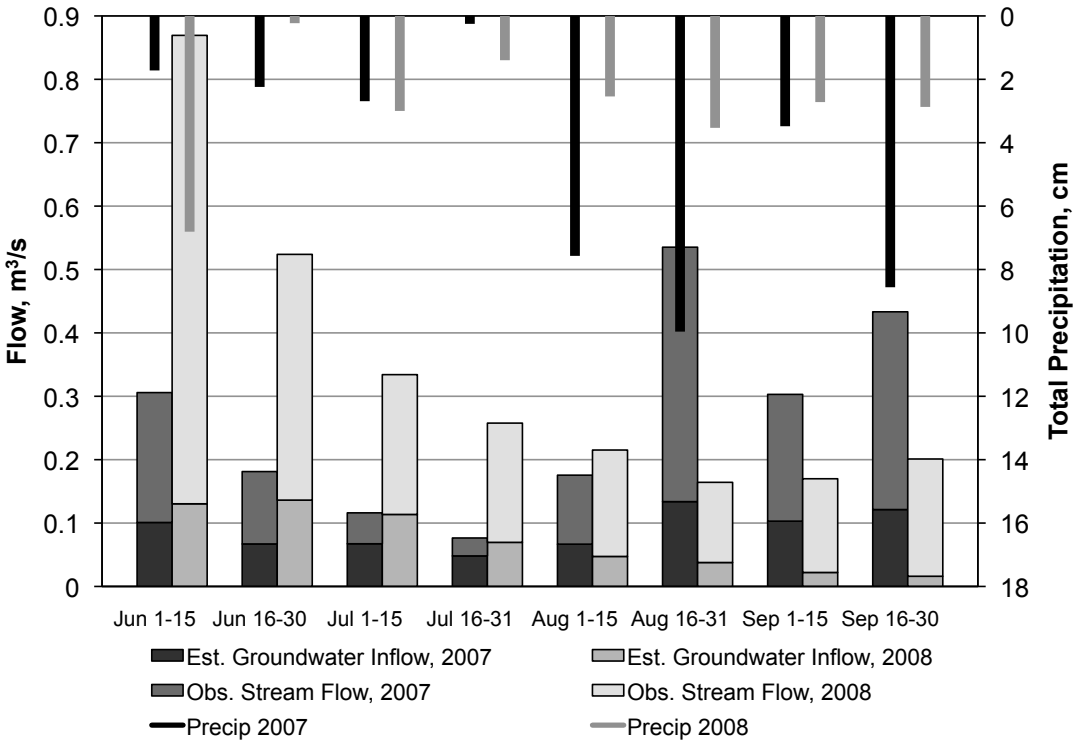

Figure 4.9: Mean observed stream flow (m^3/s) and groundwater inflow in Reach 5 (lower South Branch, a tributary of the Vermillion River) in 2007 - 2008, and total precipitation (cm) by half-month period. The groundwater inflow (cfs) in the reach (m^3/s), estimated by the model, is shown as the darker-shaded sections at the bottom of each column. Reach length is 3.0 miles. 1.0 m^3/s = 35.3 cfs.

4.7 Sensitivity of Predicted Groundwater Inflow Rates

The sensitivity of predicted groundwater inflow rates to (1) user-specified parameters (groundwater temperature and shading/sheltering) for selected time periods, and (2) data inputs (atmospheric heat transfer, stream temperature, and stream flow), is of significant interest for this model study. The sensitivity analysis is used to illustrate model dependencies and limits of applicability, and to demonstrate the importance of accurate groundwater temperature estimates.

4.7.1 Sensitivity to Groundwater Temperature and Stream Shading/Wind Sheltering

Groundwater temperature had to be a user-specified parameter in the model, along with shading and sheltering. A sensitivity analysis was therefore performed to assess the impact of these parameters on estimated groundwater inflow rate. Since the heat flux contributed by groundwater to a stream is the product of groundwater flow rate and groundwater temperature (Eq. 4.2), modification of groundwater temperature will have a direct effect on estimated groundwater inflow rate. Similarly, atmospheric heat flux, which is often the largest heat contribution to a stream (particularly during daylight hours), is directly influenced by shading, which will reduce the amount of solar radiation reaching the water surface, and by sheltering, which will reduce the wind speed at the water surface and hence evaporation and convective heat exchange between the stream surface and the atmosphere. For simplicity, shading and sheltering coefficients were assumed to be equal.

In the sensitivity analysis, groundwater inflow rates were computed for the upper Vermillion River main stem (Reach 2) for a range of groundwater temperatures and shading/sheltering coefficients. Time periods in which little or no rainfall occurred were simulated in order to minimize the effect of storm water inflow. Groundwater temperature was varied in 1°C increments over a 6 °C range (8 - 14C), and shading/sheltering values were varied in the range from 0% to 95%. Results are shown in Figure 4.10 for the week of July 1-7, 2007. This was a period of low stream flow (0.16 m^3/s), although some rainfall occurred (1.5 cm).

For this period both groundwater temperature and shading coefficient appear to

have a significant but non-linear effect on predicted groundwater inflow rate. The effect of groundwater inflow temperature (T_g) appears to be highly correlated with shading: increasing Tg from 8 °C to 14 °C for 0% shading leads to very little increase in groundwater inflow rate, while for 95% shading the same increase results in a four-fold increase in groundwater inflow rate. Similar trends (not shown) were found when this analysis was repeated for the same reach for September 8-14, 2007, a dry period in which the mean stream flow (0.47 m^3/s) was roughly 3 times higher than in the July period.

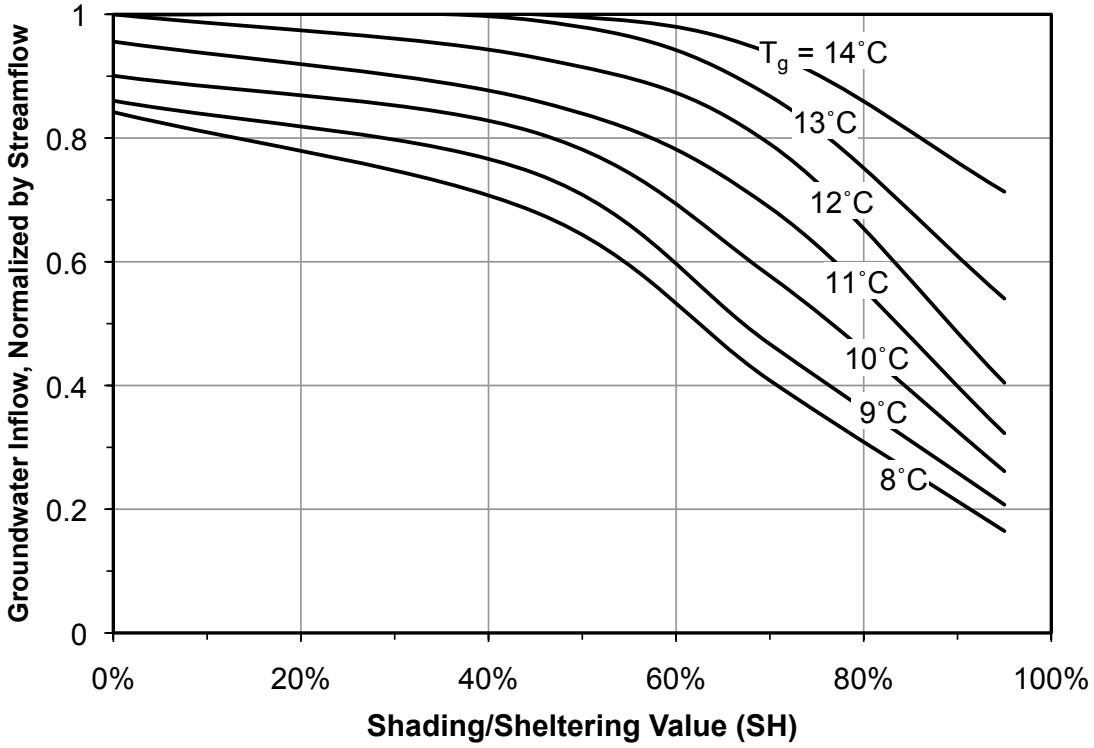

Figure 4.10: Estimated groundwater inflow rate (m^3/s) in Reach 2 (upper main stem of the Vermillion River), normalized to stream flow for July 1-7, 2007 as a function of the shading/sheltering coefficient SH and groundwater temperature T_g. Mean stream flow is 0.16 m^3/s, and reach length is 3.2 km.

These results logically indicate that stream temperature is atmosphere-dominated when the shading is low and groundwater-dominated when shading is high. The selection of groundwater temperature is crucial for using the model to extract groundwater input rates in well-shaded stream reaches. Additionally, for relatively small stream flows,

model sensitivity to input parameters may not be greatly impacted by the amount of flow carried by the stream

4.7.2 Sensitivity to Atmospheric Forcing, Stream Temperatures, and Stream Flow

An analysis was performed to correlate model output (groundwater inflow to the stream reach) with atmospheric heat flux, stream temperatures, and stream flow. This analysis was conducted to quantify the modeling constraints (conditions for which the model should not be applied) outlined in Section 4.2.6. Input quantities investigated included net atmospheric heat exchange, upstream-downstream temperature difference in the stream reach (i.e. the degree to which the stream reach was 'warming' or 'cooling'), stream temperature-groundwater temperature difference (T_s - T_g), and observed stream flow.

Very little correlation was found between atmospheric heat exchange and groundwater inflow rate for any of the reaches (R^2 = 0.009 to 0.34). Since there is no physical basis for a relationship between these two quantities, this result is encouraging.

Upstream - downstream temperature difference was computed by lagging the downstream temperature by the travel time in the reach to track the change in temperature of a parcel of water as it travels through the stream reach; a positive change indicates a warming reach. No strong trends were present in any of the reaches (R^2 = 0.06 to 0.25), although, in general, the higher groundwater inflow rates occurred in 'cooling' reaches, while smaller groundwater inflow rates occurred in 'warming' reaches (results not shown). This suggests that a stream-wise water temperature gradient in a reach, taken alone, may not be a good indicator of the amount of groundwater inflow.

Groundwater inflow rates were also related to the stream temperature-groundwater temperature difference (T_s - T_g) for every simulation period in each reach. While decreasing trends are present in plots of groundwater inflow rate versus T_s - T_g for all reaches, the strongest trends are present in the upper Vermillion River reach (Reach 2) and the middle main stem reach (Reach 3). A linear relationship fitted the data for these two sites with R^2 = 0.57 and R^2 = 0.75, respectively (Figure 4.11). These trends indicate that, as expected, the model will not give reliable groundwater inflow estimates as groundwater temperature approaches the stream temperature: a smaller

temperature difference between the stream and the groundwater requires more groundwater to 'maintain' the observed stream temperatures. The predicted inflows will then be unrealistically large. This condition also underscores the need for accurate water temperature measurements.

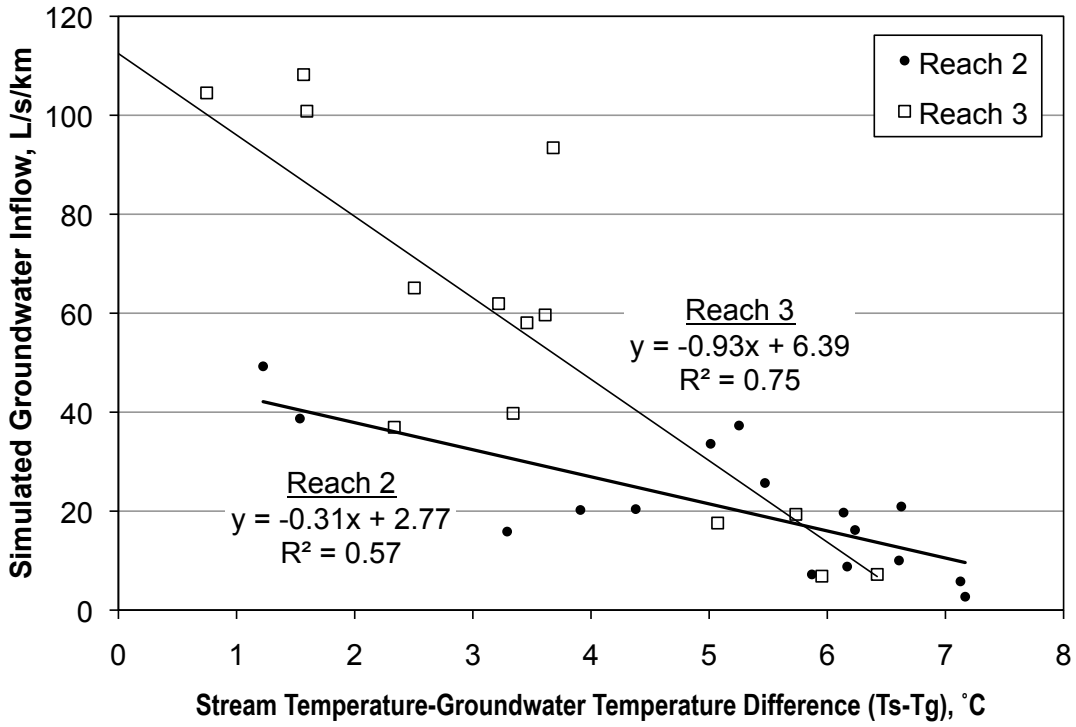

Figure 4.11: Simulated groundwater inflow in L/s/km vs. mean stream temperature - groundwater temperature difference (T_s - T_g) in °C for the upper Vermillion River main stem (Reach 2) and for the middle Vermillion River main stem (Reach 3) for the 2007 and 2008 simulation periods. Linear fits shown.

Sensitivity to stream flow was also tested. The model was not expected to perform well for periods of high flow (see Section 4.2.6), primarily for two reasons: (1) surface inflows, when present, are lumped into the groundwater inflow by the model and consequently lead to over-predicted inflow rates, and (2) groundwater will comprise a smaller portion of the overall flow as stream flow increases, meaning its contribution to the heat budget should be harder to detect accurately. Furthermore, the residual of the stream heat budget (from which groundwater inflow is calculated) becomes larger as

stream flow increases since even small changes in stream temperature represent large amounts of heat, leading also to over-predicted groundwater inflow rates. This expectation was confirmed by the discovery of a relationship between the modeled groundwater inflow and the observed stream flow ($R^2 = 0.56$ for a linear fit); it appears to hold true especially for flows higher than about 0.5 m^3/s, or 18 cfs (Figure 4.12). Above this point, groundwater inflow rates generally exceeded 35 L/s/km (roughly 2 cfs/mile), which is already an unreasonably high groundwater inflow rate for the Vermillion River stream system. In other words, the groundwater model is systematically over-predicting groundwater inflow rates for stream flows greater than 0.5 m^3/s.

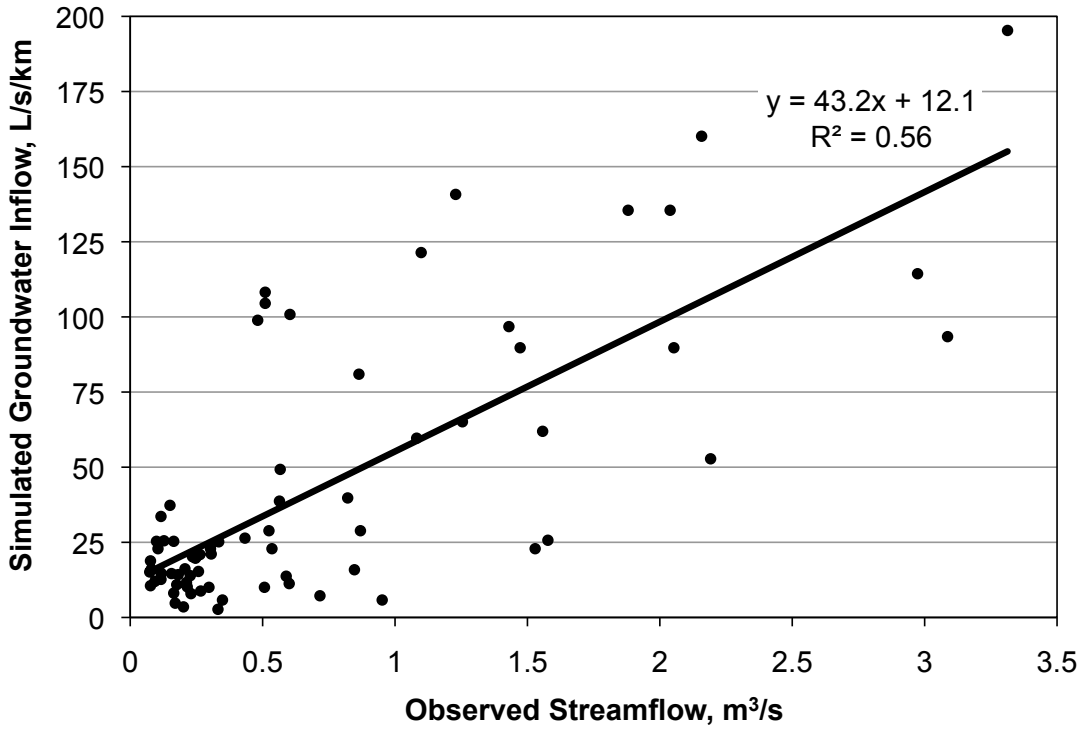

Figure 4.12: Simulated groundwater inflow (L/s/km) vs. mean observed stream flow (m^3/s) for all sites for the 2007 and 2008 simulation periods. Linear fit is shown.

In the case study there were periods of significant rainfall, most notably August-September of 2007 and June 2008. Omission of these periods had a slight impact on the seasonal averages of groundwater inflow rate for most of the modeled reaches (Table 4.2), generally causing the predicted inflow rates to decrease by 11-16%. Slightly larger

decreases logically occurred in the wetter year (2007) compared to the drier year (2008). A couple of exceptions should be noted, however. Inflow rates in North Creek increased slightly in 2008 with the omission of wet periods, which could be related to the more pronounced impact of construction dewatering at low flows. Similarly, in Reach 3, the estimated groundwater inflow rate increased by 50% in 2007 and remained largely unchanged in 2008 when wet periods were omitted; the cause of the increase in 2007 is not apparent, especially when a decrease would have been expected.

	2007			**2008**		
Reach Number	**All Periods** *L/s/km*	**Dry Periods** *L/s/km*	**% Diff.**	**All Periods** *L/s/km*	**Dry Periods** *L/s/km*	**% Diff.**
1	13.2	11.0	-16%	18.9	20.0	+6%
2	27.3	23.6	-13%	14.3	12.7	-11%
3	75.5	114.4	+51%	83.4	82.0	-2%
4	132.0	132.0	0%	n/a	n/a	n/a
5	18.0	15.1	-16%	15.6	13.7	-12%

Table 4.2: Simulated groundwater inflow rates (L/s/km) by reach and by year. Two sets of values are shown: (1) summer averages including all simulation periods for which data were available, and (2) summer averages neglecting periods in which significant rainfall occurred (August - September 2007, and early June 2008. *Reach Key:* 1 = North Creek, 2 = Upper Main Stem, 3 = Middle Main Stem (Upstream of USGS Station), 4 = Middle Main Stem (Downstream of USGS Station), 5 = South Branch.

4.8 Summary for the Vermillion River

All five modeled stream reaches in the Vermillion River watershed are groundwater-gaining reaches. Due to limitations of the modeling approach and possible errors in the input data, the estimated groundwater inflow rates should be considered with reservation. Inflow rates for the two middle main stem reaches (Reaches 3 and 4) are unrealistically high and should not be trusted; results for the other reaches are reasonable (on the order of 17.6 L/s/km, or 1.0 cfs/mile) and compare well to results found in

other studies utilizing streambed temperatures to determine input to groundwater-fed streams. For example, in a study of the Pine River in Ontario, Canada using a high spatial resolution of water level and streambed temperature measurements, Conant (2004) determined a mean summertime groundwater inflow rate of 52.5 m^3/day for a 48 m-long reach (equivalent to 12.7 L/s/km). Essaid et al. (2008) calculated mean upward groundwater velocities of roughly $1.2x10^{-6}$ m/s (0.10 m/day) for a perennial drainage ditch with a mean stream flow similar to the tributaries of the Vermillion River, and of $6.5x10^{-6}$ m/s (0.56 m/day) for a larger stream similar to the middle reaches of the Vermillion River. Groundwater velocities calculated for Reaches 1, 2, and 5 are of the same order of magnitude, ranging from 0.23 - 0.49 m/day for the simulation periods.

Application of the model to the Vermillion River system was challenging because of the presence of storm water and tributary inflows, mixed land use, and a complex hydrogeology. The temporal and spatial variability in the simulated groundwater inflows reflects these facts. However, this variability due to the hydrological diversity of the Vermillion River system may be accentuated by poor quality or low resolution of the model input data. The sensitivity analysis illustrated these limitations and led to criteria for the applicability of the model based on its limitations.

The most important limitation of the model is related to stream flow: estimated groundwater inflow rates increase with stream flow, and unrealistically high groundwater inflows (i.e. greater than 35 L/s/km, or 2.0 cfs/mile) are estimated for stream flows exceeding approximately 0.5 m^3/s (18 cfs). This dependence occurs because as stream flows increase the heat budget residual of a stream reach becomes larger due to the greater energy content of the stream flow, thus erroneously inflating the groundwater inflow rate; in reality the groundwater inflow comprises a smaller portion of a stream reachs heat budget when stream flows are large. This model limitation explains the unnaturally high (up to 195 L/s/km) groundwater inflow estimates for Reaches 3 and 4 of the Vermillion River main stem, which have year-round stream flows significantly higher than 0.5 m^3/s (see Figures 4.7 and 4.8).

Surface water inflows from storm sewers and ditches are not explicitly accounted for in the current model; this omission tends to increase groundwater inflow estimates. It is important that the model be applied to reaches with no persistent tributary inflows.

Estimated groundwater inflow rates decreased when wet periods were omitted, but

rarely by more than 16% of seasonal averages. For seasonal groundwater inflow estimates, omission of wet periods may therefore not be necessary, but for shorter time periods model results will be more realistic for dry periods.

The difference between stream temperature and groundwater temperature is a logical constraint of the method given that the groundwater inflow needs to have an impact on the stream temperature regime in order to be detectable in a heat budget. Decreasing trends for groundwater inflow rates were detected in all modeled stream reaches when the water temperature difference between the stream and the groundwater was increased. In reaches with low stream flow, groundwater inflow rates in excess of 35 L/s/km (2.0 cfs/mile) were predicted when the stream temperature-groundwater temperature difference was less than 2.0 to 3.0 °C. These relationships emphasize the need for a significant temperature difference between the stream and incoming groundwater, and stress the importance of accurate stream temperature and groundwater temperature measurements to drive the model, because errors in either will directly impact the groundwater inflow rate estimate.

Finally, the sensitivity analysis revealed that model simulation results are highly dependent on the groundwater temperature and the shading/sheltering coefficient. An increase in groundwater temperature resulted in an increase in groundwater inflow rate, but this effect was small for low shading/sheltering and large for high shading. The accurate determination of groundwater temperature is therefore of greater importance in well-shaded stream reaches than in poorly-shaded ones. The former is more likely encountered for coldwater streams.

4.9 Conclusions

A numerical model has been developed for estimation of groundwater inflow to a stream reach from measured water temperatures and weather parameters. The groundwater contribution is determined as the residual of a stream reach heat budget. The validity, sensitivities, and limitations of such an approach are assessed in a case study. The method is attractive because the required data collection is easier than the development of a simulation model for stream/aquifer interaction. Criteria were developed to guide future applications of the model:

1. The model is applicable to stream reaches that receive significant groundwater inflow relative to stream flow.

2. The stream temperature groundwater temperature difference needs to be sufficiently large for use of the heat budget approach. A difference greater than 2.0 to 3.0 °C appears to produce the most realistic results.

3. The model should be applied to small stream reaches and tributaries and preferably, when and where stream flow does not exceed roughly 0.5 m^3/s (18 cfs).

4. Stream reaches should have no persistent surface water inflows.

5. Dry weather or baseflow conditions will produce the best results. For short-term analyses (i.e. less than a season), periods should be selected when inflows from storm sewers and drainage ditches are non-existent or minimal.

6. Great care should be taken in estimation or measurement of the groundwater temperature, particularly for well-shaded reaches.

The heat budget approach is fundamentally sound, but the above limitations to the method must be borne in mind. The importance of data quality and a monitoring strategy for the data collection must be stressed: a high spatial resolution of stream and streambed temperature measurements improves the accuracy of the model results.

References

Abu-Hamdeh, N. H., Reeder, R. C., Khdair, A. I. and Al-Jalil, H. F. (2000). Thermal conductivity of disturbed soils under laboratory conditions. Transactions of the American Society of Agricultural and Biological Engineers *43*, 855–860.

American Society of Heating, Refrigeration, and Air-Conditioning Engineers, Inc. (ASHRAE). (2005). 2005 ASHRAE Handbook: Fundamentals. ASHRAE, Atlanta, GA.

Anderson, M. P. (2005). Heat as a ground water tracer. Ground Water *43*, 951–968.

Arrington, K. E. (2003). Tools to support the protection of coldwater streams from the thermal impact of development in Dane County, Wisconsin. Master's thesis Univ. of Wisconsin Madison, WI.

Barr, D. W. (2001). Turbulent flow through porous media. Ground Water *95*, 646 – 650.

Bartolino, J. R. and Niswonger, R. G. (1999). Numerical simulation of vertical groundwater flux of the Rio Grande from ground-water temperature profiles, central New Mexico. Water Resources Investigation Report 99-4212 USGS Albuquerque, NM, USA.

Baver, L., Gardner, W. and Gardner, W. (1972). The Thermal Regime of Soils. In Soil Physics chapter 7. John Wiley and Sons New York, NY, USA 4th edition.

Best, M. J. (1998). A model to predict surface temperatures. Boundary Layer Meteorology *88*, 279–306.

Bowen, I. (1926). The ratio of heat losses by conduction and by evaporation from any water surface. Physical Review *27*, 779–787.

Boyd, M. J., Bufill, M. C. and Knee, R. M. (1993). Pervious and impervious runoff in urban catchments. Hydrological Sciences Journal *38*, 463 – 478.

Carter, T. and Rasmussen, T. C. (2006). Hydrologic behavior of vegetated roofs. Journal of the American Water Resources Association *42*, 1261–1274.

Chadderton, D. (1997). Building Services Engineering Spreadsheets. 1st edition, Alden Press, Oxford.

Chow, V. T. (1964). Handbook of Applied Hydrology. McGraw-Hill Inc., New York, NY, USA.

Chow, V. T., Maidment, D. R. and Mays, L. W. (1988). Applied Hydrology. McGraw-Hill Inc., New York, NY, USA.

Conant, B. (2004). Delineating and quantifying ground water discharge zones using streambed temperatures. Ground Water *42*, 243 – 257.

Constantz, J. (2008). Heat as a tracer to determine streambed water exchanges. Water Resources Research *44*, 20 pp.

Constantz, J., Niswonger, R. G. and Stewart, A. E. (2008). Analysis of temperature gradients to determine stream exchanges with ground water. In Field techniques for estimating water fluxes between surface water and ground water, (Rosenberry, D. O. and LaBaugh, J. W., eds), chapter 4, pp. 115–128. USGS Denver, CO, USA.

Cristina, C. and Sansalone, J. (2003). Kinematic wave model of urban pavement rainfall-runoff subject to traffic loadings. Journal of Environmental Engineering *129*, 629–636.

Dakota County (2006). Dakota County ambient groundwater quality study: 1999 – 2003 Report. Dakota County, Minnesota. Available online: www.co.dakota.mn.us/CountyGovernment/Reports/Environment/Ambient.htm. Accessed May 24 2010.

Deardorff, J. (1978). Efficient prediction of ground surface temperature and moisture with inclusion of a layer of vegetation. Journal of Geophysical Research *83*, 1889–1903.

Duffie, J. A. and Beckman, W. A. (1991). Solar Engineering of Thermal Processes. 2nd edition, John Wiley and Sons, New York, NY, USA.

Dumouchelle, D. H. (2001). Evaluation of ground-water/surface-water relations, Chapman Creek, West-Central Ohio, by means of multiple methods. Water Resources Investigation Report 01-4202 USGS Columbus, OH, USA.

Duque, C., Calvache, M. L. and Engesgaard, P. (2010). Investigating river-aquifer relations using water temperature in an anthropized environment (Motil-Salobrena aquifer). Journal of Hydrology *381*, 121–133.

Eaton, J., McCormick, J., Goodno, B., O'Brien, D., Stefan, H., Hondzo, M. and Scheller, R. (1995). A field information-based system for estimating fish temperature tolerances. Fisheries *20*, 10–18.

Eckert, E. R. G. and Drake Jr., R. (1972). Analysis of Heat and Mass Transfer. McGraw-Hill, New York, NY, USA.

Edinger, J., Brady, D. and J.C., G. (1974). Heat exchange in the environment. Cooling Water Discharge Research Project RP-49 14 Electric Power Research Institute Palo Alto, CA.

Edinger, J., Duttweiler, D. and Geyer, J. (1968). The response of water temperatures to meteorological conditions. Water Resources Research *4*, 1137–1143.

Emmons and Olivier Resources, Inc. (EOR). (2007). Vermillion River headwaters groundwater recharge area inventory and protection plan. Technical report. EOR, Inc. Oakdale, MN, USA. Sep 14, 2007.

Endreny, T. A. (2005). Land Use and Land Cover Effects on Runoff Processes: Urban and Suburban Development. In Encyclopedia of Hydrological Sciences, (Anderson, M., ed.), p. 29. John Wiley and Sons New York, NY, USA.

Erickson, T. O. and Stefan, H. G. (2008a). Baseflow analysis of the upper Vermillion River, Dakota County, Minnesota. Project Report 507, St. Anthony Falls Laboratory, University of Minnesota Minneapolis, MN, USA. Available online: home.safl.umn.edu/bmackay/pub/pr/pr507.pdf. Accessed May 20 2010.

Erickson, T. O. and Stefan, H. G. (2008b). Groundwater recharge in a coldwater stream watershed during urbanization. Project Report 524, St. Anthony Falls Laboratory, University of Minnesota Minneapolis, MN, USA. Available online: home.safl.umn.edu/bmackay/pub/pr/pr524.pdf. Accessed May 20 2010.

Essaid, H., Zamora, C. M., McCarthy, K. A., Vogel, J. and Wilson, J. R. (2008). Using heat to characterize streambed water flux availability in four stream reaches. Journal of Environmental Quality *36*, 1010–1023.

Fang, X. and Stefan, H. G. (2000). Dependence of dilution of a plunging, submerged discharge over a sloping bottom on inflow and bottom friction. Journal of Hydraulic Research *38*, 15–26.

Fischer, H. B., List, E. J., Koh, R. C. Y., Imberger, J. and Brooks, N. H. (1979). Mixing in Coastal Waters. Academic Press, New York, NY, USA.

Ford, D. E. and Stefan, H. G. (1980). Thermal prediction using integral energy model. Journal of the Hydraulics Division – ASCE *106*, 39–55.

Galli, J. (1990). Thermal Impacts Associated With Urbanization and Stormwater Best Management Practices. Technical report Metropolitan Washington Council of Governments Washington, D.C., USA.

Gulliver, J. S. and Stefan, H. G. (1986). Wind function for a sheltered stream. Journal of Environmental Engineering *112*, 1–14.

Ham, J., Toran, L. and Cruz, J. (2006). Effect of upstream ponds on stream temperature. Environmental Geology *50*, 55–61.

Herb, W. R. (2008). Analysis of the effect of stormwater runoff volume regulations on thermal loading to the Vermillion River. Project Report 520, St. Anthony

Falls Laboratory, University of Minnesota Minneapolis, MN, USA. Available online: home.safl.umn.edu/bmackay/pub/pr/pr520.pdf.

Herb, W. R., Erickson, T. O. and Stefan, H. G. (2009). Stream temperature modeling of Miller Creek, Duluth, Minnesota. Project Report 535, St. Anthony Falls Laboratory, University of Minnesota Minneapolis, MN, USA. Available online: home.safl.umn.edu/bmackay/pub/pr/pr535.pdf.

Herb, W. R., Janke, B. D., Mohseni, O. and Stefan, H. G. (2006). All-weather ground surface temperature simulation. Project Report 478, St. Anthony Falls Laboratory, University of Minnesota Minneapolis, MN, USA. Available online: home.safl.umn.edu/bmackay/pub/pr/pr478.pdf.

Herb, W. R., Janke, B. D., Mohseni, O. and Stefan, H. G. (2007). Estimation of runoff temperatures and heat export from different land and water surfaces. Project Report 488, St. Anthony Falls Laboratory, University of Minnesota Minneapolis, MN, USA. Available online: home.safl.umn.edu/bmackay/pub/pr/pr488.pdf.

Herb, W. R., Janke, B. D., Mohseni, O. and Stefan, H. G. (2008). Ground surface temperature simulation for different land covers. Journal of Hydrology *356*, 327–343.

Herb, W. R., Janke, B. D., Mohseni, O. and Stefan, H. G. (2009a). MINUHET (Minnesota Urban Heat Export Tool): A software tool for the analysis of stream thermal loading by urban stormwater runoff. Project Report 526, St. Anthony Falls Laboratory, University of Minnesota Minneapolis, MN, USA. Available online: home.safl.umn.edu/bmackay/pub/pr/pr526.pdf.

Herb, W. R., Janke, B. D., Mohseni, O. and Stefan, H. G. (2009b). Runoff temperature model for paved surfaces. Journal of Hydrologic Engineering *14*, 1146–1155.

Herb, W. R., Mohseni, O. and Stefan, H. G. (2007). Heat Export and Runoff Temperature Analysis for Rainfall Event Selection. Project Report 483, St. Anthony Falls Laboratory, University of Minnesota Minneapolis, MN, USA. Available online: home.safl.umn.edu/bmackay/pub/pr/pr483.pdf.

Herb, W. R., Mohseni, O. and Stefan, H. G. (2009). Simulation of temperature mitigation by a stormwater detention pond. Journal of the American Water Resources Association *45*, 1164–1178.

Herb, W. R. and Stefan, H. G. (2008). A flow and temperature model for the Vermillion River, Part II: Response to surface runoff inputs. Project Report 525, St. Anthony Falls Laboratory, University of Minnesota Minneapolis, MN, USA. Available online: home.safl.umn.edu/bmackay/pub/pr/pr525.pdf.

Hondzo, M. (2002). Environmental Fluid Mechanics. In Mechanics of Fluids, (Potter, M., ed.), chapter 14. Brooks Cole/Thompson Learning, Pacific Grove, CA, USA, 3rd edition.

Hondzo, M. and Stefan, H. G. (1993). Lake water temperature simulation model. Journal of Hydraulic Engineering *19*, 1251– 1273.

Idso, S. (1981). A Set of Equations for Full Spectrum and 8- to 14-mm and 10.5- to 12.5-mm Thermal Radiation From Cloudless Skies. Water Resources Research *17*, 295–304.

Incropera, F. P. and DeWitt, D. P. (2002). Fundamentals of Heat and Mass Transfer. 5th edition, John Wiley and Sons, New York, NY.

James, W. and Xie, J. D. M. (1999). Modeling Thermal Enrichment of Streams Due to Solar Heating of Local Urban Stormwater. In New Applications in Modeling Urban Water Systems, (James, W., ed.), chapter 8, pp. 139–157. CHI Guelph, Canada.

Janke, B. D., Herb, W. R., Mohseni, O. and Stefan, H. G. (2006). Quasi 2-D model for runoff temperature from a paved surface. Project Report 477, St. Anthony Falls Laboratory, University of Minnesota Minneapolis, MN, USA. Available online: home.safl.umn.edu/bmackay/pub/pr/pr477.pdf.

Janke, B. D., Herb, W. R., Mohseni, O. and Stefan, H. G. (2007). Application of a runoff temperature Model (MINUHET) to a residential development in Plymouth, MN. Project Report 497, St. Anthony Falls Laboratory, University of Minnesota Minneapolis, MN, USA. Available online: home.safl.umn.edu/bmackay/pub/pr/pr497.pdf.

Janke, B. D., Herb, W. R., Mohseni, O. and Stefan, H. G. (2008). Estimation of groundwater inflow to the Vermillion River from observations of stream flow and stream temperature. Project Report 523, St. Anthony Falls Laboratory, University of Minnesota Minneapolis, MN, USA. Available online: home.safl.umn.edu/bmackay/pub/pr/pr523.pdf.

Janke, B. D., Herb, W. R., Mohseni, O. and Stefan, H. G. (2009). Simulation of heat export by rainfall/runoff from a paved surface. Journal of Hydrology *365*, 195–212.

Janke, B. D., Herb, W. R., Mohseni, O. and Stefan, H. G. (2011). Heat Release From Rooftops During Rainstorms in the Minneapolis/St. Paul Metropolitan Area, USA. Hydrological Processes *(In Press)*.

Jia, Y., Ni, G., Kawahara, Y. and Suetsugi, T. (2001). Development of WEP Model and its Application to an Urban Watershed. Hydrological Processes *15*, 2175–2194.

Klein, R. (1979). Urbanization and Stream Quality Impairment. Water Resources Bulletin *15*, 948–963.

Krause, C., Lockard, B., Newcomb, T., Kibler, D., Lohani, V. and Orth, D. (2004). Predicting the Influences of Urban Development on Thermal Habitat in a Warm Water Stream. Journal of the American Water Resources Association *40*, 1645–1658.

LeBlanc, R., Brown, R. and FitzGibbon, J. (1997). Modeling the Effects of Land Use Change on the Water Temperature in Unregulated Urban Streams. Journal of Environmental Management *49*, 445–469.

Lee, J. G. and Heaney, J. P. (2003). Estimation of urban imperviousness and its impacts on storm water systems. Journal of Water Resources Planning and Management *129*, 419 – 426.

Li, R. M., Stevens, M. A. and Simons, D. B. (1976). Solutions to Green-Ampt infiltration equation. Journal of the Irrigation and Drainage Division - ASCE *102*, 239–248.

Liu, K. and Minor, J. (2005). Performance evaluation of an extensive green roof. Technical Report NRCC-48204, National Research Council Canada, Toronto, Ontario.

Luca, J. and Mrawira, D. (2005). New Measurement of Thermal Properties of Superpave Asphalt Concrete. Journal of Materials in Civil Engineering *17*, 72–79.

Mays, L. (2001). Water Resources Engineering. 1st edition, John Wiley and Sons, New York, NY, USA.

McQuiston, F., Parker, J. and Spitler, J. D. (2000). Heating, ventilation, and air conditioning, analysis and design. 5th edition, John Wiley and Sons, New York, NY.

Neitsch, S. L., Arnold, J. G., Kiniri, J. R. and Williams, J. R. (2005). Soil and water assessment tool theoretical documentation version 2005. Technical report. Grassland Soil and Water Research Laboratory, Agriculture Research Service, US Department of Agriculture Temple, TX, USA.

Nelson, K. and Palmer, M. (2007). Stream Temperature Surges Under Urbanization and Climate Change: Data, Models, and Responses. Journal of the American Water Resources Association *43*, 440–452.

Oberndorfer, E., Lundholm, J., Bass, B., Coffman, R., Doshi, H., Dunnett, N., Gaffin, S., Kohler, M., Liu, K. K. Y. and Rowe, B. (2007). Green roofs as urban ecosystems: ecological structures, functions, and services. Bioscience *57*, 823–833.

Ochsner, T., Horton, R. and Tusheng, R. (2001). New Perspective on Soil Thermal Properties. Soil Science Society of American Journal *65*, 1641–1647.

Palen, B. M. (1990a). Geological atlas of Dakota County, Minnesota: Quaternary Hydrogeology. County Atlas Series, Atlas C-6, Plate 5 of 9. Minnesota Geological Survey, University of Minnesota St. Paul, MN, USA.

Palen, B. M. (1990b). Geological atlas of Dakota County, Minnesota: Bedrock Hydrogeology. County Atlas Series, Atlas C-6, Plate 6 of 9. Minnesota Geological Survey, University of Minnesota St. Paul, MN, USA.

Patankar, S. (1980). Numerical Heat Transfer and Fluid Flow. McGraw-Hill, New York, NY, USA.

Paul, M. J. and Meyer, J. L. (2001). Streams in the Urban Landscape. Annual Review of Ecology and Systematics *32*, 333–365.

Picksley, J. W. and Deletic, A. (1999). The Thermal Enrichment of Storm Runoff from Paved Areas – a Statistical Analysis. In New Applications in Modeling Urban Water Systems, (James, W., ed.), chapter 7, pp. 129 – 138. CHI Guelph, Canada.

Pirazzini, R., Nardino, M., Orsini, A., Georgiadis, T. and Levizzani, V. (2000). Parameterisation of the Downward Longwave Radiation from Clear and Cloudy Sky at Ny-Alesund (Svalbard). In Proceedings of the International Radiation Symposium, St. Petersburg, Russia.

Pluhowski, J. (1970). Urbanization and Its Effect on the Temperature of Streams on Long Island, New York. Professional Paper 627-D U.S. Geological Survey New York, NY, USA.

Rasmussen, A., Hondzo, M. and Stefan, H. (1995). A Test of Several Evaporation Equations for Water Temperature Simulations in Lakes. Water Resources Bulletin *31*, 1023–1028.

Rawls, W. J., Ahuja, L. R. and Brakensiek, D. L. (1989). Estimating soil hydraulic properties from soils data. In Proceedings of the International Workshop on Indirect Methods for Estimating Hydraulic Properties of Unsaturated Soils, (van Gunechten, M. T., Leij, F. J. and Lund, L. J., eds), pp. 329–340,.

Rawls, W. J., Brakensiek, D. L. and Miller, N. (1983). Green-Ampt infiltration parameters from soils data. Journal of the Hydraulics Division – ASCE *109*, 62–70.

Roa-Espinosa, A., Norman, J., Wilson, T. and Johnson, K. (2003). Predicting the Impact of Urban Development on Stream Temperature Using a Thermal Urban Runoff Model (TURM). In Proceedings of the U.S. EPA National Conference on Urban Stormwater: Enhancing Programs at the Local Level, Chicago, IL pp. 369–389,.

Roy, A. H. and Shuster, W. D. (2009). Assessing impervious surface connectivity and applications for watershed management. Journal of the American Water Resources Association *45*, 198 – 209.

Ryan, P., Harleman, D. R. F. and Stolzenbach, K. (1974). Surface heat loss from cooling ponds. Water Resources Research *10*, 930–938.

Silliman, S. E. and Booth, D. F. (1993). Analysis of time-series measurements of sediment temperature for identification of gaining vs. losing portions of Juday Creek, Indiana. Journal of Hydrology *146*, 131–148.

Stefan, H. G., Gulliver, J., Hahn, M. G. and Fu, A. Y. (1980). Water Temperature Dynamics in Experimental Field Channels: Analysis and Modeling. Project Report 193, St. Anthony Falls Laboratory, University of Minnesota Minneapolis, MN, USA.

Stonestrom, D. A. and Constantz, J. (2003). Heat as a tool for studying the movement of ground water near streams. USGS Circular 1260 U.S. Geological Survey.

Su, G. W., Jasperse, J., Seymour, D. and Constantz, J. (2004). Estimation of hydraulic conductivity in an alluvial system using temperature. Ground Water *42*, 890–901.

Taylor, C. and Stefan, H. G. (2009). Heating of shallow groundwater flow by conduction from a paved surface: requirements for coldwater stream protection. Project Report 531, St. Anthony Falls Laboratory, University of Minnesota Minneapolis, MN, USA. Available online: home.safl.umn.edu/bmackay/pub/pr/pr531.pdf.

TenWolde, A. (1997). FPL Roof Temperature and Moisture Model: Description and Verification. Research Paper FPL-RP-561 U.S. Department of Agriculture, Forest Service, Forest Products Laboratory Madison, WI, USA.

Theurer, F. D., Voos, K. A. and Miller, W. J. (1984). Instream water temperature model. Fish and Wildlife Service Instream Flow Information Paper 16, FWS/OBS-84/15. U.S. Fish and Wildlife Service, Fort Collins, CO, USA.

Thompson, A., Wilson, T. B., Norman, J. M., Gemechu, A. and Roa-Espinosa, A. (2008). Modeling the effect of summertime heating on urban runoff temperature. Journal of the American Water Resources Association *44*, 1548–1563.

Ul Haq, R. and James, W. (2002). Thermal Enrichment of Stream Temperature by Urban Storm Water. In Proceedings, International Conference on Urban Drainage. Portland, OR.

U.S. Environmental Protection Agency (E.P.A.) (1986). Quality criteria for water: 1986.

Technical Report EPA 440/5-86-001. U.S. Environmental Protection Agency, Office of Water Regulations and Standards Washington, D.C., USA.

Van Buren, M., Watt, W., Marsalek, J. and Anderson, B. (2000a). Thermal Enhancement of Stormwater Runoff by Paved Surfaces. Water Research *34*, 1359–1371.

Van Buren, M., Watt, W., Marsalek, J. and Anderson, B. (2000b). Thermal Balance of an On-stream Stormwater Management Pond. Journal of Environmental Engineering *126*, 509–517.

VanWoert, N., Rowe, D. B., Andresen, J. A., Rugh, C. L., Fernandez, R. and Xiao, L. (2005). Green roof stormwater retention: effect of roof surface, slope, and media depth. Journal of Environmental Quality *34*, 1036–1044.

Viessman Jr., W., Knapp, J., Lewis, G. and Harbaugh, T. (1977). Introduction to Hydrology. 2nd edition, Harper and Row, New York, NY, USA.

Wang, L., Lyons, J. and Kanehl, P. (2003). Impacts of urban land cover on trout streams in Wisconsin and Minnesota. Transactions of the American Fisheries Society *132*, 825–839.

Wilson, B. N. (2005). Hydrologic modeling of small watersheds. BBE 8513 Lecture Notes, University of Minnesota.

Winandy, J. E., Barnes, H. M. and Hatfield, C. A. (2000). Roof temperature histories in matched attics in Mississippi and Wisconsin. Research Paper FPL-RP-589. U.S. Department of Agriculture, Forest Service, Forest Products Laboratory Madison, WI, USA.

Winandy, J. E. and Beaumont, R. (1995). Roof temperatures in simulated attics. Research Paper FPL-RP-543. U.S. Department of Agriculture, Forest Service, Forest Products Laboratory Madison, WI, USA.

Xiong, Y. and Melching, C. (2005). Comparison of Kinetmatic-Wave and Nonlinear Reservoir Routing of Urban Watershed Runoff. Journal of Hydrologic Engineering *10*, 39–49.

Appendix A

Heat Budget Equations for a Land Surface with a Vegetated Canopy

The heat budget used by MINUHET for a land surface with vegetation cover is described in detail in Herb et al. (2006, 2008); an abbreviated description of the necessary equations is included here for reference. Two equations are used in the land surface heat budget, one for the canopy (Eq. A.1, 3.2) and another for the ground surface (Eq. A.2, 3.3). The canopy heat budget is given by:

$$h_{net,f} = 0 = h_{rad,a} + h_{lw,g} - h_{lw,f} - h_{evap,f} - h_{conv,f} \tag{A.1}$$

while the ground surface heat budget, for wet weather, is given by:

$$h_{net,g} = (1-v)h_{rad,a} + vh_{lw,f} - h_{lw,g} - (1-C_e v)h_{evap,f} - (1-C_e v)h_{conv,g} - h_{ro} \tag{A.2}$$

where v is the vegetation density factor (0 = bare soil, 1 = fully-dense canopy) and C_e is the bare soil evaporation coefficient. Note that all canopy heat budget terms (RHS of Eq. A.1) are weighted by v; however, since the canopy is assumed to have no heat storage capacity (i.e. $h_{net,f} = 0$), the weighting factor has no effect on that budget.

The equations for the radiation terms are nearly identical to those used for the Janke et al. (2009) runoff model (see Chapter 2). The incoming total (solar and longwave) radiation term, $h_{rad,a}$, is given by:

$$h_{rad,a} = \Big(1 - \alpha_f\Big)R_s + \left(\sigma\Big(CR + 0.67(1 - CR)e_a^{0.08}\Big)T_a^4\right) \tag{A.3}$$

where α_f is the canopy albedo (replaced by ground albedo, α_g, when this term is evaluated for the ground surface heat budget in A.2), R_s is the incident solar radiation (W/m^2), σ is the Stefan-Boltzmann constant, CR is a cloudiness ratio that varies from 0 (clear sky) to 1 (full cloud cover), e_a is the vapor pressure of air (Pa), and T_a is the air temperature (K). The cloudiness ratio is given by $CR = 1 - R_s/R_{s,max}$, where $R_{s,max}$ is the maximum possible solar radiation, determined using equations presented in Janke et al. (2006, see also Duffie and Beckman, 1991). The other longwave radiation terms in the canopy heat budget, $h_{lw,f}$ and $h_{lw,g}$, are formulated as follows:

$$h_{lw,f} = \epsilon_f \sigma T_f^4 \tag{A.4}$$

$$h_{lw,g} = \epsilon_g \sigma T_g^4 \tag{A.5}$$

where ϵ_f is the canopy emissivity, T_f is the canopy temperature, ϵ_g is the ground emissivity, and T_g is the ground temperature.

The canopy evaporation $h_{evap,f}$ and canopy convection $h_{conv,f}$ terms can be described with the following equations:

$$h_{evap,f} = \frac{\Big(\rho_a L_v\Big)\Big(q_{sat}(T_f) - q_a\Big)}{r_a + r_s} \tag{A.6}$$

$$h_{conv,f} = \frac{\Big(\rho_a C_{p,a}\Big)\Big(T_f - T_a\Big)}{r_a} \tag{A.7}$$

where ρ_a and $C_{p,a}$ are the density (kg/m^3) and specific heat (J/kg*K) of air, respectively, L_v is the latent heat of vaporization of water (J/kg), q_{sat} is the specific humidity of air at the canopy temperature (kg_w/kg_a), q_a is the specific humidity of air (kg_w/kg_a). The canopy evaporative and convective heat fluxes rely on the calculation of

both aerodynamic (r_a) and stomatal (r_s) resistances for the canopy (s/m). The evaporation equation includes both resistances to approximate the stomatal and atmospheric controls on evapotranspiration, while the convective heat flux equation includes the aerodynamic resistance only. These resistances are based on those given by Deardorff (1978), and are functions of wind speed (u), maximum solar radiation ($R_{s,max}$), actual solar radiation (R_s), wilting point (θ_{wp}), and soil moisture (θ):

$$r_s = 200\left(R_{s,max}/\left(R_s + 0.03R_{s,max}\right) + \left(\theta_{wp}/\theta\right)^2 \right) \tag{A.8}$$

$$r_a = 1/(c_r u_s); c_r = 0.01(1 + 0.3/u_s) \tag{A.9}$$

The terms in the ground surface heat budget (Eq. A.2) can be determined with the same equations used in the runoff temperature model (Chapter 2)) or for the canopy (Eqs. A.3 to A.9), with some minor modifications described as follows.

The radiation term $h_{rad,a}$ is identical to that for the canopy (Eq. A.3), with the albedo of the ground surface α_g used in place of the albedo of the canopy α_f. The longwave radiation terms remain unchanged; incoming longwave radiation from the canopy $h_{lw,f}$ is defined using Eq. A.4, and the outgoing longwave radiation from the ground $h_{lw,g}$ is determined with Eq. A.5.

The ground evaporation term $h_{evap,g}$ is calculated from an equation very similar to that used in the runoff model (Chapter 2):

$$h_{evap,g} = \rho_a L_v \theta' \left(C_{fc} u_s + C_{nc} \Delta\theta_v^{0.33} \right) \left(q_{sat} - q_a \right) \tag{A.10}$$

where C_{fc} and C_{nc} are coefficients for forced and natural convection, respectively, and $\Delta\theta_v$ is the difference in virtual temperature between the surface and atmosphere. For bare soil, C_{fc} and C_{nc} have values of 0.003 and 0.0015 ($^\circ C^{1/3}$m/s), respectively, determined from calibration of the surface temperature model to surface and sub-surface temperature data collected at a site on the Saint Paul, MN campus of the University of Minnesota (Herb et al., 2006, 2008). For a bare soil surface, the evaporation term is scaled directly by the soil moisture content at the surface, $\theta' = (\theta - \theta_{fc})/(\theta_s - \theta_{fc})$, where θ is the soil moisture content, θ_{fc} is the field capacity, and θ_s is the saturated soil water content (Herb et al., 2008).

The ground convection term $h_{conv,g}$ is calculated using a similar equation:

$$h_{conv,g} = \rho_a C_{p,a}\Big(C_{fc}u_s + C_{nc}\Delta\theta_v^{0.33}\Big)\Big(T_g - T_a\Big) \tag{A.11}$$

where the convection coefficients are the same as those used in the evaporation term.